

Catalytic conversion of carbon dioxide to value added chemicals

by

Sagar Dattulal Chaudhary
20EE17A26032

A thesis submitted to the
Academy of Scientific & Innovative Research
for the award of the degree of
DOCTOR OF PHILOSOPHY
in
ENGINEERING

Under the supervision of
Dr. Nilesh A. Mali (Supervisor)
Dr. Sunil S. Joshi (Co-supervisor)



CSIR- National Chemical Laboratory, Pune

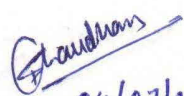


Academy of Scientific and Innovative Research
AcSIR Headquarters, CSIR-HRDC campus
Sector 19, Kamla Nehru Nagar,
Ghaziabad, U.P. – 201002, India

July 2023

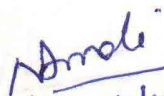
Certificate

This is to certify that the work incorporated in this Ph.D. thesis entitled, "Catalytic conversion of carbon dioxide to value added chemicals", submitted by Sagar Dattulal Chaudhary to the Academy of Scientific and Innovative Research (AcSIR) in fulfillment of the requirements for the award of the Degree of Doctor of Philosophy in Engineering embodies original research work carried-out by the student. We, further certify that this work has not been submitted to any other University or Institution in part or full for the award of any degree or diploma. Research materials obtained from other sources and used in this research work has been duly acknowledged in the thesis. Images, illustrations, figures, tables etc., used in the thesis from other sources, have also been duly cited and acknowledged.



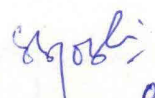
04/07/2023

(Signature of Student)



04/07/2023

(Signature of Supervisor)



04/07/2023

(Signature of Co-Supervisor)

Sagar Dattulal Chaudhary
Name with date

Dr Nilesh. A. Mali
Name with date

Dr Sunil S. Joshi
Name with date

STATEMENTS OF ACADEMIC INTEGRITY

I Sagar Dattulal Chaudhary, a Ph.D. student of the Academy of Scientific and Innovative Research (AcSIR) with Registration No. 20EE17A26032 hereby undertake that, the thesis entitled "Catalytic conversion of carbon dioxide to value added chemicals" has been prepared by me and that the document reports original work carried out by me and is free of any plagiarism in compliance with the UGC Regulations on "*Promotion of Academic Integrity and Prevention of Plagiarism in Higher Educational Institutions (2018)*" and the CSIR Guidelines for "*Ethics in Research and in Governance (2020)*".




Signature of the Student

Date : 04/07/2023

Place : CSIR-NCL, Pune

It is hereby certified that the work done by the student, under my supervision, is plagiarism-free in accordance with the UGC Regulations on "*Promotion of Academic Integrity and Prevention of Plagiarism in Higher Educational Institutions (2018)*" and the CSIR Guidelines for "*Ethics in Research and in Governance (2020)*".

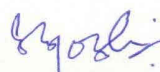


Signature of the Supervisor

Name : Dr. Nilesh A. Mali

Date : 04/07/2023

Place : CSIR - NCL, Pune



Signature of the Co-supervisor

Name : Dr. Sunil S. Joshi

Date : 04/07/2023

Place : CSIR-NCL, Pune

Dedicated to my mother

ACKNOWLEDGEMENT

It was a dream of mine to pursue a Ph.D. from my college days until I started the initial steps toward it, and today when I am about to complete it, I would like to express my gratitude to all the people and their support I received in my tenure.

First and foremost, I would like to thank my sincere gratitude to my PhD supervisors, Dr Sunil Joshi and Dr Nilesh Mali, for their advice during my doctoral research over the past few years. As my supervisors, they have constantly encouraged me to remain focused on achieving my goal. Their observations and comments helped me establish the research's overall direction. I thank them for providing me with the liberty and opportunity to work with a brilliant team of researchers. I am especially grateful for their devotion to students' research and success. I have not heard of another mentor who goes so far out of his way to make sure students are prepared for whatever the next step in their journey may be. The discipline, principles, simplicity, caring attitude, criticism and provision of a fearless work environment given by them will be helpful to grow as a researcher. Their constant effort to introduce us to several essential habits, like work planning, group meetings and weekly progress update, made me confident to start an independent scientific career and hence I preserve an everlasting gratitude for them. I am certain that the ethics and moral values which I learnt from them will go a long way in making me a better human being.

I thank my former HODs, Dr S. Tambe, and Dr S. S. Joshi, and the present head CEPD division, Dr Chetan Gadgil, for their help and support. I also thank the DAC members Dr Ashutosh Kelkar, Dr Dhiman Sarkar, Dr M Muthukrishnan, Dr Sanjay Kamble and Dr Rahul Bhambure for the evaluation of my research work. It's my privilege to thank the Director, CSIR-NCL, for giving me this opportunity and providing all necessary infrastructure and facilities. I especially thank CSIR, New Delhi, for the SRF fellowship. I thank the CMC group for their help in obtaining the analytical data. I also thank the library staff, chemical stores, purchase staff and glass-blowing section staff of NCL for their cooperation.

I also thank Dr. M. S. Shashidhar, Dr. B. L. V. Prasad, Dr. Santosh Mhaske, Ms. Kolhe, Ms. Komal, Ms. Vijaya and Ms. Vaishali Student Academic Office at NCL for their help verifying all my documents. The various members of the CEPD division have provided a diverse environment that has not only shaped me as a researcher but also as a person. Through all of

the ups and downs of the past six years that we spent together, I wouldn't replace any of the people I have had the opportunity to work with in the lab. The early lab members were helpful to me in learning lab techniques and developing thinking skills. I am lucky to make a number of friends Ajay, Priyanka, Vipin, Saurabh, Yogesh, Rahul and many more with whom I had no restriction bar to discuss anything and anytime. I am thankful to my lab members Rahul, Ajinkya, Shardul, Jayram, Meesha, Gopal, Aadharsh, Dipak, Himanshu, Yagyansh, Nikitra and Pravin for keeping the lab atmosphere joyful and supportive. I am also thankful to other lab members Ranjit, Ravindra, Nitin, Prashant, and Muzammil for supporting me in my research needs in any manner. I thank my teachers from School and College for their inspirational teaching, ethics and discipline. No words would be sufficient to express my gratitude and love to my mother for her struggle, patience, and sacrifices the main inspiration of my life. The warmth and moral value of my mother have stood me in good stead throughout my life and I would always look up to her for strength no matter what I have to go through. This Ph. D. thesis is a result of the will, efforts and sacrifices of my family. I wish to thank the great scientific community, whose constant encouragement is a source of inspiration for me. I would like to say thank you to all the people who came into my life and made it outstanding and fantastic! Though many have not been mentioned, none is forgotten.

Thank You.

Sagar Chaudhary

Table of Contents

Synopsis report	<i>i</i>
List of Figures.....	<i>vii</i>
List of Tables.....	<i>xi</i>
List of Reaction Schemes.....	<i>xii</i>
Abbreviations	<i>xiii</i>
Chapter 1: Introduction	1
1.1 CO ₂ and global warming.....	2
1.2 CO ₂ as a C ₁ feedstock.....	4
1.2.1 Current industrial applications of CO ₂	4
1.3 Need for CO ₂ utilization	5
1.4 Challenges in CO ₂ utilization.....	6
1.4.1 Thermodynamics of CO ₂ conversion.....	7
1.4.2 Strategies for CO ₂ conversion and utilization	8
1.4.3 Recent research and development in catalytic CO ₂ conversion	9
1.4.3.1 Hydrogenation of CO ₂	11
1.4.3.2 Mineral carbonation	12
1.4.3.3 Linear and cyclic carbonates	12
1.5 Motivation.....	12
1.6 References.....	13
Chapter 2: Hydrogenation of carbon dioxide to dimethyl formamide.....	18
Abstract.....	19
2.1 Introduction.....	20
2.2 Current industrial status of CO ₂ hydrogenation	21
2.3 Hydrogenation of carbon dioxide to C ₁ feedstock chemicals	21
2.3.1 CO ₂ to Methanol	21
2.3.2 CO ₂ to Methane.....	23
2.3.3 CO ₂ to CO.....	24
2.3.4 CO ₂ to formic acid and its derivatives	25
2.4 Prior art	26
2.4.1 Catalysis and mechanistic approach	26
2.4.2 Hydrotalcites as a catalyst	29
2.4.3 Thermodynamics of CO ₂ hydrogenation to formic acid.....	31

2.5 Experimental procedures	31
2.5.1 Catalyst preparation	31
2.5.2 Catalyst characterization	32
2.5.3 Batch reaction procedure and reaction monitoring	33
2.5.4 Continuous fixed bed reactor.....	35
2.6 Results and discussion	36
2.6.1 Catalyst characterization	36
2.6.1.1 Surface morphology	36
2.6.1.2 BET surface area and elemental composition	38
2.6.1.3 X-ray photo spectroscopy (XPS)	38
2.6.1.4 Fourier transform infrared (FTIR)	40
2.6.1.5 X-ray powder diffraction (XRD)	41
2.6.1.6 Temperature programmed desorption and reduction (TPD and TPR)	42
2.6.2 Catalyst screening.....	43
2.6.3 Parametric study.....	45
2.6.3.1 Effect of reaction temperature and time	45
2.6.3.2 Effect of solvent	46
2.6.3.3 Effect of H ₂ /CO ₂ mole ratio	46
2.6.3.4 Effect of phase change (pressure)	47
2.6.3.5 Effect of catalyst loading	48
2.6.3.6 Effect of base addition	49
2.6.3.7 Catalyst recycle studies	49
2.6.4 Continuous synthesis in fixed bed reactor.....	50
2.6.5 Mechanistic approach.....	51
2.6.6 Reaction kinetics	53
2.7 Conclusion and the path forward.....	56
2.8 References.....	57
Chapter 3: Cycloaddition of CO ₂ in styrene oxide	67
Abstract.....	68
3.1 Introduction.....	69
3.2 Current industrial status of cycloaddition of CO ₂ in epoxides.....	70
3.3 Cycloaddition of CO ₂ in Styrene oxide – Prior art.....	71
3.4 Experimental procedures	74
3.4.1 Batch reaction procedure and reaction monitoring	74
3.4.2 Continuous flow reactor development.....	75

3.5 Results and Discussion	77
3.5.1 Catalyst screening.....	77
3.5.2 Batch process optimization.....	78
3.5.2.1 Effect of reaction temperature	78
3.5.2.2 Effect of catalyst loading	78
3.5.2.3 Effect of pressure	80
3.5.2.4 Effect of reaction time	80
3.5.2.5 Effect of solvent	82
3.5.2.6 Effect of CO ₂ :SO mole ratio	83
3.5.3 Reaction kinetics	83
3.5.4 Continuous flow synthesis	88
3.6 Conclusion and the path forward.....	92
3.7 References.....	93
Chapter 4: Carboxylation of phenol to salicylic acid.....	99
Abstract.....	100
3.1 Introduction.....	101
3.3 Carboxylation of phenol – prior art.....	103
3.4 Experimental procedures	106
3.4.1 Catalyst synthesis.....	106
3.4.2 Catalyst characterization	106
3.4.3 Batch reaction procedure and reaction monitoring	106
3.5 Results and Discussion	108
3.5.1 Catalyst characterization	108
3.5.1.1 X-ray diffraction (XRD).....	108
3.5.1.2 Fourier transformed infrared spectroscopy (FTIR).....	108
3.5.1.3 Surface area and elemental composition.....	109
3.5.2 Catalyst screening.....	109
3.5.3 Process optimization	110
3.5.3.1 Effect of reaction tempertaure	110
3.5.3.2 Effect of catalyst loading	112
3.5.3.3 Effect of pressure.....	112
3.5.3.4 Effect of reaction time	113
3.5.3.5 Effect of solvent.....	115
3.6 Conclusion and the path forward.....	115
3.7 References	116

Chapter 5: Conclusion and future scope	120
Annexure A: Supporting information	124
Thesis Abstract	
List of publications and conferences	
Publication copies	



Synopsis of the thesis to be submitted to the Academy of Scientific and Innovative Research for the award of Doctor of Philosophy in Engineering

Name of candidate	CHAUDHARY SAGAR DATTULAL
Degree, Enrolment no. and Date	PhD in Engineering sciences (20EE17A26032) August 2017
Laboratory	CSIR – National Chemical Laboratory, Pune - 411008
Title of the thesis	Catalytic conversion of carbon dioxide to value added chemicals
Research supervisors	Dr Nilesh A. Mali and Dr Sunil S. Joshi

1. Introduction

The exponential growth of technology in almost every sector brought us an increasing demand for fossil fuels and energy. Only 16 % of global energy requirement comes from low-carbon resources like biofuels, wind, hydropower, solar and nuclear. At the same time, oil and coal are significant contributors to fulfilling the energy necessities¹. Today, carbon dioxide concentration in the atmosphere has crossed 420 ppm, and its growing trend has become a global concern. According to the latest IPCC report, the major contributors to CO₂ emissions are Asia and USA due to population density. If this trend continues, we will pass the 1.5°C threshold of average global temperature within two decades². The current industrial utilization of carbon dioxide is less than 1 % of the total global emissions, out of which 57 % is consumed in the production of urea used as agricultural fertilizer and 34 % in enhanced oil recovery³.

The major challenge for the conversion of carbon dioxide is the thermodynamic stability and its activation. Accordingly, energy must generally be supplied to drive the desired transformation. Otherwise, a proper selection of material which can activate carbon dioxide to interact with other molecules is necessary. In this thesis, we worked on different reaction schemes like hydrogenation, cyclic carbonates and carboxylation. We proposed the processes for three important industrial molecules – dimethyl formamide, styrene carbonate and salicylic acid. The detailed work in process development, process intensification and catalysis is discussed and presented in the thesis

2. Statement of the problem

2.1 Hydrogenation of CO₂ to dimethyl formamide

CO₂ is the cheapest and most readily available source, and its conversion to C₁ value-added chemicals is adopted by researchers worldwide. Hydrogenation in the presence of a catalyst leads to several essential chemicals like methanol, methane, carbon monoxide, formaldehyde and formic acid. Research and development on methanol synthesis from CO₂ have reached the level of commercial plant development, whereas geological and biological routes generally produce methane. The formic acid synthesis is explored by researchers, with most of the reports available on homogenous catalysts⁴⁻⁶. The significant challenges with the available catalyst are to overcome the use of phosphine-based toxic catalysts with greener and recyclable heterogeneous material and to increase the extent of selective hydrogenation to formic acid.

2.2 Cycloaddition of CO₂ in styrene oxide

Organic carbonates are becoming important solvents due to their low toxicity, as monomers for synthesizing polymeric materials, as electrolytes in secondary batteries and as a chemical ingredient for pharmaceutical products. The critical prerequisite for cycloaddition reaction is the presence of Lewis acids and basic sites in catalysts for epoxide ring opening and CO₂ activation. Cycloaddition of CO₂ proceeds with 100 % atom economy and several industrial processes are reported for producing ethylene and propylene carbonates^{7,8}. In regards to other cyclic carbonates like styrene carbonate, glycerol carbonate, and cyclohexane carbonate, there is a plenty of research that needs to be done with catalysis, process intensification and continuous flow synthesis.

2.3 Carboxylation of phenol to salicylic acid

The preparation of salicylic acid from phenol and carbon dioxide is well known Kolbe-Schmitt process. The current industrial process consists of 3 steps – preparation of phenoxide salt using sodium hydroxide, drying of salt followed by carbon dioxide addition with the process yield of 55 % at 80 – 90 atm pressure at 170 °C⁹. Very few reports available for carboxylation reaction suggest using potassium carbonate as a catalyst for single pot synthesis resulting in 40 – 50 % reaction yield. There is a need for significant development of the selective catalytic system with process intensification.

3. Objectives

- To develop processes for maximum conversion of CO₂ to chemicals
- To develop a green, recyclable heterogeneous catalyst for the hydrogenation of carbon dioxide to formic acid and its derivative – dimethyl formamide
- To develop the reaction kinetics understandings for the scale-up of the process
- To develop a continuous synthesis process for cyclo addition of CO₂ in styrene oxide
- To develop a novel process and catalyst system for the synthesis of ortho-salicylic acid from phenol

4. Methodology

The methodology involved an in-depth literature review, finding the gaps in the research studies, developing a newer catalytic system for the conversion of carbon dioxide, process intensification and development and continuous flow synthesis.

Studies on the hydrogenation of carbon dioxide were carried out in a high-pressure batch reactor. The different heterogeneous catalysts were prepared using the co-precipitation method as reported and tested for hydrogenation. After optimizing the catalyst system and metal compositions, detailed catalyst characterization was done to understand the catalyst properties and reaction mechanism. Process optimization was carried out in a batch reactor, and a kinetic model was developed and validated for the experimental findings. Reaction samples were analyzed using gas chromatography equipped with a polar column and FID detector

Cycloaddition of CO₂ in styrene carbonate was carried out using the reported catalyst in a batch reactor. The process optimization and kinetics study data were used to develop a continuous flow synthesis coiled reactor. The in-house developed setup of the helically coiled reactor used for the process optimization and reaction was monitored using gas chromatography on the FID detector.

A catalyst for the carboxylation of phenol was prepared using the wet-impregnation method and tested for the process in a high-pressure autoclave reactor. The carbon dioxide was fed into the reactor using a liquid CO₂ pump, and the reaction was monitored by HPLC using a UV detector.

5. Results / Summary / Conclusions

5.1 Hydrogenation of CO₂ to dimethyl formamide

In this work, we proposed dimethylformamide (DMF) synthesis using ruthenium-doped Mg/Al calcined hydrotalcite CO₂ hydrogenation in dimethylamine (DMA). At optimized conditions, complete conversion of dimethylamine was achieved with more than 92% product yield at 170 °C and 13 MPa pressure with a reaction time of 6 hrs. Fundamental catalyst properties were determined using X-ray powder diffraction (XRD), X-ray photoelectron spectroscopy (XPS), CO₂-temperature programmed desorption (TPD), H₂ temperature-programmed reduction (TPR) and Fourier transform infrared (FTIR). The surface morphology was determined using a field emission scanning electron microscope (FE-SEM) and high-resolution transmission electron microscopy (HR-TEM), and observed the planer distorted sheet morphology for the synthesized hydrotalcites. At the same time, the chemical composition was verified by energy-dispersive X-ray (EDS) and observed 1.3 mole % of ruthenium loading in the catalyst. In addition, kinetic modelling is performed using the two-site Langmuir-Hinshelwood-Hougen-Watson model. The regressed kinetic parameters gave an appropriate fit with experimental concentration values, and activation energy is calculated as 413 kJ/mol.

5.2 Cycloaddition of CO₂ in styrene oxide

In this work, we proposed the process intensification, reaction kinetics modeling and continuous flow synthesis of styrene carbonate by cycloaddition of CO₂ in styrene oxide using tetrabutylammonium bromide as a catalyst. An optimized process was developed with complete conversion of styrene oxide with 83 % of product yield at 140 °C and 2 mole % catalyst loading within 60 minutes. Important reaction parameters such as temperature and catalyst loading were optimized. The dimethylformamide used as a solution played a crucial role in CO₂ solubility and overcoming the mass transfer limitations. Due to higher CO₂ solubility, the first-order homogenous reaction kinetic model was used to determine the reaction kinetic parameter, and the activation energy was calculated as 98 kJ/mol. The process was also optimized for the continuous flow synthesis of styrene carbonate in a coiled reactor operated at 20 bar pressure.

5.3 Carboxylation of phenol to salicylic acid

Salicylic acid is industrially produced by carboxylation of phenol using sodium hydroxide as a catalyst (Kolbe-Schmitt process) in three steps. In this work, we prepared potassium-doped

NaX zeolites for the single-pot synthesis of salicylic acid. Catalyst characterization was done to interpret the catalyst properties and required sites for reaction activation. At the optimized reaction conditions, 20 % of salicylic acid yield was obtained with more than 95 % selectivity at 200 °C within 6 hrs of reaction time in supercritical conditions of CO₂. The change in the reaction phase from subcritical to supercritical phase shows the enhanced effect on reaction yield due to higher mass transfer rates.

6. Future directions

- Development of a continuous process pilot plant for the hydrogenation of CO₂ based on the understanding developed at lab scale batch reactions.
- Catalyst development for milder reaction conditions which will further improve economics of the process.
- Downstream process development for the generating commercial grade styrene carbonate.
- Pilot plant design and process validation for synthesis of styrene carbonate.
- Development better catalyst system to improve reaction kinetics and subsequently intensifying process by developing continuous reactor setup for salicylic acid synthesis.

7. References

1. Hannah Ritchie, Max Roser and Pablo Rosado (2022) - "Energy". Published online at OurWorldInData.org. Retrieved from: '<https://ourworldindata.org/energy>'
2. AR6 Climate Change 2022: Mitigation of Climate Change — IPCC. <https://www.ipcc.ch/report/sixth-assessment-report-working-group-3/>.
3. Putting CO₂ to Use – Analysis - IEA. <https://www.iea.org/reports/putting-co2-to-use>.
4. Behr, A. & Nowakowski, K. Catalytic Hydrogenation of Carbon Dioxide to Formic Acid. in *Advances in Inorganic Chemistry* (2014). doi:10.1016/B978-0-12-420221-4.00007-X.
5. Philip G. Jessop, Yi Hsiao, Takao Ikariya, and Ryoji Noyori*, †. Homogeneous Catalysis in Supercritical Fluids: Hydrogenation of Supercritical Carbon Dioxide to Formic Acid, Alkyl Formates, and Formamides. *J. Am. Chem. Soc.* **118**, 344–355 (1996).
6. Jessop, P. G., Joó, F. & Tai, C. C. Recent advances in the homogeneous hydrogenation of carbon dioxide. *Coord. Chem. Rev.* **248**, 2425–2442 (2004).

7. Clements, J. H. Reactive applications of cyclic alkylene carbonates. *Ind. Eng. Chem. Res.* **42**, 663–674 (2003).
8. Yoshida, M. & Ihara, M. Novel Methodologies for the Synthesis of Cyclic Carbonates. *Chem. – A Eur. J.* **10**, 2886–2893 (2004).
9. Lindsey, A. S. & Jeskey, H. The Kolbe-Schmitt Reaction. *Chem. Rev.* **57**, 583–620 (1957).

8. Publications and Conferences

- **Chaudhary, S. D.**, Rahatade, S. S., Joshi, S. S., & Mali, N. A. (2022). Reduction of carbon dioxide to dimethylformamide using ruthenium doped Mg/Al hydrotalcites under supercritical conditions. *Journal of CO₂ Utilization*, 61, 102055. <https://doi.org/10.1016/j.jcou.2022.102055>
- Sagar D. Chaudhary, Shardul S. Rahatade, Sunil S. Joshi, Nilesh A. Mali, “Process development for cycloaddition of CO₂ in styrene oxide, a batch and continuous synthesis approach” (Manuscript under process)
- **S. Chaudhary**, S. Joshi, “Hydrogenation of CO₂ to formic acid and its derivatives under supercritical conditions”, Carbon capture and utilization, Dec 2018, CSIR – NCL, Pune (Oral Presentation).

List of Figures

Figure No.	Details	Page No.
1.1	CO ₂ emissions sources, source: OurWorldInData.org	2
1.2	Global temperature rise and CO ₂ concentrations, source: climate.govglobal	3
1.3	Current CO ₂ consumption, projections are based on current average consumptions. Source: International Energy Agency.	4
1.4	Industrial chemical processes using CO ₂ as feedstock.	5
1.5	Carbon dioxide phase diagram.	8
1.6	Catalytic CO ₂ activation routes presented by Andrea et al	10
2.1	CO ₂ hydrogenation products	20
2.2	Suggested mechanism for formic acid on RhCl(TPPTS) ₃ by Leitner et al.	28
2.3	Suggested mechanism for formic acid on Au/Al ₂ O ₃ by Filonenko et al.	29
2.4	Hydrotalcite structure	30
2.5	Catalyst synthesis setup	32
2.6	Schematic of high pressure batch reactor	33
2.7	Fixed bed reactor for continuous CO ₂ hydrogenation	35
2.8	FE-SEM images of a) Mg-Al and b)Mg-Al-Ru calcined hydrotalcite	36
2.9	HR-TEM elemental mapping of a)Mg:Al and b)Mg:Al:Ru calcined hydrotalcite, d-spacing values of c)Mg:Al and d)Mg:Al:Ru calcined hydrotalcite, respectively.	37
2.10	XPS scan for a) Ru3d, b) Mg1s, and c) Al2p.	39
2.11	FTIR spectrum of Mg:Al and Ruthenium doped Mg:Al hydrotalcites.	40
2.12	XRD pattern for Mg:Al and Ruthenium doped Mg:Al hydrotalcites.	41
2.13	CO ₂ – TPD profiles of Mg:Al and Mg:Al:Ru hydrotalcites	42
2.14	H ₂ – TPR profile of Mg:Al:Ru hydrotalcite	43
2.15	Effect of reaction temperature and time. ■ DMA conversion; ▲ DMF yield. Reaction conditions: 1 wt % catalyst loading, solvent: MeOH, H ₂ :CO ₂ : 3:1, additive KHCO ₃ : 4.5 mmol, DMA : 80 mmol, a)time : 6 h, b) temperature : 170°C.	45
2.16	Effect of solvent. Reaction conditions: 1 wt % catalyst loading, H ₂ :CO ₂ : 3:1, additive KHCO ₃ : 4.5 mmole, DMA: 80 mmol, time : 6 h, temp: 170 °C.	48

Figure No.	Details	Page No.
2.17	Effect of H ₂ :CO ₂ mole ratio. Reaction conditions: 1 wt % catalyst loading, Solvent: MeOH, additive KHCO ₃ : 4.5 mmole, DMA: 80 mmole, time: 6 h, temperature: 170°C. Total pressure :13 MPa.	47
2.18	Effect of phase change. ■ DMA conversion; ▲ DMF yield. Reaction conditions: 1 wt % catalyst loading, solvent: MeOH, H ₂ : CO ₂ : 3:1, additive KHCO ₃ : 4.5 mmole, DMA : 80 mmole, time : 6 h, temperature : 170°C.	47
2.19	Effect of catalyst loading. ■ DMA conversion; ▲ DMF yield. Reaction conditions: Total pressure: 130 MPa, solvent: methanol, H ₂ :CO ₂ : 3:1, additive KHCO ₃ : 4.5 mmole, DMA : 80 mmole, time : 6 h, temperature : 170°C.	48
2.20	Effect of base addition. Reaction conditions: DMA 80 mmol, H ₂ : CO ₂ 3:1, time 6 h, temperature 170 °C, reaction pressure 13 MPa, catalyst Mg:Al:Ru HT (1 wt%), solvent: MeOH, base KHCO ₃ : 4.5 mmole	49
2.21	Catalyst recycle study. Reaction conditions: 1 wt % catalyst loading, Solvent: methanol, additive KHCO ₃ : 4.5 mmole, H ₂ :CO ₂ : 3:1 DMA : 80 mmole, time : 6 h, temperature : 170°C. Total pressure :13 MPa.	50
2.22	Effect of a) temperature and b) pressure in fixed bed reactor. Reaction conditions: solvent: MeOH, residence time: 2 minute, reactor volume: 5 ml, catalyst loading: 2 gms, Catalyst: Mg:Al:Ru, a) pressure: 100 bar, b) temperature: 170 °C.	51
2.23	Proposed reaction mechanism over Ru doped Mg:Al calcined hydrotalcite	52
2.24	Comparison between experimental data with the LHHW model	55
3.1	Industrial uses of cyclic carbonates	70
3.2	Asahi Kasei's polycarbonate production process ³²	71
3.3	General reaction mechanism for cycloaddition of CO ₂ to epoxide.	72
3.4	Schematic of high-pressure batch reactor	74
3.5	Actual image of high-pressure batch reactor and detailed sketch	74
3.6	Continuous flow reactor PFD for cycloaddition of CO ₂ in epoxide	76
3.7	Actual image of continuous flow reactor	76
3.8	Catalyst screening. Reaction conditions: Catalyst 5 mole %, temperature 120 °C, time 2 h, CO ₂ :SO 1.5, total pressure 20 bar, solvent: DMF 15 ml, SO 2 gms.	77

Figure No.	Details	Page No.
3.9	Effect of reaction temperature. Reaction conditions: Catalyst (TBAB) 2 mole %, time 2 h, CO ₂ :SO 1.5, total pressure 20 bar, solvent: DMF 15 ml, SO 2 gms.	78
3.10	Effect of catalyst loading. Reaction conditions: Catalyst TBAB, time 2 h, CO ₂ :SO 1.5, total pressure 20 bar, solvent: DMF - 15 ml, SO 2 gms.	79
3.11	Effect of pressure. Reaction conditions: Catalyst TBAB 2 mole %, time 2 h, CO ₂ :SO 1.5, temperature 140 °C, solvent: DMF 15 ml, SO 2 gms.	80
3.12	Effect of reaction time. Reaction conditions: Catalyst TBAB 2 mole %, CO ₂ :SO 1.5, total pressure 20 bar, solvent: DMF 15 ml, SO 2 gms.	81
3.13	Effect of solvent. Reaction conditions: time 2 h, catalyst TBAB 2 mole %, CO ₂ :SO 1.5, temperature 120 °C, total pressure 20 bar, solvent 15 ml, SO 2 gms.	82
3.14	Effect of CO ₂ :SO mole ratio. Reaction conditions: time 2 h, catalyst TBAB 2 mole %, temperature 120 °C, total pressure 20 bar, solvent DMF 15 ml, SO 2 gms.	83
3.15	Comparison between experimental data with first order kinetic model.	85
3.16	Estimated concentration profiles and experimental values at 130 °C	87
3.17	Comparison of experimental and model concentration values at different temperatures	87
3.18	Effect of temperature in a flow reactor. Reaction conditions: Catalyst TBAB 2 mole %, residence time 80 min, CO ₂ :SO mole ratio 1.7, pressure 20 bar, Solvent DMF.	88
3.19	Effect of CO ₂ :SO mole ratio in a flow reactor. Reaction conditions: catalyst TBAB 2 mole %, pressure 20 bar, residence time 80 min, solvent DMF.	89
3.20	Effect of pressure in a flow reactor. Reaction conditions: temperature 80 °C, catalyst TBAB 2 mole %, residence time 80 min, CO ₂ :SO mole ratio 1.2, solvent DMF.	90
3.21	Effect of residence time in a flow reactor. Reaction conditions: catalyst TBAB 2 mole %, pressure 15 bar, CO ₂ :SO mole ratio 1.2, solvent DMF.	91
4.1	Industrial uses of salicylic acid	102
4.2	General mechanism of Kolbe-Schmitt reaction	104

Figure No.	Details	Page No.
4.3	Reaction mechanism on K ₂ CO ₃ catalyst proposes by Iijima et al.	105
4.4	Schematic of high-pressure batch reactor	107
4.5	XRD pattern of NaX and K/NaX zeolites	108
4.6	FTIR spectra of NaX and K/NaX zeolite	109
4.7	a) Effect of temperature with K ₂ CO ₃ catalyst, b) Comparison of K/NaX and K ₂ CO ₃ with temperature. Reaction conditions: Time 5 h, reaction pressure 80 bars, catalyst amount 2 gms, phenol 2 gms.	111
4.8	Effect of catalyst loading. Reaction conditions: Temperature 200 °C, pressure 80 bar, time 5 h, phenol 2 gms. %X – conversion, % Y – yield.	112
4.9	Effect of Phase change (pressure). Reaction conditions: Temperature 200 °C, time 5 h, phenol 2 gms, catalyst K/NaX zeolite.	113
4.10	a) Effect of reaction time. b) Comparison of reaction conversions at different temperature with time. Reaction conditions: Temperature 200 °C, phenol 2 gms, catalyst 2 gms, pressure 80 bar.	114
4.11	Effect of solvent. Reaction conditions: Temperature 200 °C, pressure 80 bar, time 5 h, phenol 2 gms, catalyst 2 gms.	115
S-1.1	GC separation of DMA, DMF and TMA	124
S-1.2	Calibration curves of a)DMA, b) DMF, c) TMA	125
S-1.3	GC separation of SO, SC and SG	128
S-1.4	Calibration curves of a)SO, b) SC, c) SG	129
S-1.5	LC separation of phenol, OSA and PSA	130
S-1.6	Calibration curves of a)Phenol, b) OSA, c) PSA	131

List of Tables

Table No.	Details	Page No.
1.1	Recent catalytic systems for CO ₂ hydrogenation process	11
2.1	Summary of catalytic system reported for CO ₂ hydrogenation to formic acid	27
2.2	Thermodynamic parameters for CO ₂ hydrogenation to formic acid	31
2.3	BET surface area of different synthesized and calcined hydrotalcites	38
2.4	Catalyst Screening. Reaction conditions: DMA 80 mmol, solvent MeOH 100ml, temperature 170 °C, H ₂ : CO ₂ 3:1, reaction pressure 10 MPa, time 3 h, catalyst amount 1 wt %, additive KHCO ₃ 4.5 mmol	44
2.5	Reactions on hydrotalcite surface	53
2.6	Estimated kinetic parameters using LHHW model	56
3.1	Summary of catalytic systems for cycloaddition of CO ₂ to styrene oxide	73
3.2	Estimated kinetic parameters using first-order homogenous kinetics.	86
4.1	Catalyst screening. Reaction conditions: Phenol 2 gms, catalyst 1 gm, temperature 200 °C, time 5 h, reaction pressure 80 bar.	110
S-1.1	Gas chromatography method for detection of DMA, DMF and TMA	124
S-1.2	Gas chromatography method for detection of SO, SC, and SG	128
S-1.3	HPLC method for detection of phenol, OSA, and PSA	130

List of Reaction Schemes

Scheme No.	Details	Page No.
2.1	Hydrogenation of CO ₂ to methanol	22
2.2	Methanol synthesis by direct CO ₂ hydrogenation and via RWGS reaction	23
2.3	Hydrogenation of CO ₂ to methane	23
2.4	Hydrogenation of CO ₂ to carbon monoxide	24
2.5	CO ₂ hydrogenation to formic acid and DMF	25
3.1	Cycloaddition of CO ₂ in Epoxide	69
3.2	Reaction scheme for parallel reaction	84
4.1	Preparation of salicylic acid by carboxylation of phenol	102
4.2	Preparation of salicylic acid by hydrolysis of methyl salicylate.	103

Abbreviations

CO ₂	Carbon dioxide
H ₂	Hydrogen
NO _x	Nitrogen oxide(s)
scCO ₂	Supercritical carbon dioxide
CCS	Carbon capture and storage
CCU	Carbon capture and utilization
DAC	Direct air capture
EOR	Enhanced oil recovery
DMF	N,N-dimethyl formamide
DMA	N,N-dimethyl amine
DIMCARB	Dimethylammonium dimethyl carbonate
TMA	Trimethyl amine
SO	Styrene oxide
SG	Styrene glycol
SC	Styrene carbonate
OSA	Ortho-salicylic acid
PSA	Para-salicylic acid
HT	Hydrotalcite
XRD	X-ray diffraction
BET	Brunauer-Emmett-Teller surface area
XPS	X-ray photoelectron spectroscopy
TPD	CO ₂ -temperature programmed desorption
FTIR	Fourier transform infrared
FE-SEM	Field emission scanning electron microscope
HR-TEM	High-resolution transmission electron microscope

EDS	Energy-dispersive X-ray
LHHW	Langmuir-Hinshelwood-Hougen-Watson model
CRI	Carbon Recycling International
MTO	Methanol to olefins
DME	Dimethyl ether
ICI	Imperial Chemical Industries
DFT	Density function theory
RWGS	Reverse water gas shift reaction
FT	Fischer-Tropsch process
ΔG	Gibbs free energy
ΔH	Enthalpy
FA	Formic acid
TON	Turnover number
TOF	Turnover frequencies
GC	Gas chromatography
PFD	Process flow diagram
PID	Piping and instrumentation diagram
% X	Conversion
% Y	Yield
MFC	Mass flow controller
TBAB	Tetrabutylammonium bromide
MeOH	Methanol
EtOH	Ethanol
MPa	Mega pascal
H ₂ O	Water
5RA	5 % ruthenium on alumina

Chapter 1
Introduction

“This chapter introduces about carbon dioxide, its effects, need of CO₂ utilization and strategies to convert into value added chemicals”

Chapter 1

Introduction

1.1 CO₂ and global warming

The 21st century is experiencing exponential developments in each sector's new technologies, leading to growing energy consumption. Despite such developments, according to the World Energy Outlook Report 2021, the primary energy sources are still coal, oil, and natural gas, contributing to 81 % of total energy requirements¹. These sources emit greenhouse gases such as CO₂ and NO_x. Today, total CO₂ emission has crossed 37 billion tons per year, as shown in Figure 1.1, and it has doubled in the last five decades².

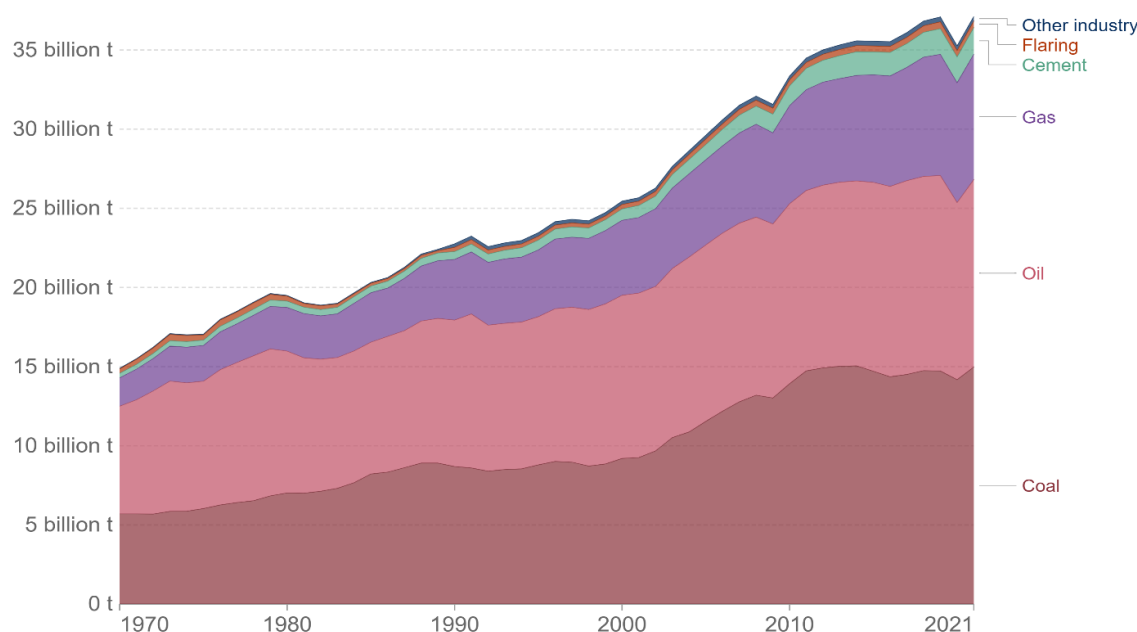


Figure 1.1: CO₂ emissions sources, source: OurWorldInData.org³

CO₂ is one of the main greenhouse gases, and its concentration in the atmosphere increased to 421 ppm in 2023. Every year, the average rise in CO₂ emission is 2 billion tons, leading to a continuous increase in concentration and eventually global warming. The rise in Earth's average temperature is primarily attributed to the accumulation of greenhouse gases in the atmosphere, which traps heat and contributes to the greenhouse effect. According to the IPCC report⁴, there is an urgent need to reduce greenhouse emissions to mitigate the effects of climate change. One of the most significant consequences of rising CO₂ levels is the intensification of the greenhouse effect. CO₂ absorbs and re-emits infrared radiation,

preventing it from escaping into space and effectively trapping heat within the atmosphere. This leads to a gradual increase in the Earth's atmosphere, which is resulting in a range of adverse effects, such as the melting of polar ice caps, sea-level rise, extreme weather events, and shifts in ecosystems⁴.

Scientific evidence indicates that the Earth's average temperature has risen by approximately 1.1 °C since the pre-industrial era (Figure 1.2), and a substantial proportion of this increase can be attributed to human-induced CO₂ emissions. This warming trend has been observed across various regions, affecting land and ocean temperatures.

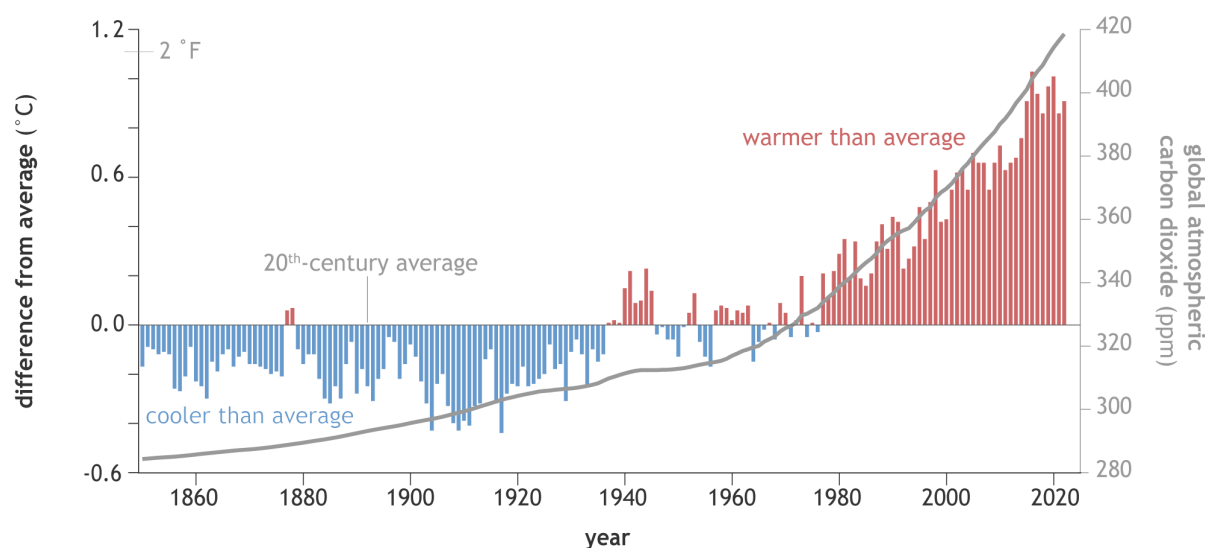


Figure 1.2: Global temperature rise and CO₂ concentrations, source: climate.govglobal⁵

To address the growing concern of global warming, international efforts have been established to limit global temperature rise to below 1.5 degrees Celsius above pre-industrial levels⁶. These targets require substantial reductions in CO₂ emissions and the adoption of renewable energy sources and practices to transition towards a low-carbon economy.

Also, the conversion of CO₂ to valuable chemicals represents a crucial avenue in the quest for a sustainable future. By harnessing the potential of CO₂ as a resource, it is possible simultaneously to address climate change, promote circular economy principles, drive innovation and economic growth, and foster the development of cleaner and more sustainable industries. As research and technological advancements continue to accelerate, the conversion of CO₂ holds tremendous promise in reshaping our approach to lowering global warming and creating a more sustainable world.

1.2 CO₂ as a C₁ feedstock

CO₂, once viewed solely as a greenhouse gas and environmental concern, is now being recognized as a valuable and abundant C₁ carbon source for the chemical industry. Many chemical processes are well established in CO₂ chemistry but are not significant for reducing its concentrations from the atmosphere. Researchers are looking at CO₂ as an alternative to C₁ sources like carbon monoxide which is challenging to handle.

Also, utilizing CO₂ as a C₁ carbon source promotes the concept of circular economy principles. By transforming CO₂ into chemicals and fuels, a closed-loop system can be established where waste becomes a valuable feedstock, minimizing waste generation and optimizing resource utilization.

1.2.1 Current industrial applications of CO₂

Today the yearly emission of CO₂ is more than 35 billion tons while the total consumption is approximately 250 million tons only which accounts for less than 1 % of total emissions. The report by International Energy Agency, suggests that early markets in CO₂ consumption are emerging but the future scale is uncertain⁷ and it is expected to rise CO₂ usage by only 10 % in the next 2-3 years based on current growth in CO₂ consumption. Figure 1.3 shows the slow growth in CO₂ consumption over the last two decades.

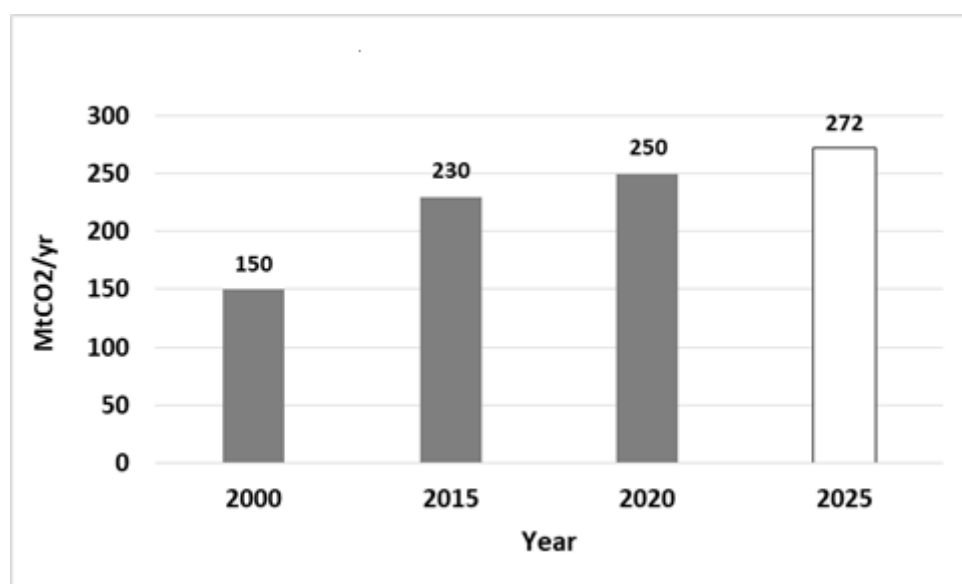


Figure 1.3: Current CO₂ consumption, projections are based on current average consumptions. Source: International Energy Agency⁷.

The majority of CO₂ currently being used is in the fertilizer industry for the production of urea where approximately 130 million tons of CO₂ is used which accounts for 57 % of total CO₂ consumption. The second large use of CO₂ is for enhanced oil recovery with a consumption of 70 to 80 million tons annually⁷. Only a small amount of CO₂ is used in extractions processes like the decaffeination of coffee, as fire extinguishers, in food industries for beverages, and in the pharmaceutical industry to produce salicylic acid. Figure 1.4 explains current industrial chemical synthesis processes using CO₂ as a feedstock and their applications.

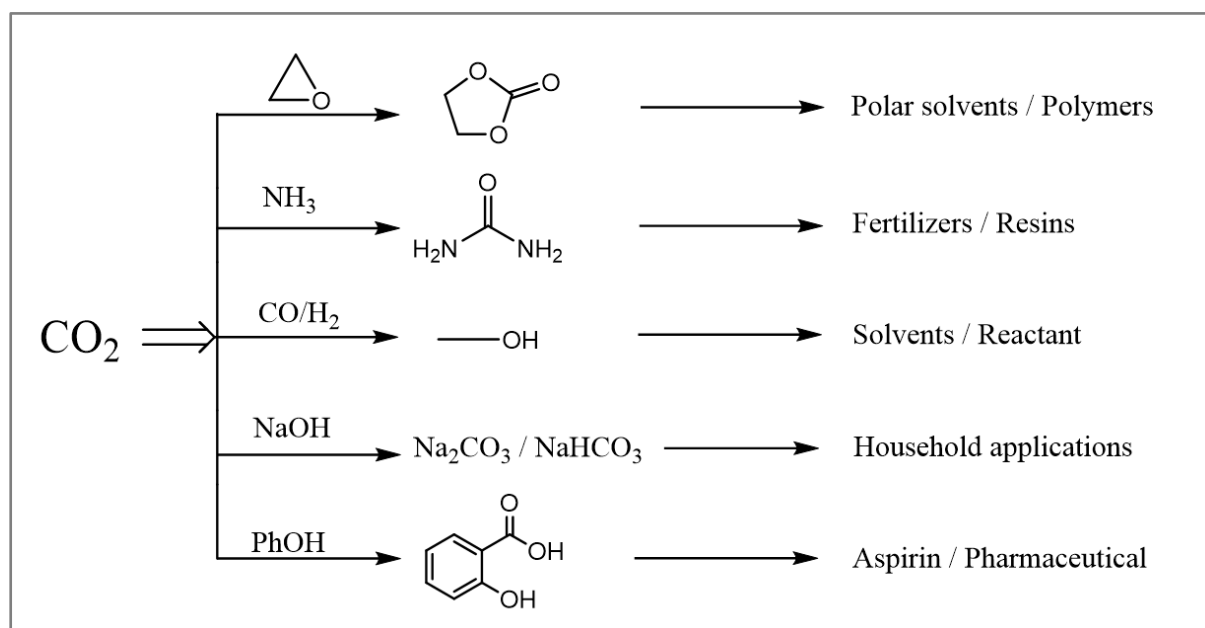


Figure 1.4: Industrial chemical processes using CO₂ as feedstock.

1.3 Need for CO₂ utilization

The need for CO₂ utilization arises from the urgent global challenges posed by climate change, resource scarcity, and the transition to a sustainable future. Reducing CO₂ emissions alone may not be sufficient to meet global climate targets. While transitioning to renewable energy sources and adopting cleaner technologies are crucial steps, it is equally important to actively remove CO₂ from the atmosphere. CO₂ utilization presents a viable pathway to accomplish this by repurposing emissions into useful and economically viable products.

Additionally, CO₂ utilization holds tremendous potential for economic growth and innovation. It presents opportunities to develop new industries and markets focused on converting CO₂ into valuable products such as chemicals, fuels, building materials, and even

food additives. By utilizing CO₂ as a raw material, reliance on fossil fuels can be reduced and it can promote the production of sustainable alternatives.

Furthermore, CO₂ utilization enables the transformation of a harmful waste stream from chemical industries into a valuable resource and chemicals. By recovering CO₂, a circular economy can be adopted minimizing waste generation and reducing dependence on finite sources. CO₂ utilization necessitates research and development in advanced technologies, catalysis, and chemical engineering. As CO₂ conversion techniques are being explored globally, technological advancements are enhancing leading to further scientific breakthroughs and innovations. This also creates economic opportunities and job prospects in energy sectors.

1.4 Challenges in CO₂ utilization

Although CO₂ is an abundant and freely available C₁ source, the utilization of CO₂ presents several challenges that need to be addressed for its effective implementation. Some key challenges include:

- Carbon capture, separation, and storage: The first step in CO₂ utilization is capturing and separating CO₂ from industrial emissions or the atmosphere. Since the concentration of CO₂ in the atmosphere is only 0.04 %, concentrating and purifying CO₂ for utilization purposes can be energy-intensive and expensive. Also, developing cost-effective, efficient, and scalable technologies for carbon capture and separation from a mixture of gases coming out of industrial emissions is crucial. Additionally, finding suitable storage sites for the captured CO₂ can be challenging as it requires geologically stable formations that can steadily store the gas without leakage.
- Energy requirements: Several processes involving CO₂ chemical conversion require significant energy input, particularly CO₂ reductions. Exploring low-energy or renewable energy pathways is essential to reduce the overall carbon footprint. Also, an efficient thermochemical catalyst is needed, which can reduce the energy required to convert carbon dioxide.
- Reactivity and conversion: Carbon dioxide is a thermodynamically stable molecule, making its conversion into valuable products challenging. Developing catalysts and chemical processes that efficiently convert CO₂ is an ongoing research area worldwide.

- Scale-up and commercialization: Many technologies involving CO₂ utilization are in the early stages of development, facing challenges in scaling up to commercial levels. While some pilot projects like the reduction of CO₂ to methanol, DME, cyclic carbonates, etc have shown promise, there is a need to demonstrate scalability and cost-effectiveness to make a significant impact on reducing CO₂ levels.
- Market size: The demand for CO₂-derived products plays an important role in the success of CO₂ utilization technologies. Creating viable markets and establishing supply chains for CO₂-based processes can be challenging, especially when competing with existing products that have well-established markets. Market policies and incentives can play a significant role in driving demand for such products
- Environmental impact: Comprehensive evaluation of CO₂ utilization processes need to be done to assess their environmental impact. Life cycle analysis considering the entire value chain from CO₂ capture to product utilization is necessary to ensure that the overall carbon footprint is reduced. Also, it is essential to assess potential negative impacts associated with the technologies. For example, the extraction of minerals required for CO₂ utilization processes can have environmental concerns if not managed appropriately.
- Policy and regulatory frameworks: There is a lack of socio-economical driving forces for enhanced CO₂ utilization and lower emissions. Regulatory bodies need to provide incentives, funding, and clear guidelines to encourage industries and people to manage CO₂ emissions and to encourage research and development of CO₂ utilization projects.

1.4.1 Thermodynamics of CO₂ conversion

CO₂ is a thermodynamically very stable molecule with standard Gibbs free energy at 298 K is – 394 kJ/mole and heat of formation at 298 K is -394 kJ/mole. The bond energy for C = O in CO₂ is 736 kJ/mol hence requires high energies to make it react. As CO₂ is highly stable and often kinetically inert, its activation is a permanent challenge for researchers to convert it into selective reactions under mild conditions. Thus, most of the reactions involving CO₂ conversions are exothermic.

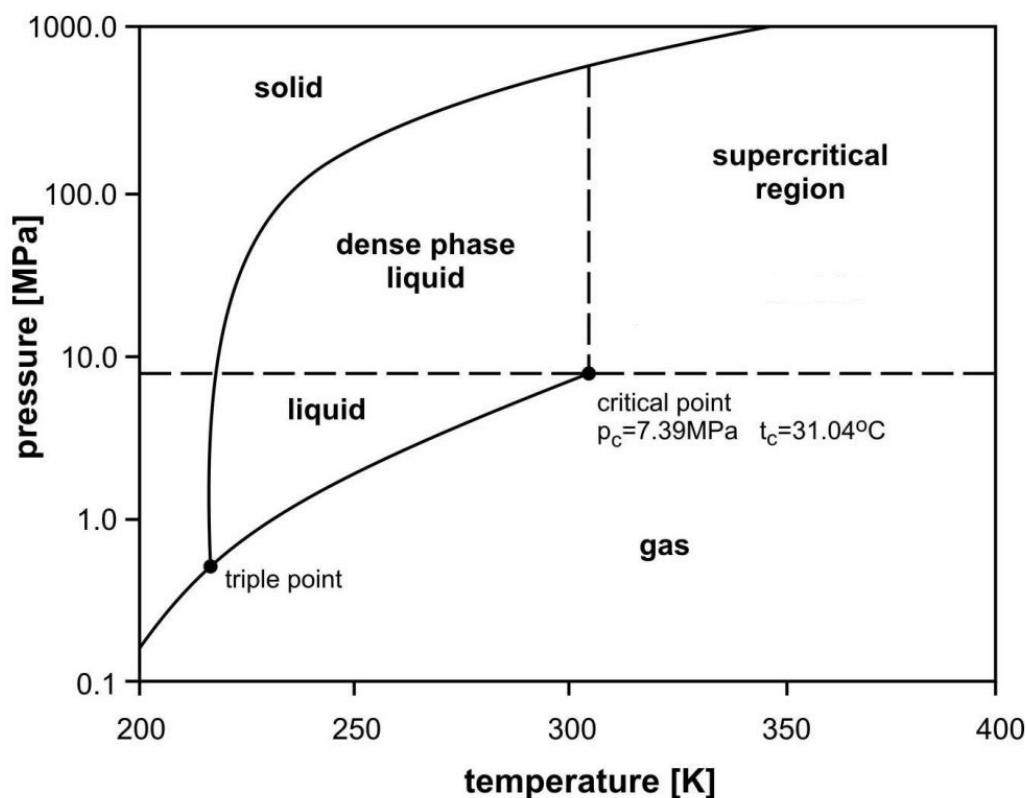


Figure 1.5: Carbon dioxide phase diagram.

Figure 1.5 shows the carbon dioxide phase diagram. The lowest pressure at which CO₂ is in liquid form is 5.1 bar and thus it sublimates at atmospheric pressure. The critical point is at 73.8 bar and 31 °C above which forms a supercritical fluid where the density of CO₂ is in the order of liquids while viscosity is in the order of gas. Compared to other solvents, the supercritical region of CO₂ occurs at relatively accessible conditions making it a perfect solvent as well as reactant due to higher diffusion rates in solid catalysts and higher mass transfer due to solubility. Also, liquid and supercritical CO₂ (scCO₂) has gained special attention as a green solvent for chemical reactions, extractions, and chromatography⁸⁻¹¹. The scCO₂ can have a range of polarity from that of pentane to pyridine by varying its density making it a versatile solvent for many chemical reactions¹².

1.4.2 Strategies for CO₂ conversion and utilization

The research on CO₂ utilization is going on which will help to achieve a sustainable future. There are several strategies which need to be considered for CO₂ conversion and utilization aimed at mitigating carbon emissions and finding productive applications. Some of the common strategies include:

- Carbon capture and storage (CCS): CCS involves capturing CO₂ emissions from industrial processes or power plants, compressing it, and storing it in underground geological formations¹³. This process prevents the release of CO₂ into the atmosphere, effectively reducing emissions.
- Carbon capture and utilization (CCU): CCU involves carbon capture and its conversion to valuable products. It can be converted to chemicals like methanol, urea, polymers etc.¹⁴ Several technologies are already developed by researchers for conversion of CO₂ to chemicals and extensive research is going on for its scalability. Also, CO₂ can react with certain minerals to form stable carbonates like calcium carbonate. CO₂ mineralization is still in its early stages of development and holds promise for long-term CO₂ storage.
- Direct air capture (DAC): This method involves capturing CO₂ directly from ambient air by technologies like absorption and cryogenic separation and storing it for further applications¹⁵. This approach is mostly used to remove CO₂ from the atmosphere.
- Biological conversion: Certain microorganisms can consume CO₂ and convert it into useful compounds¹⁶. For example, algae can be used to capture CO₂ and produce biofuel.
- Enhanced oil recovery (EOR): The majority of CO₂ is being currently used for oil recovery where it is injected into depleted oil reservoirs. This process helps in oil production as well as storing CO₂ underground¹⁷. Although, this is a commercial process, improving its efficiency is emerging research.
- Building Materials: CO₂ can be used as a feedstock for the production of building materials such as concrete, aggregates, or carbon fibre. This material can potentially sequester CO₂ for extended periods.

1.4.3 Recent research and development in catalytic CO₂ conversion

Numerous efforts are being made for the activation of CO₂ and its conversion to value-added chemicals using thermal catalysis, photocatalysis, and electrochemical methods and remarkable conclusions have been achieved by various researchers. CO₂ activation is the main research challenge for its conversion. Andrea et al. explained the various routes for its activation as shown in figure 1.6¹⁸. CO₂ conversion methods are categorised by its activation process like thermal activation, photo activation, plasma activation, and electro activation.

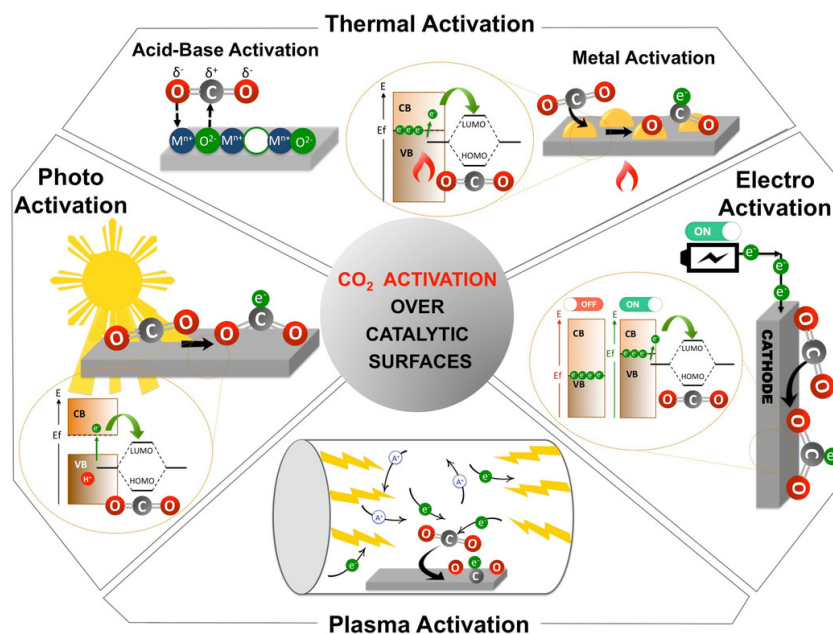


Figure 1.6: Catalytic CO₂ activation routes presented by Andrea et al¹⁸.

Thermal activation of CO₂ can be occurred by two methods – Metal activation and acid base activation. In metal activation, electron transfer takes place from metal surface to CO₂ molecule forming CO₂⁻ radical. The energy requirement for this process is higher due to large work functions of metal surfaces and thus higher temperatures promotes such type of reactions¹⁹. According to Liu, bonding of transition metals like Fe, Cu, Co, Ni with CO₂⁻ radical is stronger with lower energy barriers for CO₂ activation²⁰. Most of the metal catalysed reactions involving CO₂ are performed in the presence of hydrogen to form chemicals like CH₃OH, HCOOH, CH₄, CO. The main role of hydrogen in these reactions is the formation formate intermediate species²¹. The detailed literature on this topic is discussed in chapter 2.

Carbon dioxide is known as slightly acidic molecule and it is attracted by basic sites in solid catalytic surfaces. Generally acid-base solid catalysts are metal oxides like MgO, Al₂O₃, ZrO₂, CeO₂, etc. As shown in figure 1.6, metal oxide surface can act as Lewis base when the carbon atom of CO₂ interacts through O²⁻ sites and Lewis acid when CO₂ interacts with the surface through metal cation. CO₂ activation by acid-base sites occurred by forming intermediate species like carbonate (CO₃²⁻) and bicarbonate ions (HCO₃⁻)²².

The major advantage of acid-base solid catalysts is their fine tunability. The strength of acidic and basic sites can be tuned based on single or mixed metal oxides, compositions, structure of

catalyst, and various transition metals. The detailed study on such catalytic system is done in this thesis are represented in chapter 2.

Some of the important research areas for the thermochemical conversion of CO₂ are listed below.

1.4.3.1 Hydrogenation of CO₂

Hydrogenation of CO₂ can lead to several single-carbon products like methanol, methane, formic acid, and carbon monoxide while C₂₊ products like dimethyl ether, gasoline, higher alcohols, and liquid fuels^{23–25}. The selection of proper catalyst and reaction parameters are the main contributors to product choice^{26–28}. The hydrogenation of CO₂ to C₁ products is commercially viable while excess energy and additional active sites are required for C – C coupling.

CO₂ hydrogenation to methanol is mainly carried out on copper-based heterogeneous catalysts and its research has extended to plant-scale production^{26,29,30}. Meanwhile, formic acid production from CO₂ needs selective active sites, and researchers have proposed several catalysts worldwide^{31–34}. Although hydrogenation of CO₂ promises industrial valuable research, there is a significant need for the development of efficient catalysts with higher reaction efficiency to make the process industrially feasible. Table 1.1 shows the recent catalytic systems used for CO₂ hydrogenation processes.

Table 1.1 : Recent catalytic systems for CO₂ hydrogenation process.

Process	Product	Catalysts
	Methanol	Cu/ZnO/Al ₂ O ₃ ^{29,30} , Cu(core)-ZnO(shell) ³⁵ , Pd-Cu/SiO ₂ ³⁶ , Au/ZnO ³⁷ , Cu/Ga ₂ O ₃ /ZrO ₂ ³⁸ , Pd/ZnO/Al ₂ O ₃ ³⁹ .
CO ₂ hydrogenation	Formic acid	Ru/Mg-Al HT ³³ , Ru NP ⁴⁰ , Pd Ni/CNT ⁴¹ , Ir/Silica ⁴² , Au NP / Mg-Al HT ³² , Ir/Bpy-CTF ³¹ , Ru-DBU/Al ₂ O ₃ ⁴³ .
	Methane	Ni/ZrO ₂ ⁴⁴ , Ni/MgAl ₂ O ₄ ⁴⁵ , Ni/La ₂ O ₃ ⁴⁶ , Fe-Ni/Al ₂ O ₃ ⁴⁷ , Ni-Co/ZrO ₂ ⁴⁸ , Ru-Mn-Ni/Al ₂ O ₃ ⁴⁹ , Rh/Al ₂ O ₃ ⁵⁰ .

1.4.3.2 Mineral carbonation

The formation of stable carbonates like CaCO_3 and MgCO_3 from the carbonation of metal oxides has gained the interest of researchers due to their wide applications in pharmaceuticals, paints, explosives, and cosmetic industries.

There are mainly two routes for mineral carbonation. One is a direct method where gaseous CO_2 is directly reacted with minerals or alkaline solids. Due to very low reaction rates, this method is not been practised. While in the indirect method, aqueous carbonation is done for alkaline solids or Ca/Mg silicates are converted to hydroxide followed by dry carbonation.

1.4.3.3 Linear and cyclic carbonates

One of the actively investigated fields in recent years is the production of organic carbonates from CO_2 due to their applications in polycarbonates and polymers^{51,52}. Synthesis of these carbonates from CO_2 can replace conventional methods that use hazardous chemicals like carbon monoxide and phosgene⁵³. Synthesis of ethylene and propylene carbonate are already been accepted by industries and the research for other acyclic and cyclic carbonates promises economical and convenient processes.

Other research studies for the utilization of CO_2 like the formation of gas hydrates, fuels, polymers, and carbamates have limited applications due to their high energy demand and less market value. Although research in these areas is at the initial stages, it shows potential for better CO_2 conversions.

1.5 Motivation

The demand for energy is rising day by day, leading to excess CO_2 emissions and, eventually global warming. The primary sources of energy are still carbon-based fuels and there is a significant need to develop alternative renewable sources. Reducing CO_2 emissions alone may not be sufficient to meet global climate crises; there is a significant need to remove CO_2 from the atmosphere and convert it into viable and valuable products. Also, CO_2 utilization has huge potential for economic growth and innovation. The circular economy can be adopted by converting CO_2 , minimizing waste generation, and reducing reliance on finite sources.

In the proposed thesis, Processes for three industrially important molecules: dimethyl formamide (DMF), styrene carbonate (SC), and ortho-salicylic acid (OSA) have been developed. The current industrial synthesis of these compounds needs significant

improvement in terms of efficient and green catalysts, restricted use of toxic substrates, development of efficient process, single pot synthesis, and process intensification to maximize product viability in the market.

Considering these research gaps, the thesis work mainly focuses on sustainable and non-toxic catalyst synthesis, process development, and reaction kinetics for a scale-up protocol in the synthesis of dimethyl formamide by hydrogenation of CO₂. While process intensification was done using kinetic studies for the cycloaddition of CO₂ in styrene carbonate. The single pot synthesis of ortho-salicylic acid has been proposed using a heterogenous catalyst that is easy to recycle and reuse.

1.6 References

- (1) Energy Agency, I. World Energy Outlook 2021. **2021**.
- (2) Friedlingstein, P.; O'sullivan, M.; Jones, M. W.; Andrew, R. M.; Gregor, L.; Hauck, J.; Le Quéré, C.; Luijkx, I. T.; Olsen, A.; Peters, G. P.; Peters, W.; Pongratz, J.; Schwingshackl, C.; Sitch, S.; Canadell, J. G.; Ciais, P.; Jackson, R. B.; Alin, S. R.; Alkama, R.; Arneeth, A.; Arora, V. K.; Bates, N. R.; Becker, M.; Bellouin, N.; Bittig, H. C.; Bopp, L.; Chevallier, F.; Chini, L. P.; Cronin, M.; Evans, W.; Falk, S.; Feely, R. A.; Gasser, T.; Gehlen, M.; Gkritzalis, T.; Gloege, L.; Grassi, G.; Gruber, N.; Gürses, Ö.; Harris, I.; Hefner, M.; Houghton, R. A.; Hurtt, G. C.; Iida, Y.; Ilyina, T.; Jain, A. K.; Jersild, A.; Kadono, K.; Kato, E.; Kennedy, D.; Klein Goldewijk, K.; Knauer, J.; Korsbakken, J. I.; Landschützer, P.; Lefèvre, N.; Lindsay, K.; Liu, J.; Liu, Z.; Marland, G.; Mayot, N.; Mcgrath, M. J.; Metzl, N.; Monacci, N. M.; Munro, D. R.; Nakaoka, S. I.; Niwa, Y.; O'brien, K.; Ono, T.; Palmer, P. I.; Pan, N.; Pierrot, D.; Pockock, K.; Poulter, B.; Resplandy, L.; Robertson, E.; Rödenbeck, C.; Rodriguez, C.; Rosan, T. M.; Schwinger, J.; Séférian, R.; Shutler, J. D.; Skjelvan, I.; Steinhoff, T.; Sun, Q.; Sutton, A. J.; Sweeney, C.; Takao, S.; Tanhua, T.; Tans, P. P.; Tian, X.; Tian, H.; Tilbrook, B.; Tsujino, H.; Tubiello, F.; Van Der Werf, G. R.; Walker, A. P.; Wanninkhof, R.; Whitehead, C.; Willstrand Wranne, A.; Wright, R.; Yuan, W.; Yue, C.; Yue, X.; Zaehle, S.; Zeng, J.; Zheng, B. Global Carbon Budget 2022. *Earth Syst. Sci. Data* **2022**, *14* (11), 4811–4900. <https://doi.org/10.5194/ESSD-14-4811-2022>.
- (3) CO2 emissions by fuel - Our World in Data <https://ourworldindata.org/emissions-by-fuel#citation> (accessed Jun 21, 2023).
- (4) AR6 Climate Change 2022: Mitigation of Climate Change — IPCC <https://www.ipcc.ch/report/sixth-assessment-report-working-group-3/> (accessed Jan 6, 2023).
- (5) GlobalTemp_vs_carbon_dioxide_1850-2022.png | NOAA Climate.gov <https://www.climate.gov/media/13840> (accessed Jun 21, 2023).
- (6) Global Warming of 1.5 °C — <https://www.ipcc.ch/sr15/> (accessed Jun 21, 2023).
- (7) International Energy Agency. Putting CO₂ to Use. *Energy Rep.* **2019**, No. September, 86.
- (8) Jessop, P. G.; Hsiao, Y.; Ikariya, T.; Noyori, R. Homogeneous Catalysis in

- Supercritical Fluids: Hydrogenation of Supercritical Carbon Dioxide to Formic Acid, Alkyl Formates, and Formamides. *J. Am. Chem. Soc.* **1996**. <https://doi.org/10.1021/ja953097b>.
- (9) Rajendran, A. Design of Preparative-Supercritical Fluid Chromatography. *J. Chromatogr. A* **2012**, *1250*, 227–249. <https://doi.org/10.1016/J.CHROMA.2012.05.037>.
- (10) Sánchez-Vicente, Y.; Cabañas, A.; Renuncio, J. A. R.; Pando, C. Supercritical CO₂ as a Green Solvent for Eucalyptus and Citrus Essential Oils Processing: Role of Thermal Effects upon Mixing. *RSC Adv.* **2013**, *3* (17), 6065–6075. <https://doi.org/10.1039/C3RA23174G>.
- (11) Beckman, E. J. Supercritical and Near-Critical CO₂ in Green Chemical Synthesis and Processing. *J. Supercrit. Fluids* **2004**, *28*, 121–191. [https://doi.org/10.1016/S0896-8446\(03\)00029-9](https://doi.org/10.1016/S0896-8446(03)00029-9).
- (12) RAMSEY, E.; SUN, Q.; ZHANG, Z.; ZHANG, C.; GOU, W. Mini-Review: Green Sustainable Processes Using Supercritical Fluid Carbon Dioxide. *J. Environ. Sci.* **2009**, *21* (6), 720–726. [https://doi.org/10.1016/S1001-0742\(08\)62330-X](https://doi.org/10.1016/S1001-0742(08)62330-X).
- (13) Bui, M.; Adjiman, C. S.; Bardow, A.; Anthony, E. J.; Boston, A.; Brown, S.; Fennell, P. S.; Fuss, S.; Galindo, A.; Hackett, L. A.; Hallett, J. P.; Herzog, H. J.; Jackson, G.; Kemper, J.; Krevor, S.; Maitland, G. C.; Matuszewski, M.; Metcalfe, I. S.; Petit, C.; Puxty, G.; Reimer, J.; Reiner, D. M.; Rubin, E. S.; Scott, S. A.; Shah, N.; Smit, B.; Trusler, J. P. M.; Webley, P.; Wilcox, J.; Mac Dowell, N. Carbon Capture and Storage (CCS): The Way Forward. *Energy Environ. Sci.* **2018**, *11* (5), 1062–1176. <https://doi.org/10.1039/c7ee02342a>.
- (14) Ghiat, I.; Al-Ansari, T. A Review of Carbon Capture and Utilisation as a CO₂ Abatement Opportunity within the EWF Nexus. *J. CO₂ Util.* **2021**, *45*, 101432. <https://doi.org/10.1016/J.JCOU.2020.101432>.
- (15) Sanz-Pérez, E. S.; Murdock, C. R.; Didas, S. A.; Jones, C. W. Direct Capture of CO₂ from Ambient Air. *Chem. Rev.* **2016**, *116* (19), 11840–11876. <https://doi.org/10.1021/acs.chemrev.6b00173>.
- (16) Li, H.; Liao, J. C. Biological Conversion of Carbon Dioxide to Photosynthetic Fuels and Electrofuels. *Energy Environ. Sci.* **2013**, *6* (10), 2892–2899. <https://doi.org/10.1039/c3ee41847b>.
- (17) Al-Shargabi, M.; Davoodi, S.; Wood, D. A.; Rukavishnikov, V. S.; Minaev, K. M. Carbon Dioxide Applications for Enhanced Oil Recovery Assisted by Nanoparticles: Recent Developments. *ACS Omega* **2022**, *7* (12), 9984–9994. https://doi.org/10.1021/ACSOMEGA.1C07123/ASSET/IMAGES/LARGE/AO1C07123_0005.JPEG.
- (18) Álvarez, A.; Borges, M.; Corral-Pérez, J. J.; Olcina, J. G.; Hu, L.; Cornu, D.; Huang, R.; Stoian, D.; Urakawa, A. CO₂ Activation over Catalytic Surfaces. *ChemPhysChem* **2017**, *18* (22), 3135–3141. <https://doi.org/10.1002/cphc.201700782>.
- (19) Solymosi, F. The Bonding, Structure and Reactions of CO₂ Adsorbed on Clean and Promoted Metal Surfaces. *J. Mol. Catal.* **1991**, *65* (3), 337–358. [https://doi.org/10.1016/0304-5102\(91\)85070-I](https://doi.org/10.1016/0304-5102(91)85070-I).
- (20) Liu, C.; Cundari, T. R.; Wilson, A. K. CO₂ Reduction on Transition Metal (Fe, Co, Ni, and Cu) Surfaces: In Comparison with Homogeneous Catalysis. *J. Phys. Chem. C*

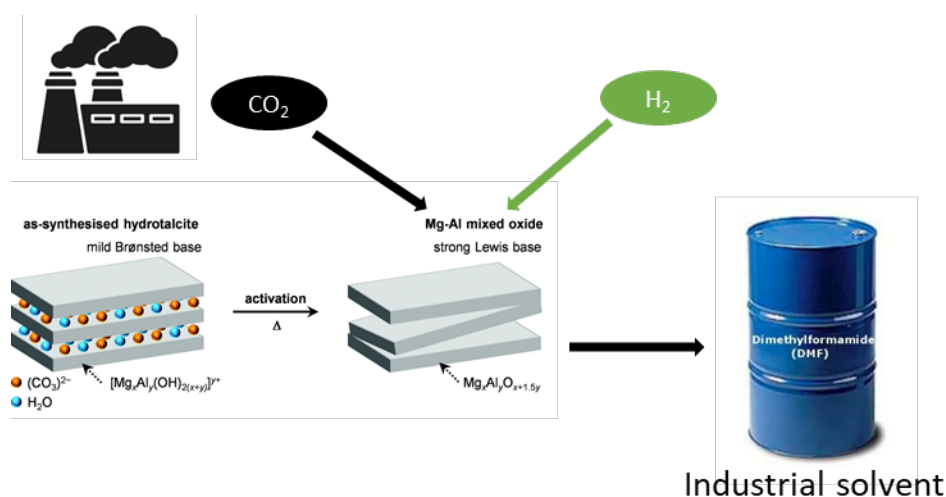
- 2012, *116* (9), 5681–5688. <https://doi.org/10.1021/jp210480c>.
- (21) Chen, C. S.; Cheng, W. H.; Lin, S. S. Mechanism of CO Formation in Reverse Water-Gas Shift Reaction over Cu/Al₂O₃ Catalyst. *Catal. Letters* **2000**, *68* (1–2), 45–48. <https://doi.org/10.1023/A:1019071117449/METRICS>.
- (22) Hahn, K. R.; Iannuzzi, M.; Seitsonen, A. P.; Hutter, J. Coverage Effect of the CO₂ Adsorption Mechanisms on CeO₂(111) by First Principles Analysis. *J. Phys. Chem. C* **2013**, *117* (4), 1701–1711. https://doi.org/10.1021/JP309565U/SUPPL_FILE/JP309565U_SI_001.PDF.
- (23) Gao, P.; Li, S.; Bu, X.; Dang, S.; Liu, Z.; Wang, H.; Zhong, L.; Qiu, M.; Yang, C.; Cai, J.; Wei, W.; Sun, Y. Direct Conversion of CO₂ into Liquid Fuels with High Selectivity over a Bifunctional Catalyst. *Nat. Chem.* **2017**, *9* (10), 1019–1024. <https://doi.org/10.1038/nchem.2794>.
- (24) Roy, S.; Cherevotan, A.; Peter, S. C. Thermochemical CO₂ Hydrogenation to Single Carbon Products: Scientific and Technological Challenges. *ACS Energy Lett.* **2018**, *3* (8), 1938–1966. <https://doi.org/10.1021/acsenergylett.8b00740>.
- (25) Kattel, S.; Liu, P.; Chen, J. G. Tuning Selectivity of CO₂ Hydrogenation Reactions at the Metal/Oxide Interface. *J. Am. Chem. Soc.* **2017**, *139* (29), 9739–9754. https://doi.org/10.1021/JACS.7B05362/ASSET/IMAGES/LARGE/JA-2017-05362S_0014.JPEG.
- (26) Álvarez, A.; Bansode, A.; Urakawa, A.; Bavykina, A. V.; Wezendonk, T. A.; Makkee, M.; Gascon, J.; Kapteijn, F. Challenges in the Greener Production of Formates/Formic Acid, Methanol, and DME by Heterogeneously Catalyzed CO₂ Hydrogenation Processes. *Chem. Rev.* **2017**, *117* (14), 9804–9838. https://doi.org/10.1021/ACS.CHEMREV.6B00816/ASSET/IMAGES/LARGE/CR-2016-00816H_0019.JPEG.
- (27) Wang, W.; Wang, S.; Ma, X.; Gong, J. Recent Advances in Catalytic Hydrogenation of Carbon Dioxide. *Chem. Soc. Rev.* **2011**. <https://doi.org/10.1039/c1cs15008a>.
- (28) Jia, J.; Qian, C.; Dong, Y.; Li, Y. F.; Wang, H.; Ghossoub, M.; Butler, K. T.; Walsh, A.; Ozin, G. A. Heterogeneous Catalytic Hydrogenation of CO₂ by Metal Oxides: Defect Engineering – Perfecting Imperfection. *Chem. Soc. Rev.* **2017**, *46* (15), 4631–4644. <https://doi.org/10.1039/C7CS00026J>.
- (29) Bansode, A.; Urakawa, A. Towards Full One-Pass Conversion of Carbon Dioxide to Methanol and Methanol-Derived Products. *J. Catal.* **2014**, *309*, 66–70. <https://doi.org/10.1016/J.JCAT.2013.09.005>.
- (30) Gaikwad, R.; Bansode, A.; Urakawa, A. High-Pressure Advantages in Stoichiometric Hydrogenation of Carbon Dioxide to Methanol. *J. Catal.* **2016**, *343*, 127–132. <https://doi.org/10.1016/J.JCAT.2016.02.005>.
- (31) Park, K.; Gunasekar, G. H.; Prakash, N.; Jung, K. D.; Yoon, S. A Highly Efficient Heterogenized Iridium Complex for the Catalytic Hydrogenation of Carbon Dioxide to Formate. *ChemSusChem* **2015**, *8* (20), 3410–3413. <https://doi.org/10.1002/CSSC.201500436>.
- (32) Filonenko, G. A.; Vrijburg, W. L.; Hensen, E. J. M.; Pidko, E. A. On the Activity of Supported Au Catalysts in the Liquid Phase Hydrogenation of CO₂ to Formates. *J. Catal.* **2016**, *343*, 97–105. <https://doi.org/10.1016/J.JCAT.2015.10.002>.

- (33) Chaudhary, S. D.; Rahatade, S. S.; Joshi, S. S.; Mali, N. A. Reduction of Carbon Dioxide to Dimethylformamide Using Ruthenium Doped Mg/Al Hydrotalcites under Supercritical Conditions. *J. CO₂ Util.* **2022**, *61* (May), 102055. <https://doi.org/10.1016/j.jcou.2022.102055>.
- (34) Filonenko, G. A.; Van Putten, R.; Schulpen, E. N.; Hensen, E. J. M.; Pidko, E. A. Highly Efficient Reversible Hydrogenation of Carbon Dioxide to Formates Using a Ruthenium PNP-Pincer Catalyst. *ChemCatChem* **2014**, *6* (6), 1526–1530. <https://doi.org/10.1002/CCTC.201402119>.
- (35) Le Valant, A.; Comminges, C.; Tisseraud, C.; Canaff, C.; Pinard, L.; Pouilloux, Y. The Cu–ZnO Synergy in Methanol Synthesis from CO₂, Part 1: Origin of Active Site Explained by Experimental Studies and a Sphere Contact Quantification Model on Cu + ZnO Mechanical Mixtures. *J. Catal.* **2015**, *324*, 41–49. <https://doi.org/10.1016/J.JCAT.2015.01.021>.
- (36) Jiang, X.; Koizumi, N.; Guo, X.; Song, C. Bimetallic Pd–Cu Catalysts for Selective CO₂ Hydrogenation to Methanol. *Appl. Catal. B Environ.* **2015**, *170–171*, 173–185. <https://doi.org/10.1016/J.APCATB.2015.01.010>.
- (37) Hartadi, Y.; Widmann, D.; Behm, R. J. Methanol Synthesis via CO₂ Hydrogenation over a Au/ZnO Catalyst: An Isotope Labelling Study on the Role of CO in the Reaction Process. *Phys. Chem. Chem. Phys.* **2016**, *18* (16), 10781–10791. <https://doi.org/10.1039/C5CP06888F>.
- (38) Fornero, E. L.; Sanguineti, P. B.; Chiavassa, D. L.; Bonivardi, A. L.; Baltanás, M. A. Performance of Ternary Cu–Ga₂O₃–ZrO₂ Catalysts in the Synthesis of Methanol Using CO₂-Rich Gas Mixtures. *Catal. Today* **2013**, *213*, 163–170. <https://doi.org/10.1016/J.CATTOD.2013.03.012>.
- (39) Xu, J.; Su, X.; Liu, X.; Pan, X.; Pei, G.; Huang, Y.; Wang, X.; Zhang, T.; Geng, H. Methanol Synthesis from CO₂ and H₂ over Pd/ZnO/Al₂O₃: Catalyst Structure Dependence of Methanol Selectivity. *Appl. Catal. A Gen.* **2016**, *514*, 51–59. <https://doi.org/10.1016/J.APCATA.2016.01.006>.
- (40) Umegaki, T.; Enomoto, Y.; Kojima, Y. Metallic Ruthenium Nanoparticles for Hydrogenation of Supercritical Carbon Dioxide. *Catal. Sci. Technol.* **2016**, *6* (2), 409–412. <https://doi.org/10.1039/C5CY00994D>.
- (41) Nguyen, L. T. M.; Park, H.; Banu, M.; Kim, J. Y.; Youn, D. H.; Magesh, G.; Kim, W. Y.; Lee, J. S. Catalytic CO₂ Hydrogenation to Formic Acid over Carbon Nanotube-Graphene Supported PdNi Alloy Catalysts. *RSC Adv.* **2015**, *5* (128), 105560–105566. <https://doi.org/10.1039/C5RA21017H>.
- (42) Xu, Z.; Mcnamara, N. D.; Neumann, G. T.; Schneider, W. F.; Hicks, J. C. Catalytic Hydrogenation of CO₂ to Formic Acid with Silica-Tethered Iridium Catalysts. *ChemCatChem* **2013**, *5* (7), 1769–1771. <https://doi.org/10.1002/CCTC.201200839>.
- (43) Yang, H.; Zhang, C.; Gao, P.; Wang, H.; Li, X.; Zhong, L.; Wei, W.; Sun, Y. A Review of the Catalytic Hydrogenation of Carbon Dioxide into Value-Added Hydrocarbons. *Catalysis Science and Technology*. Royal Society of Chemistry October 16, 2017, pp 4580–4598. <https://doi.org/10.1039/c7cy01403a>.
- (44) Yang Lim, J.; McGregor, J.; Sederman, A. J.; Dennis, J. S. Kinetic Studies of CO₂ Methanation over a Ni/γ-Al₂O₃ Catalyst Using a Batch Reactor. *Chem. Eng. Sci.* **2016**, *141*, 28–45. <https://doi.org/10.1016/J.CES.2015.10.026>.

- (45) Fan, Z.; Sun, K.; Rui, N.; Zhao, B.; Liu, C. J. Improved Activity of Ni/MgAl₂O₄ for CO₂ Methanation by the Plasma Decomposition. *J. Energy Chem.* **2015**, *24* (5), 655–659. <https://doi.org/10.1016/J.JECHEM.2015.09.004>.
- (46) SONG, H.; YANG, J.; ZHAO, J.; CHOU, L. Methanation of Carbon Dioxide over a Highly Dispersed Ni/La₂O₃ Catalyst. *Chinese J. Catal.* **2010**, *31* (1), 21–23. [https://doi.org/10.1016/S1872-2067\(09\)60036-X](https://doi.org/10.1016/S1872-2067(09)60036-X).
- (47) Pandey, D.; Deo, G. Effect of Support on the Catalytic Activity of Supported Ni–Fe Catalysts for the CO₂ Methanation Reaction. *J. Ind. Eng. Chem.* **2016**, *33*, 99–107. <https://doi.org/10.1016/J.JIEC.2015.09.019>.
- (48) Ren, J.; Qin, X.; Yang, J. Z.; Qin, Z. F.; Guo, H. L.; Lin, J. Y.; Li, Z. Methanation of Carbon Dioxide over Ni–M/ZrO₂ (M = Fe, Co, Cu) Catalysts: Effect of Addition of a Second Metal. *Fuel Process. Technol.* **2015**, *137*, 204–211. <https://doi.org/10.1016/J.FUPROC.2015.04.022>.
- (49) Wan Abu Bakar, W. A.; Ali, R.; Mohammad, N. S. The Effect of Noble Metals on Catalytic Methanation Reaction over Supported Mn/Ni Oxide Based Catalysts. *Arab. J. Chem.* **2015**, *8* (5), 632–643. <https://doi.org/10.1016/J.ARABJC.2013.06.009>.
- (50) Beuls, A.; Swalus, C.; Jacquemin, M.; Heyen, G.; Karelavic, A.; Ruiz, P. Methanation of CO₂: Further Insight into the Mechanism over Rh/γ-Al₂O₃ Catalyst. *Appl. Catal. B Environ.* **2012**, *113–114*, 2–10. <https://doi.org/10.1016/J.APCATB.2011.02.033>.
- (51) Sun, J.; Fujita, S. I.; Zhao, F.; Hasegawa, M.; Arai, M. A Direct Synthesis of Styrene Carbonate from Styrene with the Au/SiO₂-ZnBr₂/Bu₄NBr Catalyst System. *J. Catal.* **2005**, *230* (2), 398–405. <https://doi.org/10.1016/j.jcat.2004.12.015>.
- (52) Fu, X.; Jing, H. Quaternary Onium Modified SalenCoXY Catalysts for Alternating Copolymerization of CO₂ and Propylene Oxide: A Kinetic Study. *J. Catal.* **2015**, *329*, 317–324. <https://doi.org/10.1016/J.JCAT.2015.05.030>.
- (53) Fukuoka, S.; Kawamura, M.; Komiya, K.; Tojo, M.; Hachiya, H.; Hasegawa, K.; Aminaka, M.; Okamoto, H.; Fukawa, I.; Konno, S. A Novel Non-Phosgene Polycarbonate Production Process Using by-Product CO₂ as Starting Material. *Green Chem.* **2003**, *5* (5), 497–507. <https://doi.org/10.1039/B304963A>.

Chapter 2

Hydrogenation of carbon dioxide to dimethyl formamide



“This chapter reports heterogeneous calcined hydrotalcites as a catalyst presenting excellent activity towards hydrogenation of carbon dioxide with detailed process development and reaction kinetics”

Chapter 2

Hydrogenation of carbon dioxide to dimethyl formamide

Abstract

Increasing demand for fossil fuels and consequently increasing carbon dioxide (CO₂) concentrations in the atmosphere has become a global concern for environmentalists and researchers. CO₂ is one of the main contributors to global warming and its chemical conversion to industrial chemicals is an attractive route to lower its impact. Due to thermodynamic challenges and high industrial demand, its conversion to formic acid is been studied worldwide for a few decades and remarkable progress has been made in terms of homogeneous catalytic systems and process parameter optimization. The main gap in research so far is to replace phosphine-based metal-organic homogenous catalysts which makes the process non-feasible concerning economics and safety. In this work, a process involving in-situ derivatization of formic acid to dimethyl formamide (DMF) to increase the reaction yields is developed using ruthenium-doped Mg/Al calcined hydrotalcite in the presence of dimethyl amine (DMA).

The current work focuses on synthesising a non-toxic, cheap, and recyclable solid catalyst for CO₂ hydrogenation to formic acid and process development for batch and continuous synthesis. At the optimum conditions, complete conversion of DMA is achieved with more than 92 mole % selectivity of product at 170 °C and 13 MPa pressure within 6 hours of reaction time. Key catalyst properties were determined using X-ray powder diffraction (XRD), X-ray photoelectron spectroscopy (XPS), CO₂-temperature programmed desorption (TPD), H₂ temperature-programmed reduction (TPR), and Fourier transform infrared (FTIR). The surface morphology was determined using a field emission scanning electron microscope (FE-SEM) and high-resolution transmission electron microscopy (HR-TEM). At the same time, the chemical composition was verified by energy-dispersive X-ray (EDS). In addition, kinetic modelling is performed using the two-site Langmuir-Hinshelwood-Hougen-Watson (LHHW) model. The regressed kinetic parameters gave an appropriate fit with experimental concentration values, and activation energy is calculated as 413 kJ mol⁻¹.

2.1 Introduction

Utilizing a large amount of captured carbon dioxide has been a massive challenge for industries realizing its activation and other viable, economical, and available synthesis routes. Considering the historical process of producing fossils by natural carbon-hydrogenation during the photosynthesis process, the hydrogenation of CO₂ is probably the best modern approach to regenerate exhausted hydrocarbons. The thermal stability of CO₂ indicated by high bond energy of 806 kJ/mole and the required high cost of renewable energy restricts the large-scale CO₂ hydrogenation processes. Tackett et al. also stated that the net reduction in CO₂ would be achieved if a process emits less than 0.2 kg of CO₂ / kWh of electricity¹.

CO₂ reduction to chemicals is generally carried out by three routes- thermocatalytic, electrochemical and photocatalytic. As the activation and subsequent conversion of CO₂ are energy-demanding, its reduction using hydrogen produced by renewable energy and thermal catalysis is a promising research direction due to flexibility in catalyst combinations and its greater reaction dynamics². At the same time, photocatalysis and electrocatalysis have low energy efficiency³⁻⁵.

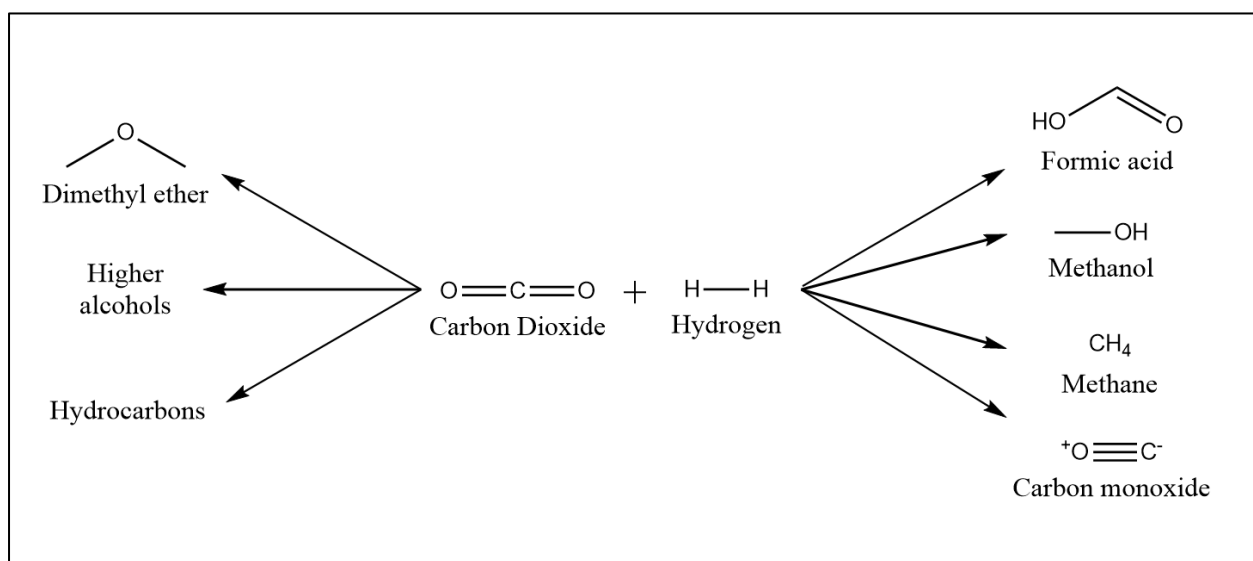


Figure 2.1: CO₂ hydrogenation products

Hydrogenation of carbon dioxide can lead to several hydrocarbon products, as shown in figure 2.1. The selection of proper catalyst and reaction parameters are the main contributors to product choice⁶⁻⁹.

2.2 Current industrial status of CO₂ hydrogenation

Even though CO₂ hydrogenation to speciality fine chemicals and fuels studies are currently limited to lab scale, only methanol is scaled up to industrial level. Carbon Recycling International (CRI), Iceland developed the process to produce renewable methanol (Green methanol) and recycled carbon to methanol using hydrogen produced from water electrolysis executed using renewable sources and hydrogen from waste gases combined with CO₂. The production started in Anyang, China and the process is based on Emissions to Liquids (ETL) technology and can capture 160,000 tonnes of carbon dioxide every year, producing 110,000 tonnes of methanol. CRI's second project in China is also announced and is expected to start by the end of 2023. Although some industries start commercial synthesis of methanols, global acceptance will be achieved if technology with mild reaction conditions is developed.

Various researchers are exploring the methods for the volarization of CO₂ to chemicals and making it industrially feasible.

2.3 Hydrogenation of carbon dioxide to C₁ feedstock chemicals

Carbon dioxide is the cheapest C₁ source of carbon, and its hydrogenation to single carbon products like methanol, methane, carbon monoxide and formic acid are commercially viable with selective catalyst and reaction conditions. While, the hydrogenation of CO₂ to C₂₊ products like liquid fuels, light olefins, dimethyl ether, gasoline and higher alcohols occurs via the Fischer-Tropsch mechanism or methanol-mediated route needs excess energy and additional active sites in a catalyst for C – C coupling¹⁰⁻¹³.

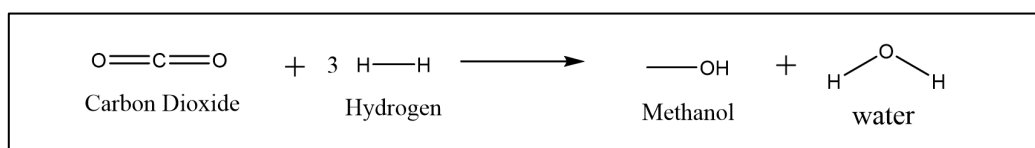
2.3.1 CO₂ to Methanol

The catalytic hydrogenation of CO₂ into methanol exhibits strong potential due to commonly reported high reaction rates. Historically, methanol also called wood alcohol was produced as a byproduct in the charcoal synthesis from wood and was used for lighting, cooling and heating purposes¹⁴.

Methanol is a primary raw material for the chemical industry, used in the MTO (methanol to olefins) process, as an intermediate for the production of chemicals like formaldehyde, methyl ter-butyl ether, and acetic acid¹⁴. Most of these chemicals are building blocks for many commodity products in our daily life including paints, plastics, resins, adhesives, and

antifreezants. Additionally, methanol can be directly used in fuel cells, and is also proven to be a good fuel blend for internal combustion engines. The derivative of methanol, dimethyl ether (DME) with a high cetane number of 55 offers attractive properties over standard diesel fuel with a cetane number of 40 – 55¹⁵.

In the early nineteenth century, BASF developed processes for organic oxygenates and methanol from syngas and commercialized methanol production process from syngas using sulphur-resistant zinc chromite (ZnO-Cr₂O₃) catalyst at 320 °C and 250 – 350 bar pressure.

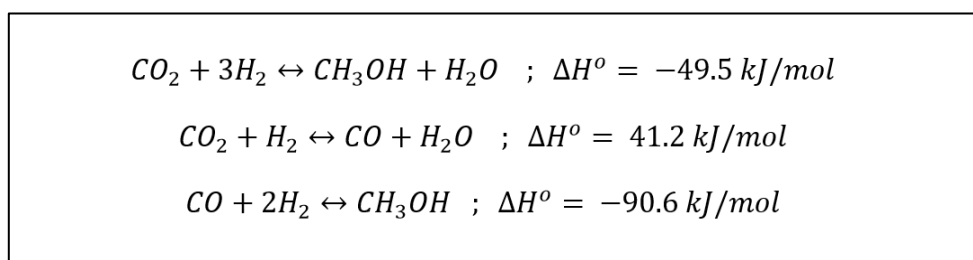


Scheme 2.1: Hydrogenation of CO₂ to methanol

Later in the 1960s, Imperial Chemical Industries (ICI) developed copper-based zinc oxide supported on alumina catalyst with higher selectivity of methanol for CO₂ hydrogenation. Although many catalysts with different compositions have been found active for the selective synthesis of methanol by CO₂ hydrogenation, the Cu-ZnO system remains most investigated due to its high activity and methanol selectivity¹⁶⁻²³. Typically, copper-based catalysts used for methanol synthesis commercially are prepared by co-precipitation method and contain about 50 – 70 mole % of copper, 20 – 50 % of zinc and 5 – 20 % of aluminium. These catalysts are generally calcined and reduced under a hydrogen atmosphere to obtain specific copper (0) sites. It is proposed that Cu⁰ metal is the main catalytic site for the reactivity in CO₂ activation while Arena et al. stated that ZnO acts as a reservoir for hydrogen and eventually speeds up the hydrogenation of intermediates²⁴. Kunkes et al. did the DFT calculations and concluded that intermediates in CO₂ hydrogenation are bound through an oxygen atom to the catalyst surface and the addition of Zn acts as a promoter while CO hydrogenation is activated through carbon atoms and Zn blocks these sites and hindered hydrogenations²⁵.

Various reports indicated the reaction mechanism for methanol synthesis via formate route via transformation to dioxymethylene (CH₂O₂*), formaldehyde (CH₂O*), and then to methoxy (CH₃O*), however only formate and methoxy species were observable as intermediates²⁶. Chen et al. explored the possibilities of the RWGS reaction route for the

methanol synthesis as direct hydrogenation and RWGS are two major competing reactions as shown in Scheme 2.2²⁷.

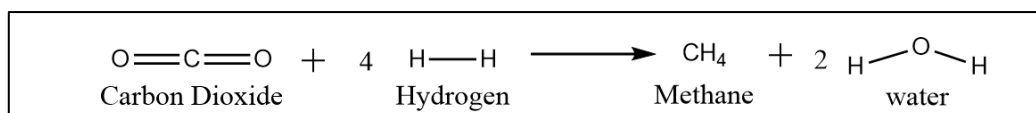


Scheme 2.2: Methanol synthesis by direct CO₂ hydrogenation and via RWGS reaction

By Le Chatelier's principle, it can be stated that the use of high pressures and low temperatures should be advantageous due to the exothermic nature of direct hydrogenation of CO₂ towards methanol formation and has been proved by several authors^{17,28}.

2.3.2 CO₂ to Methane

French chemist Paul Sabatier reported CO₂ methanation for the first time in 1902. Due to the increasing demand for mitigating global warming and storing surplus renewable power, this ancient art has attracted renewed attention. The Sabatier reaction is an advantageous way to store renewable energy such as wind and solar power, to transfer biogas effectively to biomethane, and to convert CO₂ to chemical feedstock and fuels^{29,30}.



Scheme 2.3: Hydrogenation of CO₂ to methane

CO₂ methanation can be catalyzed by various transition metal-based catalysts like Co, Ni, Ru, Rh, and Pd. Out of which, Ruthenium and rhodium showed greater activity for hydrogenation³¹⁻³⁵. Nickel-based catalysts are preferred for industrial purposes due to their ease of availability and higher CH₄ selectivity. The insertion of second metal on the surface of a monometallic catalyst changes the electronic and geometric structures of the catalyst and with this concept, Beuls et al. proposed the complete selective hydrogenation of CO₂ towards methane at 150 °C and 2 bar pressure using rhodium doping on gamma alumina surface. In most cases, loading more than one metal makes a significant synergic effect on CO₂ methanation. Rh and Ni catalysts give low selectivity when used separately while when used

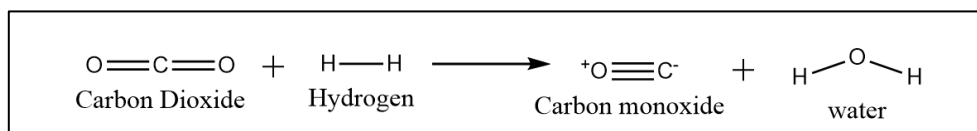
together, activity is increased due to the supportive properties of each metal site. Rhodium is used as a storage source of CO₂ adsorption and also helps in dissociation, while nickel sites help in hydrogen adsorption and activation via spillover mechanism³⁶.

CO₂ methanation is an exothermic reaction with high equilibrium conversion between 25 – 400 °C and studied by various authors^{37,38}, Whereas it can proceed via either the CO route or formate route which is explained by various activity of metals and their supports.

Although CO₂ methanation can be an alternative way of utilizing CO₂, the geothermal availability of methane makes it non-feasible for commercialization until the new technology develops with better activity at milder reaction conditions.

2.3.3 CO₂ to CO

Hydrogenation of CO₂ to carbon monoxide (CO) is a well-known reverse water gas shift (RWGS) reaction with positive enthalpy of 41 kJ/mol. Due to the endothermic nature of the reaction, higher reaction temperatures favour the conversion of CO₂ according to Le Chatelier's principle. Also, the CO₂ conversions are maximized by increasing the H₂/CO₂ ratio by various authors³⁹⁻⁴¹. It's been noticed that, lower temperature favour the CO₂ methanation and equilibrium reaches for RWGS⁴¹.



Scheme 2.4: Hydrogenation of CO₂ to carbon monoxide

RWGS reaction plays a crucial role in chemical industries due to its usage in methanol synthesis and Fischer – Tropsch (FT) process to synthesize a variety of hydrocarbons. CO₂ hydrogenation can proceed via two routes – redox mechanism and association mechanism. In redox mechanism, CO₂ is directly reduced to CO on catalyst surface while hydrogen reduced catalyst again to regain its activity⁴². Iron based catalyst are the most explored in this regard due to its high temperature stability and oxygen mobility^{43,44}.

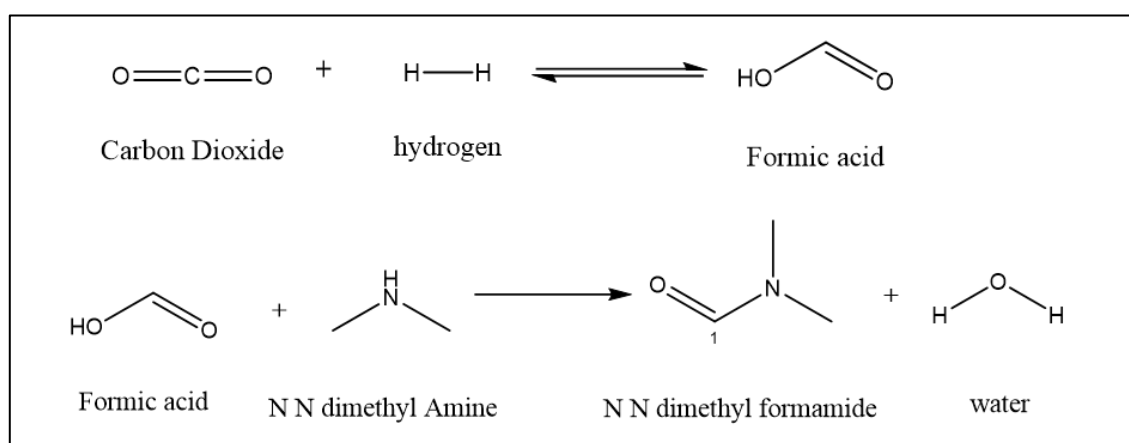
In association mechanism, intermediate species like formate, carbonate, carboxyl, and bicarbonate forms with dissociated hydrogen and adsorbed CO₂ on the catalyst surface which further decomposed to CO and water. Whereas the intermediate varies with catalyst composition and activity⁴⁵⁻⁴⁷. Although the RWGS reaction can proceed via different

mechanism, the key properties in the catalyst requires adsorption of CO₂, dissociation of hydrogen, disruption of one carbon oxygen bond, and formation of water by dissociated hydrogen.

Even though the RWGS reaction is commercially practiced, direct hydrogenation of CO₂ to value added chemicals has increasing demand considering the integrated processes and minimizing the risk associated with toxicity of carbon monoxide.

2.3.4 CO₂ to formic acid and its derivatives

CO₂ hydrogenation to formic acid (FA) has gained special attention from researchers due to its non-favourable thermodynamics⁴⁸ and its emerging role as a green energy carrier⁴⁹. It is a highly reversible endergonic reaction with Gibbs free energy of 32.9 kJ/mole, and formic acid exhibits significant potential as a liquid hydrogen carrier with a hydrogen capacity of 53 g/L⁵⁰. In addition, formic acid is considered a crucial intermediate for synthesizing valuable oxygen-containing compounds like alcohols, esters and acids⁵¹. Though various homogenous catalysts comprising molecular metal complexes and ligands are reported for hydrogenation of CO₂ to formic acid with exceptional activities⁵²⁻⁵⁸, research concerning heterogeneous catalyst systems and non-toxic compounds needs more attention. Also, to break the reaction equilibrium according to Le Chatelier's principle, the derivatization of formic acid in situ has become an important step.



Scheme 2.5: CO₂ hydrogenation to formic acid and DMF

Formic acid can be derivatized to N,N dimethyl formamide (DMF) using dimethyl amine as a reactant substrate as shown in scheme 2.5. DMF is used primarily as a solvent in chemical processes and is being industrially produced at 70 – 100 °C and 2 – 10 MPa by carbonylation

of N,N dimethyl amine (DMA)⁵⁹. Many authors explored the production of DMF by CO₂ hydrogenation and DMA using different transition metal-based homogenous catalysts with high turnover numbers (TON) and frequencies (TOF)^{53,60-64}. Although few heterogeneous catalytic systems without halides and phosphine have been reported in recent years^{8,65}, efficient, non-toxic, cheap and green catalysts are needed for commercial applications. Most of the available reports suggest the use of noble metals in the heterogeneous catalyst, which are well known for hydrogenation reactions^{9,64-66}. In this work, ruthenium-doped hydrotalcite as a phosphine-free heterogeneous catalytic system is proposed for the direct hydrogenation of carbon dioxide to dimethyl formamide using dimethyl amine under supercritical conditions of carbon dioxide.

2.4 Prior art

2.4.1 Catalysis and mechanistic approach

Catalyst plays crucial role in CO₂ hydrogenation to formic acid to overcome the high kinetic barrier and research has resulted in remarkable success for catalyst development to both homogenous and heterogeneous catalyst⁶⁷⁻⁶⁹. Various metal complexes with metal centres and ligands have demonstrated exceptional activities for homogeneous CO₂ reduction to formic acid. Filonenko et al.⁷⁰ presented Ru-PNP pincer complex with activity up to 1100000 h⁻¹ TOF while Nozaki et al.⁷¹ reported similar Ir-PNP complex with TON as high as 3500000 where pyridine part of the Ir-PNP complex was proposed to enhance H₂ activation and proton transfer over Ir centres.

In spite of excellent activity of molecular complexes, its application became impractical due to difficult separation and recycling of metal complexes, and air sensitive ligands. Thus, easy handling, recyclable heterogeneous catalyst system gained importance to researchers and series of supported metal based catalyst have been reported in last two decades^{68,72,73} although it usually show lower catalytic activity due to poor atom utilization efficiency. The table 2.1 shows the various reported homogenous and heterogeneous catalyst with their activities towards CO₂ hydrogenation to formic acid and DMF.

Table 2.1: Summary of catalytic system reported for CO₂ hydrogenation to formic acid

Catalyst	Solvent	Additives	p, atm	T, °C	T, h	TON / %X _{CO2}	TOF / %Y _{FA}	Reference
RhCl(TPPTS) ₃	Water	DMA	40	23	--	--	1364	Leitner et al. ⁷⁴
RuCl ₂ (PMe ₃) ₄	scCO ₂	TEA	220	50	47	7200	153	Jessop et al. ⁶⁶
RuCl ₃ + PPh ₃	Ethanol	TEA, water	120	60	5	200	40	Zhang et al. ⁷⁵
RuCl(OAc)(PMe ₃) ₄	scCO ₂	TEA	190	50	0.3	31667	95000	Munshi et al. ⁷⁶
PdCl ₂	water	KOH	110	160	3	1580	530	Kudo et al. ⁷⁷
PdCl ₂ (PPh ₃) ₂	Benzene	TEA, water	100	30	--	15	--	Sakamoto et al. ⁷⁸
RuCl ₂ (PTA) ₄	--	--	120	80	--	--	807	Laurencyzy et al. ⁷⁹
[RuCl ₂ (CO) ₂] _n	water	TEA	110	80	0.3	400	1300	Xia et al. ⁵⁴
Ni(dppe) ₂	Benzene	TEA, water	50	30	20	7	0.4	Inoue et al. ⁸⁰
NiCl ₂ (dcppe)	DMSO	DBU	200	50	22	4400	200	Tai et al. ⁵⁶
Ru-DBU/Al ₂ O ₃	Ethanol	TEA	80	120	1	197	197	Zhang et al. ⁸¹
Ru-PPh ₃ /Al ₂ O ₃	Ethanol	TEA	80	120	1	751	751	Zhang et al. ⁸²
Au NP / Mg-Al HT	Ethanol	TEA	70	40	20	91	4.6	Filonenko et al. ⁸³
PdNi / CNT	Water	--	50	40	15	6.4	--	Nguyen et al. ⁵⁷
Aeroxide P 90 TiO ₂	Water	--	1	90	6	--	98.98 % yield	Kamble et al. ⁸⁴
Ru NP	Water	TEA	80	20	3	6351	2117	Umegaki et al. ⁸⁵
Ir/Silica	Water	TEA	120	40	2	2300	1150	Xu et al. ⁸⁶
Ir/Bpy-CTF	Water	TEA	120	80	2	5000	2500	Park et al. ⁸⁷

Reaction pathway for the formation of formic acid over metal complexes were explained by various researchers. Leitner et al.⁷⁴ explained the reaction mechanism on $\text{RhCl}(\text{TPPTS})_3$ catalyst using ^1H and ^{31}P NMR spectroscopic measurements as shown in figure 2.2.

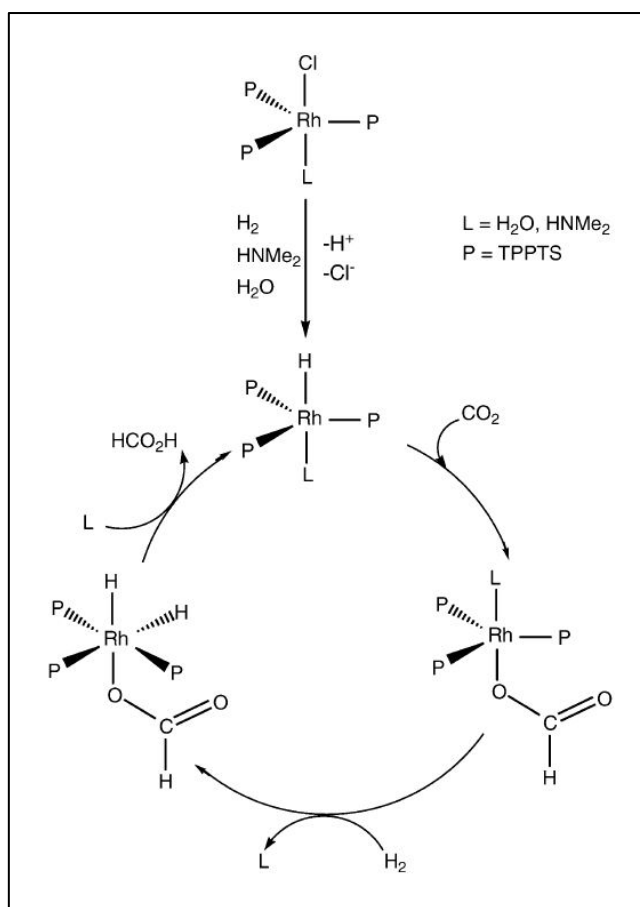


Figure 2.2: Suggested mechanism for formic acid on $\text{RhCl}(\text{TPPTS})_3$ by Leitner et al.

Leitner explained that in the absence of dimethylamine, $\text{RhCl}(\text{TPPTS})_3$ was shown to react with H_2 yielding the expected $\text{RhH}_2\text{Cl}(\text{TPPTS})_3$ and the cationic $[\text{RhH}_2(\text{TPPTS})_3]\text{Cl}$ dihydrides. While, the key intermediate in this mechanism is the monohydridorhodium complex, $\text{RhH}(\text{TPPTS})_3\text{L}$ (L = H_2O or HNMe_2) which forms only in the presence of HNMe_2 . Therefore, HNMe_2 is not only a sink for formic acid but also plays an active role in the formation of the catalytically active rhodium species. At the time of the investigations, no direct NMR evidence could be obtained for $\text{RhH}(\text{TPPTS})_3\text{L}$. Later, the analogous monohydrido complex $\text{RhH}(\text{TPPMS})_3(\text{H}_2\text{O})$, formed in strongly basic aqueous solutions, was explicitly characterized by Joo et al.⁸⁸

In case of heterogenized molecular catalyst, reaction mechanisms are similar to their homogeneous counterparts whereas, support plays important role towards affinity of reactants, reaction products, and solvent. Filonenko et al.⁸³ proposed gold nanoparticles

supported on alumina for the formation of formic acid with formates and bicarbonates are the key intermediates in the catalytic process. In the proposed mechanism as shown in figure 2.3, dissociation of hydrogen occurs on Au/support interface producing surface hydroxyl and metal hydride species.

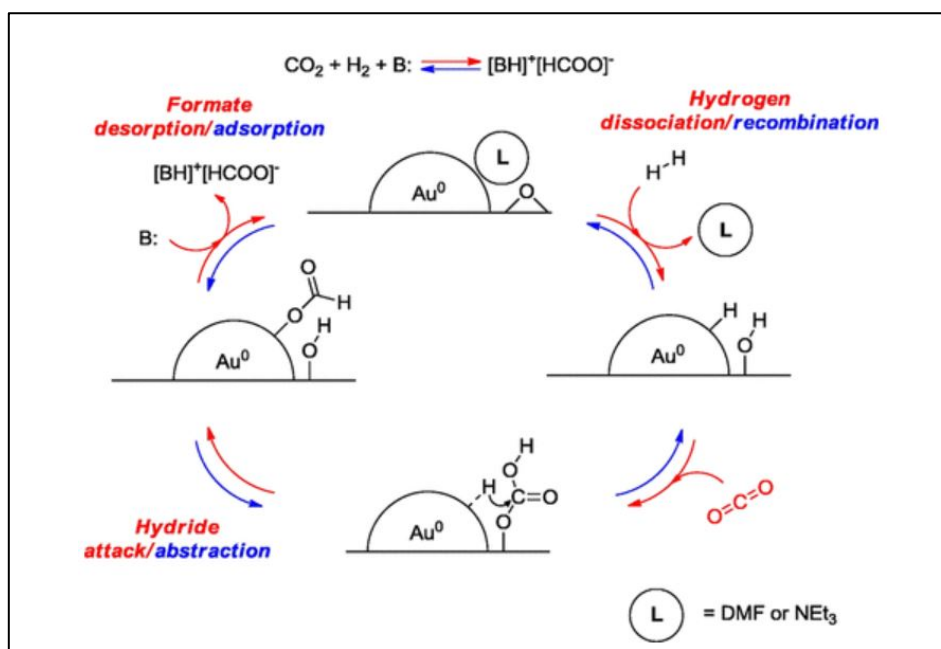


Figure 2.3: Suggested mechanism for formic acid on Au/Al₂O₃ by Filonenko et al.

Since the reaction was performed in DMF as a solvent, which adsorbed on the catalyst surface, hydrogen dissociation is followed by DMF desorption. This is followed by CO₂ reaction with surface hydroxyl groups forming bicarbonate species on the catalytic surface. The hydride ion from Au surface reacts with bicarbonate species to form formate ion on Au-support interface.

It was observed that, the main steps in reaction mechanism are – CO₂ activation and hydrogen dissociation. For the activation of CO₂, surface oxides which are basic in nature are found to be more active while noble metals are proven for hydrogenation reactions. Considering these factors, Ruthenium doped hydrotalcites is proposed as catalyst in this work.

2.4.2 Hydrotalcites as a catalyst

Hydrotalcites are a basic anionic layered clay material. These are the types of lamellar ionic compounds used as adsorbents, ion-exchangers, stabilizers, and catalyst precursors⁸⁹, and it has a greater CO₂ adsorption capacity than other basic materials. The structure of hydrotalcite

resembles the form of brucite $\text{Mg}(\text{OH})_2$ with fractional change in M(II) ions replaced with M(III) as shown in figure 2.4. A positive charge is balanced by balancing anions in the inter-lamellar space apart from water molecules.

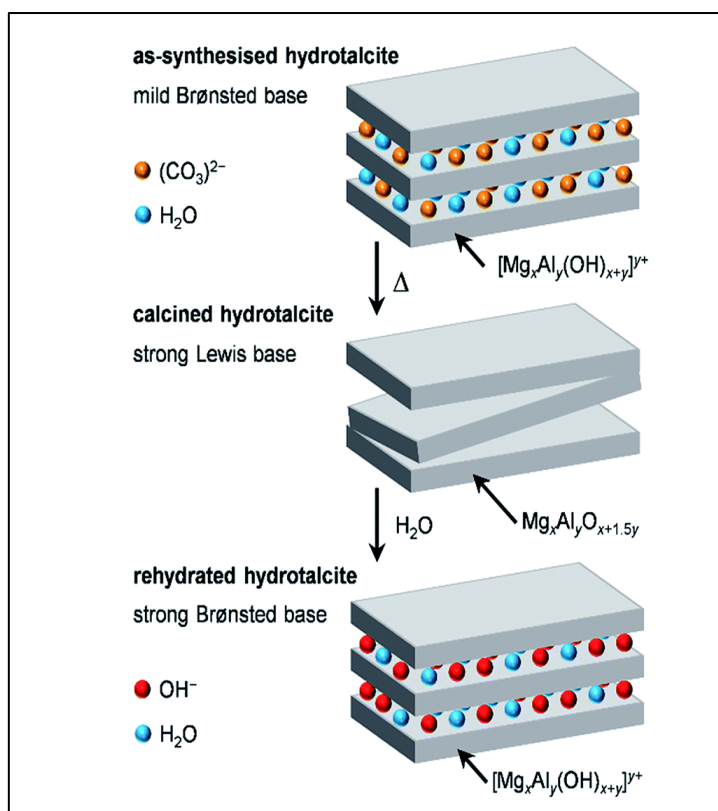


Figure 2.4: Hydrotalcite structure

The composition of hydrotalcites can be varied by replacing M(II) with isomorphs M(III) cations having nearly the same size⁹⁰. The dependency of adsorption capacity for CO_2 on microporous volume, interlayer spacing, and charge density of hydrotalcite has been explained by Alirio E. Rodrigues et al.^{91,92}. Basicity of hydrotalcite can be tuned by changing the nature and ratio of $\text{M}^{2+}/\text{M}^{3+}$ metal or by replacing a suitable anion between the interlayer. It can also be achieved by doping various elements or controlling thermal activation. Mg:Al calcined hydrotalcite have intermediate basic sites that form bi-dentate carbonates on the adsorption of CO_2 . High surface area, uniform distribution of cations, and high thermal stability makes hydrotalcite-based metal oxides a suitable catalyst. The Hydrotalcite structure can hold significant variations in the type of interlayer anions and different cations with +2 and +3 oxidation states

2.4.3 Thermodynamics of CO₂ hydrogenation to formic acid

The formation of formic acid from carbon dioxide and hydrogen involves a phase change from gaseous reagents into liquid product and its highly reversible reaction and thermodynamically not favourable with positive Gibbs free energy of 32.9 kJ/mol as discussed earlier.

However, CO₂ hydrogenation becomes favourable at higher pressures, in aqueous medium or with the use of base such as amines, alkali or ammonia in the reaction to remove the formic acid formed from the reaction system by forming an complex in a subsequent reaction^{93,94}. Jessop et al. suggested to hydrate all the reactants and products to decrease the Gibbs free energy in slightly negative value of -4 kJ/mol and in the presence of bases such as NaOH, NaHCO₃ or amines as it absorb the generated proton decreasing the gibbs free energy further to -9.5 kJ/mol⁹⁵ as shown in table 2.2

Table 2.2: Thermodynamic parameters for CO₂ hydrogenation to formic acid

Reaction	ΔG° (kJ/mol)	ΔH° (kJ/mol)	ΔS° (J/molK)
CO ₂ (g) + H ₂ (g) → HCOOH (l)	32.9	-31.2	-215
CO ₂ (aq) + H ₂ (aq) → HCOOH (aq)	- 4	--	--
CO ₂ (aq) + H ₂ (aq) + NH ₃ (aq) → NH ₄ ⁺ (aq) + HCOO ⁻ (aq)	-9.5	-84.3	-250

Enthaler et al. suggested not to separate the formic acid from the amine if the purpose for formic acid synthesis is to use it for hydrogen storage⁹⁶ and Dobrovolna et al. did the decomposition of ammonium salt of formic acid into hydrogen, CO₂ and ammonia over Pd/C at room temperature⁹⁷.

2.5 Experimental procedures

2.5.1 Catalyst preparation

The hydrotalcites with required metals and their mole ratios were prepared using the co-precipitation method at constant pH, as reported by Cavani et al. and Basile et al.^{89,98}. For the preparation of ruthenium doped Mg:Al calcined hydrotalcite, Magnesium nitrate hexahydrate (40 mmol) and Aluminium nitrate nonahydrate (10 mmol) supplied by Merck limited and Ruthenium (III) chloride hydrate (0.5 mmol) supplied by Sigma-Aldrich was dissolved in 100

ml of water and mixed on a magnetic stirrer. The second solution of 0.5 M Na_2CO_3 was prepared and added dropwise to the nitrate mixture at 80 °C, as shown in figure 2.5. The blend was aged for 24 h at 80 °C. After filtration, the solid cake was washed with warm water to remove potassium and nitrate ions and dried at 100 °C for 12 h. The resulting dried catalyst powder was calcined at 550 °C in the air for 4 h and tested for reaction activity.

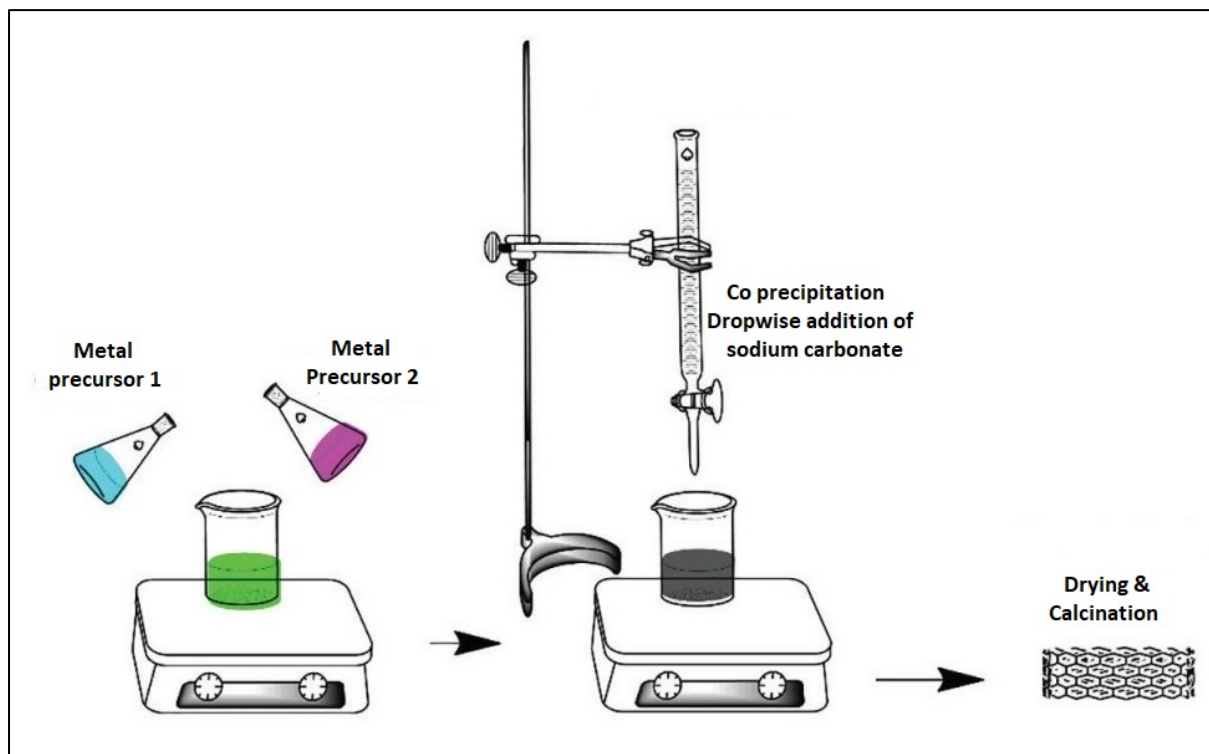


Figure 2.5: Catalyst synthesis setup

2.5.2 Catalyst characterization

X-ray diffraction (XRD) patterns of the catalysts were measured by Rigaku Dmax 500 diffractometer using nickel filtered $\text{Cu K}\alpha$ radiation. The sample was rotated to minimize the textural effect. The diffractometer was recorded in a range between 10° to 80° 2θ at a scanning rate of 0.01°/s at a temperature of 25 °C.

The surface areas of the catalyst samples were determined by nitrogen adsorption with the Thermo-Scientific Surfer instrument at – 196 °C and calculated using the Brunauer-Emmett-Teller (BET) surface area analysis method.

Basic sites of the catalyst were determined by CO_2 – temperature programmed desorption (TPD) and reduction properties of the catalyst were quantified by H_2 – temperature programmed reduction (TPR) studies.

Surface morphology studies were performed using a field emission scanning electron microscope (FE-SEM) at an accelerating voltage of 10 kV and a high-resolution transmission electron microscope (HR-TEM) on the Jeol JEM 200 model operated at an accelerating voltage of 200 kV. Catalyst surface composition was confirmed by Energy dispersive X-ray (EDS) analysis coupled with HR-TEM observations.

X-ray photoelectron spectroscopy (XPS) measurements were performed on Thermo Fisher Scientific Instrument equipped with Al K α source and multichannel plate (MCP) detector.

The Infrared (IR) spectra were recorded in 600-4000 cm⁻¹ using Perkin Elmer Spectrum One Fourier transform infrared spectrometer.

2.5.3 Batch reaction procedure and reaction monitoring

CO₂ hydrogenation was carried out in 300 ml stainless steel high-pressure batch reactor supplied by Parr Instrument. The reactor is equipped with overhead magnetic stirrer, PID temperature controller, pressure gauge, and digital pressure transmitter. The gaseous reactants – hydrogen and carbon dioxide was connected to dip tube present in the reactor as shown in figure 2.6.

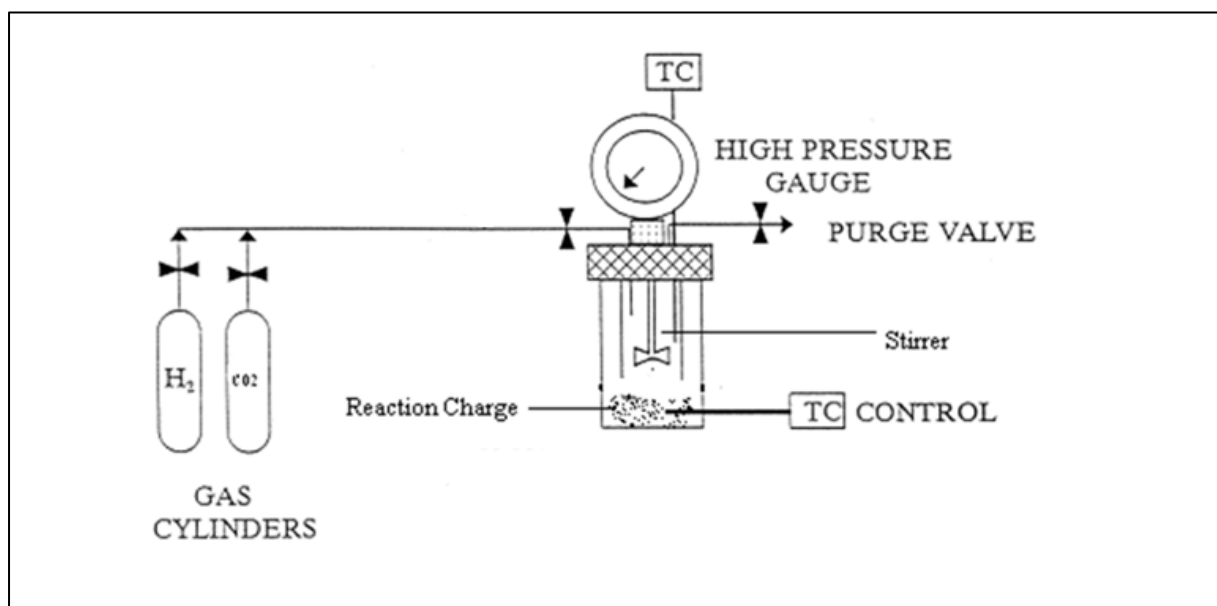


Figure 2.6: Schematic of high pressure batch reactor

In a specific experiment, 40% aqueous DMA, catalyst, KHCO₃, and methanol as solvent were charged with required quantities into the reactor. After purging with hydrogen, the reactor was pressurized to 5-10 MPa with hydrogen and carbon dioxide with requisite mole

ratio and heated to the necessary temperature. The reaction mixture was then kept for stirring at a constant temperature for a pre-determined time. After the reaction, reactor was cooled to room temperature and unreacted gases were vent off through scrubber and liquid reaction charge was collected in sample container.

The reaction sample was filtered to remove solid catalyst, diluted with methanol analysed using Agilent 7890B gas chromatography(GC) installed with an auto sampler and HP - carbowax 30m capillary column with 250 micron of pore diameter connected to a flame ionization detector. Also, the gas samples were analysed using Agilent Micro GC 490 to identify any gaseous reaction side products.

Reaction activity was monitored using external standard calibration method on GC where response factor of all reaction components were recorded prior to experiment using pre-defined quantities. The calibration curves and their response factors with detailed GC method are mentioned in supporting information, table S-1.1 and figure S-1.1. Also, figure S-1.2 in supporting information shows GC separation of compounds.

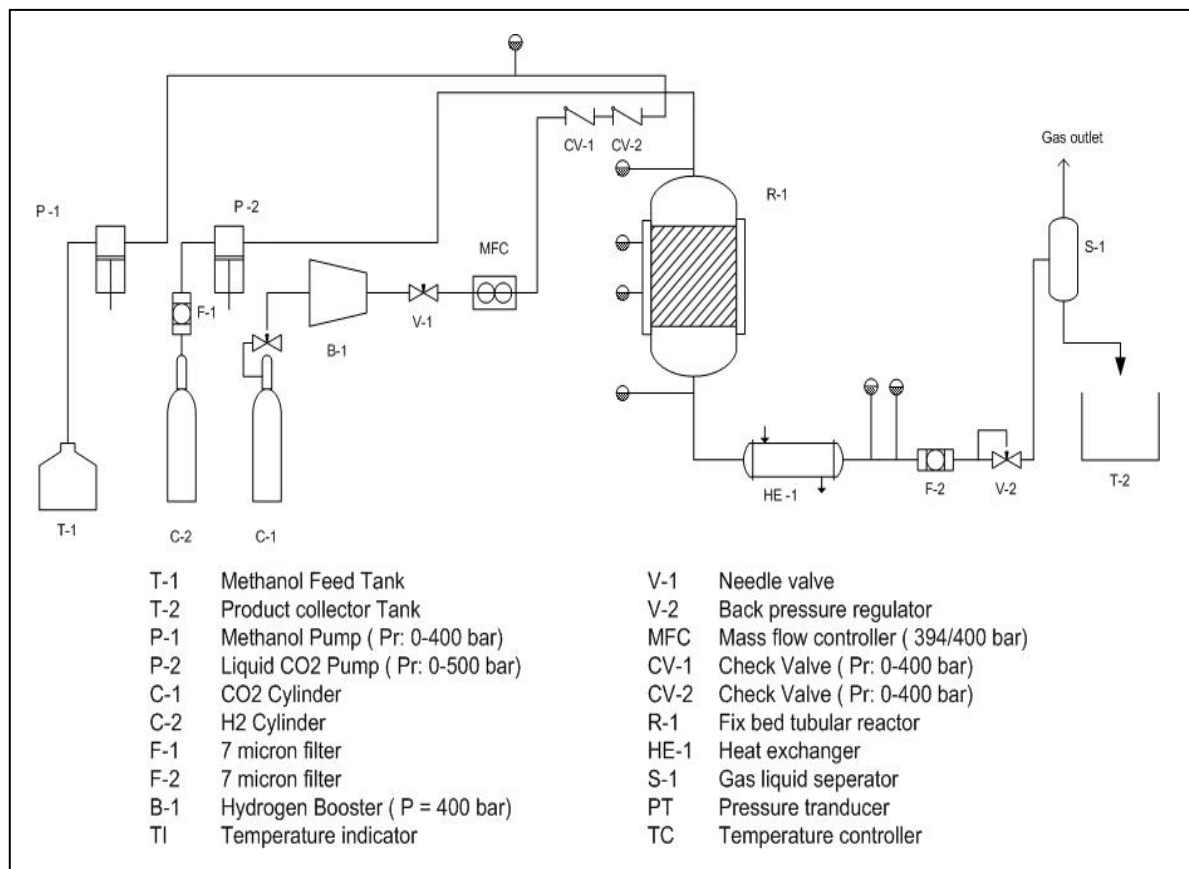
The reaction outcome parameters are calculated using standard equations as shown in eq. 1 to eq. 3

$$\% \text{ Conversion} = \frac{\text{Initial moles} - \text{final moles of DMA}}{\text{Initial moles of DMA}} * 100 \quad (1)$$

$$\% \text{ Selectivity} = \frac{\text{Moles of desired product formed}}{\text{Moles of DMA converted}} * 100 \quad (2)$$

$$\% \text{ Yield} = \frac{\text{Moles of desired product formed}}{\text{Initial moles of DMA}} * 100 \quad (3)$$

2.5.4 Continuous fixed bed reactor

Figure 2.7: Fixed bed reactor for continuous CO₂ hydrogenation

The fixed bed reactor, as shown in figure 2.7 was made with SS 316 tube and fittings in-house for the continuous synthesis of DMF. Liquid reactant (DMA in methanol) was fed through a high-pressure piston pump (P-1) supplied by Gilson, Inc., CO₂ was fed using a liquid CO₂ pump (P-2) supplied by Jasco, and hydrogen through a mass flow controller (MFC) provide by Bronkhsort. The catalyst was pelletized, sieved in the 500 – 1000 micron range and filled to the tubular reactor (R-1), and the reactor was installed with 7-micron stainless steel frit on both ends to prevent entrainment of catalyst particles in the downstream process. A product cooler (HE-1) was installed after the reactor, followed by a filter element and back pressure regulator (V-2) to maintain the required pressure in the complete system. Finally, the gas-liquid separator (S-1) was installed after the back pressure regulator separated the liquid products and unreacted gases, which were sent for analysis purposes.

2.6 Results and discussion

2.6.1 Catalyst characterization

2.6.1.1 Surface morphology

The hydrotalcite structure is stable below 300 °C and upon calcination at 550 °C, it transforms to distorted sheet of Mg/Al mixed oxides. From the FE – SEM images, it clearly showed the expected sheet morphology for calcined Mg:Al hydrotalcite as shown in figure 2.8. The similar surface behaviour is explained by Venugopal et al.⁹⁹ for hydrotalcites.

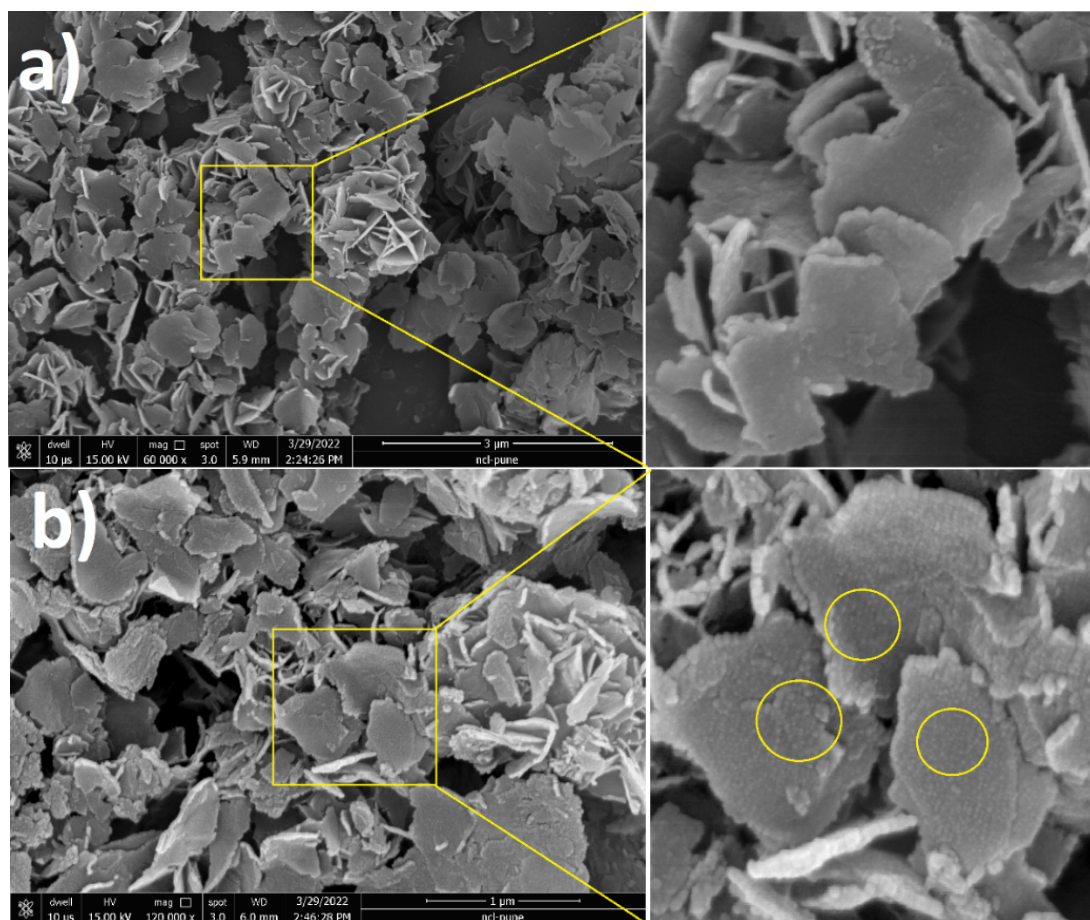


Figure 2.8: FE-SEM images of a) Mg-Al and b) Mg-Al-Ru calcined hydrotalcite

As shown in figure 2.8 a, planer sheets are observed for Mg/Al oxide whereas, deposition of particles are observed on the surface of ruthenium doped Mg/Al hydrotalcite (figure 2.8 b). The deposition features the ruthenium metal doped over the surface of hydrotalcite.

HR – TEM elemental mapping as shown in figure 2.9 (a&b) shows the uniform distribution of all metals in the catalyst. Also the d-spacing values of Mg/Al hydrotalcite (194.7 pm) and

ruthenium doped hydrotalcite (197.5) shows no difference in inter lattice as shown in figure 2.9 (c) and supports the claim that doping of ruthenium occurred on the surface of hydrotalcite.

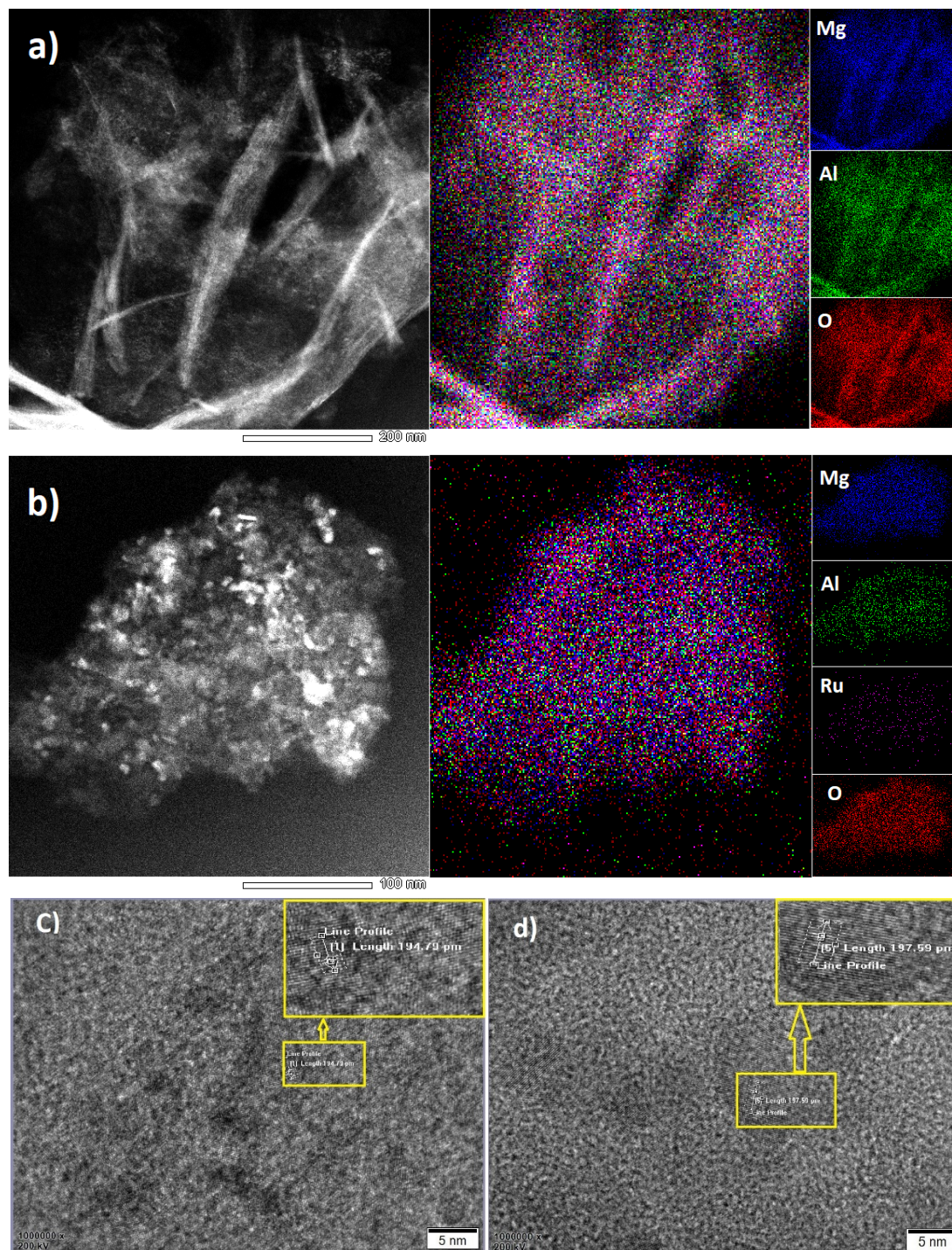


Figure 2.9: HR-TEM elemental mapping of a)Mg:Al and b)Mg:Al:Ru calcined hydrotalcite, d-spacing values of c)Mg:Al and d)Mg:Al:Ru calcined hydrotalcite, respectively.

2.6.1.2 BET surface area and elemental composition

BET surface area of different hydrotalcites with and without noble metal doping are presented in table 2.3. The loss of interstitial water and carbon dioxide in calcined hydrotalcite leads to amorphous oxide with a high surface area¹⁰⁰. A decrease in surface area after noble metal doping as shown in table 2.3 is due to meal blocking by large-size ruthenium particles on the catalyst's external edge surface, which can be also seen from FE-SEM images (figure 2.8). A similar decrease in surface area and pore size after the insertion of ruthenium is observed by Maru et al¹⁰¹.

Table 2.3: BET surface area of different synthesized and calcined hydrotalcites

SN	Catalyst	BET surface area (m ² /gm)
1	Mg:Al (4:1)	851.3
2	Cu:Al (4:1)	413.4
3	Mg:Al:Ru (4:1)	337.7
4	Mg:Al:Ir (4:1)	315.2
5	Mg:Al:Pd (4:1)	403.5
6	Cu:Al:Ru (4:1)	219.9

Energy dispersive X-ray (EDS) analysis confirmed the atomic percentage of metals available in the catalyst. For ruthenium doped Mg:Al hydrotalcite, atomic mole of Ru is found to be 1.3 % of total metals present in the catalyst.

2.6.1.3 X – ray photo spectroscopy (XPS)

The electronic states of metals present in the catalyst were confirmed using XPS analysis. As shown in figure 2.10-a, Ru3d scan showed the presence of different oxidation states of ruthenium. Peak *i* at B.E. 280.3 eV shows the Ru (IV)O₂, peak *ii* at 282.5 eV represents Ru(VI)O₃, while peaks *iii* and *iv* at B.E. 284.5 eV and 286.1 shows the metal incorporation of ruthenium oxide and Ru(II)O respectively^{99,102}. The marginal shifting in binding energies of ruthenium could be due to the stress of metal (M²⁺/M³⁺) incorporation in the catalyst. These observations can also be cross-linked with FE-SEM morphological study and even dispersion of ruthenium in elemental mapping, as described in figure 2.8 and figure 2.9.

The Mg1s and Al2p scan showed the different characteristics peaks of magnesium oxide and aluminium oxide as represented in figure 2.10 – b & c. The additional binding energies also show the crosslinking of aluminium and magnesium metals available in hydrotalcites.

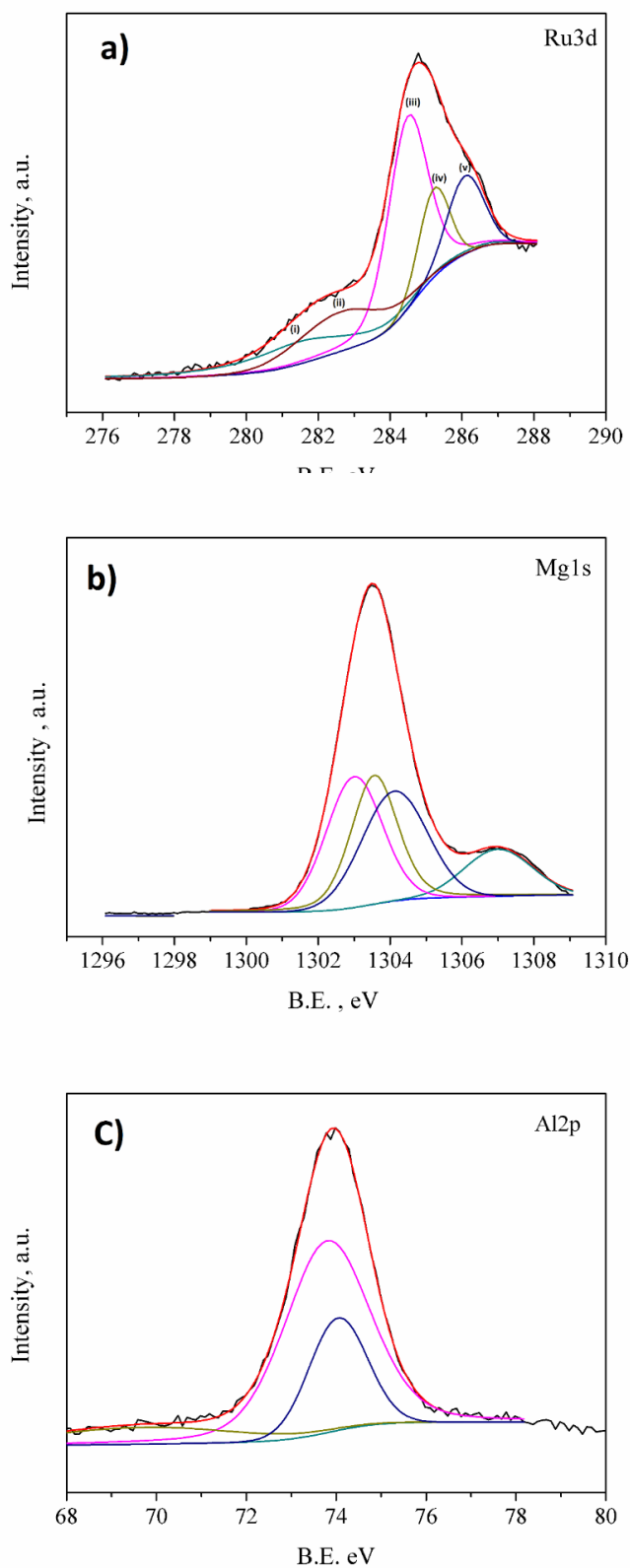


Figure 2.10: XPS scan for a) Ru3d, b) Mg1s, and c) Al2p.

2.6.1.4 Fourier transform infrared (FTIR)

The FTIR spectrum of the uncalcined Mg:Al:Ru hydrotalcite is shown in figure 2.11. The concentrated broadband between 3800 – 3000 cm^{-1} represents vibrations of structural OH-groups, physically adsorbed water, and vibrations of carbonate-hydroxyl and hydroxyl-hydroxyl groups in hydrotalcite. This broadband may also represent stretching vibration of magnesium-hydroxide bond in hydrotalcite as suggested by Parida et al.¹⁰³. The band at 1360 cm^{-1} represents the presence of carbonate ions and some impurities of nitrate ions due to synthesis solution in uncalcined hydrotalcite. Finally, the broadband at 663 cm^{-1} was implied in reports as a superposition of the characteristic bonds of hydrotalcites. Upon calcination of HT, it is observed that carbonate and water peaks have vanished, and the loss of hydrotalcite structure is confirmed by the absence of broadband at 663 cm^{-1} . FTIR spectrum of spent calcined hydrotalcite showed the intact nature of the catalyst as represented in figure 2.11.

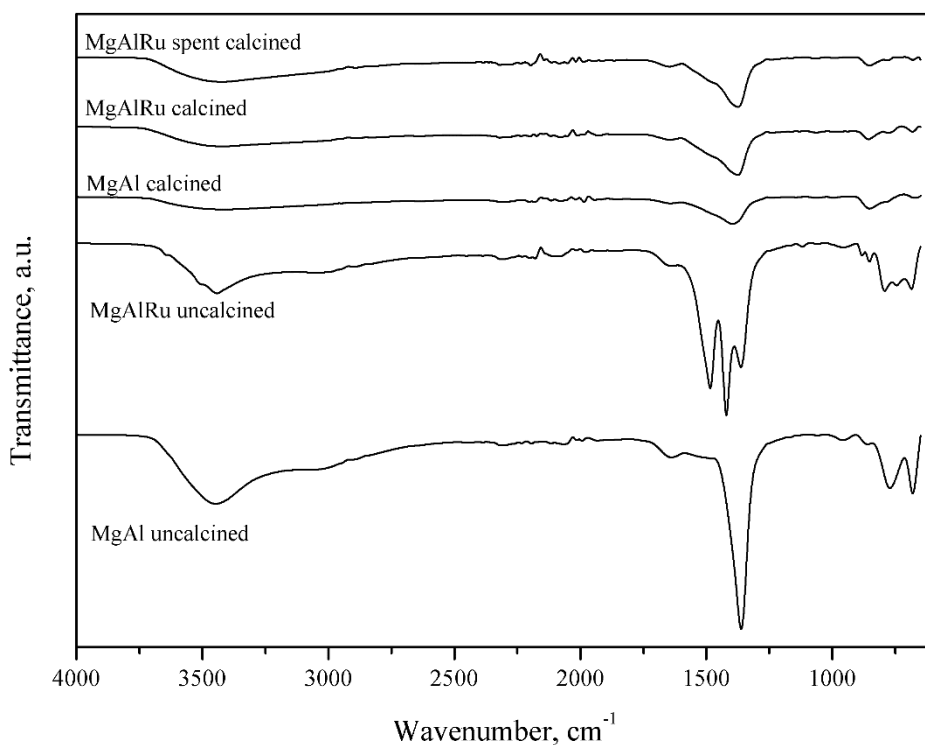


Figure 2.11: FTIR spectrum of Mg:Al and Ruthenium doped Mg:Al hydrotalcites.

2.6.1.5 X-ray powder diffraction (XRD)

The hydrotalcite structure was stable below 300 °C and transformed into a distorted sheet of Mg/Al mixed oxides after calcination to 550 °C. It is known that the hydrotalcite structure was demolished upon calcination and can be regenerated by the addition of water or being exposed to the atmosphere^{104,105}. Powder XRD pattern of uncalcined Mg:Al hydrotalcite depicted all representative peaks of pure carbonate-containing hydrotalcites as given by sharma et al.¹⁰⁶. A comparison of the XRD spectra of Mg:Al (4:1) hydrotalcite and after doping with ruthenium is shown in figure 2.12. The absence of any additional peak in ruthenium doped hydrotalcite confirmed the original crystalline nature. Whereas, slight decrease in intensity after doping of ruthenium shows the decrease in crystalline nature. This may be due to penetration of some amount of ruthenium particles in the intra-crystalline spaces (hydrotalcite spaces) of magnesium and aluminium. The spent catalyst in the reaction was washed with water and re-calcined at 550 °C for 4 h, and its XRD pattern showed no loss in crystalline nature.

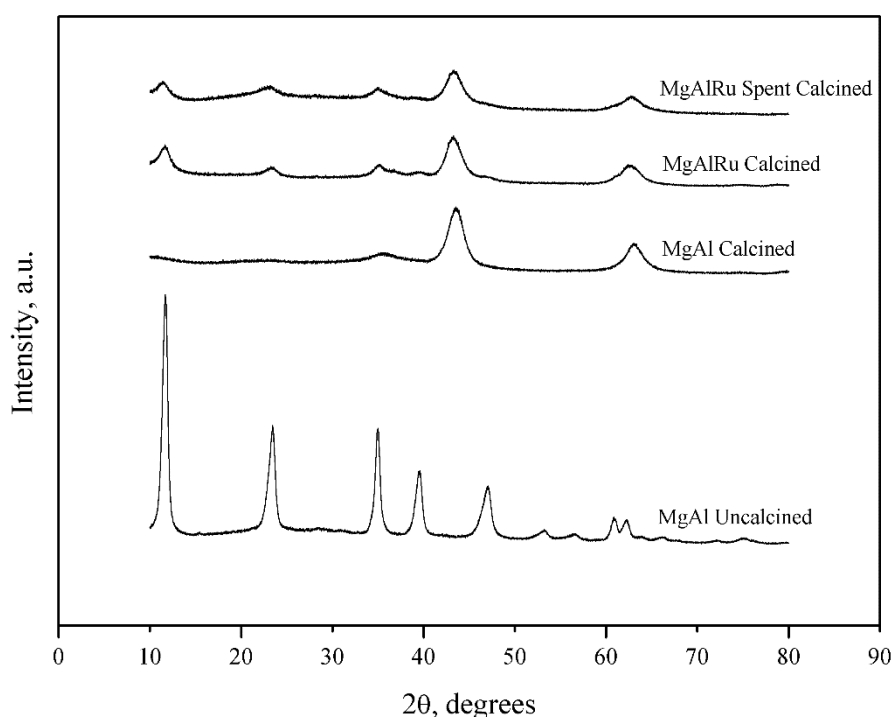


Figure 2.12: XRD pattern for Mg:Al and Ruthenium doped Mg:Al hydrotalcites.

2.6.1.6 Temperature programmed desorption and reduction (TPD and TPR)

The basic sites on ruthenium doped Mg:Al calcined hydrotalcite were quantified by CO₂-TPD at different desorption peaks at 100 – 190 °C and 200 – 500 °C, representing weak and medium sites. As shown in figure 2.13, Mg-Al catalyst has a large amount of medium basic sites while, after insertion of ruthenium on Mg/Al oxide support, medium basic sites are decreased due to the acidic nature of ruthenium. These basic sites on Mg/Al oxide layer are responsible for CO₂ activation, while ruthenium helps in hydrogenation. According to Shen et al.¹⁰⁷, calcined Mg-Al hydrotalcite at higher temperatures possess stronger basic sites than acidic ones. With the increase in calcination temperature up to 600 °C, acidic sites are reduced to a minimum while basic sites attain a peak.

Reduction of Mg:Al:Ru calcined hydrotalcite was studied using H₂-TPR. Major Peaks at 200 – 400 °C and small, broad peak at 450 – 600 °C shows the reduction of Ru₂O with different degree of interaction on Mg-Al oxide support as represented in figure 2.14. These interpretations are in line with Apuzzo et al.¹⁰⁸.

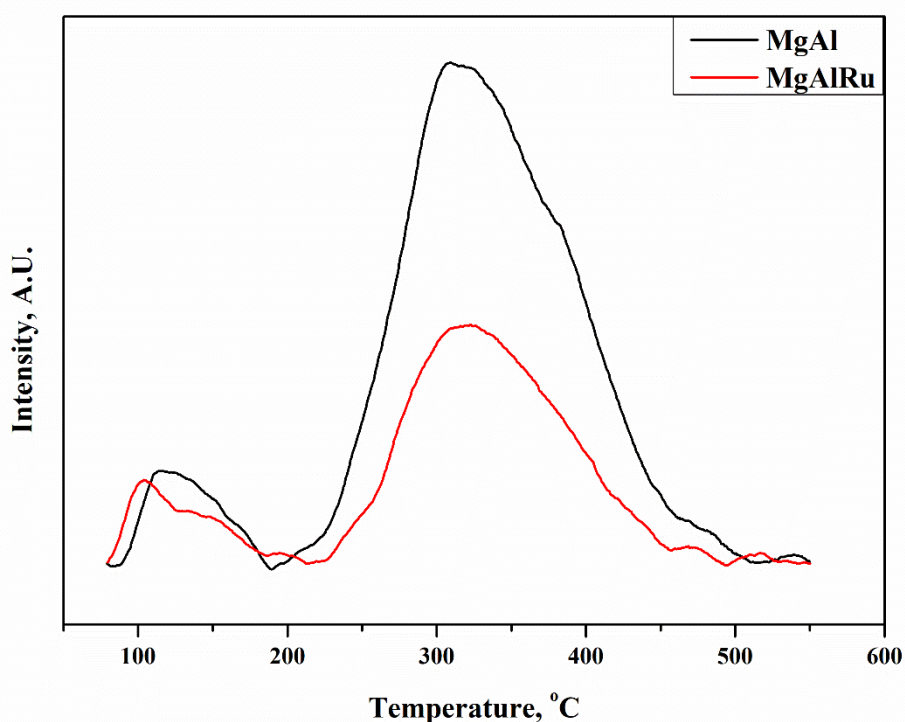
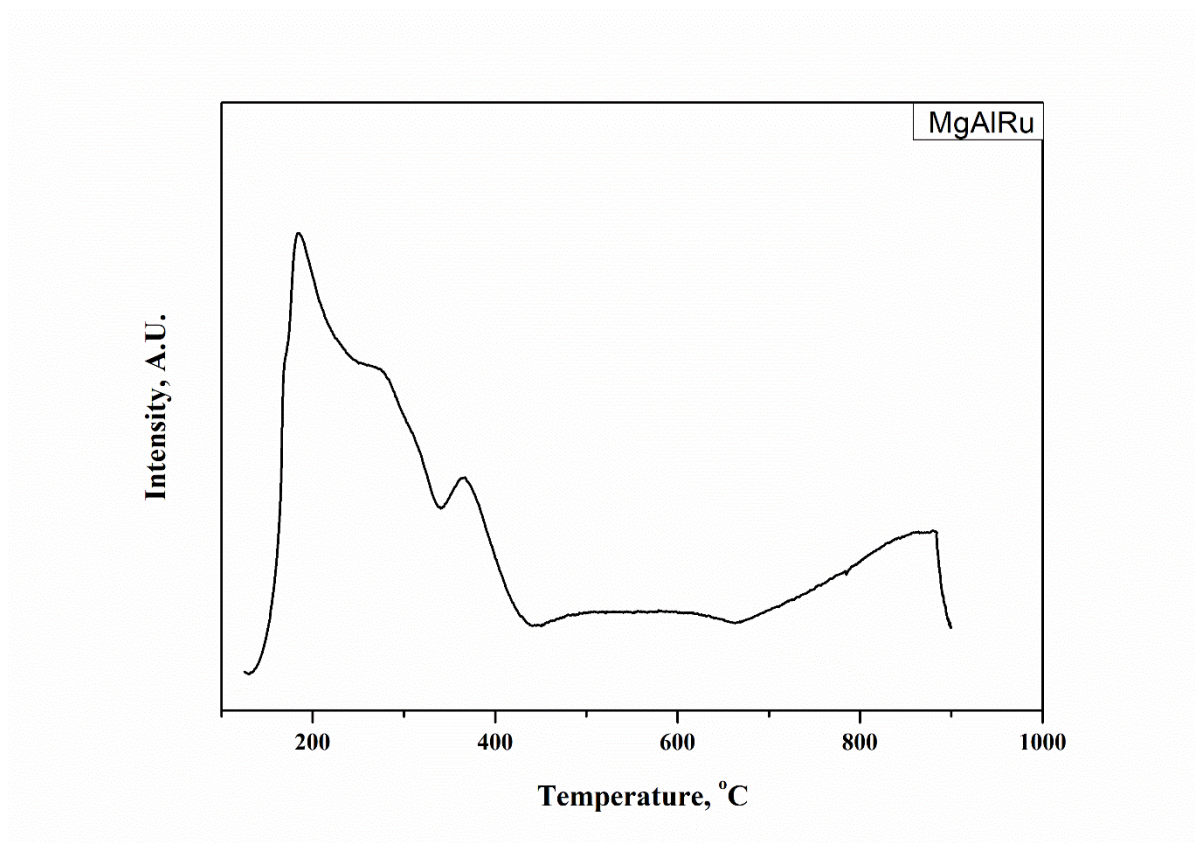


Figure 2.13: CO₂ – TPD profiles of Mg:Al and Mg:Al:Ru hydrotalcites

Figure 2.14: H₂ – TPR profile of Mg:Al:Ru hydrotalcite

2.6.2 Catalyst screening

In initial studies, a series of calcined hydrotalcites were tested for hydrogenation of CO₂ in a high pressure batch reactor with the general formula M(II): M(III), where M(II) = Mg, Cu, and Zn, and M(III) = Al and Cr with atomic ratio 4:1. Among the catalyst studied, Mg:Al and Cu:Al HT showed a considerable yield of DMF as presented in table 2.4. This suggests that appropriate basic sites in Mg and Cu systems contribute to mediating the reaction. As per the reports, the basicity of HT can be adjusted by varying Mg/Al molar ratio or activation at a suitable temperature¹⁰⁹, and it is mainly due to their O²⁻ (Lewis basicity) and hydroxyl groups (Bronsted basicity) present in it. The increased Mg content in HT resulted in higher DMF selectivity due to the increased basic character of HT. A trace amount of trimethylamine (TMA) was formed in the reaction as a side product by methylation of dimethylamine¹¹⁰, and in the case of a lesser extent of CO₂ hydrogenation, DMF yield is low, and DMA conversion is higher due to formation of dimethylammonium dimethylcarbamate (DIMCARB) with excess CO₂ in the reaction¹¹¹.

Table 2.4: Catalyst Screening. Reaction conditions: DMA 80 mmol, solvent MeOH 100ml, temperature 170 °C, H₂: CO₂ 3:1, reaction pressure 10 MPa, time 3 h, catalyst amount 1 wt %, additive KHCO₃ 4.5 mmol

Entry	Catalyst (HT)	DMA conversion (%)	DMF yield (%)
1	Cu:Al(4:1)	33.0	7.6
2	Zn:Al(4:1)	6.7	0.3
3	Mg:Cr(4:1)	1.2	0.2
4	Mg:Al(4:1)	24.2	7.0
5	Mg:Al(2:1)	23.3	4.2
6	Mg:Al(6:1)	22.7	2.4
7	Mg:Al:Cu(4:1:0.05)	11.1	6.8
8	Mg:Al:Ni(4:1:0.05)	5.2	2.2
9	Mg:Al:Zn(4:1:0.05)	5.7	0.4
10	Mg:Al:Co(4:1:0.05)	2.1	1.5
11	Mg:Al:Cr(4:1:0.05)	4.5	0.3
12	Mg:Al:Pd(4:1:0.05)	7.9	3.5
13	Mg:Al:Rh(4:1:0.05)	20.3	8.6
14	Mg:Al:Ir(4:1:0.05)	57.3	46.1
15	Mg:Al:Ru(4:1:0.05)	88.4	78.8

Further, different transition and noble metal (1 mol %) doped Mg/Al HT were studied. According to Basile et al.¹¹², Al³⁺ ions may partially replace by Rh³⁺, Ru³⁺, and Ir³⁺, having in octahedral coordination ionic radius values in the range required for the synthesis of HT phases, whereas Mg²⁺ ions may be substituted by Pd²⁺, Ni²⁺, Co²⁺ and Cu²⁺. Comparing the results obtained with Ru, Ir, Pd, and Rh-containing catalysts (Table 2.4, entry 12-15) with other transition metal catalysts (Table 2.4, entry 7-11) makes it perceptible that preferential coordination is possible to play a more critical role than the ion size. Ruthenium forms a strong coordinated covalent bond in the form of Lewis acid-base interaction, which promotes the hydrogenation step in the reaction mechanism. Higher selectivity and conversion with Ru-HT show that ruthenium has major active sites for the reaction (Table 2.4, entry 15).

2.6.3 Parametric study

2.6.3.1 Effect of reaction temperature and time

The reaction temperature and time greatly influence catalyst performance towards the hydrogenation reaction by supplying the required activation energy and interaction time. The screened ruthenium doped Mg:Al calcined hydrotalcite was tested for different temperature and observed that DMF yield increased with temperature up to 170 °C as shown in figure 2.15-a . The further increase in temperature promoted the side reaction of DMA with methanol to yield trimethyl amine (DMA) which is a temperature driven process as reported by Kita et al¹¹³. Also, gradual increase in reaction product observed with time resulting the complete conversion of DMA with 92.5 % yield of DMF as presented in figure 2.15-b. Detail reaction kinetics are discussed in subsequent section 2.6.6.

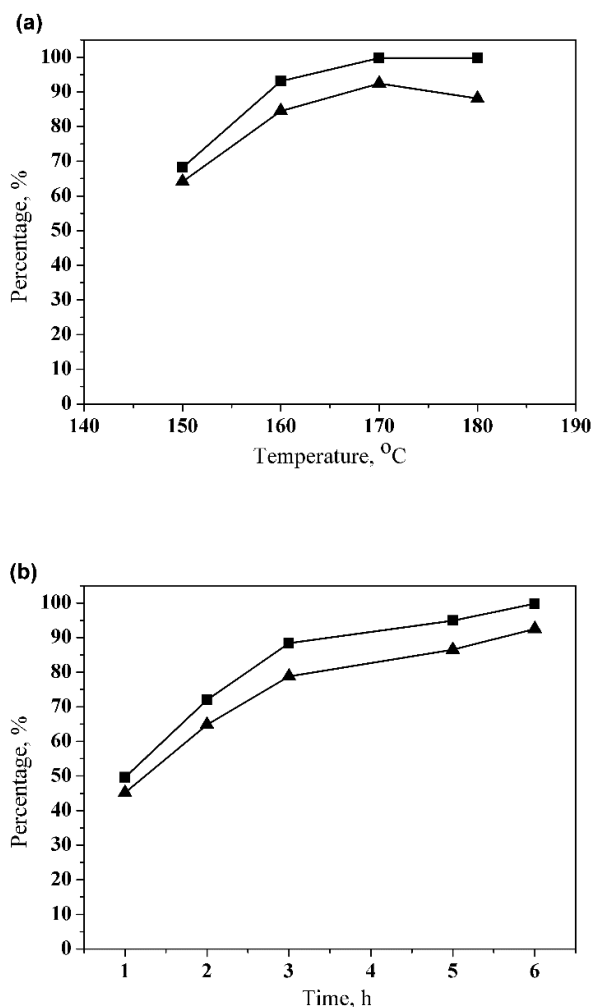


Figure 2.15: Effect of reaction temperature and time. ■ DMA conversion; ▲ DMF yield. Reaction conditions: 1 wt % catalyst loading, solvent: MeOH, H₂:CO₂: 3:1, additive KHCO₃: 4.5 mmole, DMA : 80 mmole, a) time : 6 h, b) temperature : 170°C.

2.6.3.2 Effect of solvent

The experiments were carried out using different polar and non-polar solvents and observed that the reaction yields were maximum with methanol and ethanol as a solvent as shown in figure 2.16. This effect is might be due to the involvement of alcohols as a hydrogen bond donor or proton donor in concerted ionic hydrogenation mechanism. Solvents may not involve directly in the mechanism in the presence of CO₂ and base, but it may also interact with catalyst surface, change surface properties, and increase the solubility of reactants. Reaction with water as a solvent resulted in formation of DIMCARB salt instead of hydrogenation due to solubility of CO₂ and DMA in water. Non-polar solvent like toluene did not showed the reaction activity as shown in figure 2.16 due to non-miscible phase formation inside the reaction.

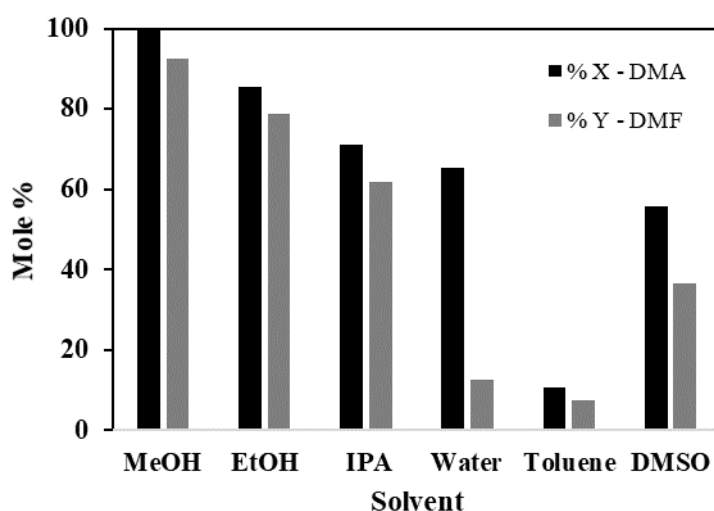


Figure 2.16: Effect of solvent. Reaction conditions: 1 wt % catalyst loading, H₂:CO₂: 3:1, additive KHCO₃: 4.5 mmole, DMA : 80 mmole, time : 6 h, temperature : 170 °C.

2.6.3.3 Effect of H₂ / CO₂ mole ratio

Although the theoretical requirement of CO₂ and H₂ for formic acid synthesis is equimolar, higher concentration of hydrogen resulted in optimum reaction yields as shown in figure 2.17. The excess amount of hydrogen up to three equivalent showed the maximum yield and further increase in mole ratio did not made any effect due to the fact that, excess available hydrogen occupies the ruthenium active sites and suppress the parallel reactions forming TMA and DIMCARB.

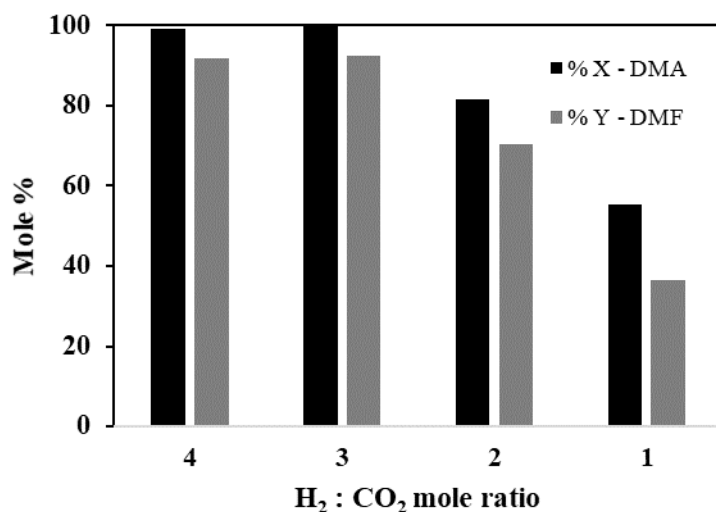


Figure 2.17: Effect of H₂:CO₂ mole ratio. Reaction conditions: 1 wt % catalyst loading, Solvent: MeOH, additive KHCO₃: 4.5 mmole, DMA: 80 mmole, time: 6 h, temperature: 170°C. Total pressure :13 MPa.

2.6.3.4 Effect of phase change (pressure)

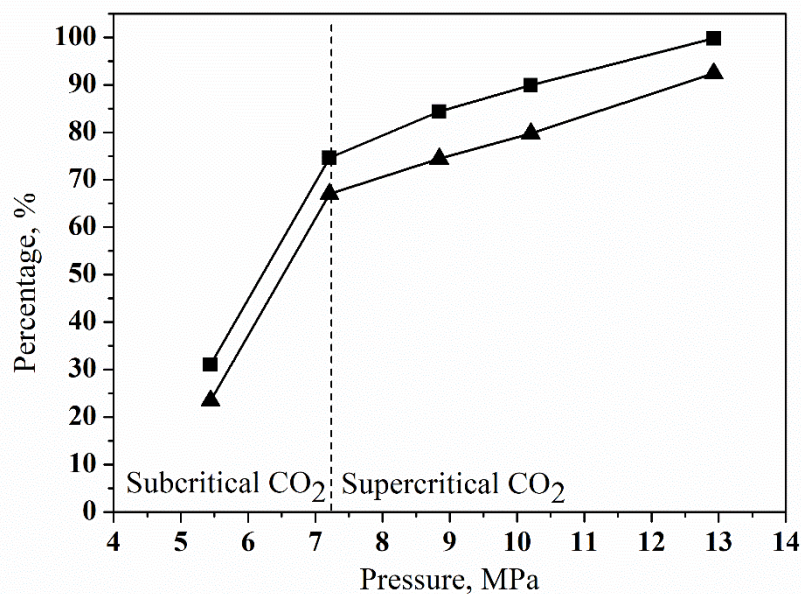


Figure 2.18: Effect of phase change. ■ DMA conversion; ▲ DMF yield. Reaction conditions: 1 wt % catalyst loading, solvent: MeOH, H₂: CO₂: 3:1, additive KHCO₃: 4.5 mmole, DMA : 80 mmole, time : 6 h, temperature : 170°C.

The total pressure in the reaction plays a significant role in the diffusion of reactants on solid catalyst surfaces. Several reports indicate the benefits of supercritical phase of CO₂ in terms of higher diffusion and solubility of compounds leading to lower mass transfer limitations and higher reaction yields^{66,114,115}. The same trend of DMF yield is observed in the current study. With increased pressure up to 13 MPa, complete conversion of DMA is observed with 92.5 % DMF yield. As shown in figure 2.18, reaction yield and conversion is comparatively low in the subcritical phase than in the supercritical phase of CO₂.

2.6.3.5 Effect of catalyst loading

The catalyst amount reliability on reaction conversion and yield is shown in figure 2.19. DMF yield is gradually increased with catalyst amount up to 1 wt % of DMA at 170 °C for 6 h. Further increase in catalyst loading does not have any effect on product yield. Whereas, with lower catalyst loading, side reactions like DIMCARB and TMA formation are governing over hydrogenation reaction leading to higher conversions of DMA but poor DMF selectivity as shown in figure 2.19. In addition, the experimental studies show that the reaction does not proceed at all in the absence of the catalyst.

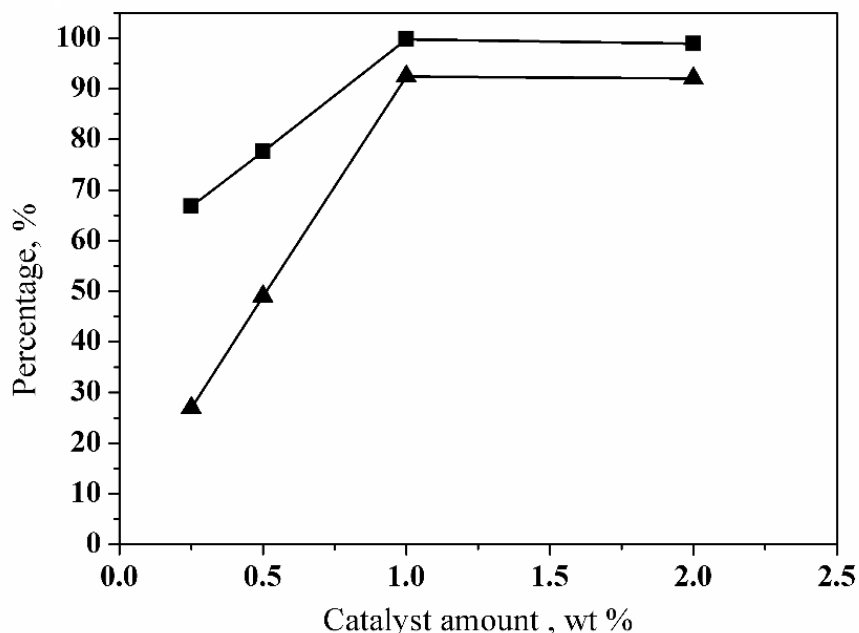


Figure 2.19: Effect of catalyst loading. ■ DMA conversion; ▲ DMF yield. Reaction conditions: Total pressure: 130 MPa, solvent: methanol, H₂:CO₂ : 3:1, additive KHCO₃: 4.5 mmole, DMA : 80 mmole, time : 6 h, temperature : 170°C.

2.6.3.6 Effect of base addition

Addition of base in reaction promote the equilibrium in forward direction by trapping formed acid molecules and different homogeneous bases like triethylamine are explored by various researchers⁷⁶. In current work, the different basic salts like KOH, KHCO₃, NaOH, K₂CO₃ are compared as an additive in reaction medium and observed that reaction proceeds better with potassium bicarbonate (KHCO₃) as it may help in reaction mechanism by trapping formate ions. With other salts, instead of hydrogenation of CO₂, carbonation of salts is occurred in greater extend. Also, the comparison study of reaction monitoring with and without addition of additive base explained the required basic sites in the prepared catalyst as shown in figure 2.20. It can be also deduced that, addition of base enhanced the reaction rate reducing the total time required for complete conversion.

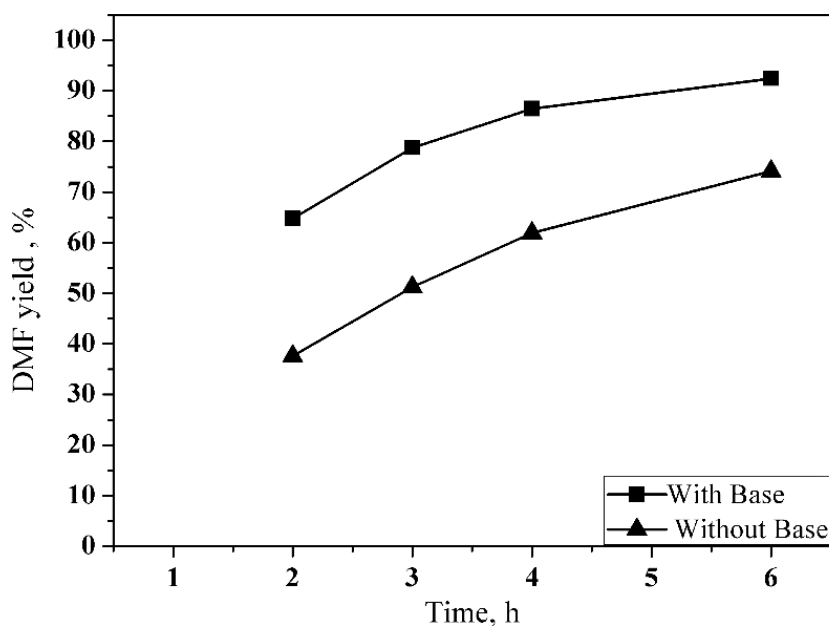


Figure 2.20: Effect of base addition. Reaction conditions: DMA 80 mmol, H₂: CO₂ 3:1, time 6 h, temperature 170 °C, reaction pressure 13 MPa, catalyst Mg:Al:Ru HT (1 wt%), solvent: MeOH, base KHCO₃: 4.5 mmole

2.6.3.7 Catalyst recycle studies

The used ruthenium doped catalyst was filtered, washed with water, dried at 110 °C, and reused for the reaction to check its activity. It was observed that catalyst activity is slightly reduced with yield of DMF decreased to 72 mole % from 92 mole %. The ICP analysis confirmed the leaching of ruthenium in reaction mass and ruthenium content is decreased from 1.3 atomic percent to 1.05. This is due to the removal of weakly interacted ruthenium on

Mg/Al surface. Further recycle studies shown no change in catalyst activity as shown in figure 2.21 indicates no further ruthenium leaching.

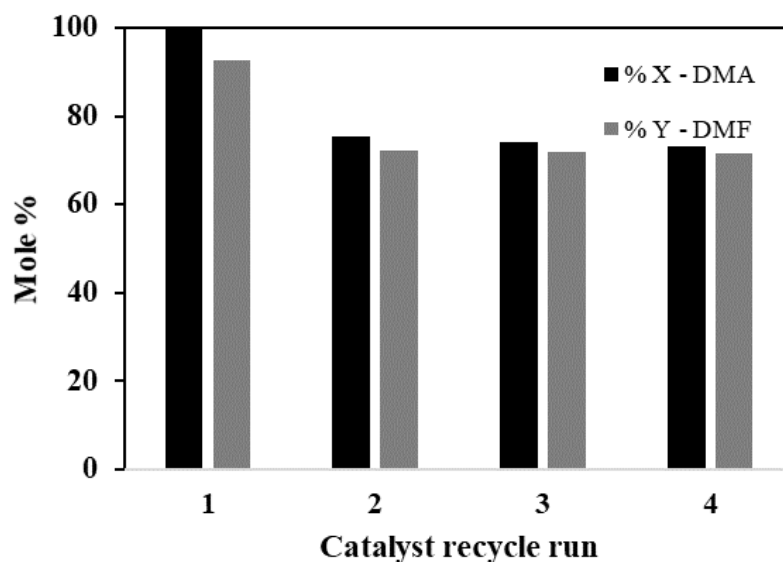


Figure 2.21: Catalyst recycle study. Reaction conditions: 1 wt % catalyst loading, Solvent: methanol, additive KHCO_3 : 4.5 mmole, H_2 : CO_2 : 3:1 DMA : 80 mmole, time : 6 h, temperature : 170°C. Total pressure :13 MPa.

2.6.4 Continuous synthesis in fixed bed reactor

The proof of concept for continuous flow synthesis of formic acid is developed on an available fixed bed reactor which was developed in-house the lab as discussed in experimental procedures. In the study of temperature, it was found that maximum reaction selectivity is observed at 170 °C. Increasing temperature beyond 170 °C resulted in the loss of selectivity as the enhanced temperature promoted side reactions, as shown in figure 2.22-a. Unlike batch process, supercritical conditions favoured the reaction, and a 16 % yield was observed within two minutes of residence time, as shown in figure 2.22-b.

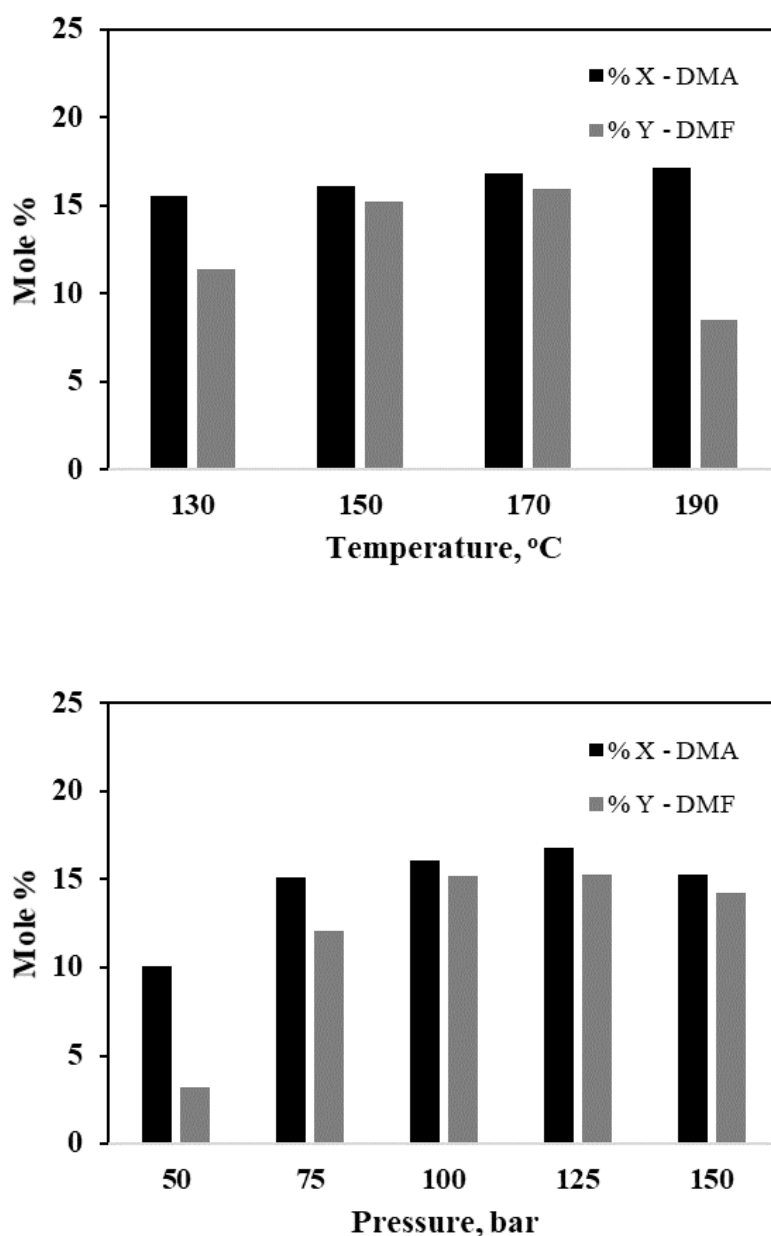


Figure 2.22: Effect of a) temperature and b) pressure in fixed bed reactor. Reaction conditions: solvent: MeOH, residence time: 2 minute, reactor volume: 5 ml, catalyst loading: 2 gms, Catalyst: Mg:Al:Ru, a) pressure: 100 bar, b) temperature: 170 °C.

2.6.5 Mechanistic approach

CO₂ hydrogenation to formic acid mainly requires the basic sites in the catalyst for CO₂ activation and noble metals are well known for hydrogenation reactions. In the proposed reaction system, the formation mechanism of DMF requires cooperation between both the acidic and basic sites. Base catalyzed hydrogenation was observed with heterolytic dissociation of hydrogen in H⁺ and H⁻ species as shown in figure 2.23, whereas amination

involves DMA dissociating into $^-NR_2$ and H^+ . In the reaction, basic Mg/Al oxides sites are responsible for CO_2 activation, whereas Ru^{2+} and O^{2-} act as hydrogenation sites.

Reaction proceeds with hydrogenation or hydrogen adsorption on the ruthenium surface, followed by CO_2 activation by creating carbonate species on Mg/Al calcined hydrotalcite surface as shown in figure 2.23. The similar mechanism for CO_2 hydrogenation are given by Maru et al.¹⁰¹ for rhodium as a active species and Jia et al.⁶ for metal oxides as a promoting sites.

Once the carbonate species forms on catalyst surface, the lone pair on oxygen atom attacks the hydronium ion of ruthenium surface and subsequently, hydride ion attacks on electrophilic carbon centre releasing formic acid and catalyst. Further reaction of formed formic acid with DMA forms dimethyl formate, which can be easily dehydrated to form DMF.

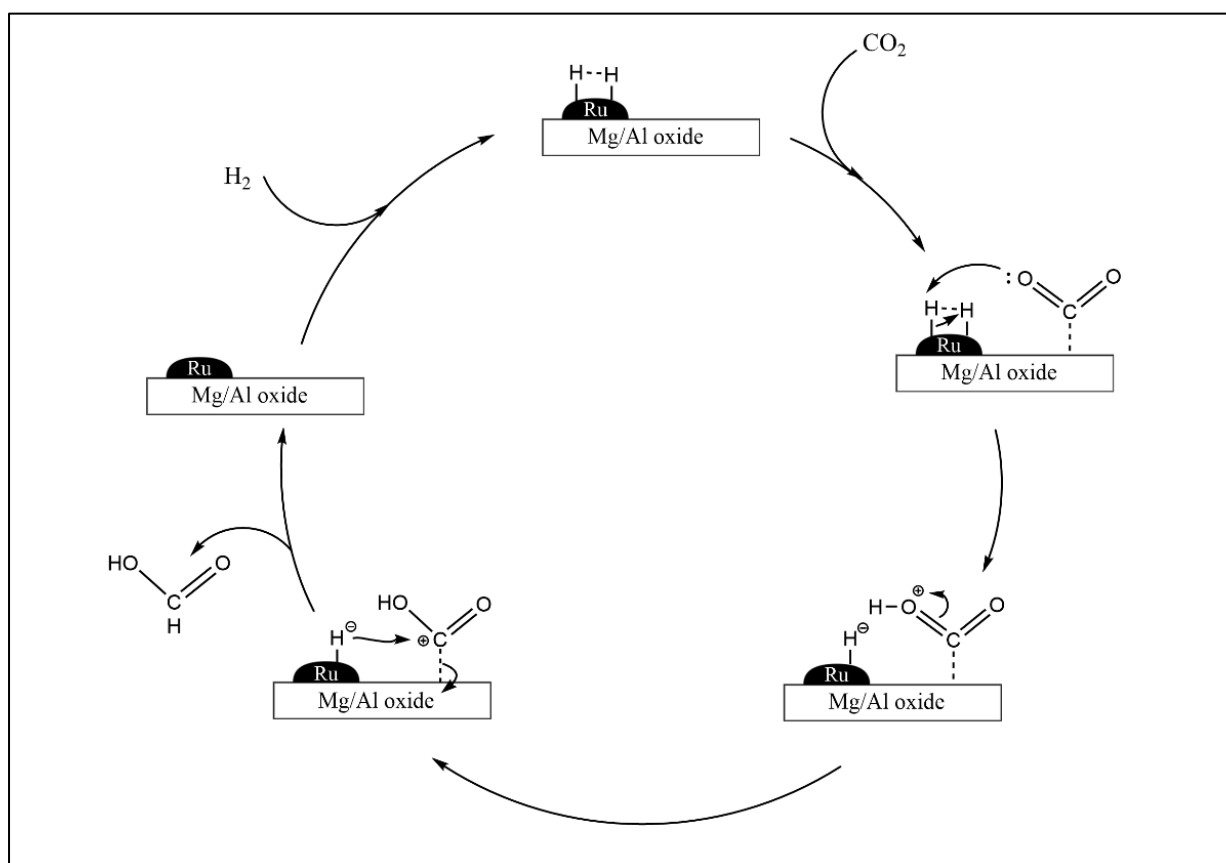


Figure 2.23: Proposed reaction mechanism over Ru doped Mg:Al calcined hydrotalcite

2.6.6 Reaction kinetics

The kinetic model was developed to understand the reaction dynamics and experiments were performed at various process temperature for model regression. As discussed earlier in catalytic mechanism, reaction proceeds with two active sites in the catalyst and accordingly Langmuir-Hinshelwood-Haugen-Watson (LHHW) kinetic model was established. The general procedure to develop and solve LHHW model is executed as described by Vernuccio et al. for hydrogenation reaction ¹¹⁶. The table 2.5 illustrates the surface mechanism considering the non-competitive adsorption of CO₂ and H₂ on two types of active sites.

Table 2.5: Reactions on hydrotalcite surface

i) $H_2 + 2S_H$	\rightleftharpoons	$2H.S_H$
ii) $CO_2 + S_C$	\rightleftharpoons	$CO_2.S_C$
iii) $H.S_H + CO_2.S_C$	\longrightarrow	$COOH.S_C + S_H$
iv) $COOH.S_C + H.S_H$	\rightleftharpoons	$HCOOH.S_C + S_H$
v) $HCOOH.S_C$	\rightleftharpoons	$HCOOH + S_C$

From the above table, step *i* and *ii* are adsorption steps for hydrogen and carbon dioxide on the catalyst surface, respectively, while step *iii* is considered as rate-limiting irreversible surface reaction between adsorbed hydrogen and CO₂ species. Under these assumptions, the rate equation generated for hydrogenation is as follows (equation 4). Step *iv* is the formation of adsorbed formic acid species, while step *v* is the desorption step of formic acid from the catalyst's surface.

$$r_R = K_R \cdot S'_H \cdot S_{CO_2.C} \quad (4)$$

Where,

Occupied Hydrogen Sites: $S'_H = H.S_H$

Unoccupied Hydrogen Sites: S_H

Occupied CO₂ sites: $S_{i.C}$

Unoccupied CO₂ sites: S_C

The concentration of Components' i' : C_i

The equilibrium constants for the surface reactions mentioned in the table 2.5 are stated as follows:

$$K_1 : \text{H}_2 \text{ adsorption constant} = \frac{S_H'^2}{C_H \cdot S_H} \quad (5)$$

$$K_2 : \text{CO}_2 \text{ adsorption constant} = \frac{S_{CO_2 \cdot C}}{C_{CO_2} \cdot S_C} \quad (6)$$

$$K_4 : \text{Reaction rate constant of step iv} = \frac{S_{HCOOH \cdot C} \cdot S_H}{S_{COOH \cdot C} \cdot S_H'} \quad (7)$$

$$K_5 : \text{Formic acid desorption constant} = \frac{S_{HCOOH \cdot C}}{HCOOH \cdot S_C} \quad (8)$$

The fractional coverages of occupied and unoccupied sites are derived from the mass balance equations (9) and (10). Equation (9) demonstrates the active sites for hydrogen species while, equation (10) represents the mass balance of all carbon dioxide adsorbed sites.

$$S_H + S_H' = 1 \quad (9)$$

$$S_{CO_2 \cdot C} + S_{HCOOH \cdot C} + S_{COOH \cdot C} + S_C = 1 \quad (10)$$

The equations (5) and (9) are combined to yield,

$$S_H' = \frac{\sqrt{K_1 \cdot C_H}}{\sqrt{K_1 \cdot C_H} + 1} \quad (11)$$

$$S_H = \frac{1}{\sqrt{K_1 \cdot C_H} + 1} \quad (12)$$

Similarly, equations (6), (7), (8), and (10) are solved simultaneously, and the final equation is expressed as equation (13),

$$S_{CO_2 \cdot C} = \frac{K_2 \cdot C_{CO_2}}{(K_2 \cdot C_{CO_2} + K_5 \cdot C_{HCOOH} + 1)} \quad (13)$$

Finally, equations (11) and (13) are substituted in equation (4) to deduce the final reaction rate equation as,

$$r_R = K_R \cdot \frac{\sqrt{K_1 \cdot C_H}}{\sqrt{K_1 \cdot C_H} + 1} * \frac{K_2 \cdot C_{CO_2}}{(K_2 \cdot C_{CO_2} + K_5 \cdot C_{HCOOH} + 1)} \quad (14)$$

The developed kinetic model was solved in MATLAB using an *ode45* solver and appropriate initial conditions. The variation in experimental and calculated data concentration values was minimized using *fminsearch*, and regressed parameters were recorded. The detailed MATLAB code is presented in supporting information.

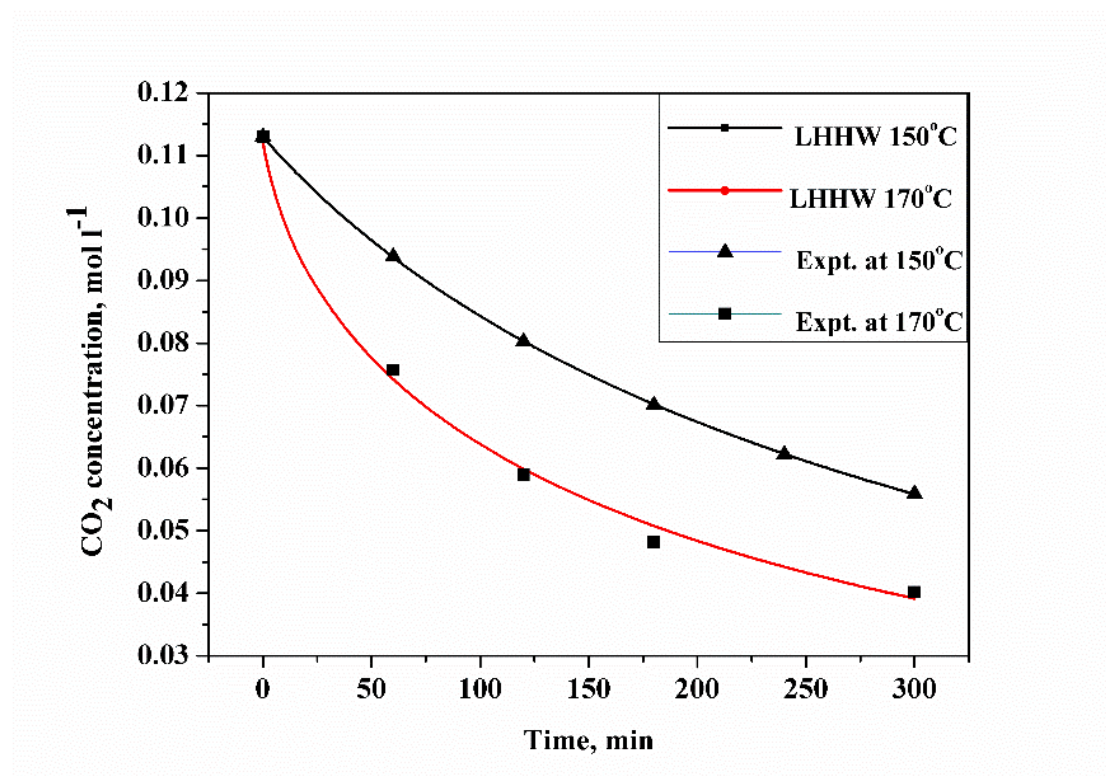


Figure 2.24: Comparison between experimental data with the LHHW model

The regressed kinetic parameter fitted well with the coefficient of determination (R^2) between calculated and experimental values is more than 0.99 for both experimental trials of 150°C and 170 °C as shown in figure 2.24

The model accurately describes the observed trends with changes in operating temperature, as shown in figure 2.24. The kinetic parameters were optimized with good precision after multiple iterations.

The estimated kinetic parameters are known to follow the Arrhenius temperature dependence as shown in equation (15) and are depicted in the table 2.6.

$$K_R = k_0 \exp\left(\frac{-Ea}{R.T}\right) \quad (15)$$

Where,

k_0 : Pre-Exponential Factor ($L \cdot mol^{-1} \cdot min^{-1}$)

Ea : Activation Energy ($kJ \cdot mol^{-1}$)

R : Universal Gas Constant ($J \cdot mol^{-1} \cdot K^{-1}$)

Table 2.6: Estimated kinetic parameters using LHHW model

Temperature Parameters	150 °C	170 °C	Units
K_i	0.3717	0.00018	$mol.mol_{cat}^{-1}.min^{-1}$
K_{ii}	0.7109	0.5329	$mol.mol_{cat}^{-1}.min^{-1}$
K_v	9.98	63.805	$mol.mol_{cat}^{-1}.min^{-1}$
K_R	0.03153	7.68	$L.mol^{-1}.min^{-1}$
E_a	413.1		$kJ.mol^{-1}$

2.7 Conclusion and the path forward

Different hydrotalcite-like compounds with a molar ratio 4:1 were prepared and have been tested for hydrogenation of CO₂ to DMF under supercritical conditions of CO₂. Results show that the basic sites in the catalyst have a considerable influence on the reaction yield. The optimum yield can be obtained from balancing the number of basic and metallic sites, and the hydrogenation was favoured by a topology of metallic sites. Mg/Al HT with a molar ratio 4 was found to be most active within other bimetallic hydrotalcite. The activity of the catalyst increased by impregnating various noble metals on hydrotalcite. The selectivity of DMF increases with the increase in the basicity of catalysts, suggesting that formic acid is the primary product. This might be because catalyst particles have a large surface area and have sufficient basic sites to carry out hydrogenation. Among the four noble metal promoters, the Ruthenium effect is more noticeable than the other promoters. This could be due to the different effects of these promoters on CO₂ adsorption, hydrogenation, or product formation. Thus it is concluded that Mg:Al:Ru CHTIs with higher thermal stability and a molar ratio of 4:1:0.05 is a promising candidate for hydrogenation of CO₂ to DMF with 92.5% yield and would be able to replace traditional homogeneous catalysts. The kinetic model developed is in-line with the experimental trends, and the regression performed resulted in kinetic parameters with desirable accuracy.

Reaction kinetics suggests a slower reaction rate, and proof of concept for continuous flow synthesis in fixed bed reactor is developed for the system. While development of pilot scale continuous reactor and its process development is the next goal for the system, making it industrially feasible.

2.8 References

- (1) Tackett, B. M.; Gomez, E.; Chen, J. G. Net Reduction of CO₂ via Its Thermocatalytic and Electrocatalytic Transformation Reactions in Standard and Hybrid Processes. *Nat. Catal.* **2019**, *2* (5), 381–386. <https://doi.org/10.1038/s41929-019-0266-y>.
- (2) Li, W.; Wang, H.; Jiang, X.; Zhu, J.; Liu, Z.; Guo, X.; Song, C. A Short Review of Recent Advances in CO₂ Hydrogenation to Hydrocarbons over Heterogeneous Catalysts. **2018**. <https://doi.org/10.1039/c7ra13546g>.
- (3) Yoon, Y.; Hall, A. S.; Surendranath, Y. Tuning of Silver Catalyst Mesostructure Promotes Selective Carbon Dioxide Conversion into Fuels. *Angew. Chemie* **2016**, *128* (49), 15508–15512. <https://doi.org/10.1002/ANGE.201607942>.
- (4) Li, K.; Peng, B.; Peng, T. Recent Advances in Heterogeneous Photocatalytic CO₂ Conversion to Solar Fuels. *ACS Catal.* **2016**, *6* (11), 7485–7527. https://doi.org/10.1021/ACSCATAL.6B02089/ASSET/IMAGES/LARGE/CS-2016-02089T_0023.JPEG.
- (5) Zhou, L.; Wang, Q.; Ma, L.; Chen, J.; Ma, J.; Zi, Z. CeO₂ Promoted Mesoporous Ni/ γ -Al₂O₃ Catalyst and Its Reaction Conditions for CO₂ Methanation. *Catal. Letters* **2015**, *145* (2), 612–619. <https://doi.org/10.1007/S10562-014-1426-Y/FIGURES/9>.
- (6) Jia, J.; Qian, C.; Dong, Y.; Li, Y. F.; Wang, H.; Ghossoub, M.; Butler, K. T.; Walsh, A.; Ozin, G. A. Heterogeneous Catalytic Hydrogenation of CO₂ by Metal Oxides: Defect Engineering – Perfecting Imperfection. *Chem. Soc. Rev.* **2017**, *46* (15), 4631–4644. <https://doi.org/10.1039/C7CS00026J>.
- (7) Álvarez, A.; Bansode, A.; Urakawa, A.; Bavykina, A. V.; Wezendonk, T. A.; Makkee, M.; Gascon, J.; Kapteijn, F. Challenges in the Greener Production of Formates/Formic Acid, Methanol, and DME by Heterogeneously Catalyzed CO₂ Hydrogenation Processes. *Chem. Rev.* **2017**, *117* (14), 9804–9838. https://doi.org/10.1021/ACS.CHEMREV.6B00816/ASSET/IMAGES/LARGE/CR-2016-00816H_0019.JPEG.
- (8) Wang, W.; Wang, S.; Ma, X.; Gong, J. Recent Advances in Catalytic Hydrogenation of Carbon Dioxide. *Chem. Soc. Rev.* **2011**. <https://doi.org/10.1039/c1cs15008a>.
- (9) Jessop, P. G.; Ikariya, T.; Noyori, R. Homogeneous Hydrogenation of Carbon Dioxide. *Chem. Rev.* **1995**. <https://doi.org/10.1021/cr00034a001>.
- (10) Kattel, S.; Liu, P.; Chen, J. G. Tuning Selectivity of CO₂ Hydrogenation Reactions at the Metal/Oxide Interface. *J. Am. Chem. Soc.* **2017**, *139* (29), 9739–9754. https://doi.org/10.1021/JACS.7B05362/ASSET/IMAGES/LARGE/JA-2017-05362S_0014.JPEG.
- (11) Roy, S.; Cherevotan, A.; Peter, S. C. Thermochemical CO₂ Hydrogenation to Single Carbon Products: Scientific and Technological Challenges. *ACS Energy Lett.* **2018**, *3* (8), 1938–1966. https://doi.org/10.1021/ACSENERGYLETT.8B00740/ASSET/IMAGES/LARGE/NZ-2018-00740W_0014.JPEG.
- (12) Gao, P.; Li, S.; Bu, X.; Dang, S.; Liu, Z.; Wang, H.; Zhong, L.; Qiu, M.; Yang, C.; Cai, J.; Wei, W.; Sun, Y. Direct Conversion of CO₂ into Liquid Fuels with High

- Selectivity over a Bifunctional Catalyst. *Nat. Chem.* 2017 910 **2017**, 9 (10), 1019–1024. <https://doi.org/10.1038/nchem.2794>.
- (13) Wei, J.; Ge, Q.; Yao, R.; Wen, Z.; Fang, C.; Guo, L.; Xu, H.; Sun, J. Directly Converting CO₂ into a Gasoline Fuel. *Nat. Commun.* 2017 81 **2017**, 8 (1), 1–9. <https://doi.org/10.1038/ncomms15174>.
- (14) Olah, G. A.; Goeppert, A.; Prakash, G. K. S. Chemical Recycling of Carbon Dioxide to Methanol and Dimethyl Ether: From Greenhouse Gas to Renewable, Environmentally Carbon Neutral Fuels and Synthetic Hydrocarbons. *J. Org. Chem.* **2009**, 74 (2), 487–498. <https://doi.org/10.1021/jo801260f>.
- (15) Arcoumanis, C.; Bae, C.; Crookes, R.; Kinoshita, E. The Potential of Di-Methyl Ether (DME) as an Alternative Fuel for Compression-Ignition Engines: A Review. *Fuel* **2008**, 87 (7), 1014–1030. <https://doi.org/10.1016/J.FUEL.2007.06.007>.
- (16) Bansode, A.; Urakawa, A. Towards Full One-Pass Conversion of Carbon Dioxide to Methanol and Methanol-Derived Products. *J. Catal.* **2014**, 309, 66–70. <https://doi.org/10.1016/J.JCAT.2013.09.005>.
- (17) Gaikwad, R.; Bansode, A.; Urakawa, A. High-Pressure Advantages in Stoichiometric Hydrogenation of Carbon Dioxide to Methanol. *J. Catal.* **2016**, 343, 127–132. <https://doi.org/10.1016/J.JCAT.2016.02.005>.
- (18) Le Valant, A.; Comminges, C.; Tisseraud, C.; Canaff, C.; Pinard, L.; Pouilloux, Y. The Cu–ZnO Synergy in Methanol Synthesis from CO₂, Part 1: Origin of Active Site Explained by Experimental Studies and a Sphere Contact Quantification Model on Cu + ZnO Mechanical Mixtures. *J. Catal.* **2015**, 324, 41–49. <https://doi.org/10.1016/J.JCAT.2015.01.021>.
- (19) Baltés, C.; Vukojević, S.; Schüth, F. Correlations between Synthesis, Precursor, and Catalyst Structure and Activity of a Large Set of CuO/ZnO/Al₂O₃ Catalysts for Methanol Synthesis. *J. Catal.* **2008**, 258 (2), 334–344. <https://doi.org/10.1016/J.JCAT.2008.07.004>.
- (20) Raudaskoski, R.; Niemelä, M. V.; Keiski, R. L. The Effect of Ageing Time on Co-Precipitated Cu/ZnO/ZrO₂ Catalysts Used in Methanol Synthesis from CO₂ and H₂. *Top. Catal.* 2007 451 **2007**, 45 (1), 57–60. <https://doi.org/10.1007/S11244-007-0240-9>.
- (21) Li, L.; Mao, D.; Yu, J.; Guo, X. Highly Selective Hydrogenation of CO₂ to Methanol over CuO–ZnO–ZrO₂ Catalysts Prepared by a Surfactant-Assisted Co-Precipitation Method. *J. Power Sources* **2015**, 279, 394–404. <https://doi.org/10.1016/J.JPOWSOUR.2014.12.142>.
- (22) Witton, T.; Chalorngtham, J.; Dumrongbunditkul, P.; Chareonpanich, M.; Limtrakul, J. CO₂ Hydrogenation to Methanol over Cu/ZrO₂ Catalysts: Effects of Zirconia Phases. *Chem. Eng. J.* **2016**, 293, 327–336. <https://doi.org/10.1016/J.CEJ.2016.02.069>.
- (23) Fornero, E. L.; Sanguineti, P. B.; Chiavassa, D. L.; Bonivardi, A. L.; Baltanás, M. A. Performance of Ternary Cu–Ga₂O₃–ZrO₂ Catalysts in the Synthesis of Methanol Using CO₂-Rich Gas Mixtures. *Catal. Today* **2013**, 213, 163–170. <https://doi.org/10.1016/J.CATTOD.2013.03.012>.
- (24) Arena, F.; Mezzatesta, G.; Spadaro, L.; Trunfio, G. Latest Advances in the Catalytic

- Hydrogenation of Carbon Dioxide to Methanol/Dimethylether. **2014**, 103–130. https://doi.org/10.1007/978-3-642-44988-8_5.
- (25) Kunkes, E. L.; Studt, F.; Abild-Pedersen, F.; Schlögl, R.; Behrens, M. Hydrogenation of CO₂ to Methanol and CO on Cu/ZnO/Al₂O₃: Is There a Common Intermediate or Not? *J. Catal.* **2015**, *328*, 43–48. <https://doi.org/10.1016/J.JCAT.2014.12.016>.
- (26) Fitzpatrick, T. Synthesis of Methanol: Part 1. Catalysts and Kinetics. *Appl. Catal.* **1988**, *36* (9), 1–65. [https://doi.org/10.1016/S0166-9834\(00\)80103-7](https://doi.org/10.1016/S0166-9834(00)80103-7).
- (27) Chen, W. H.; Lin, B. J.; Lee, H. M.; Huang, M. H. One-Step Synthesis of Dimethyl Ether from the Gas Mixture Containing CO₂ with High Space Velocity. *Appl. Energy* **2012**, *98*, 92–101. <https://doi.org/10.1016/J.APENERGY.2012.02.082>.
- (28) van Bennekom, J. G.; Venderbosch, R. H.; Winkelman, J. G. M.; Wilbers, E.; Assink, D.; Lemmens, K. P. J.; Heeres, H. J. Methanol Synthesis beyond Chemical Equilibrium. *Chem. Eng. Sci.* **2013**, *87*, 204–208. <https://doi.org/10.1016/J.CES.2012.10.013>.
- (29) Thampi, K. R.; Kiwi, J.; Grätzel, M. Methanation and Photo-Methanation of Carbon Dioxide at Room Temperature and Atmospheric Pressure. *Nat. 1987 3276122* **1987**, *327* (6122), 506–508. <https://doi.org/10.1038/327506a0>.
- (30) Tomsett, A. D.; Hagiwara, T.; Miyamoto, A.; Inui, T. Highly Active Catalysts for CO₂ Methanation to Provide the Second Reactor of Two Stage Process for High BTU SNG Synthesis. *Appl. Catal.* **1986**, *26* (C), 391–394. [https://doi.org/10.1016/S0166-9834\(00\)82566-X](https://doi.org/10.1016/S0166-9834(00)82566-X).
- (31) Janlamool, J.; Praserthdam, P.; Jongsomjit, B. Ti-Si Composite Oxide-Supported Cobalt Catalysts for CO₂ Hydrogenation. *J. Nat. Gas Chem.* **2011**, *20* (5), 558–564. [https://doi.org/10.1016/S1003-9953\(10\)60213-7](https://doi.org/10.1016/S1003-9953(10)60213-7).
- (32) Rossetti, I.; Biffi, C.; Bianchi, C. L.; Nichele, V.; Signoretto, M.; Menegazzo, F.; Finocchio, E.; Ramis, G.; Di Michele, A. Ni/SiO₂ and Ni/ZrO₂ Catalysts for the Steam Reforming of Ethanol. *Appl. Catal. B Environ.* **2012**, *117–118*, 384–396. <https://doi.org/10.1016/J.APCATB.2012.02.006>.
- (33) Theleritis, D.; Souentie, S.; Siokou, A.; Katsaounis, A.; Vayenas, C. G. Hydrogenation of CO₂ over Ru/YSZ Electropromoted Catalysts. *ACS Catal.* **2012**, *2* (5), 770–780. https://doi.org/10.1021/CS300072A/ASSET/IMAGES/LARGE/CS-2012-00072A_0005.JPEG.
- (34) Kwak, J. H.; Kovarik, L.; Szanyi, J. CO₂ Reduction on Supported Ru/Al₂O₃ Catalysts: Cluster Size Dependence of Product Selectivity. *ACS Catal.* **2013**, *3* (11), 2449–2455. https://doi.org/10.1021/CS400381F/ASSET/IMAGES/LARGE/CS-2013-00381F_0006.JPEG.
- (35) Park, J. N.; McFarland, E. W. A Highly Dispersed Pd–Mg/SiO₂ Catalyst Active for Methanation of CO₂. *J. Catal.* **2009**, *266* (1), 92–97. <https://doi.org/10.1016/J.JCAT.2009.05.018>.
- (36) Hammer, B.; Nørskov, J. K. Theoretical Surface Science and Catalysis—Calculations and Concepts. *Adv. Catal.* **2000**, *45* (C), 71–129. [https://doi.org/10.1016/S0360-0564\(02\)45013-4](https://doi.org/10.1016/S0360-0564(02)45013-4).
- (37) Gao, J.; Wang, Y.; Ping, Y.; Hu, D.; Xu, G.; Gu, F.; Su, F. A Thermodynamic

- Analysis of Methanation Reactions of Carbon Oxides for the Production of Synthetic Natural Gas. *RSC Adv.* **2012**, 2 (6), 2358–2368. <https://doi.org/10.1039/C2RA00632D>.
- (38) Koschany, F.; Schlereth, D.; Hinrichsen, O. On the Kinetics of the Methanation of Carbon Dioxide on Coprecipitated NiAl(O)X. *Appl. Catal. B Environ.* **2016**, 181, 504–516. <https://doi.org/10.1016/J.APCATB.2015.07.026>.
- (39) Loiland, J. A.; Wulfers, M. J.; Marinkovic, N. S.; Lobo, R. F. Fe/ γ -Al₂O₃ and Fe–K/ γ -Al₂O₃ as Reverse Water-Gas Shift Catalysts. *Catal. Sci. Technol.* **2016**, 6 (14), 5267–5279. <https://doi.org/10.1039/C5CY02111A>.
- (40) Pastor-Pérez, L.; Baibars, F.; Le Sache, E.; Arellano-García, H.; Gu, S.; Reina, T. R. CO₂ Valorisation via Reverse Water-Gas Shift Reaction Using Advanced Cs Doped Fe-Cu/Al₂O₃ Catalysts. *J. CO₂ Util.* **2017**, 21, 423–428. <https://doi.org/10.1016/J.JCOU.2017.08.009>.
- (41) Daza, Y. A.; Kuhn, J. N. CO₂ Conversion by Reverse Water Gas Shift Catalysis: Comparison of Catalysts, Mechanisms and Their Consequences for CO₂ Conversion to Liquid Fuels. *RSC Adv.* **2016**, 6 (55), 49675–49691. <https://doi.org/10.1039/C6RA05414E>.
- (42) Ginés, M. J. L.; Marchi, A. J.; Apesteguía, C. R. Kinetic Study of the Reverse Water-Gas Shift Reaction over CuO/ZnO/Al₂O₃ Catalysts. *Appl. Catal. A Gen.* **1997**, 154 (1–2), 155–171. [https://doi.org/10.1016/S0926-860X\(96\)00369-9](https://doi.org/10.1016/S0926-860X(96)00369-9).
- (43) Wenzel, M.; Aditya Dharanipragada, N. V. R.; Galvita, V. V.; Poelman, H.; Marin, G. B.; Rihko-Struckmann, L.; Sundmacher, K. CO Production from CO₂ via Reverse Water–Gas Shift Reaction Performed in a Chemical Looping Mode: Kinetics on Modified Iron Oxide. *J. CO₂ Util.* **2017**, 17, 60–68. <https://doi.org/10.1016/J.JCOU.2016.10.015>.
- (44) Chen, C. S.; Cheng, W. H.; Lin, S. S. Study of Iron-Promoted Cu/SiO₂ Catalyst on High Temperature Reverse Water Gas Shift Reaction. *Appl. Catal. A Gen.* **2004**, 257 (1), 97–106. [https://doi.org/10.1016/S0926-860X\(03\)00637-9](https://doi.org/10.1016/S0926-860X(03)00637-9).
- (45) Goguet, A.; Meunier, F. C.; Tibiletti, D.; Breen, J. P.; Burch, R. Spectrokinetic Investigation of Reverse Water-Gas-Shift Reaction Intermediates over a Pt/CeO₂ Catalyst. *J. Phys. Chem. B* **2004**, 108 (52), 20240–20246. <https://doi.org/10.1021/JP047242W/ASSET/IMAGES/MEDIUM/JP047242WE00005.GIF>.
- (46) Chen, X.; Su, X.; Liang, B.; Yang, X.; Ren, X.; Duan, H.; Huang, Y.; Zhang, T. Identification of Relevant Active Sites and a Mechanism Study for Reverse Water Gas Shift Reaction over Pt/CeO₂ Catalysts. *J. Energy Chem.* **2016**, 25 (6), 1051–1057. <https://doi.org/10.1016/J.JECHEM.2016.11.011>.
- (47) Jacobs, G.; Davis, B. H. Reverse Water-Gas Shift Reaction: Steady State Isotope Switching Study of the Reverse Water-Gas Shift Reaction Using in Situ DRIFTS and a Pt/Ceria Catalyst. *Appl. Catal. A Gen.* **2005**, 284 (1–2), 31–38. <https://doi.org/10.1016/J.APCATA.2005.01.013>.
- (48) Schaub, T.; Paciello, R. A. A Process for the Synthesis of Formic Acid by CO₂ Hydrogenation: Thermodynamic Aspects and the Role of CO. *Angew. Chemie Int. Ed.* **2011**, 50 (32), 7278–7282. <https://doi.org/10.1002/ANIE.201101292>.

- (49) Enthaler, S.; Von Langermann, J.; Schmidt, T. Carbon Dioxide and Formic Acid—the Couple for Environmental-Friendly Hydrogen Storage? *Energy Environ. Sci.* **2010**, *3* (9), 1207–1217. <https://doi.org/10.1039/B907569K>.
- (50) Eppinger, J.; Huang, K. W. Formic Acid as a Hydrogen Energy Carrier. *ACS Energy Letters*. American Chemical Society January 13, 2017, pp 188–195. <https://doi.org/10.1021/acsenergylett.6b00574>.
- (51) Lin, T.; Qi, X.; Wang, X.; Xia, L.; Wang, C.; Yu, F.; Wang, H.; Li, S.; Zhong, L.; Sun, Y.; Qi, X.; Wang, X.; Xia, L.; Wang, C.; Yu, F.; Wang, H.; Li, S.; Zhong, L.; Sun, Y. Direct Production of Higher Oxygenates by Syngas Conversion over a Multifunctional Catalyst. *Angew. Chemie Int. Ed.* **2019**, *58* (14), 4627–4631. <https://doi.org/10.1002/ANIE.201814611>.
- (52) Munshi, P.; Main, A. D.; Linehan, J. C.; Tai, C. C.; Jessop, P. G. Hydrogenation of Carbon Dioxide Catalyzed by Ruthenium Trimethylphosphine Complexes: The Accelerating Effect of Certain Alcohols and Amines. *J. Am. Chem. Soc.* **2002**, *124* (27), 7963–7971. <https://doi.org/10.1021/ja0167856>.
- (53) Gassner, F.; Leitner, W. Hydrogenation of Carbon Dioxide to Formic Acid Using Water-Soluble Rhodium Catalysts. *J. Chem. Soc. Chem. Commun.* **1993**. <https://doi.org/10.1039/C39930001465>.
- (54) Theoretical Study on the Carbon Dioxide Hydrogenation Catalyzed by Ru Dihydride Complexes XIA, Guangjie. **2017**.
- (55) Yang, H.; Zhang, C.; Gao, P.; Wang, H.; Li, X.; Zhong, L.; Wei, W.; Sun, Y. A Review of the Catalytic Hydrogenation of Carbon Dioxide into Value-Added Hydrocarbons. *Catalysis Science and Technology*. Royal Society of Chemistry October 16, 2017, pp 4580–4598. <https://doi.org/10.1039/c7cy01403a>.
- (56) Tai, C. C.; Pitts, J.; Linehan, J. C.; Main, A. D.; Munshi, P.; Jessop, P. G. In Situ Formation of Ruthenium Catalysts for the Homogeneous Hydrogenation of Carbon Dioxide. *Inorg. Chem.* **2002**, *41* (6), 1606–1614. <https://doi.org/10.1021/ic010866l>.
- (57) Nguyen, L. T. M.; Park, H.; Banu, M.; Kim, J. Y.; Youn, D. H.; Magesh, G.; Kim, W. Y.; Lee, J. S. Catalytic CO₂ Hydrogenation to Formic Acid over Carbon Nanotube-Graphene Supported PdNi Alloy Catalysts. *RSC Adv.* **2015**, *5* (128), 105560–105566. <https://doi.org/10.1039/C5RA21017H>.
- (58) Jin, F.; Gao, Y.; Jin, Y.; Zhang, Y.; Cao, J.; Wei, Z.; Smith, R. L. High-Yield Reduction of Carbon Dioxide into Formic Acid by Zero-Valent Metal/Metal Oxide Redox Cycles. *Energy Environ. Sci.* **2011**, *4* (3), 881–884. <https://doi.org/10.1039/C0EE00661K>.
- (59) Weissrnel, K.; Arpe, H. *Industrial Organic Chemistry*; Wiley, 1997. <https://doi.org/10.1002/9783527616688>.
- (60) Behr, A.; Nowakowski, K. Catalytic Hydrogenation of Carbon Dioxide to Formic Acid. *Adv. Inorg. Chem.* **2014**, *66*, 223–258. <https://doi.org/10.1016/B978-0-12-420221-4.00007-X>.
- (61) Graf, E.; Leitner, W. Direct Formation of Formic Acid from Carbon Dioxide and Dihydrogen Using the [Rh(Cod)Cl]₂-Ph₂P(CH₂)₄PPh₂ Catalyst System. *J. Chem. Soc. Chem. Commun.* **1992**. <https://doi.org/10.1039/C39920000623>.

- (62) Gunasekar, G. H.; Padmanaban, S.; Park, K.; Jung, K.; Yoon, S. An Efficient and Practical System for the Synthesis of *N,N*-Dimethylformamide by CO₂ Hydrogenation Using a Heterogeneous Ru Catalyst: From Batch to Continuous Flow. *ChemSusChem* **2020**, *13* (7), 1735–1739. <https://doi.org/10.1002/cssc.201903364>.
- (63) Ezhova, N. N.; Kolesnichenko, N. V.; Bulygin, A. V.; Slivinskii, E. V.; Han, S. Hydrogenation of CO₂ to Formic Acid in the Presence of the Wilkinson Complex. *Russ. Chem. Bull.* **2002**. <https://doi.org/10.1023/A:1022162713837>.
- (64) Jessop, P. G.; Hsiao, Y.; Ikariya, T.; Noyori, R. Catalytic Production of Dimethylformamide from Supercritical Carbon Dioxide. *J. Am. Chem. Soc.* **1994**. <https://doi.org/10.1021/ja00098a072>.
- (65) Liu, J.; Guo, C.; Zhang, Z.; Jiang, T.; Liu, H.; Song, J.; Fan, H.; Han, B. Synthesis of Dimethylformamide from CO₂, H₂ and Dimethylamine over Cu/ZnO. *Chem. Commun.* **2010**, *46* (31), 5770–5772. <https://doi.org/10.1039/c0cc00751j>.
- (66) Philip G. Jessop; Yi Hsiao; Takao Ikariya, and; Ryoji Noyori*, †. Homogeneous Catalysis in Supercritical Fluids: Hydrogenation of Supercritical Carbon Dioxide to Formic Acid, Alkyl Formates, and Formamides. *J. Am. Chem. Soc.* **1996**, *118* (2), 344–355. <https://doi.org/10.1021/JA953097B>.
- (67) Wang, W. H.; Himeda, Y.; Muckerman, J. T.; Manbeck, G. F.; Fujita, E. CO₂ Hydrogenation to Formate and Methanol as an Alternative to Photo- and Electrochemical CO₂ Reduction. *Chem. Rev.* **2015**, *115* (23), 12936–12973. https://doi.org/10.1021/ACS.CHEMREV.5B00197/ASSET/IMAGES/LARGE/CR-2015-00197P_0002.JPEG.
- (68) Álvarez, A.; Bansode, A.; Urakawa, A.; Bavykina, A. V.; Wezendonk, T. A.; Makkee, M.; Gascon, J.; Kapteijn, F. Challenges in the Greener Production of Formates/Formic Acid, Methanol, and DME by Heterogeneously Catalyzed CO₂ Hydrogenation Processes. *Chem. Rev.* **2017**, *117* (14), 9804–9838. https://doi.org/10.1021/ACS.CHEMREV.6B00816/ASSET/IMAGES/LARGE/CR-2016-00816H_0019.JPEG.
- (69) Dong, K.; Razzaq, R.; Hu, Y.; Ding, K. Homogeneous Reduction of Carbon Dioxide with Hydrogen. *Top. Curr. Chem.* **2017**, *375* (2). <https://doi.org/10.1007/S41061-017-0107-X>.
- (70) Filonenko, G. A.; Van Putten, R.; Schulpen, E. N.; Hensen, E. J. M.; Pidko, E. A. Highly Efficient Reversible Hydrogenation of Carbon Dioxide to Formates Using a Ruthenium PNP-Pincer Catalyst. *ChemCatChem* **2014**, *6* (6), 1526–1530. <https://doi.org/10.1002/CCTC.201402119>.
- (71) Tanaka, R.; Yamashita, M.; Nozaki, K. Catalytic Hydrogenation of Carbon Dioxide Using Ir(III)-Pincer Complexes. *J. Am. Chem. Soc.* **2009**, *131* (40), 14168–14169. https://doi.org/10.1021/JA903574E/SUPPL_FILE/JA903574E_SI_002.PDF.
- (72) Bulushev, D. A.; Ross, J. R. H. Heterogeneous Catalysts for Hydrogenation of CO₂ and Bicarbonates to Formic Acid and Formates. <https://doi.org/10.1080/01614940.2018.1476806> **2018**, *60* (4), 566–593. <https://doi.org/10.1080/01614940.2018.1476806>.
- (73) Zhou, K.; Li, Y. Catalysis Based on Nanocrystals with Well-Defined Facets. *Angew. Chemie Int. Ed.* **2012**, *51* (3), 602–613. <https://doi.org/10.1002/ANIE.201102619>.

- (74) Aqueous-phase organometallic catalysis: concepts and applications | WorldCat.org <https://www.worldcat.org/title/aqueous-phase-organometallic-catalysis-concepts-and-applications/oclc/39740757> (accessed Sep 8, 2022).
- (75) Zhang, J. Z.; Li, Z.; Wang, H.; Wang, C. Y. Homogeneous Catalytic Synthesis of Formic Acid (Salts) by Hydrogenation of CO₂ with H₂ in the Presence of Ruthenium Species. *J. Mol. Catal. A Chem.* **1996**, *112* (1), 9–14. [https://doi.org/10.1016/1381-1169\(96\)00185-9](https://doi.org/10.1016/1381-1169(96)00185-9).
- (76) Munshi, P.; Main, A. D.; Linehan, J. C.; Tai, C. C.; Jessop, P. G. Hydrogenation of Carbon Dioxide Catalyzed by Ruthenium Trimethylphosphine Complexes: The Accelerating Effect of Certain Alcohols and Amines. *J. Am. Chem. Soc.* **2002**, *124* (27), 7963–7971. <https://doi.org/10.1021/JA0167856/ASSET/IMAGES/LARGE/JA0167856H00001.JPG>.
- (77) Kudo, K.; Phala, H.; Sugita, N.; Takezaki, Y. Synthesis of Dimethyl Formamide From Carbon Dioxide, Hydrogen and Dimethyl Amine Catalyzed By Palladium(Ii) Chloride. *Chem. Lett.* **1977**, *6* (12), 1495–1496. <https://doi.org/10.1246/cl.1977.1495>.
- (78) Sakamoto, M.; Shimizu, I.; Yamamoto, A. Synthesis of the First Carbon Dioxide Coordinated Palladium(0) Complex, Pd(H₂-CO₂)(PMePh₂)₂. *Organometallics* **1994**, *13* (2), 407–409. <https://doi.org/10.1021/om00014a003>.
- (79) Laurency, G.; Joo, F.; Nadasdi, L. Formation and Characterization of Water-Soluble Hydrido-Ruthenium(II) Complexes of 1,3,5-Triaza-7-Phosphaadamantane and Their Catalytic Activity in Hydrogenation of CO₂ and HCO₃⁻ in Aqueous Solution. *Inorg. Chem.* **2000**, *39* (22), 5083–5088. <https://doi.org/10.1021/IC000200B>.
- (80) Inoue, Y.; Izumida, H.; Sasaki, Y.; Hashimoto, H. Catalytic Fixation of Carbon Dioxide To Formic Acid By Transition-Metal Complexes Under Mild Conditions. *Chem. Lett.* **1976**, *5* (8), 863–864. <https://doi.org/10.1246/cl.1976.863>.
- (81) Zhang, W.; Wang, S.; Zhao, Y.; Xinbin, M. Hydrogenation of ScCO₂ to Formic Acid Catalyzed by Heterogeneous Ruthenium(III)/Al₂O₃ Catalysts. <https://doi.org/10.1246/cl.160013> **2016**, *45* (5), 555–557. <https://doi.org/10.1246/CL.160013>.
- (82) Zhang, W.; Wang, S.; Zhao, Y.; Ma, X. Hydrogenation of CO₂ to Formic Acid Catalyzed by Heterogeneous Ru-PPh₃/Al₂O₃ Catalysts. *Fuel Process. Technol.* **2018**, *178*, 98–103. <https://doi.org/10.1016/J.FUPROC.2018.05.024>.
- (83) Filonenko, G. A.; Vrijburg, W. L.; Hensen, E. J. M.; Pidko, E. A. On the Activity of Supported Au Catalysts in the Liquid Phase Hydrogenation of CO₂ to Formates. *J. Catal.* **2016**, *343*, 97–105. <https://doi.org/10.1016/j.jcat.2015.10.002>.
- (84) PANDURAG, K. S.; GUNDAPPA, K. R.; VENKATARAMASUBRAMANIAN, V.; ARUMUGAM, S. METAL CATALYZED PROCESS FOR REDUCTION OF CO₂ TO SODIUM FORMATE AND FORMIC ACID, 2016.
- (85) Umegaki, T.; Enomoto, Y.; Kojima, Y. Metallic Ruthenium Nanoparticles for Hydrogenation of Supercritical Carbon Dioxide. *Catal. Sci. Technol.* **2016**, *6* (2), 409–412. <https://doi.org/10.1039/C5CY00994D>.
- (86) Xu, Z.; Mcnamara, N. D.; Neumann, G. T.; Schneider, W. F.; Hicks, J. C. Catalytic

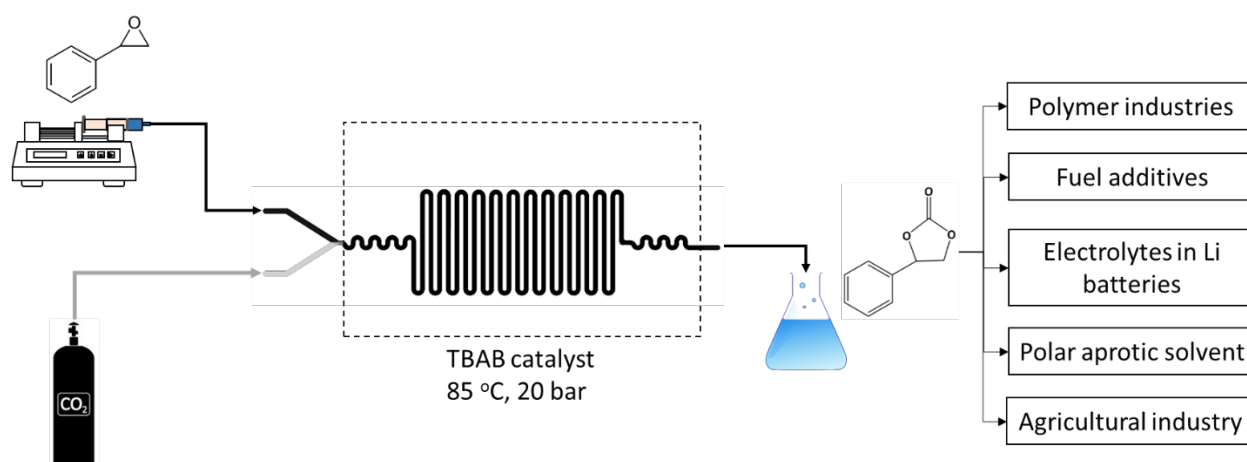
- Hydrogenation of CO₂ to Formic Acid with Silica-Tethered Iridium Catalysts. *ChemCatChem* **2013**, 5 (7), 1769–1771. <https://doi.org/10.1002/CCTC.201200839>.
- (87) Park, K.; Gunasekar, G. H.; Prakash, N.; Jung, K. D.; Yoon, S. A Highly Efficient Heterogenized Iridium Complex for the Catalytic Hydrogenation of Carbon Dioxide to Formate. *ChemSusChem* **2015**, 8 (20), 3410–3413. <https://doi.org/10.1002/CSSC.201500436>.
- (88) Joó, F.; Kovács, J.; Bényei, A. C.; Nádasdi, L.; Laurenczy, G. The Effect of PH on the Reactions of Catalytically Important RhI Complexes in Aqueous Solution: Reaction of [RhCl(Tppms)₃] and Trans-[RhCl(CO)(Tppms)₂] with Hydrogen (TPPMS = Mono-Sulfonated Triphenylphosphine). *Chem. - A Eur. J.* **2001**, 7 (1), 193–199. [https://doi.org/10.1002/1521-3765\(20010105\)7:1<193::aid-chem193>3.3.co;2-h](https://doi.org/10.1002/1521-3765(20010105)7:1<193::aid-chem193>3.3.co;2-h).
- (89) Cavani, F.; Trifirò, F.; Vaccari, A. Hydrotalcite-Type Anionic Clays: Preparation, Properties and Applications. *Catal. Today* **1991**, 11 (2), 173–301. [https://doi.org/10.1016/0920-5861\(91\)80068-K](https://doi.org/10.1016/0920-5861(91)80068-K).
- (90) Bravo-Suárez, J. J.; Páez-Mozo, E. A.; Oyama, S. T. Review of the Synthesis of Layered Double Hydroxides: A Thermodynamic Approach. *Quim. Nova* **2004**, 27 (4), 601–614. <https://doi.org/10.1590/S0100-40422004000400015>.
- (91) Yong, Z.; Rodrigues, A. E. Hydrotalcite-like Compounds as Adsorbents for Carbon Dioxide. *Energy Convers. Manag.* **2002**, 43 (14), 1865–1876. [https://doi.org/10.1016/S0196-8904\(01\)00125-X](https://doi.org/10.1016/S0196-8904(01)00125-X).
- (92) Yong, Z.; Mata, V.; Rodrigues, A. E. Adsorption of Carbon Dioxide onto Hydrotalcite-like Compounds (HTlcs) at High Temperatures. *Ind. Eng. Chem. Res.* **2001**, 40 (1), 204–209. <https://doi.org/10.1021/IE000238W/ASSET/IMAGES/LARGE/IE000238WF00009.JPG>.
- (93) Maity, D. K. How Much Water Is Needed to Ionize Formic Acid? *J. Phys. Chem. A* **2013**, 117 (36), 8660–8670. https://doi.org/10.1021/JP403032E/ASSET/IMAGES/LARGE/JP-2013-03032E_0006.JPEG.
- (94) Schmidt, I.; Müller, K.; Arlt, W. Evaluation of Formic-Acid-Based Hydrogen Storage Technologies. *Energy and Fuels* **2014**, 28 (10), 6540–6544. https://doi.org/10.1021/EF501802R/SUPPL_FILE/EF501802R_SI_001.PDF.
- (95) Affan, M. A.; Jessop, P. G. Catalytic Formylation of Primary and Secondary Amines with CO₂ and H₂ Using Abundant-Metal Catalysts. **2017**. <https://doi.org/10.1021/acs.inorgchem.7b01242>.
- (96) Enthaler, S.; Von Langermann, J.; Schmidt, T. Carbon Dioxide and Formic Acid —the Couple for Environmental-Friendly Hydrogen Storage? *Energy Environ. Sci.* **2010**, 3 (9), 1207–1217. <https://doi.org/10.1039/B907569K>.
- (97) Dobrovolná, Z.; Červený, L. Ammonium Formate Decomposition Using Palladium Catalyst. *Res. Chem. Intermed.* **2000**, 26 (5), 489–497. <https://doi.org/10.1163/156856700X00480>.
- (98) Basile, F.; Basini, L.; Fornasari, G.; Gazzano, M.; Trifirò, F.; Vaccari, A. New Hydrotalcite-Type Anionic Clays Containing Noble Metals. *Chem. Commun.* **1996**,

- No. 21, 2435–2436. <https://doi.org/10.1039/CC9960002435>.
- (99) Venugopal, A. K.; Venugopalan, A. T.; Kaliyappan, P.; Raja, T. Oxidative Dehydrogenation of Ethyl Benzene to Styrene over Hydrotalcite Derived Cerium Containing Mixed Metal Oxides. *Green Chem.* **2013**, *15* (11), 3259–3267. <https://doi.org/10.1039/C3GC41321G>.
- (100) Kuśtrowski, P.; Chmielarz, L.; Bozek, E.; Sawalha, M.; Roessner, F. Acidity and Basicity of Hydrotalcite Derived Mixed Mg–Al Oxides Studied by Test Reaction of MBOH Conversion and Temperature Programmed Desorption of NH₃ and CO₂. *Mater. Res. Bull.* **2004**, *39* (2), 263–281. <https://doi.org/10.1016/J.MATERRESBULL.2003.09.032>.
- (101) Maru, M. S.; Ram, S.; Adwani, J. H.; Shukla, R. S. Selective and Direct Hydrogenation of CO₂ for the Synthesis of Formic Acid over a Rhodium Hydrotalcite (Rh-HT) Catalyst. *ChemistrySelect* **2017**, *2* (13), 3823–3830. <https://doi.org/10.1002/SLCT.201700130>.
- (102) Morgan, D. J. Resolving Ruthenium: XPS Studies of Common Ruthenium Materials. *Surf. Interface Anal.* **2015**, *47* (11), 1072–1079. <https://doi.org/10.1002/sia.5852>.
- (103) Parida, K.; Das, J. Mg/Al Hydrotalcites: Preparation, Characterisation and Ketonisation of Acetic Acid. *J. Mol. Catal. A Chem.* **2000**, *151* (1–2), 185–192. [https://doi.org/10.1016/S1381-1169\(99\)00240-X](https://doi.org/10.1016/S1381-1169(99)00240-X).
- (104) Corma, A.; Fornés, V.; Martín-Aranda, R. M.; Rey, F. Determination of Base Properties of Hydrotalcites: Condensation of Benzaldehyde with Ethyl Acetoacetate. *J. Catal.* **1992**, *134* (1), 58–65. [https://doi.org/10.1016/0021-9517\(92\)90209-Z](https://doi.org/10.1016/0021-9517(92)90209-Z).
- (105) Tichit, D.; Coq, B. Catalysis by Hydrotalcites and Related Materials. *CATTECH* **2003**, *7* (6), 206–217. <https://doi.org/10.1023/B:CATT.0000007166.65577.34/METRICS>.
- (106) Sharma, S. K.; Parikh, P. A.; Jasra, R. V. Solvent Free Aldol Condensation of Propanal to 2-Methylpentenal Using Solid Base Catalysts. *J. Mol. Catal. A Chem.* **2007**, *278* (1–2), 135–144. <https://doi.org/10.1016/J.MOLCATA.2007.09.002>.
- (107) Shen, J.; Tu, M.; Hu, C. Structural and Surface Acid/Base Properties of Hydrotalcite-Derived MgAlO Oxides Calcined at Varying Temperatures. *J. Solid State Chem.* **1998**, *137* (2), 295–301. <https://doi.org/10.1006/JSSC.1997.7739>.
- (108) Apuzzo, J.; Cimino, S.; Lisi, L. Ni or Ru Supported on MgO/γ-Al₂O₃ Pellets for the Catalytic Conversion of Ethanol into Butanol. *RSC Adv.* **2018**, *8* (45), 25846–25855. <https://doi.org/10.1039/C8RA04310H>.
- (109) Kim, T. W.; Sahimi, M.; Tsotsis, T. T. The Preparation and Characterization of Hydrotalcite Thin Films. *Ind. Eng. Chem. Res.* **2009**, *48* (12), 5794–5801. https://doi.org/10.1021/IE900371R/ASSET/IMAGES/IE-2009-00371R_M011.GIF.
- (110) Alshakova, I. D.; Nikonov, G. I. Selective Synthesis of Secondary and Tertiary Amines by Reductive N-Alkylation of Nitriles and N-Alkylation of Amines and Ammonium Formate Catalyzed by Ruthenium Complex. *ChemCatChem* **2019**, *11* (21), 5370–5378. <https://doi.org/10.1002/CCTC.201900561>.
- (111) SCHROTH, W.; ANDERSCH, J.; SCHAEGLER, H.-D. +; SPITZNER, R. ChemInform Abstract: The Dimethylamine - Carbon Dioxide - Complex Dimcarb and Its Preparative Use. *ChemInform* **1990**, *21* (7), no-no.

- <https://doi.org/10.1002/CHIN.199007144>.
- (112) Basile, F.; Fornasari, G.; Gazzano, M.; Vaccari, A. Synthesis and Thermal Evolution of Hydrotalcite-Type Compounds Containing Noble Metals. *Appl. Clay Sci.* **2000**, *16* (3–4), 185–200. [https://doi.org/10.1016/S0169-1317\(99\)00053-8](https://doi.org/10.1016/S0169-1317(99)00053-8).
- (113) Kita, Y.; Kuwabara, M.; Yamadera, S.; Kamata, K.; Hara, M. Effects of Ruthenium Hydride Species on Primary Amine Synthesis by Direct Amination of Alcohols over a Heterogeneous Ru Catalyst. *Chem. Sci.* **2020**, *11* (36), 9884–9890. <https://doi.org/10.1039/D0SC03858J>.
- (114) Jessop, P. G.; Hsiao, Y.; Ikariya, T.; Noyori, R. Homogeneous Catalysis in Supercritical Fluids: Hydrogenation of Supercritical Carbon Dioxide to Formic Acid, Alkyl Formates, and Formamides. *J. Am. Chem. Soc.* **1996**. <https://doi.org/10.1021/ja953097b>.
- (115) Kröcher, O.; Köppel, R. A.; Baiker, A. Sol-Gel Derived Hybrid Materials as Heterogeneous Catalysts for the Synthesis of N,N-Dimethylformamide from Supercritical Carbon Dioxide. *Chem. Commun.* **1996**. <https://doi.org/10.1039/CC9960001497>.
- (116) Vernuccio, S.; Von Rohr, P. R.; Medlock, J. General Kinetic Modeling of the Selective Hydrogenation of 2-Methyl-3-Butyn-2-ol over a Commercial Palladium-Based Catalyst. *Ind. Eng. Chem. Res.* **2015**, *54* (46), 11543–11551. <https://doi.org/10.1021/acs.iecr.5b03424>.

Chapter 3

Cycloaddition of CO₂ in styrene oxide



“This chapter introduces about process intensification in flow reactor for the synthesis of styrene carbonate with detailed process development and reaction kinetics”

Chapter 3

Cycloaddition of CO₂ in styrene oxide

Abstract

The need for CO₂ utilization lies in transforming a greenhouse gas into valuable chemicals, addressing climate change and resource scarcity. Utilization technologies offer sustainable pathways to reduce CO₂ emissions while producing valuable products. In the proposed work, a sustainable process was developed for the utilization of CO₂ in one of the highly demandable product, styrene carbonate (SC), by cycloaddition of CO₂ in styrene oxide (SO).

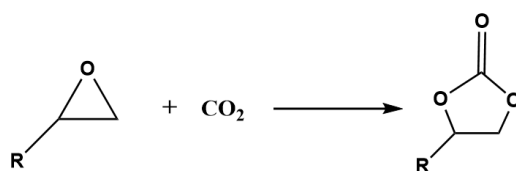
The cycloaddition of CO₂ in epoxides is a 100 % atom efficiency reaction that occurs on the catalytic surface with both acidic and basic sites. Styrene carbonate is five-membered cyclic carbonate with applications in several industries. In the present work, the batch and continuous flow processes are developed for styrene carbonate synthesis using tetrabutylammonium bromide as a catalyst. At the optimum conditions in the batch reactor, complete conversion of SO is observed with 85 % yield of SC at 120 °C, 20 bar pressure, 2 mole % catalyst, and CO₂:SO ratio of 1.5 within 2 hours. The reaction kinetics studies suggested fast reaction rates with the required activation energy of 97.9 kJ/mol to proceed with the reaction. Also, the estimated reaction conversion using obtained kinetic parameters resulted in a good fit with the experimental values with an r-squared value of 0.982.

The developed continuous flow process has several advantages over batch reactors in terms of high heat transfer rates, high surface-to-volume ratio, improved mixing, and reduced reactant concentrations at any particular time. At optimum flow conditions, 95 % conversion of SO is observed with 79 % SC yield at 80 °C within 80 minutes of residence time.

The developed continuous flow process provides a practical and sustainable approach towards CO₂ utilization and cyclic carbonate synthesis.

3.1 Introduction

The increasing concentration of carbon dioxide (CO₂) in the earth's atmosphere has become a pressing global concern. CO₂ is a waste from various chemical and mechanical industries making it an inexpensive, renewable and infinite carbon source. Hence, it is a fascinating challenge for the development of chemical processes which can use CO₂ as a feedstock for the production of valuable industrial chemicals, fuels, plastic precursors, etc¹⁻⁵. Although CO₂ is cheaply available, its utilization has become challenging due to several limitations like energy requirements, scale and efficiency, selectivity and catalysts, purified source of CO₂, and indirect carbon cost to power CO₂ conversion due to its thermodynamic stability^{6,7}. Despite such limitations, remarkable progress has been made in recent years in the utilization of CO₂ to value chemicals⁸⁻¹⁶.



Scheme 3.1: Cycloaddition of CO₂ in Epoxide

One potential strategy is to convert CO₂ to five-membered cyclic carbonates by 100 % atom economical reaction cycloaddition of CO₂ in epoxides, as shown in scheme 3.1^{17,18}. This transformation not only provides a practical and sustainable route for the utilization of CO₂ but also allows the synthesis of valuable compounds with diverse applications.

Epoxides, also known as oxiranes, are three-membered cyclic ethers containing a reactive strained oxygen bridge. Their unique reactivity and versatility have made them key intermediates in various organic transformations. The cycloaddition of CO₂ to epoxides is a highly efficient and atom-economical process leading to the formation of cyclic carbonates. These carbonates are valuable compounds due to their stability, polarity, and potential as building blocks for the synthesis of polymers, pharmaceuticals, and fine chemicals^{19,20} as shown in Figure 3.1.

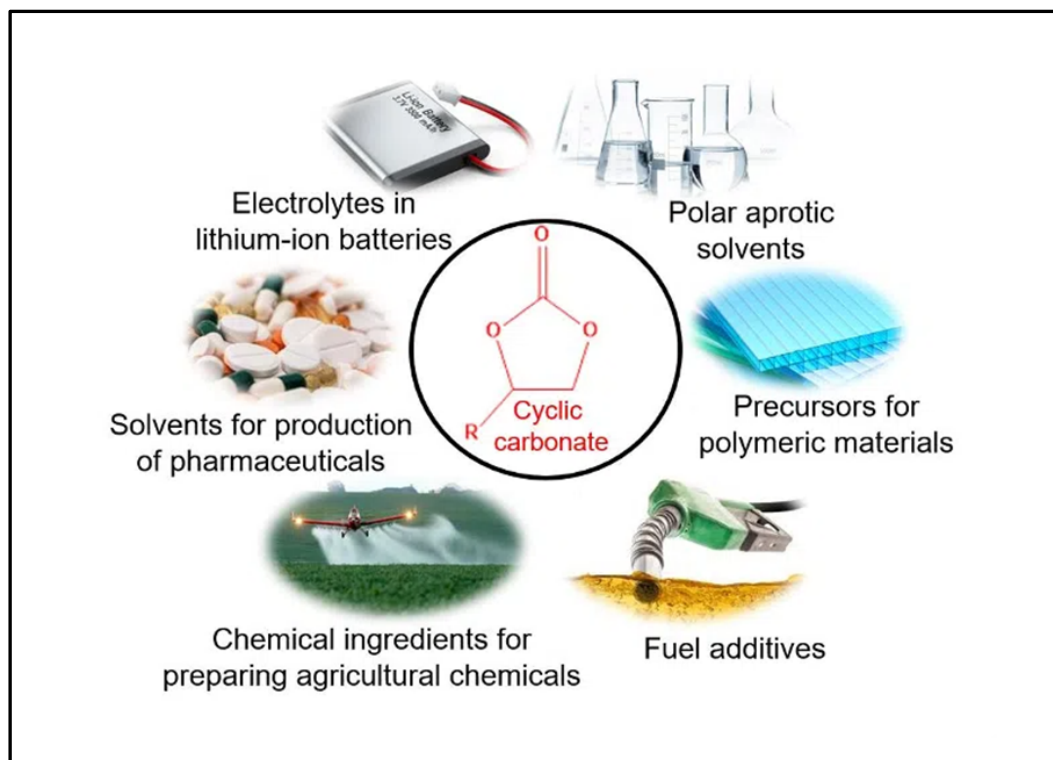


Figure 3.1: Industrial uses of cyclic carbonates²¹

Catalysts with both acidic and basic sites are required for the activation of epoxides and CO₂, and different homogeneous and heterogeneous catalysts like amines, quaternary ammonium salts, metal complexes, metal oxides, organo-catalyst, ionic liquids etc., are reported by several authors for this reaction^{22–29}. However, the detailed process development, reaction kinetics, and continuous flow synthesis of cyclic carbonates are scarcely available in the literature.

In this work, the process development with detailed reaction kinetics in a batch reactor is developed along with continuous flow reactor for the synthesis of styrene carbonate by cycloaddition of CO₂ in styrene oxide using tetrabutylammonium bromide (TBAB) as a catalyst.

3.2 Current industrial status cycloaddition of CO₂ in epoxides

Several industries have adopted the process for the synthesis of ethylene and propylene carbonates using the cycloaddition of the CO₂ route. The shell omega process uses ethylene carbonate produced from cycloaddition to synthesize ethylene glycol by hydrolysis, while in Japan, Asahi Kasei process, ethylene carbonate is reacted with methanol to produce dimethyl carbonate and ethylene glycol^{30,31} which is used to produce polycarbonate as shown in Figure 3.2.

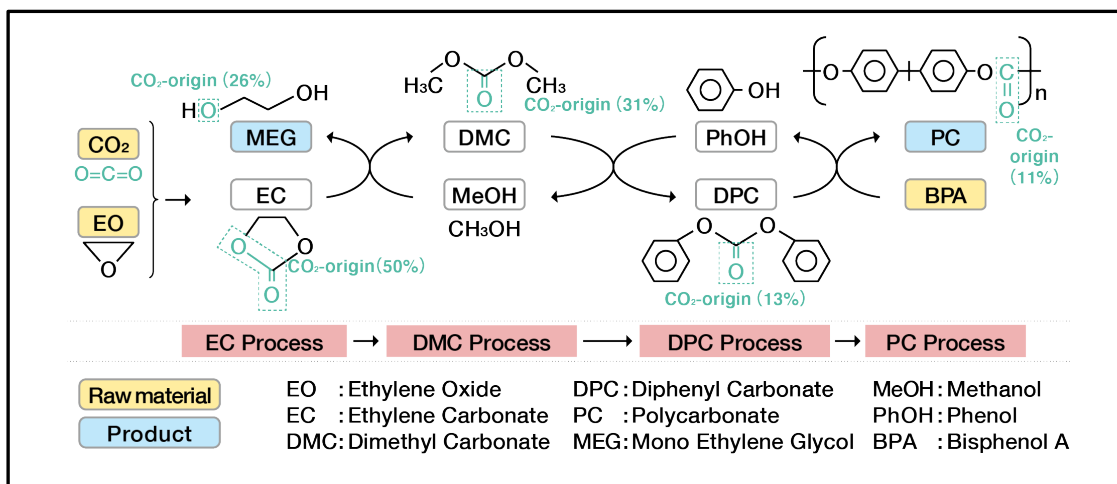


Figure 3.2: Asahi Kasei's polycarbonate production process³²

Earlier polycarbonate was produced using the phosgene route but with the developed process by Asahi Kasei, the process became phosgene-free, methylene chloride free and process water free.

Propylene carbonate is also being manufactured by industries like Huntsman Corp., BASF SE, Solvay SA, and Eastman chemical company by cycloaddition of CO₂ in propylene oxide using ammonium salts as a catalyst.

3.3 Cycloaddition of CO₂ in Styrene oxide – Prior art

Styrene oxide is a chemical compound from the family of epoxides derived from styrene, an aromatic hydrocarbon. It is highly reactive due to the presence of epoxy functional group, making it very useful in various industrial applications. The cycloaddition of CO₂ in styrene oxide results in lower reaction yields compared to ethylene and propylene oxide, probably due to the bulky epoxide and low reactivity of the β – carbon atom of SO³³. Various authors explored the homogenous and heterogeneous catalytic systems for the synthesis of styrene carbonate and proposed the mechanistic approach for the reaction.

Very scarce literature is available on the thermodynamics and reaction kinetics for the cycloaddition of CO₂ to styrene oxide. Rehman et al. studied the reaction kinetics with ZnBr₂ catalyst and TBAB as a co-catalyst³⁴. The authors found the reaction to be kinetically controlled and endergonic with positive values of enthalpy ($\Delta H = 18.5$ kJ/mol) of activation and Gibb's free energy ($\Delta G = 77.3$ kJ/mol) of activation.

The summary of different catalytic systems and their performance for the cycloaddition of CO₂ in styrene oxide is shown in Table 3.1. Although these catalysts show a radical effect on the reaction yields, their synthesis procedures and cost make it challenging for the process to scale up to an industrial scale. In the proposed research, styrene carbonate synthesis is optimized across tetrabutylammonium bromide (TBAB) catalyst with complete conversion of SO and more than 85 % yield of SC. The detailed process parameters, reaction kinetics, and flow synthesis are presented in the results and discussion section. Generally, the acid-base catalyst is required for the cycloaddition of CO₂ in an epoxide ring which is activated by the interaction with Lewis acid on an oxygen atom and ring opening by Lewis base or nucleophile to form an alkoxide intermediate as shown in figure 3.3 by Rehman et al³⁴. The negatively charged alkoxide helps to insert CO₂ and carbonate intermediate forms after rearrangement and displacement of nucleophiles. A similar mechanism is reported with various catalysts like metal halides, metal oxides, ammonium salts, ionic liquids, and organocatalyst-containing acid-base sites by researchers worldwide³⁵⁻⁴¹.

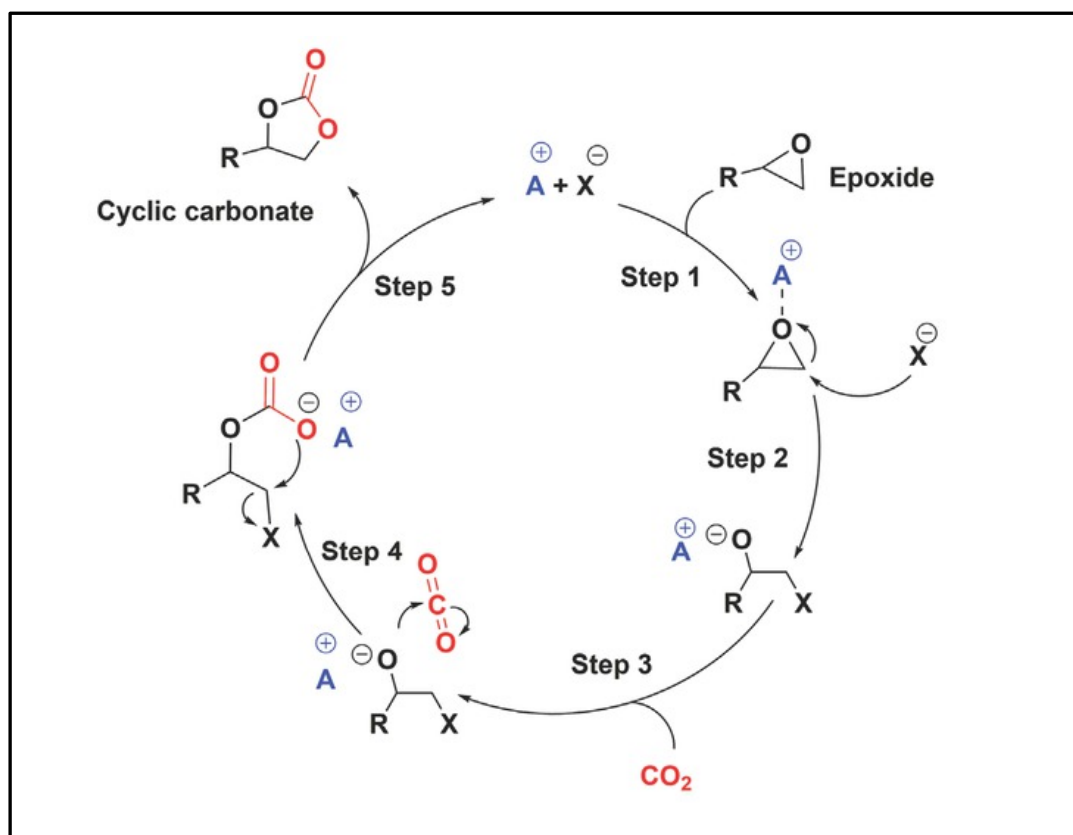


Figure 3.3: General reaction mechanism for cycloaddition of CO₂ to epoxide.

Table 3.1: Summary of catalytic systems for cycloaddition of CO₂ to styrene oxide

Catalyst	Co-Catalyst	Operating parameters				Catalyst performance			Ref.
		Temperature °C	Pressure bar	Time h	Conversion Mole %	Yield Mole %	TOF h ⁻¹		
MCM-41- Imi/Br	--	140	40	6	84.0	81.5	--	Appaturi et al. ⁴²	
ZnBr ₂	TBAB	100	6	1	86.0	--	--	Rehman et al. ³⁴	
ZnBr ₂	TBAI	80	80	--	--	--	686	Sun et al. ⁴³	
ZnBr ₂	TBAI	100	30	--	--	--	67	Ono et al. ⁴⁴	
MgO	--	135	20	6	--	--	14	Yamaguchi et al. ⁴⁵	
Zn-HAP	DMAP	100	10	10	--	--	308	Mori et al. ⁴⁶	
Co-Porphyrin complex	DMAP	100	26	6	--	--	38	Kruper et al. ⁴⁷	
[TBA] ₂ ZnBr ₂	--	80	50	0.5	94	94	--	Sun et al. ⁴⁸	
Cr-Salophen	TBAB/Silica	80	11	7	92	92	--	Balas et al. ⁴⁹	
Au/SiO ₂	ZnBr ₂ +TBAB	80	10	4	--	42	--	Sun et al. ⁵⁰	
Co - HMBED	DMAP	100	15	3	100	87.1	--	Pradhan et al. ⁵¹	
NAI/PPh ₃	PhOH	120	40	4	97	96	--	Shim et al. ⁵²	
PPNI / H ₂ O	--	45	10	--	39	38	--	Alassmy et al. ⁵³	
[BMIM]Cl	ZnBr ₂	80	140	1	100	100	--	Sun et al. ⁴⁸	

3.4 Experimental procedures

3.4.1 Batch reaction procedure and reaction monitoring

Experiments were carried out in a 50ml high-pressure reactor supplied by Parr instrument company. The reactor was equipped with a dip tube, pressure gauge, digital pressure sensor, temperature sensor and overhead magnetic drive, as shown in Figures 3.4 and 3.5.

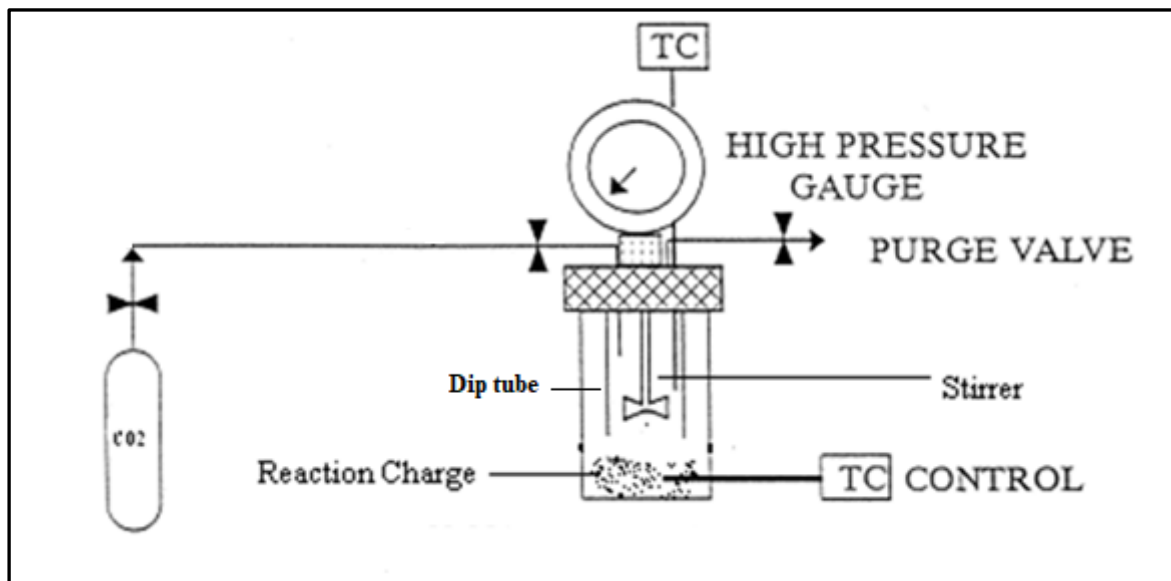


Figure 3.4: Schematic of high-pressure batch reactor

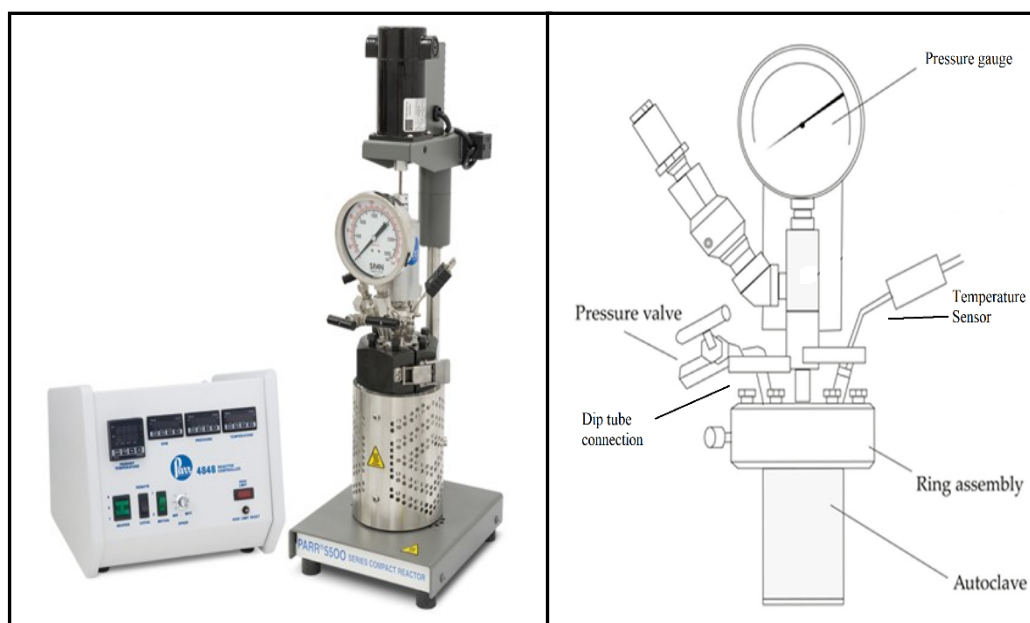


Figure 3.5: Actual image of high-pressure batch reactor and detailed sketch

The liquid solvent and reactants with catalyst were fed to the reactor vessel, and after packing the reactor bomb with its head, CO₂ was purged through a dip tube 2 – 3 times to remove air present in the reactor. After cleansing, CO₂ was fed to the reactor with the required amount from the cylinder directly, and the reactor was heated to the required temperature. On completion of the reaction, unreacted CO₂ was removed using a valve and liquid reaction mass was analyzed for composition.

GC-MS confirmed the products, and their distribution was quantified using gas chromatography supplied by Agilent technologies equipped with an HP-50 column connected to an FID detector by an external calibration method. In this method, the calibration curve of known concentrations for compounds to their GC responses was determined first. The response factor is used to quantify the exact quantities present in the reaction mass. The detailed GC method, calibration curve and GC peak separation is shown in supporting information table S-1.2 and figures S- 1.3 and 1.4 respectively. The reaction parameters were calculated using traditional formulae as mentioned below:

$$\% \text{ Conversion} = \frac{\text{Initial moles} - \text{final moles of SO}}{\text{Initial moles of SO}} * 100 \quad (1)$$

$$\% \text{ Selectivity} = \frac{\text{Moles of desired product formed}}{\text{Moles of SO converted}} * 100 \quad (2)$$

$$\% \text{ Yield} = \frac{\text{Moles of desired product formed}}{\text{Initial moles of SO}} * 100 \quad (3)$$

3.4.2 Continuous flow reactor development

Depending upon the batch reaction kinetics, a continuous flow coil tube reactor is developed in-house, as shown in Figures 3.6 and 3.7. The solvent (DMF), styrene oxide, and catalyst (TBAB) were mixed and fed using a high-pressure syringe pump supplied by Teledyne ISCO, and CO₂ was inserted through a mass flow controller provided by Bronkhorst Instrumentation. Both the reactants were passed through a static mixer to ensure diffusion of CO₂ in a solvent, followed by a preheater and coiled reactor. The temperature of the reactor was controlled with a PID controller, and the reaction mass was cooled down using a coiled condenser connected to the reactor. Jasco's back pressure regulator connected after the condenser maintained the required pressure throughout the system. The actual image of the reactor setup is shown in Figure 3.7.

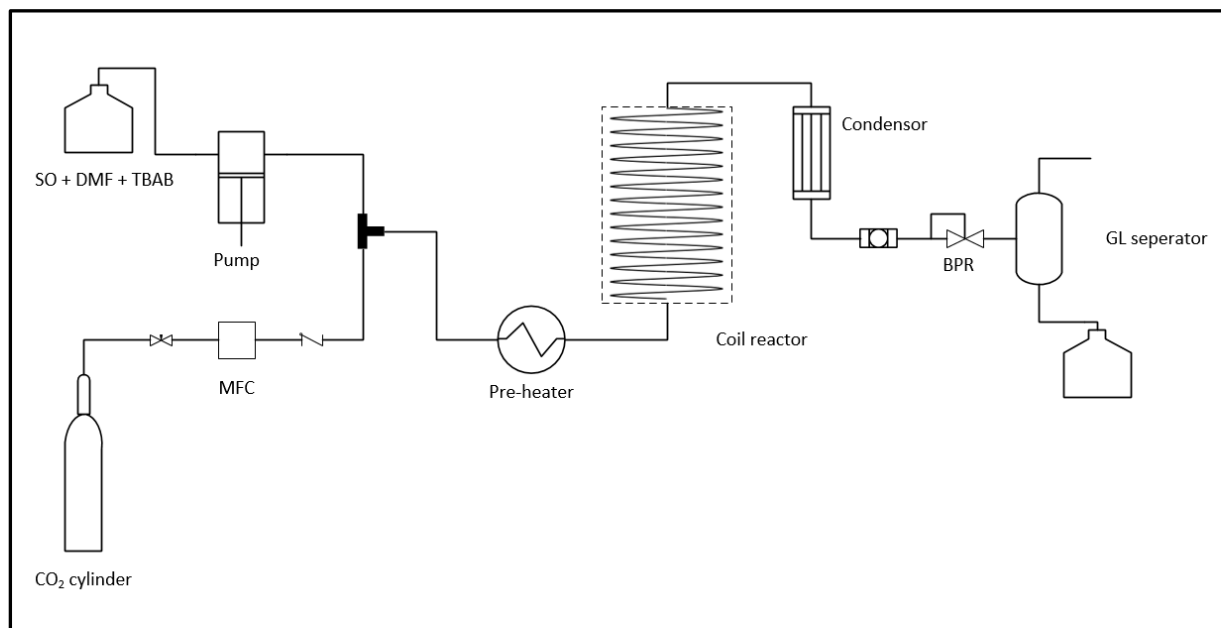


Figure 3.6: Continuous flow reactor PFD for cycloaddition of CO₂ in epoxide

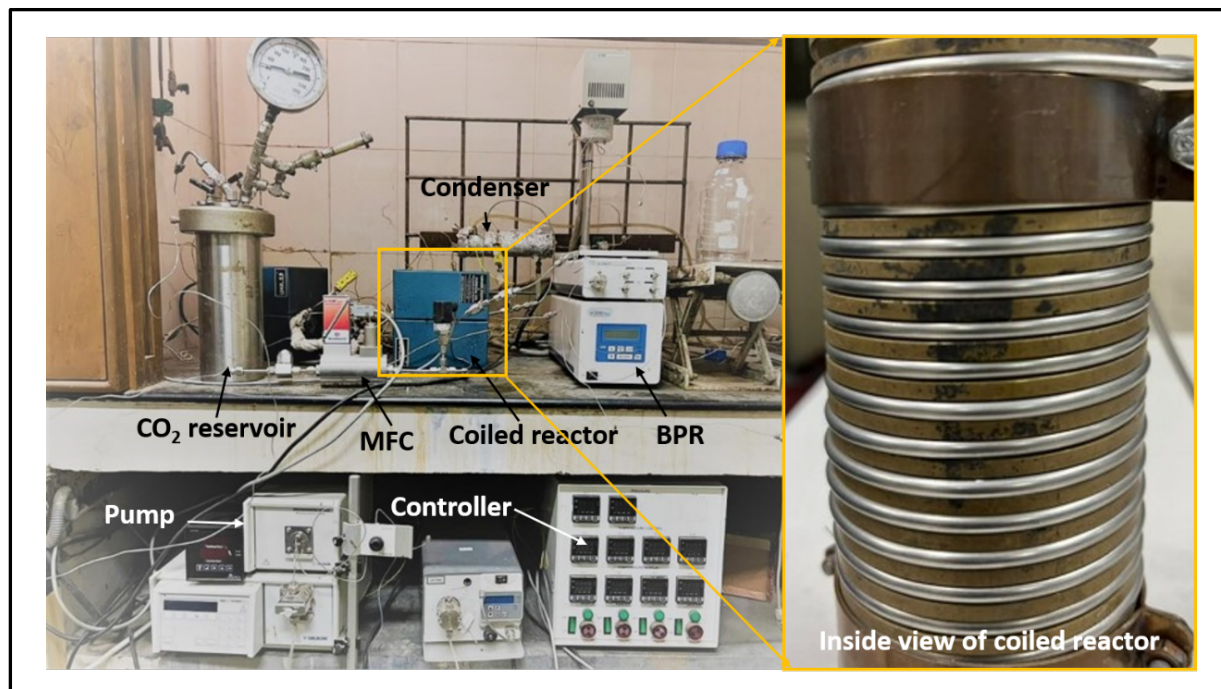


Figure 3.7: Actual image of continuous flow reactor

3.5 Results and Discussion

3.5.1 Catalyst screening

As discussed earlier in the mechanistic approach for cycloaddition reaction, catalysts with both acidic and basic sites are required to carry out the reaction. A series of catalysts with these properties are screened for the reaction, as shown in Figure 3.8. The heterogeneous catalysts like 5% Ru/Al₂O₃ (5 % RA), pseudo-boehmite (PB), and mixed metal oxides of transition metals (CLR, CSR and MAR) shown the conversion of styrene oxide, but the selectivity is more towards the parallel reaction resulting phenyl acetaldehyde formed by isomerization reaction^{54,55}. The phenyl acetaldehyde can also be produced by dehydration of styrene glycol in the presence of acidic sites⁵⁶. While using TBAB as a co-catalyst with these heterogeneous catalysts has resulted in partial styrene carbonate yield. It was observed that the catalyst - tetra butyl ammonium bromide (TBAB) alone shows the maximum output without the addition of a co-catalyst which various authors have also reported. It is concluded that the cycloaddition requires a specific combination of basic and acidic sites present in TBAB; any additional site can lead to the formation of by-products. Also, the quantity of the catalyst (TBAB) loading plays very crucial role in selective product formation and discussed in further sections. Thus, the same catalyst is considered for further optimization and development of continuous flow process.

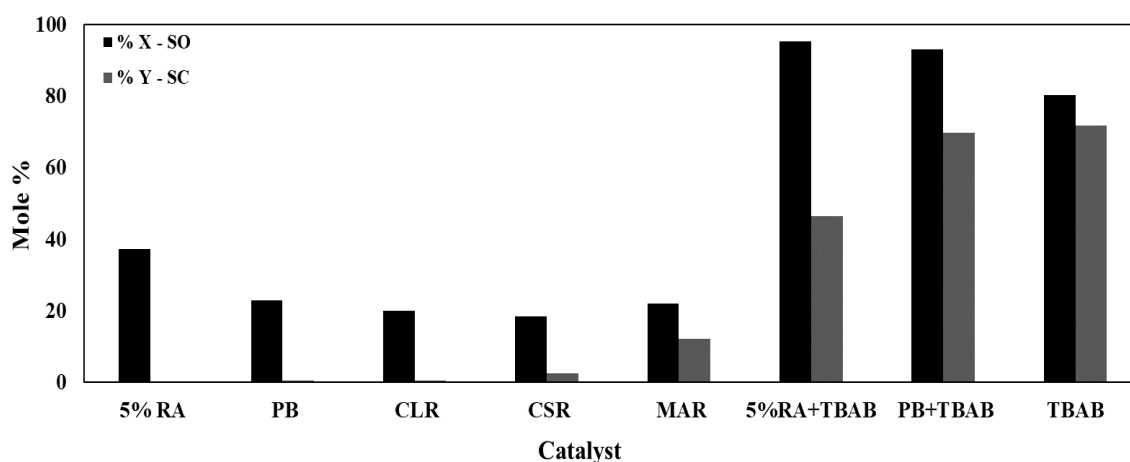


Figure 3.8: Catalyst screening. Reaction conditions: Catalyst 5 mole %, temperature 120 °C, time 2 h, CO₂:SO 1.5, total pressure 20 bar, solvent: DMF 15 ml, SO 2 gms.

3.5.2 Batch process optimization

3.5.2.1 Effect of reaction temperature

The reaction temperature showed a radical effect on the selection of products due to the close activation energies of side reactions. The isomerization of styrene oxide can lead to phenyl acetaldehyde and dehydration of styrene glycol, which produces in reaction yields to phenyl acetaldehyde in the presence of acidic sites as discussed earlier⁵⁴⁻⁵⁶. As shown in Figure 3.9, with 2 mole % of TBAB as a catalyst, a CO₂:SO mole ratio of 1.5 and pressure of 20 bar, the yield of styrene carbonate (% Y) increases till 140 °C to the maximum value of 84 % while, sudden drop in selectivity is observed after a further increase in temperature resulting the formation of phenyl acetaldehyde within 2 hours.

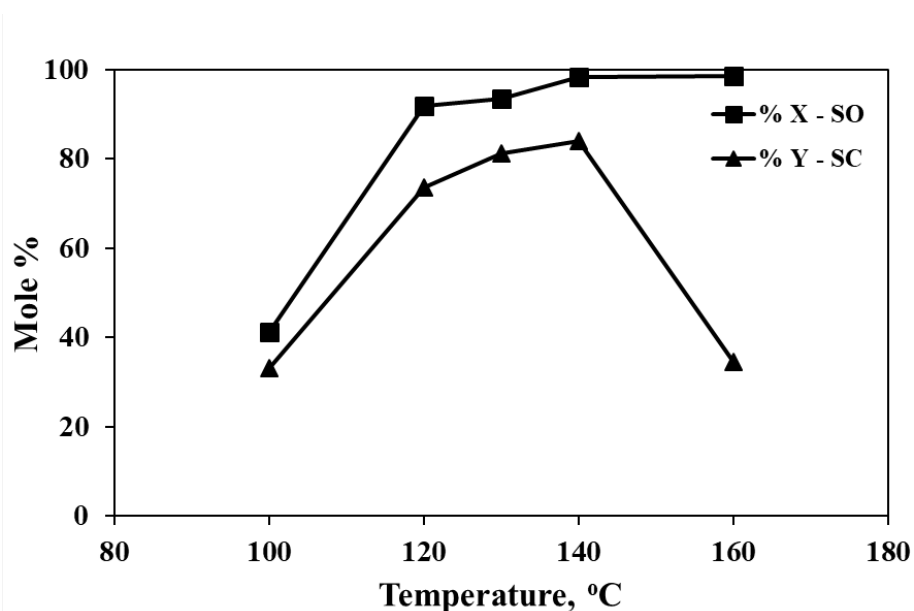


Figure 3.9: Effect of reaction temperature. Reaction conditions: Catalyst (TBAB) 2 mole %, time 2 h, CO₂:SO 1.5, total pressure 20 bar, solvent: DMF 15 ml, SO 2 gms.

3.5.2.2 Effect of catalyst loading

TBAB has strong cation and anion, making it both acidic and basic sites available for reactions. Its concentration in the reaction media plays a vital role in the selective cycloaddition of CO₂ in styrene oxide. As shown in Figure 3.10 a, at 140 °C, the increased concentration of TBAB promotes side reactions, while at lower temperatures (Figure 3.10 b&c), the yield of by-products is less due to a lack of activation energy.

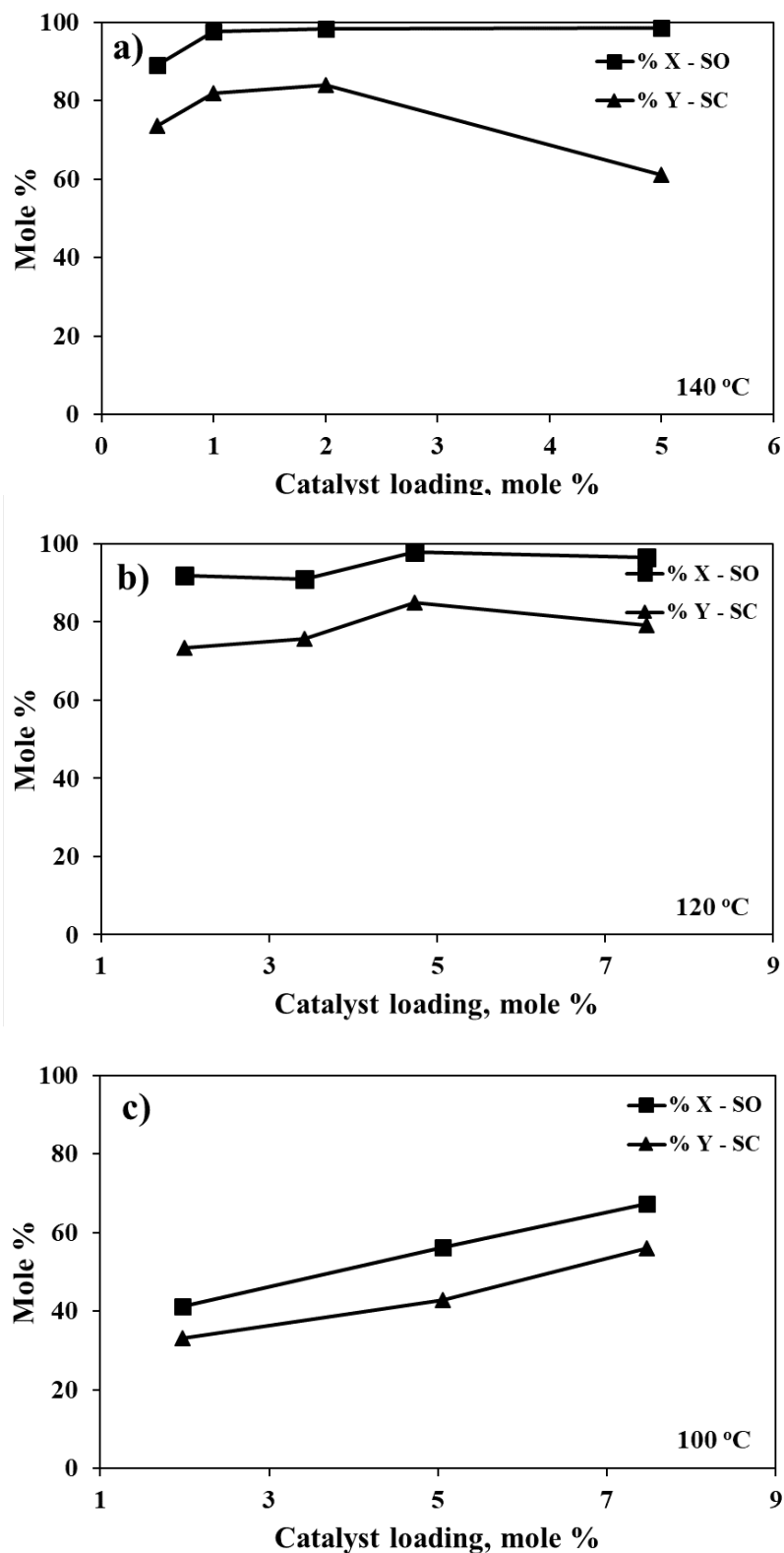


Figure 3.10: Effect of catalyst loading. Reaction conditions: Catalyst TBAB, time 2 h, CO₂:SO 1.5, total pressure 20 bar, solvent: DMF - 15 ml, SO 2 gms.

3.5.2.3 Effect of pressure

CO₂ is highly soluble in DMF with solubility of 3.3 mol/kg at 20 bar pressure⁵⁷, making the reaction homogeneous in liquid form and proceeding without mass transfer limitations. The elevated pressure increases the solubility of CO₂ in DMF as a solvent, and as shown in Figure 3.11, the reaction conversion (% X) increases with pressure up to 20 bar. The complete conversion with 84 % yield (% Y) of styrene carbonate was observed at 140 °C, 2 mole % catalyst, and 20 bar pressure within 2 hours. Further, the increase in pressure did not have any effect on reaction parameters. At lower pressure(s), reaction yield and conversions are less due to the lesser diffusion of CO₂.

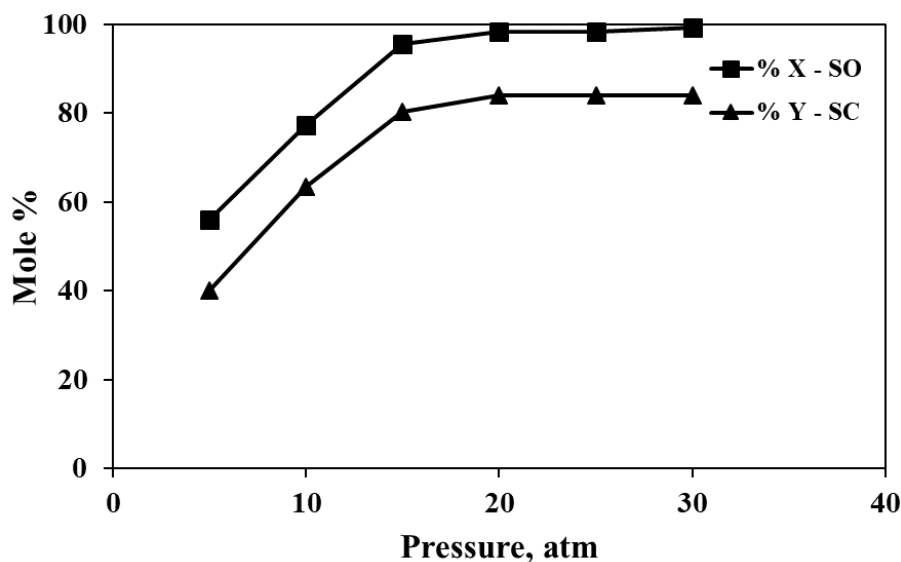


Figure 3.11: Effect of pressure. Reaction conditions: Catalyst TBAB 2 mole %, time 2 h, CO₂:SO 1.5, temperature 140 °C, solvent: DMF 15 ml, SO 2 gms.

3.5.2.4 Effect of reaction time

The cycloaddition of CO₂ in styrene oxide is relatively fast, and the reaction conversions with respect to time are shown in Figure 3.12. Complete conversion of styrene oxide is observed within 2 hours at 140 °C, whereas the initial rate is very high, and 85 % conversion was achieved within the first 40 minutes. The reaction conversion and yield at lower temperatures gradually increase with time and are shown in Figures 3.12 b & c. Also, as seen in Figure 3.12, at the very initial stage (0 – 10 min), the selectivity towards styrene carbonate is complete. With respect to time, the formation of styrene glycol is increasing, resulting in a lower yield of carbonate. The detailed reaction kinetics are discussed in the following section.

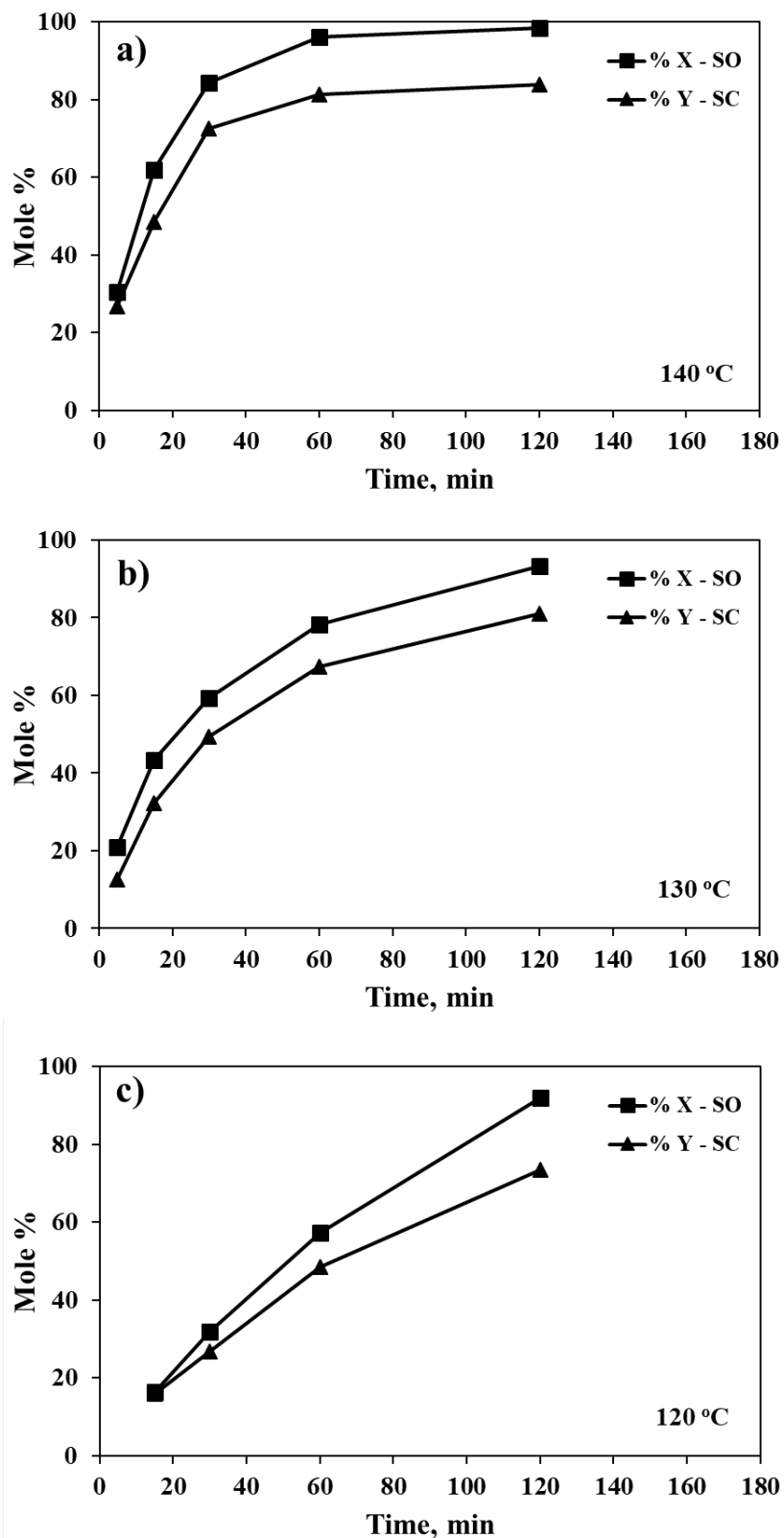


Figure 3.12: Effect of reaction time. Reaction conditions: Catalyst TBAB 2 mole %, CO₂:SO 1.5, total pressure 20 bar, solvent: DMF 15 ml, SO 2 gms.

3.5.2.5 Effect of solvent

The effect of solvent for cycloaddition of CO₂ in styrene oxide was studied at 120 °C reaction temperature for 2 hours of residence time in a batch reactor. As shown in Figure 3.13, dimethyl formamide (DMF) has shown the best activity for CO₂ addition in styrene oxide, probably due to the polar nature and the amide group may act as a good promoter⁵⁸. Also, the solubility of CO₂ in DMF is more significant than other solvents compared, making the reaction mass homogenous and free from mass transfer limitations⁵⁹. With water as a solvent, complete styrene oxide is converted to styrene glycol by hydration reaction and with methanol also the same trend is observed where selectivity for styrene glycol is more than styrene carbonate.

Reactions without solvents are considered one of the main principles in green chemistry⁶⁰ and within 2 hours, 45 % conversion with 90 % selectivity is observed without the use of any solvent. The lesser conversions are due to gas–liquid mass transfer limitation in batch reaction, but the selectivity number suggests better reaction yields for a longer time.

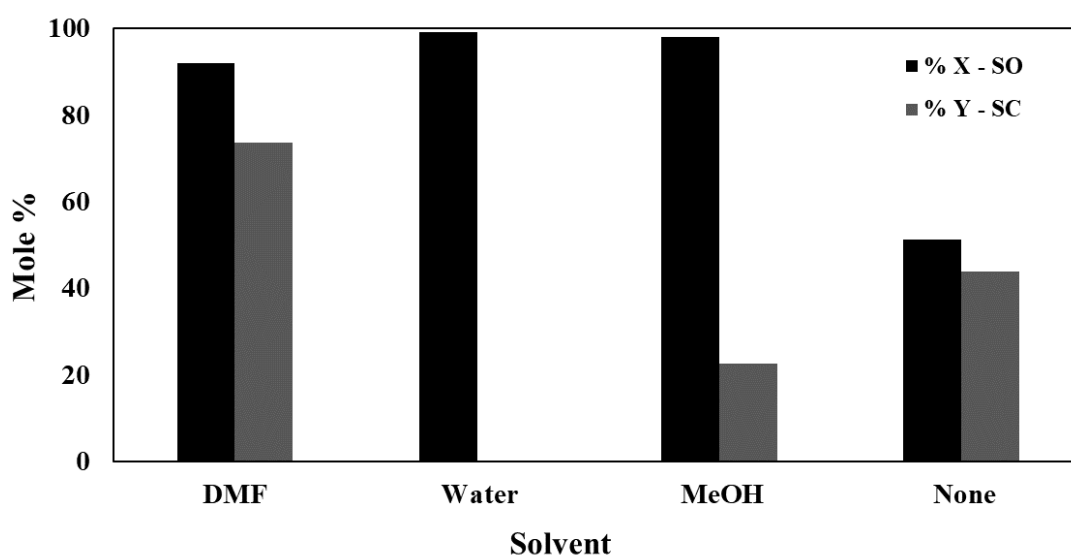


Figure 3.13: Effect of solvent. Reaction conditions: time 2 h, catalyst TBAB 2 mole %, CO₂:SO 1.5, temperature 120 °C, total pressure 20 bar, solvent 15 ml, SO 2 gms.

3.5.2.6 Effect of CO₂:SO mole ratio

Experiments were carried out with excess CO₂ and observed that with a CO₂:SO mole ratio of 2.5 and further, there is no effect on reaction conditions, while at a mole ratio of 1 and 1.5, there is only a slight decrease in reaction yield, as shown in Figure 3.14. This indicates the excess CO₂ is not promoting any further reaction while the soluble CO₂ in the reaction media of SO and solvent (DMF) is reacting to yield SC. Thus the 1.5-mole ratio is considered the optimum with 95 % conversion of SO and 80 % yield at 120 °C within 2 hours.

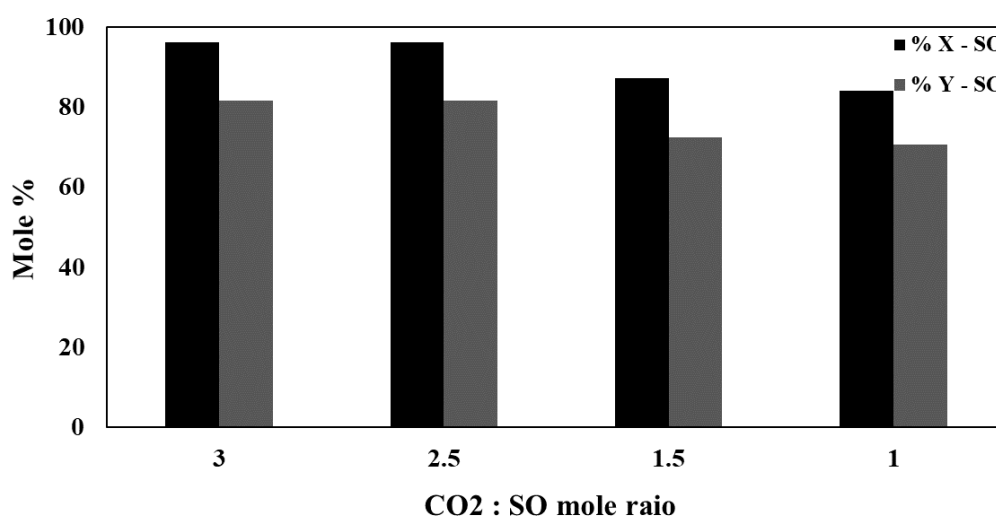
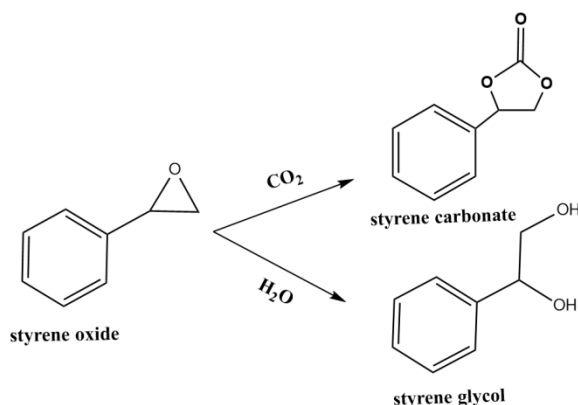


Figure 3.14: Effect of CO₂:SO mole ratio. Reaction conditions: time 2 h, catalyst TBAB 2 mole %, temperature 120 °C, total pressure 20 bar, solvent DMF 15 ml, SO 2 gms.

3.5.3 Reaction kinetics.

The kinetics were studied to understand reaction dynamics, and experiments were performed at various temperatures and times for model regression. The solubility of CO₂ in DMF (solvent) at higher pressure makes the reaction medium homogenous, and first-order reaction kinetic equations were used for parallel reactions, as mentioned in Scheme 3.2. The formation of styrene glycol occurs due to the presence of a small amount of water in the catalyst (TBAB).



Scheme 3.2: Reaction scheme for parallel reaction

The overall reaction rate for the consumption of styrene oxide (SO) can be written as :

$$-\frac{d[SO]}{dt} = k_1[SO] + k_2[SO] \quad (4)$$

Where, k_1 is the reaction rate constant for SC formation and

k_2 is the reaction rate constant for SG formation.

Subsequently, the rate of formation of styrene carbonate (SC) and styrene glycol (SG) can also be stated as follows:

$$\frac{d[SC]}{dt} = k_1[SO] \quad (5)$$

$$\frac{d[SG]}{dt} = k_2[SO] \quad (6)$$

Integrating equation (4) with respect to time leads to the final rate expression for SO as:

$$[SO] = [SO]_0 e^{-(k_1+k_2)t} \quad (7)$$

Where, $[SO]_0$ is the initial concentration of SO in the reaction medium.

The concentration equations for SC and SG were derived by substituting equation (7) in equations (5) & (6), resulting in the following equations.

$$\frac{d[SC]}{dt} = k_1 e^{-(k_1+k_2)t} \quad \text{and} \quad \frac{d[SG]}{dt} = k_2 e^{-(k_1+k_2)t}$$

Upon integrating the above equations with boundary conditions of the initial concentration of SG and SC to zero, the final concentration profiles were estimated.

$$[SC] = \frac{k_1 [SO]_0}{k_1+k_2} [1 - e^{-(k_1+k_2)t}] \quad (8)$$

$$[SG] = \frac{k_2 [SO]_0}{k_1 + k_2} [1 - e^{-(k_1 + k_2)t}] \quad (9)$$

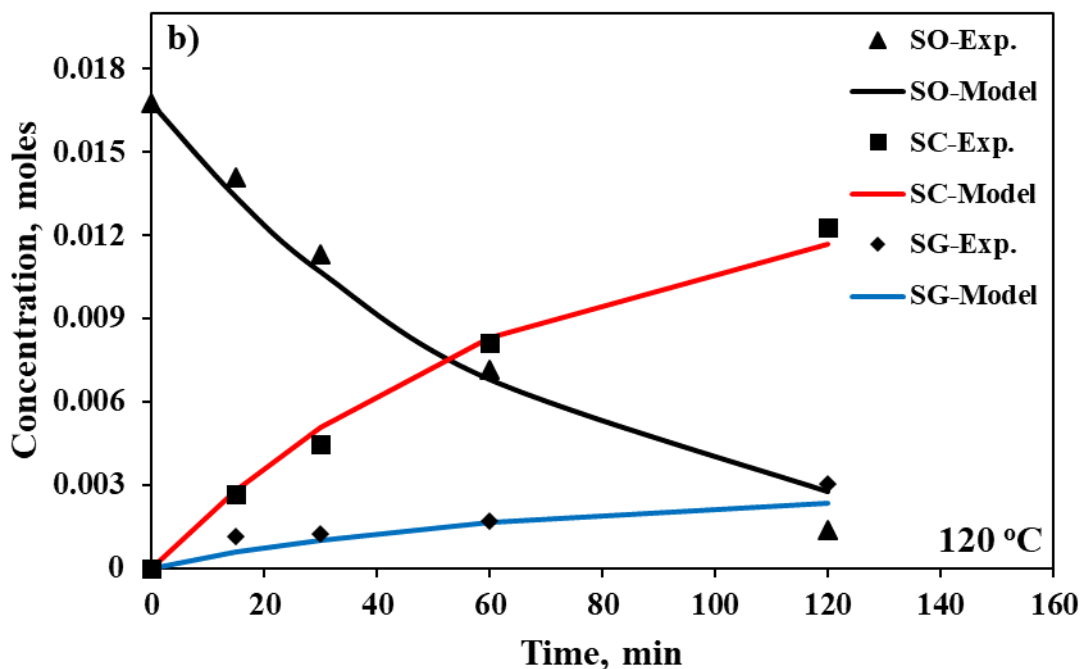
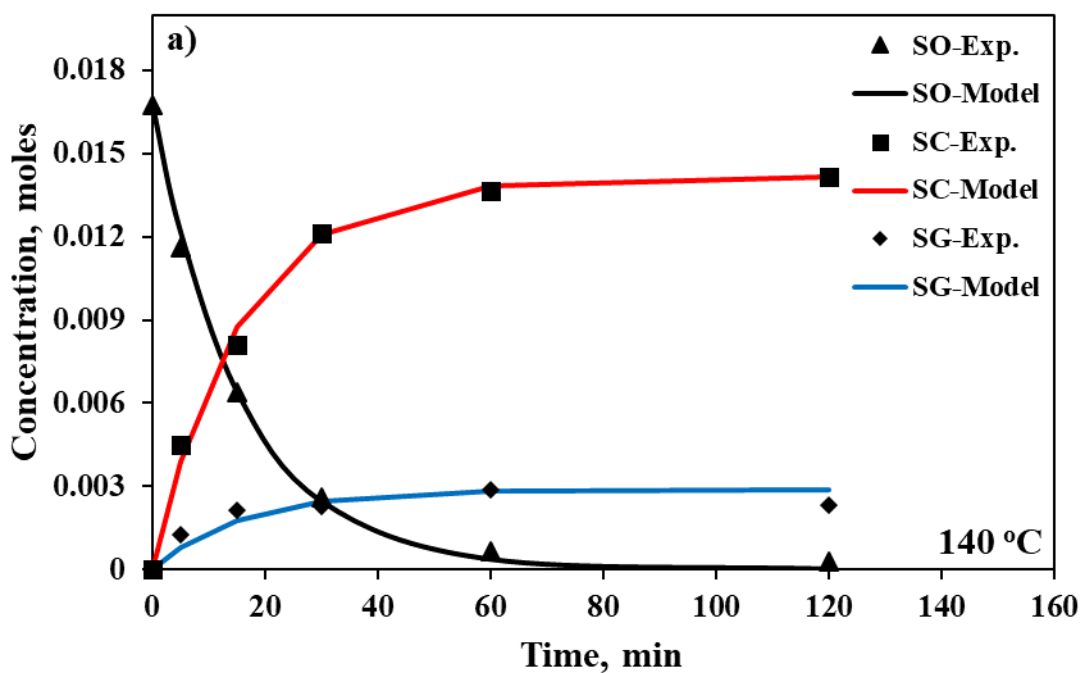


Figure 3.15: Comparison between experimental data with first order kinetic model.

The final model equations (7), (8) and (9) for concentrations were solved in the solver function of Microsoft Excel using an appropriate initial guess of kinetic coefficient and the least mean square error between experimental values and calculated values was minimized. Figure 3.15 compares the concentration values of all components using regressed kinetic parameters with experimental values at 140 °C and 120 °C. The model fitted very well with r-squared (R²) values of 0.995 and 0.990, respectively for both temperatures.

The estimated kinetic rate constant was used to calculate the activation energy of the reaction using the Arrhenius temperature dependence, as shown in equation (10).

$$k_R = k_0 \exp\left(\frac{-E_a}{R.T}\right) \quad \text{where, } k_R = k_1 + k_2 \quad (10)$$

The above equation is modified to estimate activation energy (E_a) using two rate constants at different temperatures as,

$$E_a = R \cdot \ln\left(\frac{k_{R1}}{k_{R2}}\right) * \left(\frac{T_1 \cdot T_2}{T_1 - T_2}\right) \quad (11)$$

Where, k_{R1} and k_{R2} are rate constant at 120 °C and 140 °C, respectively.

The final regressed kinetic parameters are shown in the following table:

Table 3.2: Estimated kinetic parameters using first-order homogenous kinetics.

Temperature Parameters	120 °C	140 °C	Units
$k_R (k_1 + k_2)$	0.015	0.065	min^{-1}
k_1	0.0125	0.054	min^{-1}
k_2	0.0025	0.011	min^{-1}
E_a	97.9		kJ.mol^{-1}

The above kinetic parameters were used to estimate reaction concentrations at 130 °C and it was observed the excellent fit of experimental data with estimated values and an r-squared value of 0.982, as shown in Figure 3.16. Also, the comparison of concentration values at different temperatures with experimental and estimated values is shown in Figure 3.17.

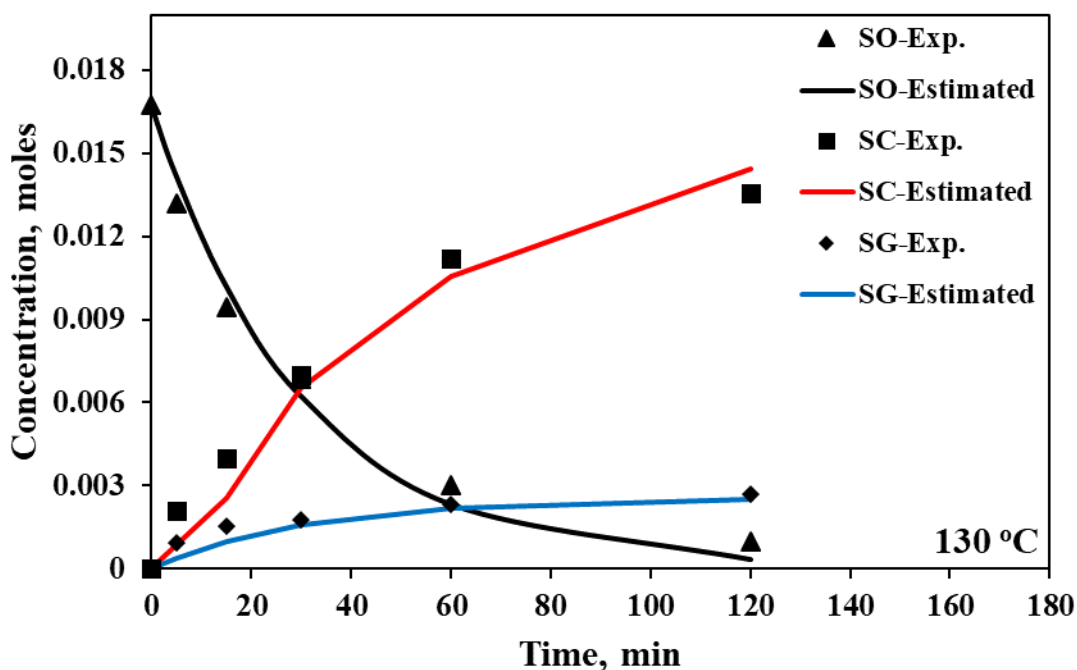


Figure 3.16: Estimated concentration profiles and experimental values at 130 °C

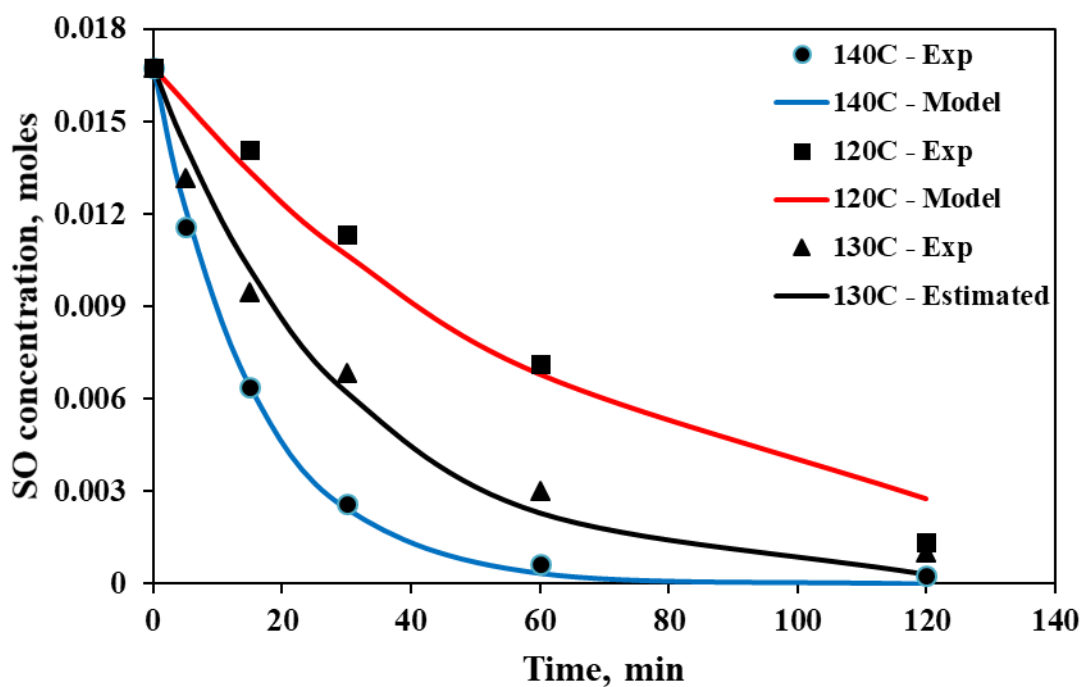


Figure 3.17: Comparison of experimental and model concentration values at different temperatures

3.5.4 Continuous flow synthesis

A flow reactor was built in-house for the continuous flow synthesis of styrene carbonate, as discussed in Figures 3.6 and 3.7 in the experimental section. Continuous flow reactors can often perform at lower temperatures than batch reactors due to higher heat transfer efficiency, reduced reactant concentration at any time, improved mixing, and lower heat loss⁶¹⁻⁶⁶. The same effect is observed when the cycloaddition of CO₂ was done in a flow reactor. Figure 3.18 shows that the reaction yields 80 % of styrene carbonate with 95 % SO conversion at 80 °C only with 80 min of residence time, 1.7 CO₂:SO mole ratio, and 2 mole % of catalyst loading. At the same time, it took 120 °C for batch reaction for similar performance. The increased temperature of 85 °C promoted the formation of phenyl acetaldehyde, as observed in the batch reactor also.

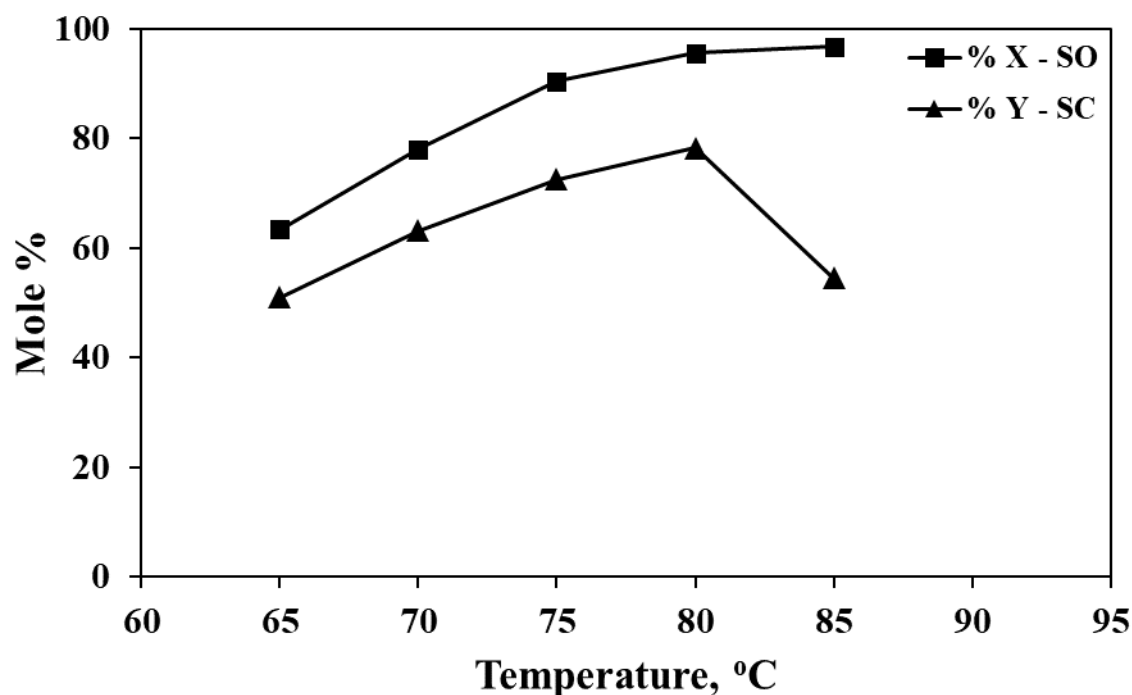


Figure 3.18: Effect of temperature in a flow reactor. Reaction conditions: Catalyst TBAB 2 mole %, residence time 80 min, CO₂:SO mole ratio 1.7, pressure 20 bar, Solvent DMF.

The study of excess CO₂ (CO₂:SO mole ratio) at different temperatures confirmed that reaction is not mass transfer controlled as the excess amount of CO₂ did not make any remarkable effect of reactions progress. As shown in Figure 3.19 a and b, reaction yields are similar at a CO₂:SO mole ratio of 1.2 and further. SC yield at 85 °C is lower due to the formation of isomer phenyl acetaldehyde, as discussed earlier.

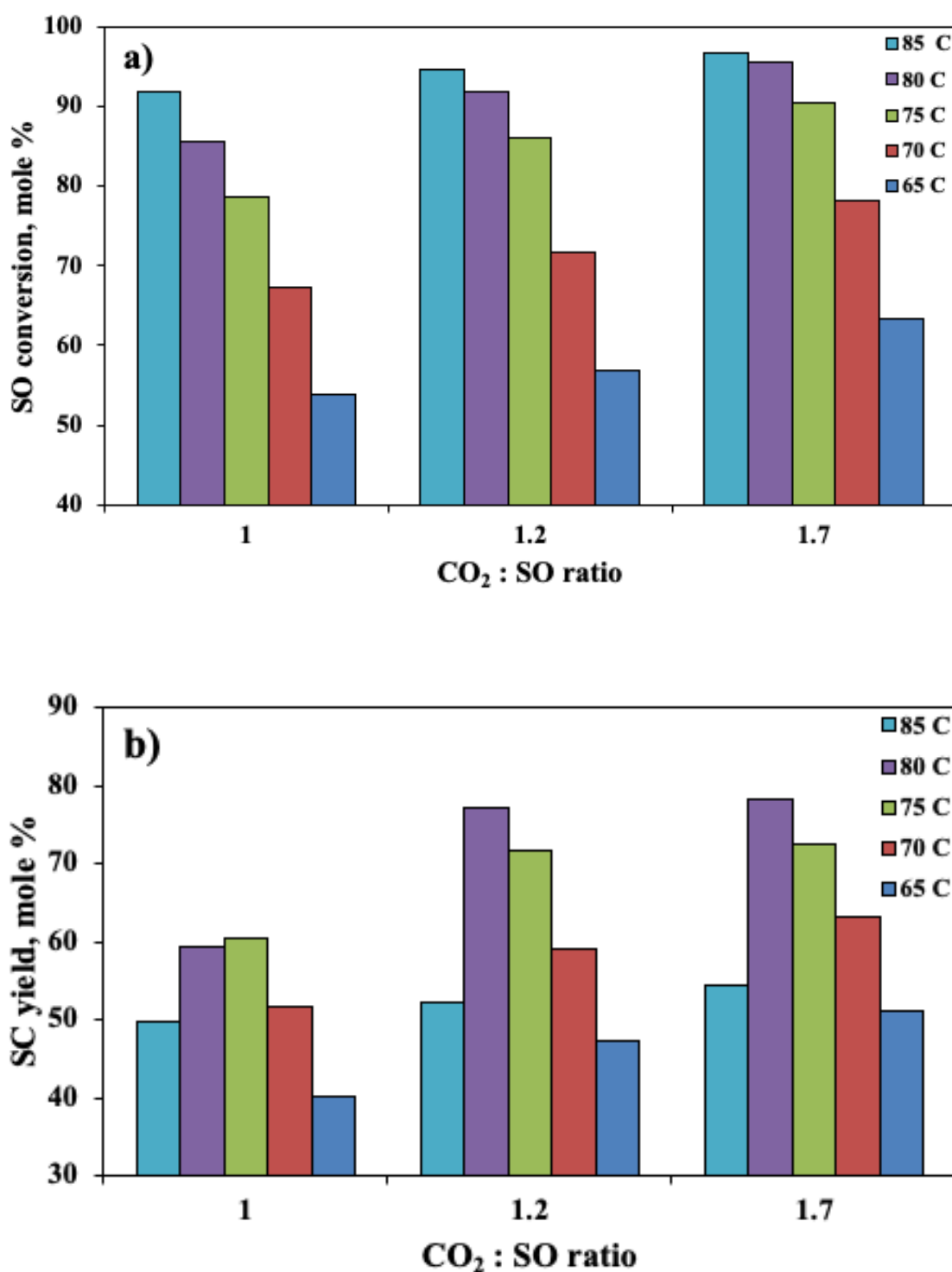


Figure 3.19: Effect of CO₂:SO mole ratio in a flow reactor. Reaction conditions: catalyst TBAB 2 mole %, pressure 20 bar, residence time 80 min, solvent DMF.

The increased pressure helped in increased solubility of CO₂ in solvent (DMF) and eventually resulted in higher reaction selectivity and conversion. As observed in the batch reactor, the

same trend is seen in the flow process (figure 3.20) that the reaction conversion and yield gradually increased up to 15 bar and further increased in pressure did not improve results.

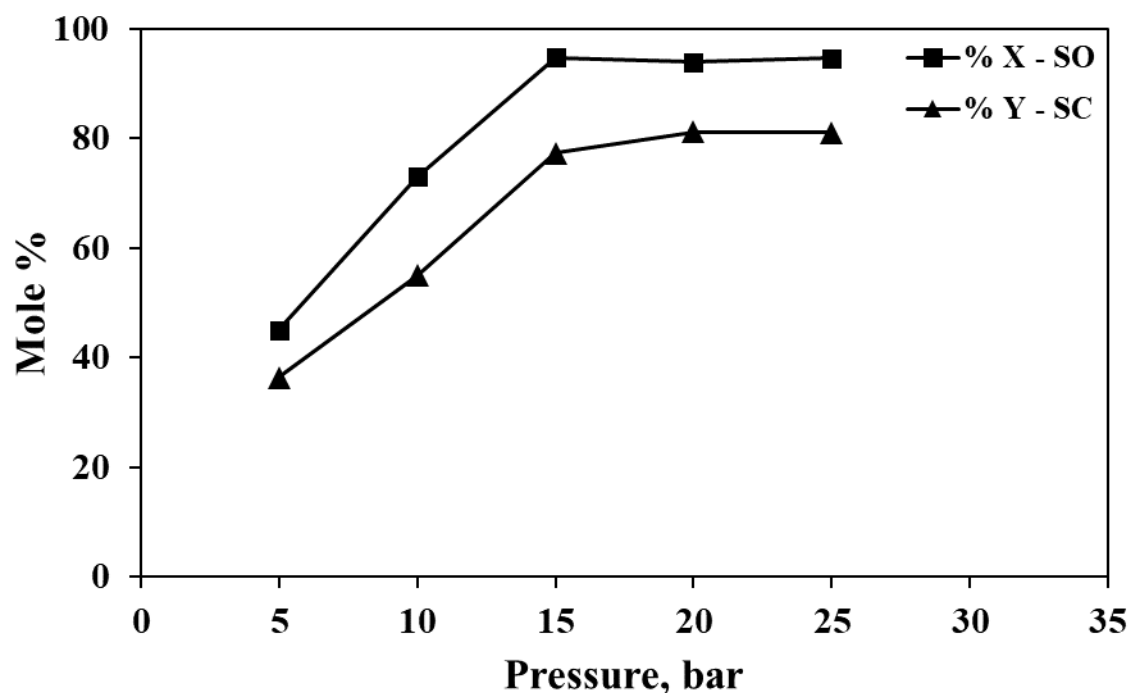


Figure 3.20: Effect of pressure in a flow reactor. Reaction conditions: temperature 80 °C, catalyst TBAB 2 mole %, residence time 80 min, CO₂:SO mole ratio 1.2, solvent DMF.

Finally, the effect of residence time was studied in the flow synthesis, and it was observed that, reaction conversion and SC selectivity gradually increased with residence time, as shown in Figure 3.21 and optimum conditions obtained for continuous flow synthesis of cycloaddition of CO₂ in styrene oxide.

As shown in Figure 3.21 a, the conversion of SO gradually increased with residence time and temperature and similar trends are observed for SC yield (Figure 3.21 b). With an increased residence time of 100 minutes, the reaction results are similar for 75 °C and 80 °C.

The final reaction parameters for the continuous flow synthesis of styrene carbonate are optimized to 80 °C, 80 min residence time, 15 bar pressure, and 1.2 CO₂:SO mole ratio with 95 % conversion of SO and 79 % yield of SC.

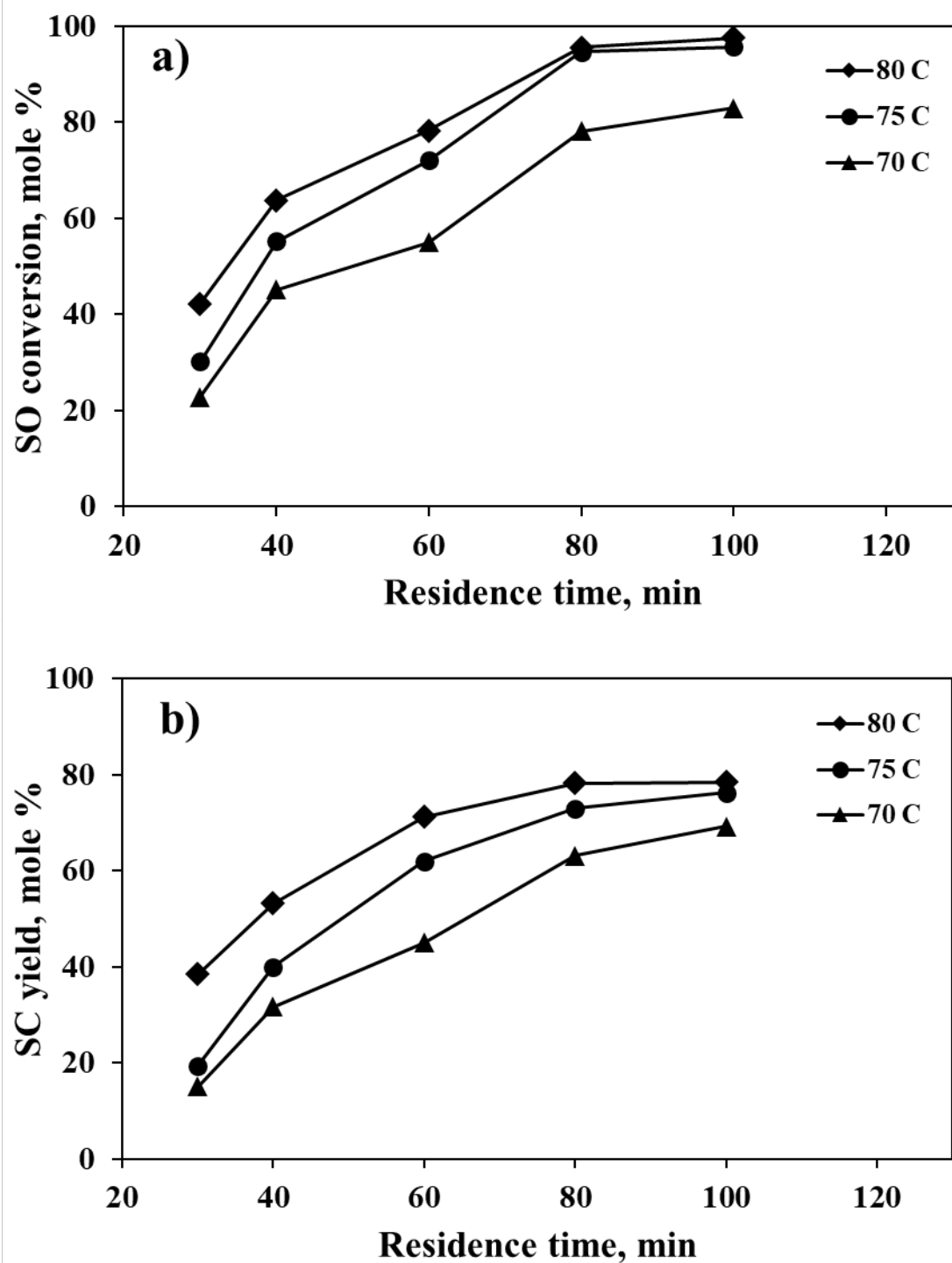


Figure 3.21: Effect of residence time in a flow reactor. Reaction conditions: catalyst TBAB 2 mole %, pressure 15 bar, CO₂:SO mole ratio 1.2, solvent DMF.

3.6 Conclusion and the path forward

Process for batch and continuous synthesis is developed for the cycloaddition of CO₂ to styrene oxide in the presence of tetrabutylammonium bromide as a catalyst. The reaction mechanism suggests the requirement of both basic and acid sites in the catalyst for the reaction, and TBAB has both strong cations and anions. Process optimization results show that the amount of catalyst and temperature plays a crucial role in the reaction to avoid side reactions. At the optimum conditions of 120 °C temperature, 20 bar pressure, 2 mole % catalyst loading, and 1.5-mole ratio of CO₂ to SO, complete conversion of styrene oxide is achieved with more than 85 % selectivity of styrene carbonate within 2 hours. Other side products like styrene glycol and phenyl acetaldehyde also get formed by the isomerization of SO. The choice of temperature and catalyst loading was a key factor in minimizing the by-products.

Reaction kinetics suggested fast reaction dynamics with an activation energy of 97.9 kJ/mol. The obtained kinetic parameters were used to estimate reaction conversions and yield at 130 °C, and it was observed a good fit of estimated and experimental values with an r-squared value of 0.983. Based on the reaction kinetics, a continuous flow reactor was developed, and the process was optimized at 80 °C, 80 minutes of residence time with 95 % conversion of SO and 80 % yield of SC.

The process is optimized in terms of reaction conversion and selectivities. The development of comprehensive kinetic model with mass transfer considerations and the downstream process development comprising the separation of products and solvents is the system's next goal, making it an industrially feasible process.

3.7 References

- (1) Lee, S. Y. T.; Ghani, A. A.; D'Elia, V.; Cokoja, M.; Herrmann, W. A.; Basset, J. M.; Kühn, F. E. Liberation of Methyl Acrylate from Metallalactone Complexes via M-O Ring Opening (M = Ni, Pd) with Methylation Agents. *New J. Chem.* **2013**, 37 (11), 3512–3517. <https://doi.org/10.1039/c3nj00693j>.
- (2) Hu, J.; Ma, J.; Zhu, Q.; Zhang, Z.; Wu, C.; Han, B. Transformation of Atmospheric CO₂ Catalyzed by Protic Ionic Liquids: Efficient Synthesis of 2-Oxazolidinones. *Angew. Chemie - Int. Ed.* **2015**, 54 (18), 5399–5403. <https://doi.org/10.1002/anie.201411969>.
- (3) Song, Q. W.; He, L. N. Robust Silver(I) Catalyst for the Carboxylative Cyclization of Propargylic Alcohols with Carbon Dioxide under Ambient Conditions. *Adv. Synth. Catal.* **2016**, 358 (8), 1251–1258. <https://doi.org/10.1002/adsc.201500639>.
- (4) Centi, G.; Quadrelli, E. A.; Perathoner, S. Catalysis for CO₂ Conversion: A Key Technology for Rapid Introduction of Renewable Energy in the Value Chain of Chemical Industries. *Energy Environ. Sci.* **2013**, 6 (6), 1711–1731. <https://doi.org/10.1039/C3EE00056G>.
- (5) Tsuji, Y.; Fujihara, T. Carbon Dioxide as a Carbon Source in Organic Transformation: Carbon–Carbon Bond Forming Reactions by Transition-Metal Catalysts. *Chem. Commun.* **2012**, 48 (80), 9956–9964. <https://doi.org/10.1039/c2cc33848c>.
- (6) Advances in Energy Systems Engineering. *Adv. Energy Syst. Eng.* **2017**. <https://doi.org/10.1007/978-3-319-42803-1>.
- (7) Von Der Assen, N.; Jung, J.; Bardow, A. Life-Cycle Assessment of Carbon Dioxide Capture and Utilization: Avoiding the Pitfalls. *Energy Environ. Sci.* **2013**, 6 (9), 2721–2734. <https://doi.org/10.1039/c3ee41151f>.
- (8) Li, X.; Duan, R.; Pang, X.; Gao, B.; Wang, X.; Chen, X. Rigid Linked Dinuclear Salph-Co(III) Catalyst for Carbondioxide/Epoxydes Copolymerization. *Appl. Catal. B Environ.* **2016**, 182, 580–586. <https://doi.org/10.1016/J.APCATB.2015.10.019>.
- (9) Darensbourg, D. J.; Kyran, S. J. Carbon Dioxide Copolymerization Study with a Sterically Encumbering Naphthalene-Derived Oxide. *ACS Catal.* **2015**, 5 (9), 5421–5430. https://doi.org/10.1021/ACSCATAL.5B01375/SUPPL_FILE/CS5B01375_SI_002.CIF.
- (10) Honda, M.; Tamura, M.; Nakagawa, Y.; Nakao, K.; Suzuki, K.; Tomishige, K. Organic Carbonate Synthesis from CO₂ and Alcohol over CeO₂ with 2-Cyanopyridine: Scope and Mechanistic Studies. *J. Catal.* **2014**, 318, 95–107. <https://doi.org/10.1016/J.JCAT.2014.07.022>.
- (11) Laserna, V.; Fiorani, G.; Whiteoak, C. J.; Martin, E.; Escudero-Adán, E.; Kleij, A. W. Carbon Dioxide as a Protecting Group: Highly Efficient and Selective Catalytic Access to Cyclic Cis-Diol Scaffolds. *Angew. Chemie Int. Ed.* **2014**, 53 (39), 10416–10419. <https://doi.org/10.1002/ANIE.201406645>.
- (12) Tóth, A.; Halasi, G.; Solymosi, F. Reactions of Ethane with CO₂ over Supported Au. *J. Catal.* **2015**, 330, 1–5. <https://doi.org/10.1016/J.JCAT.2015.07.006>.

- (13) Jiang, X.; Gou, F.; Jing, H. Alternating Copolymerization of CO₂ and Propylene Oxide Catalyzed by C₂v-Porphyrin Cobalt: Selectivity Control and a Kinetic Study. *J. Catal.* **2014**, *313*, 159–167. <https://doi.org/10.1016/J.JCAT.2014.03.008>.
- (14) Gao, X.; Yu, B.; Yang, Z.; Zhao, Y.; Zhang, H.; Hao, L.; Han, B.; Liu, Z. Ionic Liquid-Catalyzed C-S Bond Construction Using CO₂ as a C1 Building Block under Mild Conditions: A Metal-Free Route to Synthesis of Benzothiazoles. *ACS Catal.* **2015**, *5* (11), 6648–6652. https://doi.org/10.1021/ACSCATAL.5B01874/ASSET/IMAGES/LARGE/CS-2015-018745_0004.JPEG.
- (15) Lescot, C.; Nielsen, D. U.; Makarov, I. S.; Lindhardt, A. T.; Daasbjerg, K.; Skrydstrup, T. Efficient Fluoride-Catalyzed Conversion of CO₂ to CO at Room Temperature. *J. Am. Chem. Soc.* **2014**, *136* (16), 6142–6147. <https://doi.org/10.1021/JA502911E>.
- (16) Fu, X.; Jing, H. Quaternary Onium Modified SalenCoXY Catalysts for Alternating Copolymerization of CO₂ and Propylene Oxide: A Kinetic Study. *J. Catal.* **2015**, *329*, 317–324. <https://doi.org/10.1016/J.JCAT.2015.05.030>.
- (17) Yasuda, H.; He, L. N.; Sakakura, T.; Hu, C. Efficient Synthesis of Cyclic Carbonate from Carbon Dioxide Catalyzed by Polyoxometalate: The Remarkable Effects of Metal Substitution. *J. Catal.* **2005**, *233* (1), 119–122. <https://doi.org/10.1016/J.JCAT.2005.04.030>.
- (18) Werner, T.; Büttner, H. Phosphorus-Based Bifunctional Organocatalysts for the Addition of Carbon Dioxide and Epoxides. *ChemSusChem* **2014**, *7* (12), 3268–3271. <https://doi.org/10.1002/CSSC.201402477>.
- (19) Zou, B.; Hao, L.; Fan, L. Y.; Gao, Z. M.; Chen, S. L.; Li, H.; Hu, C. W. Highly Efficient Conversion of CO₂ at Atmospheric Pressure to Cyclic Carbonates with in Situ-Generated Homogeneous Catalysts from a Copper-Containing Coordination Polymer. *J. Catal.* **2015**, *329*, 119–129. <https://doi.org/10.1016/J.JCAT.2015.05.002>.
- (20) Ahmed, M.; Sakthivel, A. Preparation of Cyclic Carbonate via Cycloaddition of CO₂ on Epoxide Using Amine-Functionalized SAPO-34 as Catalyst. *J. CO₂ Util.* **2017**, *22*, 392–399. <https://doi.org/10.1016/J.JCOU.2017.10.021>.
- (21) Marciniak, A. A.; Lamb, K. J.; Ozorio, L. P.; Mota, C. J. A.; North, M. Heterogeneous Catalysts for Cyclic Carbonate Synthesis from Carbon Dioxide and Epoxides. *Curr. Opin. Green Sustain. Chem.* **2020**, *26*, 100365. <https://doi.org/10.1016/J.COGSC.2020.100365>.
- (22) Paddock, R. L.; Nguyen, S. T. Chemical CO(2) Fixation: Cr(III) Salen Complexes as Highly Efficient Catalysts for the Coupling of CO(2) and Epoxides. *J. Am. Chem. Soc.* **2001**, *123* (46), 11498–11499. <https://doi.org/10.1021/JA0164677>.
- (23) Yano, T.; Matsui, H.; Koike, T.; Ishiguro, H.; Fujihara, H.; Yoshihara, M.; Maeshima, T. Magnesium Oxide-Catalysed Reaction of Carbon Dioxide with Anepoxide with Retention of Stereochemistry. *Chem. Commun.* **1997**, No. 12, 1129–1130. <https://doi.org/10.1039/A608102I>.
- (24) Xu, J.; Xu, M.; Wu, J.; Wu, H.; Zhang, W. H.; Li, Y. X. Graphene Oxide Immobilized with Ionic Liquids: Facile Preparation and Efficient Catalysis for Solvent-Free Cycloaddition of CO₂ to Propylene Carbonate. *RSC Adv.* **2015**, *5* (88), 72361–72368. <https://doi.org/10.1039/C5RA13533H>.

- (25) Whiteoak, C. J.; Kielland, N.; Laserna, V.; Escudero-Adán, E. C.; Martin, E.; Kleij, A. W. A Powerful Aluminum Catalyst for the Synthesis of Highly Functional Organic Carbonates. *J. Am. Chem. Soc.* **2013**, *135* (4), 1228–1231. https://doi.org/10.1021/JA311053H/SUPPL_FILE/JA311053H_SI_004.CIF.
- (26) Zhou, H.; Wang, G. X.; Zhang, W. Z.; Lu, X. B. CO₂ Adducts of Phosphorus Ylides: Highly Active Organocatalysts for Carbon Dioxide Transformation. *ACS Catal.* **2015**, *5* (11), 6773–6779. https://doi.org/10.1021/ACSCATAL.5B01409/ASSET/IMAGES/LARGE/CS-2015-01409B_0009.JPEG.
- (27) Liu, M.; Liang, L.; Li, X.; Gao, X.; Sun, J. Novel Urea Derivative-Based Ionic Liquids with Dual-Functions: CO₂ Capture and Conversion under Metal- and Solvent-Free Conditions. *Green Chem.* **2016**, *18* (9), 2851–2863. <https://doi.org/10.1039/C5GC02605A>.
- (28) Carvalho Rocha, C.; Onfroy, T.; Pilmé, J.; Denicourt-Nowicki, A.; Roucoux, A.; Launay, F. Experimental and Theoretical Evidences of the Influence of Hydrogen Bonding on the Catalytic Activity of a Series of 2-Hydroxy Substituted Quaternary Ammonium Salts in the Styrene Oxide/CO₂ Coupling Reaction. *J. Catal.* **2016**, *333*, 29–39. <https://doi.org/10.1016/J.JCAT.2015.10.014>.
- (29) Aoyagi, N.; Furusho, Y.; Endo, T. Convenient Synthesis of Cyclic Carbonates from CO₂ and Epoxides by Simple Secondary and Primary Ammonium Iodides as Metal-Free Catalysts under Mild Conditions and Its Application to Synthesis of Polymer Bearing Cyclic Carbonate Moiety. *J. Polym. Sci. Part A Polym. Chem.* **2013**, *51* (5), 1230–1242. <https://doi.org/10.1002/POLA.26492>.
- (30) Fukuoka, S.; Kawamura, M.; Komiya, K.; Tojo, M.; Hachiya, H.; Hasegawa, K.; Aminaka, M.; Okamoto, H.; Fukawa, I.; Konno, S. A Novel Non-Phosgene Polycarbonate Production Process Using by-Product CO₂ as Starting Material. *Green Chem.* **2003**, *5* (5), 497–507. <https://doi.org/10.1039/B304963A>.
- (31) Han, Z.; Rong, L.; Wu, J.; Zhang, L.; Wang, Z.; Ding, K. Catalytic Hydrogenation of Cyclic Carbonates: A Practical Approach from CO₂ and Epoxides to Methanol and Diols. *Angew. Chemie Int. Ed.* **2012**, *51* (52), 13041–13045. <https://doi.org/10.1002/ANIE.201207781>.
- (32) Chemistry No, S. GSC JACI Textbook Learning from Social Practice Cases That Received the GSC Awards.
- (33) Kawanami, H.; Sasaki, A.; Matsui, K.; Ikushima, Y. A Rapid and Effective Synthesis of Propylene Carbonate Using a Supercritical CO₂-Ionic Liquid System. *Chem. Commun.* **2003**, *3* (7), 896–897. <https://doi.org/10.1039/B212823C>.
- (34) Rehman, A.; Gunam Resul, M. F. M.; Eze, V. C.; Harvey, A. A Kinetic Study of Zn Halide/TBAB-Catalysed Fixation of CO₂ with Styrene Oxide in Propylene Carbonate. *Green Process. Synth.* **2019**, *8* (1), 719–729. https://doi.org/10.1515/GPS-2019-0042/ASSET/GRAPHIC/J_GPS-2019-0042_FIG_014.JPG.
- (35) Casadei, M. A.; Inesi, A.; Rossi, L. Electrochemical Activation of Carbon Dioxide: Synthesis of Organic Carbonates. *Tetrahedron Lett.* **1997**, *38* (20), 3565–3568. [https://doi.org/10.1016/S0040-4039\(97\)00664-3](https://doi.org/10.1016/S0040-4039(97)00664-3).
- (36) Metcalfe, I. S.; North, M.; Pasquale, R.; Thursfield, A. An Integrated Approach to

- Energy and Chemicals Production. *Energy Environ. Sci.* **2010**, *3* (2), 212–215. <https://doi.org/10.1039/B918417A>.
- (37) Man, M. L.; Lam, K. C.; Sit, W. N.; Ng, S. M.; Zhou, Z.; Lin, Z.; Lau, C. P. Synthesis of Heterobimetallic Ru–Mn Complexes and the Coupling Reactions of Epoxides with Carbon Dioxide Catalyzed by These Complexes. *Chem. – A Eur. J.* **2006**, *12* (4), 1004–1015. <https://doi.org/10.1002/CHEM.200500780>.
- (38) Udayakumar, S.; Raman, V.; Shim, H. L.; Park, D. W. Cycloaddition of Carbon Dioxide for Commercially-Imperative Cyclic Carbonates Using Ionic Liquid-Functionalized Porous Amorphous Silica. *Appl. Catal. A Gen.* **2009**, *368* (1–2), 97–104. <https://doi.org/10.1016/J.APCATA.2009.08.015>.
- (39) Udayakumar, S.; Lee, M. K.; Shim, H. L.; Park, S. W.; Park, D. W. Imidazolium Derivatives Functionalized MCM-41 for Catalytic Conversion of Carbon Dioxide to Cyclic Carbonate. *Catal. Commun.* **2009**, *10* (5), 659–664. <https://doi.org/10.1016/J.CATCOM.2008.11.017>.
- (40) Sun, J.; Ren, J.; Zhang, S.; Cheng, W. Water as an Efficient Medium for the Synthesis of Cyclic Carbonate. *Tetrahedron Lett.* **2009**, *50* (4), 423–426. <https://doi.org/10.1016/J.TETLET.2008.11.034>.
- (41) Jutz, F.; Grunwaldt, J. D.; Baiker, A. In Situ XAS Study of the Mn(III)(Salen)Br Catalyzed Synthesis of Cyclic Organic Carbonates from Epoxides and CO₂. *J. Mol. Catal. A Chem.* **2009**, *297* (2), 63–72. <https://doi.org/10.1016/J.MOLCATA.2008.10.009>.
- (42) Appaturi, J. N.; Adam, F. A Facile and Efficient Synthesis of Styrene Carbonate via Cycloaddition of CO₂ to Styrene Oxide over Ordered Mesoporous MCM-41-Imi/Br Catalyst. *Appl. Catal. B Environ.* **2013**, *136–137*, 150–159. <https://doi.org/10.1016/J.APCATB.2013.01.049>.
- (43) Sun, J.; Fujita, S. I.; Zhao, F.; Arai, M. A Highly Efficient Catalyst System of ZnBr₂/n-Bu₄NI for the Synthesis of Styrene Carbonate from Styrene Oxide and Supercritical Carbon Dioxide. *Appl. Catal. A Gen.* **2005**, *287* (2), 221–226. <https://doi.org/10.1016/J.APCATA.2005.03.035>.
- (44) Ono, F.; Qiao, K.; Tomida, D.; Yokoyama, C. Rapid Synthesis of Cyclic Carbonates from CO₂ and Epoxides under Microwave Irradiation with Controlled Temperature and Pressure. *J. Mol. Catal. A Chem.* **2007**, *263* (1–2), 223–226. <https://doi.org/10.1016/J.MOLCATA.2006.08.037>.
- (45) Yamaguchi, K.; Ebitani, K.; Yoshida, T.; Yoshida, H.; Kaneda, K. Mg–Al Mixed Oxides as Highly Active Acid–Base Catalysts for Cycloaddition of Carbon Dioxide to Epoxides. *J. Am. Chem. Soc.* **1999**, *121* (18), 4526–4527. <https://doi.org/10.1021/JA9902165/ASSET/IMAGES/LARGE/JA9902165H00001.JPEG>.
- (46) Mori, K.; Mitani, Y.; Hara, T.; Mizugaki, T.; Ebitani, K.; Kaneda, K. A Single-Site Hydroxyapatite-Bound Zinc Catalyst for Highly Efficient Chemical Fixation of Carbon Dioxide with Epoxides. *Chem. Commun.* **2005**, No. 26, 3331–3333. <https://doi.org/10.1039/B502636A>.
- (47) Kruper, W. J.; Dellar, D. V. Catalytic Formation of Cyclic Carbonates from Epoxides

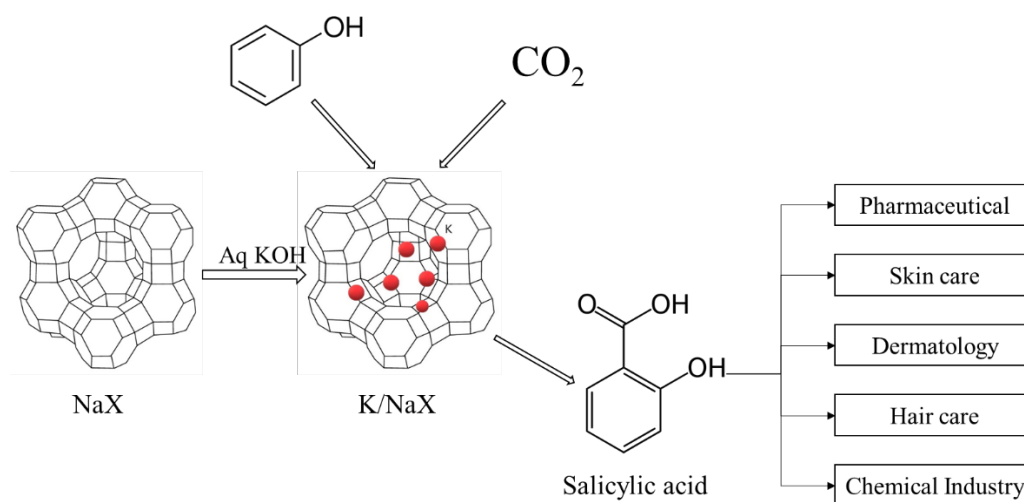
- and CO₂ with Chromium Metalloporphyrinates. *J. Org. Chem.* **1995**, *60* (3), 725–727. https://doi.org/10.1021/JO00108A042/ASSET/JO00108A042.FP.PNG_V03.
- (48) Sun, J.; Fujita, S. I.; Zhao, F.; Arai, M. Synthesis of Styrene Carbonate from Styrene Oxide and Carbon Dioxide in the Presence of Zinc Bromide and Ionic Liquid under Mild Conditions. *Green Chem.* **2004**, *6* (12), 613–616. <https://doi.org/10.1039/b413229g>.
- (49) Balas, M.; K/Bidi, L.; Launay, F.; Villanneau, R. Chromium-Salophen as a Soluble or Silica-Supported Co-Catalyst for the Fixation of CO₂ Onto Styrene Oxide at Low Temperatures. *Front. Chem.* **2021**, *9* (October), 1–7. <https://doi.org/10.3389/fchem.2021.765108>.
- (50) Sun, J.; Fujita, S. I.; Zhao, F.; Hasegawa, M.; Arai, M. A Direct Synthesis of Styrene Carbonate from Styrene with the Au/SiO₂-ZnBr₂/Bu₄NBr Catalyst System. *J. Catal.* **2005**, *230* (2), 398–405. <https://doi.org/10.1016/j.jcat.2004.12.015>.
- (51) Pradhan, H. C.; Mantri, S.; Routaray, A.; Maharana, T.; Sutar, A. K. Cobalt (II) Complex Catalyzed Polymerization of Lactide and Coupling of CO₂ and Styrene Oxide into Cyclic Styrene Carbonate. *J. Chem. Sci.* **2020**, *132* (1). <https://doi.org/10.1007/s12039-019-1722-6>.
- (52) Shim, J. J.; Kim, D.; Choon, S. R. Carboxylation of Styrene Oxide Catalyzed by Quaternary Onium Salts under Solvent-Free Conditions. *Bull. Korean Chem. Soc.* **2006**, *27* (5), 744–746. <https://doi.org/10.5012/bkcs.2006.27.5.744>.
- (53) Alassmy, Y. A.; Pescarmona, P. P. The Role of Water Revisited and Enhanced: A Sustainable Catalytic System for the Conversion of CO₂ into Cyclic Carbonates under Mild Conditions. *ChemSusChem* **2019**, *12* (16), 3856–3863. <https://doi.org/10.1002/CSSC.201901124>.
- (54) Choo, J. P. S.; Kammerer, R. A.; Li, X.; Li, Z. High-Level Production of Phenylacetaldehyde Using Fusion-Tagged Styrene Oxide Isomerase. *Adv. Synth. Catal.* **2021**, *363* (6), 1714–1721. <https://doi.org/10.1002/ADSC.202001500>.
- (55) Salla, I.; Bergadà, O.; Salagre, P.; Cesteros, Y.; Medina, F.; Sueiras, J. E.; Montanari, T. Isomerisation of Styrene Oxide to Phenylacetaldehyde by Fluorinated Mordenites Using Microwaves. *J. Catal.* **2005**, *232* (1), 239–245. <https://doi.org/10.1016/J.JCAT.2004.10.011>.
- (56) Guenic, S. Le; Ceballos, C.; Len, C. Synthesis of Phenylacetaldehyde from 1-Phenylethan-1,2-Diol by Microwave-Assisted Dehydration in Water. *Catal. Letters* **2015**, *145* (10), 1851–1855. <https://doi.org/10.1007/S10562-015-1606-4/TABLES/4>.
- (57) Jo, M.; Pe, Ivaro; Kamps, rez-S.; Maurer, G. An Experimental Investigation of the Solubility of CO₂ in (N,N-Dimethylmethanamide + Water). **2012**. <https://doi.org/10.1021/je300105q>.
- (58) Aresta, M.; Dibenedetto, A.; Gianfrate, L.; Pastore, C. Nb(V) Compounds as Epoxides Carboxylation Catalysts: The Role of the Solvent. *J. Mol. Catal. A Chem.* **2003**, *204–205*, 245–252. [https://doi.org/10.1016/S1381-1169\(03\)00305-4](https://doi.org/10.1016/S1381-1169(03)00305-4).
- (59) Jödecke, M.; Pérez-Salado Kamps, Á.; Maurer, G. An Experimental Investigation on the Influence of NaCl on the Solubility of CO₂ in (N,N-Dimethylmethanamide+water). *Fluid Phase Equilib.* **2012**, *334*, 106–116.

<https://doi.org/10.1016/j.fluid.2012.07.024>.

- (60) Srivastava, R.; Srinivas, D.; Ratnasamy, P. Zeolite-Based Organic–Inorganic Hybrid Catalysts for Phosgene-Free and Solvent-Free Synthesis of Cyclic Carbonates and Carbamates at Mild Conditions Utilizing CO₂. *Appl. Catal. A Gen.* **2005**, *289* (2), 128–134. <https://doi.org/10.1016/J.APCATA.2005.04.055>.
- (61) Gerbaud, V.; Rodriguez-Donis, I.; Hegely, L.; Lang, P.; Denes, F.; You, X. Q. Review of Extractive Distillation. Process Design, Operation, Optimization and Control. *Chem. Eng. Res. Des.* **2019**, *141*, 229–271. <https://doi.org/10.1016/J.CHERD.2018.09.020>.
- (62) Fox, R. O. CFD Models for Analysis and Design of Chemical Reactors. *Adv. Chem. Eng.* **2006**, *31*, 231–305. [https://doi.org/10.1016/S0065-2377\(06\)31004-6](https://doi.org/10.1016/S0065-2377(06)31004-6).
- (63) Baumann, M.; Moody, T. S.; Smyth, M.; Wharry, S. A Perspective on Continuous Flow Chemistry in the Pharmaceutical Industry. *Org. Process Res. Dev.* **2020**, *24* (10), 1802–1813. <https://doi.org/10.1021/ACS.OPRD.9B00524>.
- (64) Sattari-Najafabadi, M.; Nasr Esfahany, M.; Wu, Z.; Sunden, B. Mass Transfer between Phases in Microchannels: A Review. *Chem. Eng. Process. - Process Intensif.* **2018**, *127*, 213–237. <https://doi.org/10.1016/J.CEP.2018.03.012>.
- (65) Rossetti, I.; Compagnoni, M. Chemical Reaction Engineering, Process Design and Scale-up Issues at the Frontier of Synthesis: Flow Chemistry. *Chem. Eng. J.* **2016**, *296*, 56–70. <https://doi.org/10.1016/J.CEJ.2016.02.119>.
- (66) Akwi, F. M.; Watts, P. Continuous Flow Chemistry: Where Are We Now? Recent Applications, Challenges and Limitations. *Chem. Commun.* **2018**, *54* (99), 13894–13928. <https://doi.org/10.1039/C8CC07427E>.

Chapter 4

Carboxylation of phenol to salicylic acid



“This chapter presents the single pot synthesis of salicylic acid by carboxylation of phenol on potassium impregnated NaX zeolites”

Chapter 4

Carboxylation of phenol to salicylic acid

Abstract

Salicylic acid has a wide range of applications in the pharmaceutical and chemical industries. The market demand for salicylic acid is over 100 kilotons per annum, increasing rapidly. Industrially it is produced by the carboxylation of phenol using CO₂ over an alkaline catalyst and requires multiple steps. The main challenge in the current process is obtaining an anhydrous reaction intermediate, which is needed for selective carboxylation reaction and formation of sodium chloride as by product. As its demand increases, this process offers a helping hand in CO₂ mitigation technologies.

The present work presents the single-pot synthesis of salicylic acid using potassium-impregnated NaX zeolites. Zeolites are known for CO₂ adsorption, high surface area and volumes. At the same time, potassium ion is active in the carboxylation reaction due to its great tendency to form phenolate salt, which is the primary intermediate in this reaction.

The potassium-impregnated catalyst is characterised to understand its properties and detailed process optimization was carried out in a high-pressure batch reactor. X-ray diffraction (XRD) study confirmed the dispersion of potassium on the zeolite surface and the original structure of zeolite upon potassium impregnation. At the same time, Fourier transformed infra-red (FTIR) study indicated the main characteristic properties of NaX zeolite. The decrease in the surface area has been observed after impregnating potassium on zeolite due to uniform dispersion covering the pores of the zeolite.

At optimized conditions, more than 98 % selectivity of salicylic acid is obtained with 20 % conversion at 200 °C within 5 hours under supercritical conditions of CO₂ and without the use of any additional solvent. The CO₂ above its critical point offers several advantages in terms of higher product solubility, enhanced diffusion, and lower mass transfer limitations.

3.1 Introduction

Carboxylation is a fundamental chemical process involving adding a carboxyl group (-COOH) to a compound. This transformation plays a crucial role in various areas of organic chemistry, including the synthesis of pharmaceuticals and fine chemicals. One notable example of carboxylation is the Kolbe-Schmitt process for preparing salicylic acid from phenol. According to the global salicylic acid market report by Skyquest, the market demand for salicylic acid is 102 kilotons valued at USD 510 million and expected to grow to 880 million USD by 2030¹.

The carboxylation of phenol to salicylic acid typically involves using carbon dioxide (CO₂) as the carboxylating agent and is often catalysed by a base like sodium hydroxide. The preparation of salicylic acid offers a practical and efficient route for synthesising valuable compounds from CO₂.

As shown in Figure 4.1, salicylic acid has many applications in the pharmaceutical, cosmetic, and chemical industries. Some of the essential applications are listed below:

- **Pharmaceutical applications:** Salicylic acid is commonly used to formulate analgesics, anti-inflammatory, and antipyretic drugs². One of its most famous derivatives is acetylsalicylic acid, also known as aspirin which is widely used as a pain reliever and blood thinner.
- **Skincare applications:** Salicylic acid is a popular ingredient in skincare products, particularly targeting acne. It is often found in facial cleansers, toners, spot treatments, and peels to combat acne, blemishes, and blackheads³.
- **Dermatological applications:** Salicylic acid treats dermatological conditions like psoriasis, seborrheic dermatitis, and warts. It helps to remove dead skin, promote skin shedding, and reduce scaling and itching³.
- **Haircare applications:** Salicylic acid is used in shampoos and scalp treatments to address dandruff and scalp conditions⁴.
- **Industrial applications:** Salicylic acid finds various applications in producing dyes, fragrances, and rubber chemicals^{5,6}. It is also utilised in the synthesis of agrochemicals, including herbicides and plant growth regulators⁷.

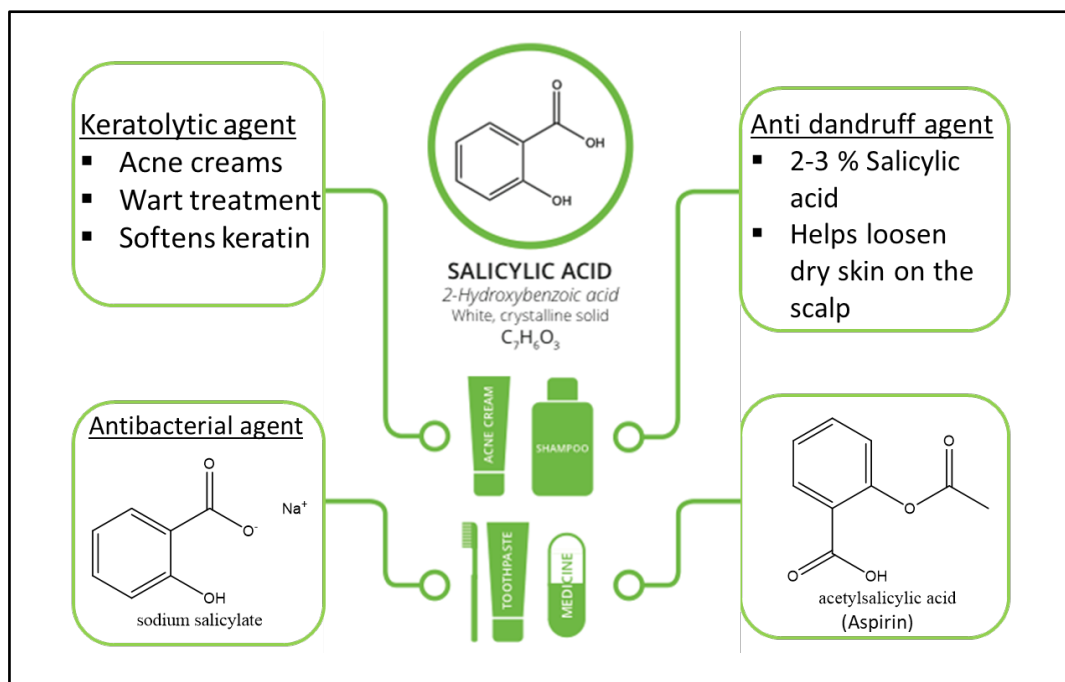
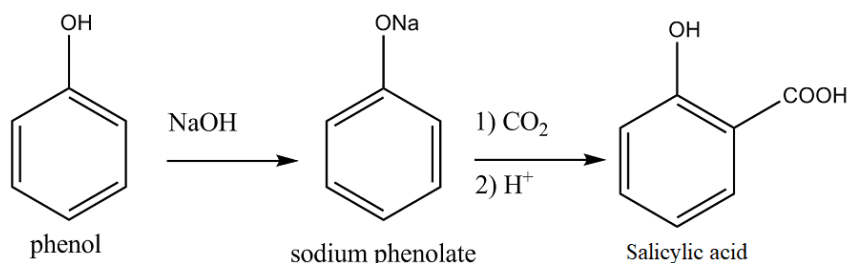


Figure 4.1: Industrial uses of salicylic acid

3.2 Current industrial status salicylic acid production

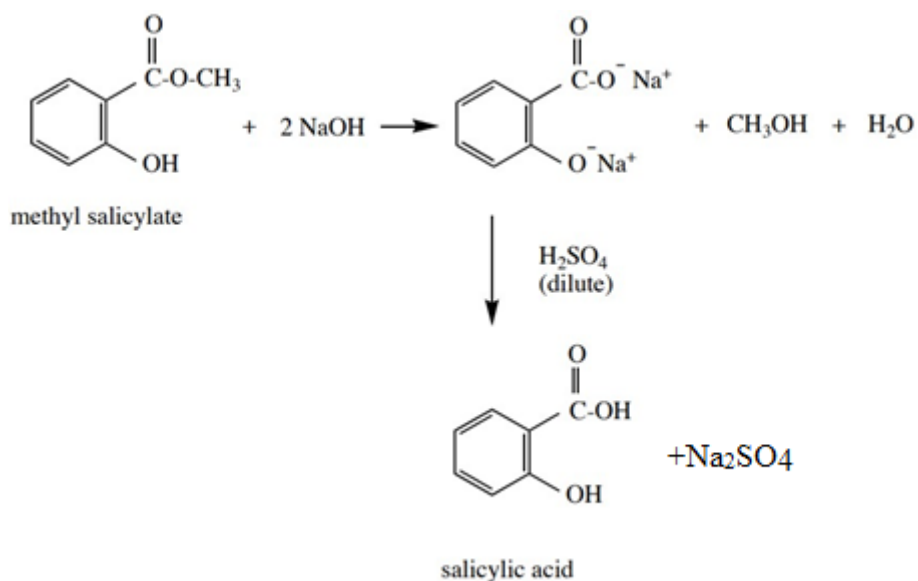
The most common processes for the industrial preparation of salicylic acid are the carboxylation of phenol and hydrolysis of methyl salicylate.



Scheme 4.1: Preparation of salicylic acid by carboxylation of phenol.

As discussed earlier, carboxylation of phenol is a well-known Kolbe-Schmitt process and is a widely employed method for the industrial synthesis of salicylic acid^{8,9,10}. In this process, phenol is first treated with sodium hydroxide to form sodium phenoxide, which later reacts with carbon dioxide under elevated temperatures of 120 – 130 °C and pressures of 80 – 90 bar to yield sodium salicylate salt. Salicylic acid is formed along with sodium chloride upon hydrolysis of sodium salicylate. The salicylic acid can be further purified through crystallization. The main challenge in carrying out this reaction is the difficulty of getting anhydrous sodium phenoxide for carboxylation¹⁰.

Another method for industrial production involves the hydrolysis of methyl salicylate, which is commonly obtained from natural sources such as wintergreen oil^{11,12}.



Scheme 4.2: Preparation of salicylic acid by hydrolysis of methyl salicylate.

Methyl salicylate is first reacted with sodium hydroxide to yield sodium salicylate and methanol. Then the sodium salicylate is acidified with sulphuric acid to form salicylic acid and sodium sulphate.

Although, these two are most common methods used for industrial production of salicylic acid, various attempts are made by researchers to develop other technologies and catalytic system for carboxylation of phenol.

3.3 Carboxylation of phenol – prior art

Carboxylation of phenol is well known Kolbe-Schmitt process for the synthesis of ortho salicylic acid (OSA). In general, substitution of carboxylic acid occurs at the ortho position of phenol, but in some cases para substitution is also known to lead to para-salicylic acid (PSA).

In 1860, Kolbe first proposed salicylic acid synthesis by heating a mixture of phenol with sodium in the presence of carbon dioxide. The salicylic acid was generated by acid precipitation of sodium salicylate formed in this reaction. This process needed various improvements due to formation of by-products like sodium carbonate and sodium phenoxide. In addition, some amount of phenol was volatilized from the reaction mixture due to direct heating.

Later, Schmitt modified the process and proposed three step process for of salicylic acid where in the first step, phenol was reacted with an aqueous solution of equivalent sodium hydroxide

to form sodium phenoxide. The water from sodium phenoxide is evaporated completely at 180 °C to make dried sodium phenoxide in the second step. Later, CO₂ was inserted in reaction mass in a closed vessel at 80 – 90 bar pressure and heated for several hours at 120 – 130 °C. Under these conditions, sodium salicylate was formed which is treated with acid solution to precipitate salicylic acid⁸. The modified Kolbe-Schmitt method remains the standard method for the preparation of wide range of aromatic hydroxyl acids.

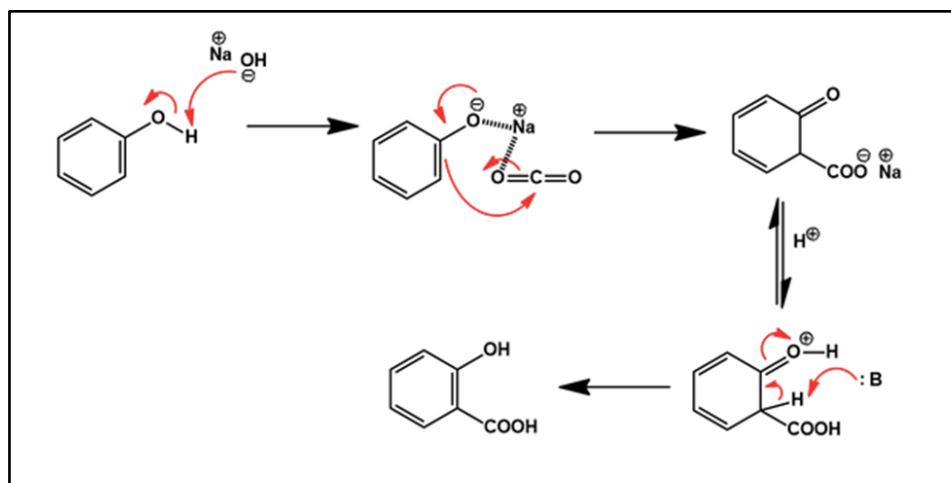


Figure 4.2: General mechanism of Kolbe-Schmitt reaction

The general reaction mechanism as shown in figure 4.2, suggest the formation of sodium phenolate salt by the interaction of strong electrophile with the lone pair on oxygen atom present in phenol. After CO₂ insertion, sodium metal interacts with oxygen connected to carbon forming sodium salicylate. Upon acid hydrolysis, salicylic acid gets precipitates with sodium chloride as a by-product.

Considering this mechanistic study, researchers have explored different catalytic system for the synthesis of salicylic acids and its derivatives. Iijima et al. proposed the direct synthesis of salicylic acid catalyzed by K₂CO₃ under supercritical CO₂¹³. As shown in figure 4.3, authors suggested the reaction mechanism on solid base catalyst where initial absorption of phenol occurs with Lewis acid centre on base catalyst producing phenoxy anion. Simultaneously, an oxygen atom from CO₂ donates a charge to the cation to which phenoxy group is attached, forming a carboxyl group. Salicylic acid is formed by the transfer of a hydrogen atom to the carboxyl group. Tsuji proposed that the migration of CO₂ on an oxide surface has been observed over strong solid bases like metal oxides¹⁴. Iijima et al.¹⁵ also stated a similar mechanism with AlBr₃ as a catalyst.

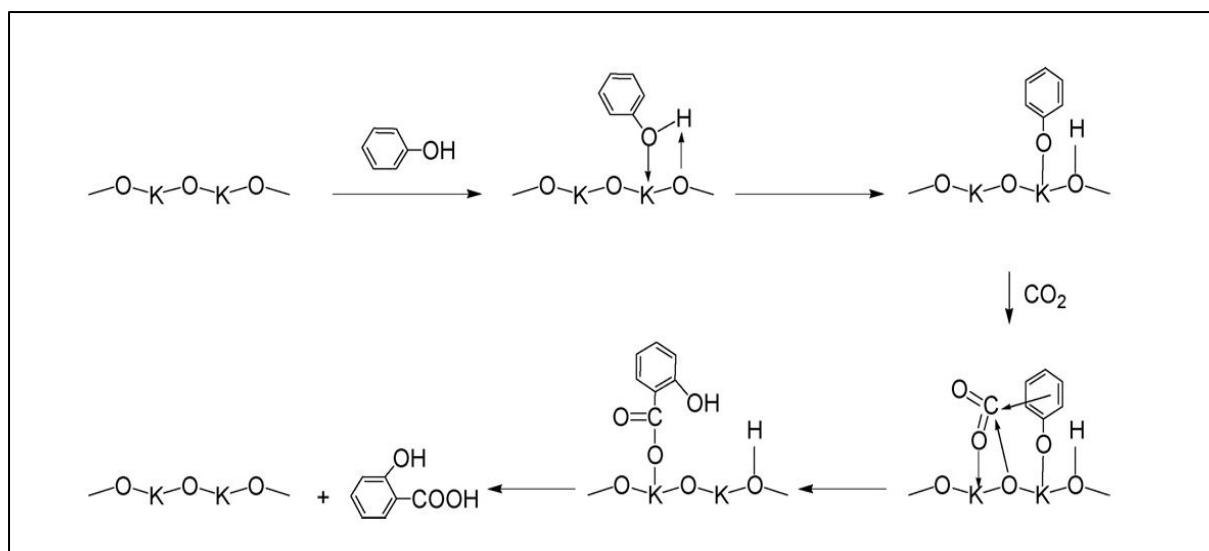


Figure 4.3: Reaction mechanism on K_2CO_3 catalyst proposed by Iijima et al.¹³

Miaofei et al.¹⁶ studied hybrid effects of K_2CO_3 on the synthesis of salicylic acid and derivatives using various alkaline earth metal phenoxides. The authors used different combinations of catalysts like ionic liquids, tetrabutylammonium bromide with potassium and sodium carbonate. Rahim et al. also investigated the effects of alkaline earth metals on Kolbe-Schmitt reactions and observed the better selectivities of ortho products with sodium and potassium phenoxides¹⁷.

Zeolites are a class of porous crystalline materials with unique three-dimensional framework structures composed of interconnected channels and cages. NaX and NaY, the sodium forms of zeolites, have shown CO_2 adsorption applications due to their high surface area and unique pore structure. Boer et al. studies the adsorption capacity of NaX zeolites and offers valuable information for the development of efficient CO_2 capture system¹⁸.

In the proposed work, potassium-doped NaX zeolites (K/NaX) were explored for carboxylation reaction as zeolite has good CO_2 adsorption capabilities and potassium shows activity towards phenol activation for phenoxide formation. The potassium-doped zeolites has higher basic sites compared to plane NaX zeolite due to the addition of active potassium sites. Siriporn et al. showed the effect of potassium doping on basic sites of NaX zeolites¹⁹.

3.4 Experimental procedures

3.4.1 Catalyst synthesis

The NaX zeolite was prepared using reported method by Georgiev et al²⁰. The kaolin with Si/Al ratio of 1.3 was calcined in muffle furnace at 600 °C for 3 hours. The obtained product was mixed with silica to get homogenous mixture. The dried homogenous mixture was added into sodium-alumosilicate to obtain gel like solution. The blend was mixed for 1 hour followed by calcination at 700 °C and dried NaX was obtained.

The obtained NaX zeolite was impregnated with an aqueous solution of KOH as mentioned by Wenlei et al²¹. In a typical experiment, 4 gms of zeolite was stirred with 40 ml of 10 % aqueous KOH solution for 12 h at ambient temperature. After impregnation, the slurry was filtered using Whatman filter paper and dried in an oven at 120 °C for 12 hours to evaporate complete water followed by calcination at 500 °C for 3 hours.

3.4.2 Catalyst characterization

X-ray diffraction (XRD) patterns of the catalysts were measured by Rigaku Dmax 500 diffractometer using nickel filtered Cu K α radiation. The sample was rotated to minimize the textural effect. The diffractometer was recorded in a range between 10° to 80° 2 θ at a scanning rate of 0.01°/s at a temperature of 25 °C.

The surface areas of the catalyst samples were determined by nitrogen adsorption with the Thermo-Scientific Surfer instrument at – 196 °C and calculated using the Brunauer-Emmett-Teller (BET) surface area analysis method.

Catalyst surface composition was confirmed by Energy dispersive X-ray (EDS) analysis.

The Infrared (IR) spectra were recorded in 600-4000 cm⁻¹ using Perkin Elmer Spectrum One Fourier transform infrared spectrometer.

3.4.3 Batch reaction procedure and reaction monitoring

Experiments were carried out in a 50 ml high-pressure reactor supplied by Parr Instrument Company. The reactor was equipped with a dip tube, pressure gauge, digital pressure sensor, temperature sensor and overhead magnetic drive, as shown in figure 4.4.

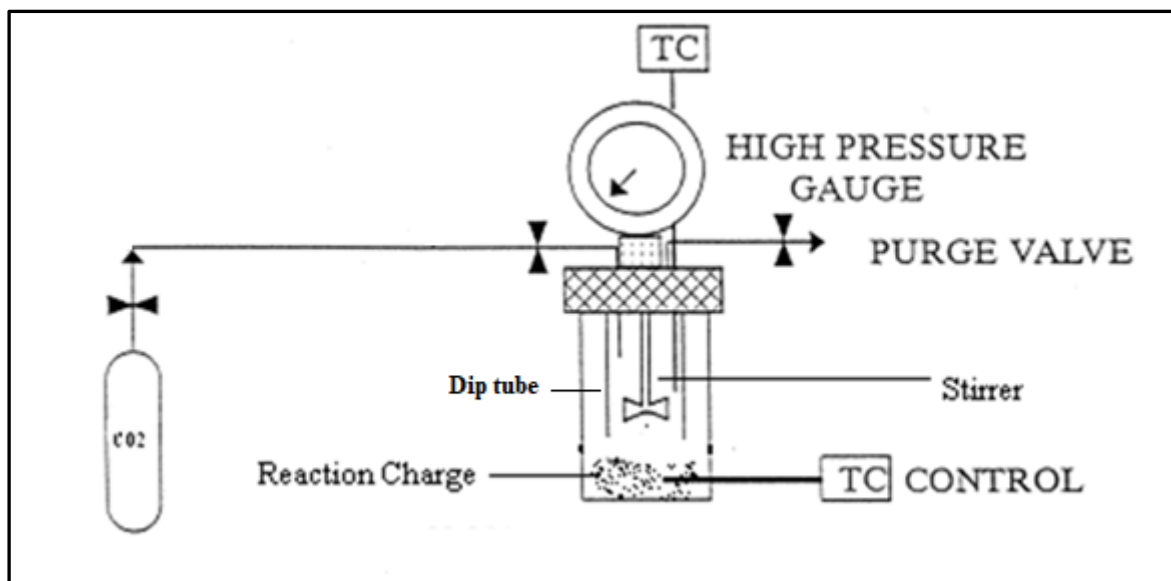


Figure 4.4: Schematic of high-pressure batch reactor

The phenol and catalyst were fed to the reactor vessel, and after packing the reactor bomb with its head, CO₂ was purged through a dip tube 2 – 3 times to remove air present in the reactor. After cleansing, CO₂ was fed to the reactor with the required amount from the cylinder directly, and the reactor was heated to the required temperature. On completion of the reaction, unreacted CO₂ was removed using a valve and the reaction mass was analyzed for composition.

The products were quantified using high pressure liquid chromatography (HPLC) supplied by Agilent technologies equipped with an C-18 column on UV detector with phosphate buffer as a mobile phase by an external calibration method. In this method, the calibration curve of known concentrations for compounds to their HPLC areas/responses was recorded first. The response factor is used to quantify the exact quantities present in the reaction mass. The detailed HPLC method with calibration curves and peak separations are mentioned in supporting information table S-1.3 and figures S-1.5 and S-1.6. The reaction parameters were calculated using traditional formulae as mentioned below:

$$\% \text{ Conversion} = \frac{\text{Initial moles} - \text{final moles of phenol}}{\text{Initial moles of Phenol}} * 100 \quad (1)$$

$$\% \text{ Selectivity} = \frac{\text{Moles of desired product formed}}{\text{Moles of phenol converted}} * 100 \quad (2)$$

$$\% \text{ Yield} = \frac{\text{Moles of desired product formed}}{\text{Initial moles of phenol}} * 100 \quad (3)$$

3.5 Results and Discussion

3.5.1 Catalyst characterization

3.5.1.1 X-ray diffraction (XRD)

Figure 4.5 shows XRD pattern of NaX and potassium-impregnated NaX zeolite. After impregnation of potassium using KOH solution, the main characteristic peaks were still observed but with a decrease in the intensities. This represents the intact zeolite structure upon impregnation. However, some structure may have collapsed due to hydrolysis of Si-O-Al bonds²²⁻²⁴. The decrease in intensities also implies that potassium molecules cover the external surface of NaX as suggested by Siriporn et al¹⁹.

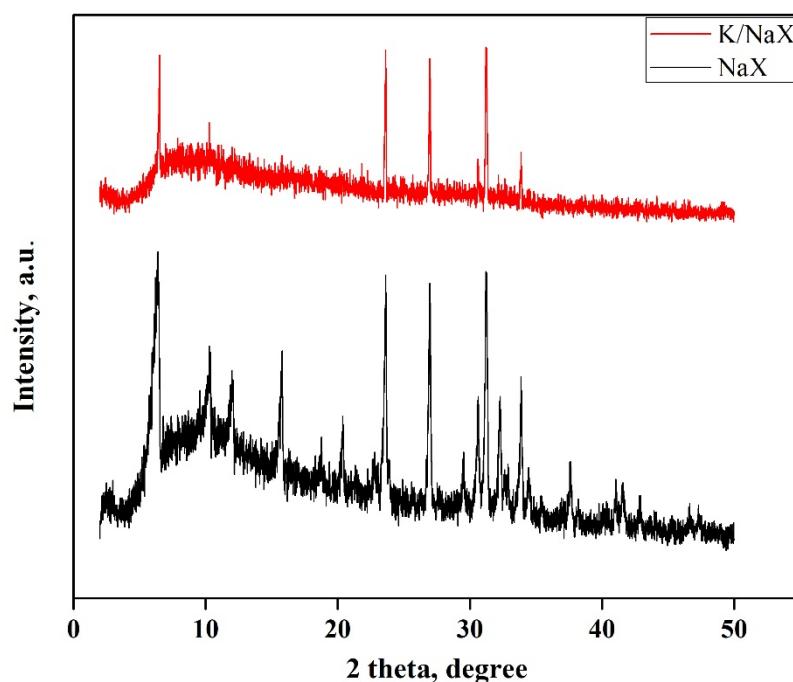


Figure 4.5: XRD pattern of NaX and K/NaX zeolites.

3.5.1.2 Fourier transformed infrared spectroscopy (FTIR)

Figure 4.6 presents the FTIR spectra of plain NaX zeolite and potassium-impregnated zeolite. NaX zeolite shows all the characteristic peaks. The intensity of band stretching at 950 cm^{-1} is decreased in potassium-doped zeolite corresponding to Si-O-Al due to the dispersion of potassium and thermal hydrolysis during decomposition in the calcination process²³. The peak

at 1425 cm^{-1} for K/NaX zeolite corresponds to carbonate ion stretching probably due to adsorption of CO_2 on potassium sites^{25,26}. All these findings for potassium-doped zeolites are in line with Rakmae et al²³. and Manadee et al²⁶.

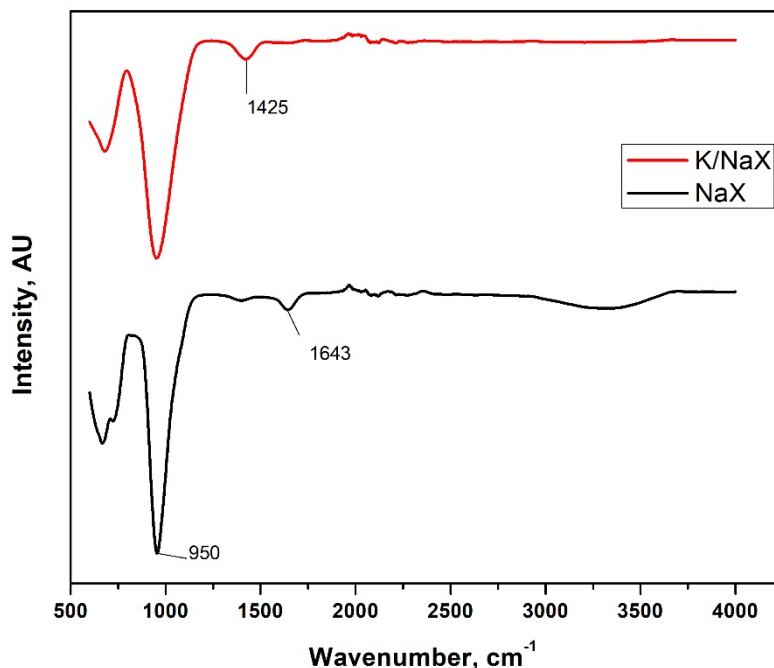


Figure 4.6: FTIR spectra of NaX and K/NaX zeolite

3.5.1.3 Surface area and elemental composition

The Nitrogen sorption isotherms of NaX and K/NaX zeolite confirmed the occupation of impregnated species in the zeolite structure as BET surface area is decreased from $604\text{ m}^2/\text{gm}$ to $332\text{ m}^2/\text{gm}$ after impregnation of potassium on NaX zeolite. These results also confirm the decrease in XRD intensity upon impregnation. Similar trend has been observed by several researchers^{22–24,26,27}. The elemental composition measurements analysed on energy dispersive X-ray spectroscopy confirmed the presence of 11.2 atomic % of potassium in K/NaX zeolite.

3.5.2 Catalyst screening

Considering the required basic sites in the catalyst for carboxylation of phenol to salicylic acid from reaction mechanism understanding, various catalyst were explored, as shown in table 4.1. It was observed that the catalyst with potassium precursors or doping is more active towards

the reactions, probably due to the tendency to form phenoxide salts with phenol^{16,28}. NaX zeolites are known for CO₂ adsorption capacities¹⁸ and with potassium impregnation (table 4.1, entry 8 & 9) its activity towards ortho-salicylic acid is increased. The other isomer, para salicylic acid is produced in less quantity as electronic effects are stronger in ortho positions. Further reaction optimization was carried out with K/NaX zeolite.

Table 4.1: Catalyst screening. Reaction conditions: Phenol 2 gms, catalyst 1 gm, temperature 200 °C, time 5 h, reaction pressure 80 bar.

Entry	Catalyst	Phenol conversion Mole %	OSA selectivity Mole %	PSA selectivity Mole %
1	K ₂ CO ₃	9.2	92.3	7.7
2	MgO	5.0	96.0	4.0
3	Li/MgO	7.1	97.1	2.9
4	K/MgO	7.5	98.6	1.4
5	ZnBr ₂	2.3	86.9	13.1
6	LiBr	3.2	93.7	6.3
7	Mg:Al (4:1) HT	3.5	94.3	5.7
8	NaX zeolite	7.3	97.3	2.7
9	K/NaX zeolite	13.5	97.7	2.3

3.5.3 Process optimization

3.5.3.1 Effect of reaction temperature

Temperature is one of the main parameter for reaction to carry out. As shown in figure 4.7 a, increasing trend of phenol conversion is observed with temperature up to 200 °C and further there is a drop in its activity due to decomposition of salicylic acid into phenol and CO₂ again^{29,30}. Figure 4.7 b compares the phenol conversion of K₂CO₃ and K/NaX zeolite and it is observed that K/NaX better activity than plain K₂CO₃ due to more CO₂ adsorption on zeolite surface and high surface area and pore volume of zeolites. At 200 °C, K₂CO₃ showed maximum 12 % phenol conversion (%X) while K/NaX resulted in maximum 20 % phenol conversion with 98 % salicylic acid selectivity within 5 hours of time and 2 gms catalyst loading.

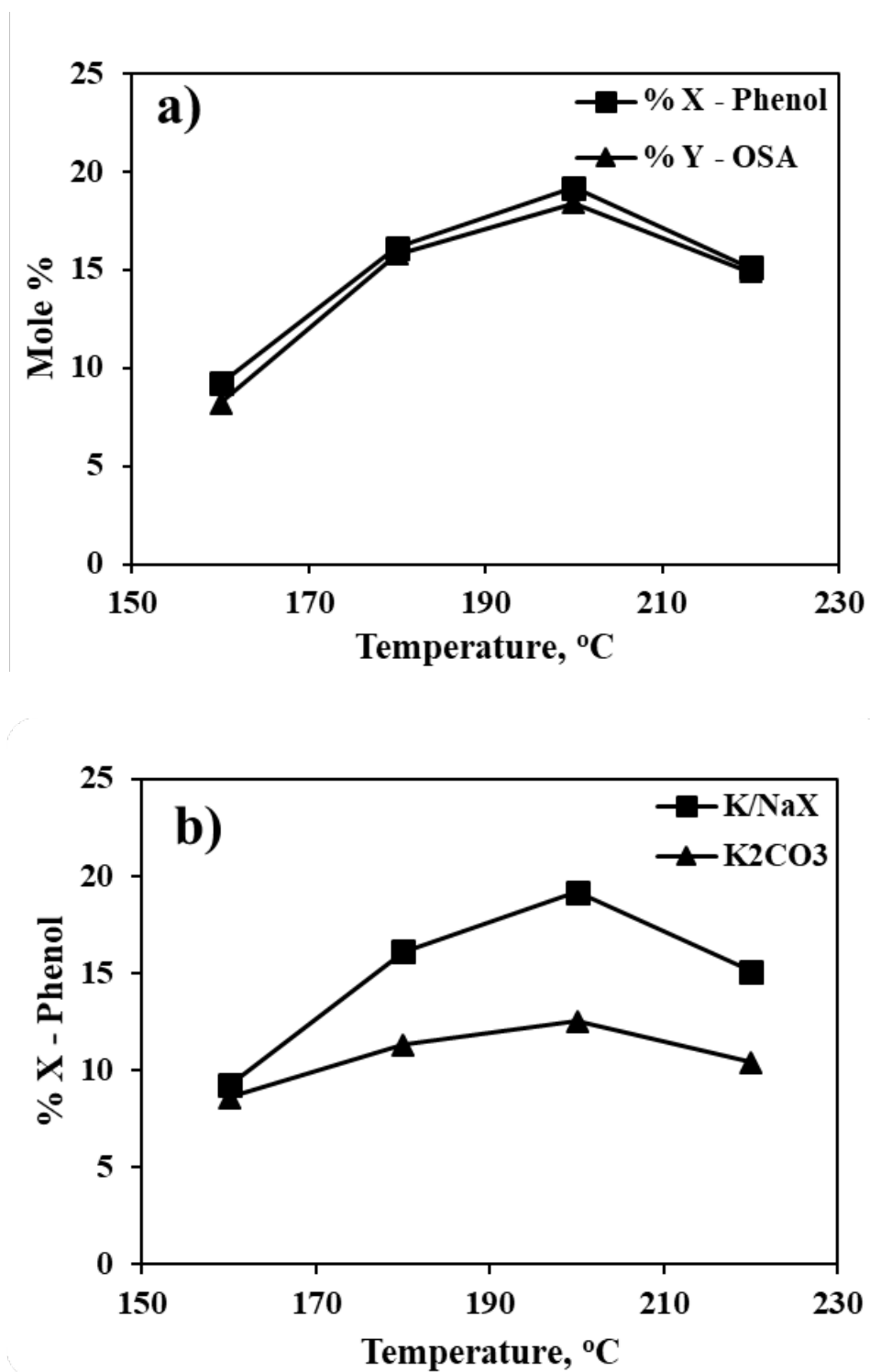


Figure 4.7: a) Effect of temperature with K_2CO_3 catalyst, b) Comparison of K/NaX and K_2CO_3 with temperature. Reaction conditions: Time 5 h, pressure 80 bars, catalyst amount 2 gms, phenol 2 gms.

3.5.3.2 Effect of catalyst loading

In the carboxylation of aromatics, Olah et al³¹. stated that the amount of catalyst is directly dependent on carboxylic acid formed and similar trend is observed with K/NaX catalyst as shown in figure 4.8. The yield of salicylic acid significantly increases with an increase in catalyst quantity upto 2 gms while the selectivity remains more than 95 %. With lesser catalyst loading, the selectivity of ortho-salicylic acid is 100 % as shown in figure but the conversions are very less. The higher loading is slightly promoting para substitution also due to higher number of active sites present.

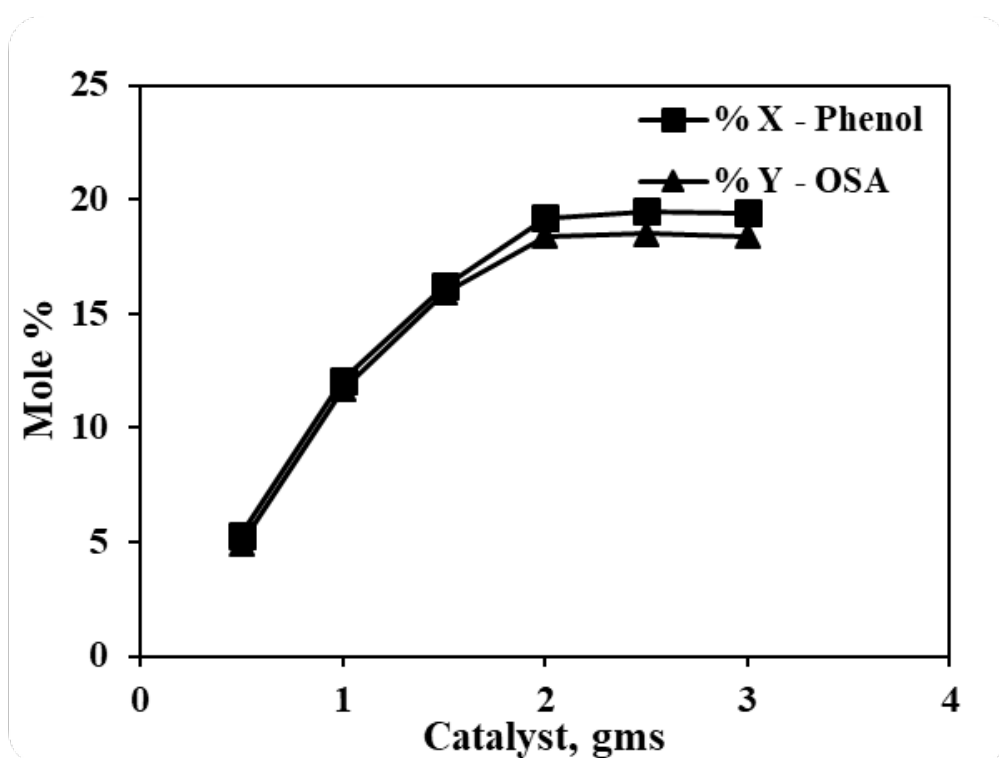


Figure 4.8: Effect of catalyst loading. Reaction conditions: Temperature 200 °C, pressure 80 bar, time 5 h, phenol 2 gms. %X – conversion, % Y – yield.

3.5.3.3 Effect of pressure

The increased pressure of CO₂ results to higher density and eventually higher solubility of phenol in carbon dioxide. As shown in figure 4.9, the reaction yield drastically changed with phase change of CO₂ from subcritical to supercritical. Also, it's been reported that the reactivity of CO₂ is maximum near its critical pressure^{32,33}. Figure 4.9 also states that there is no change with further increase for pressure beyond supercritical point.

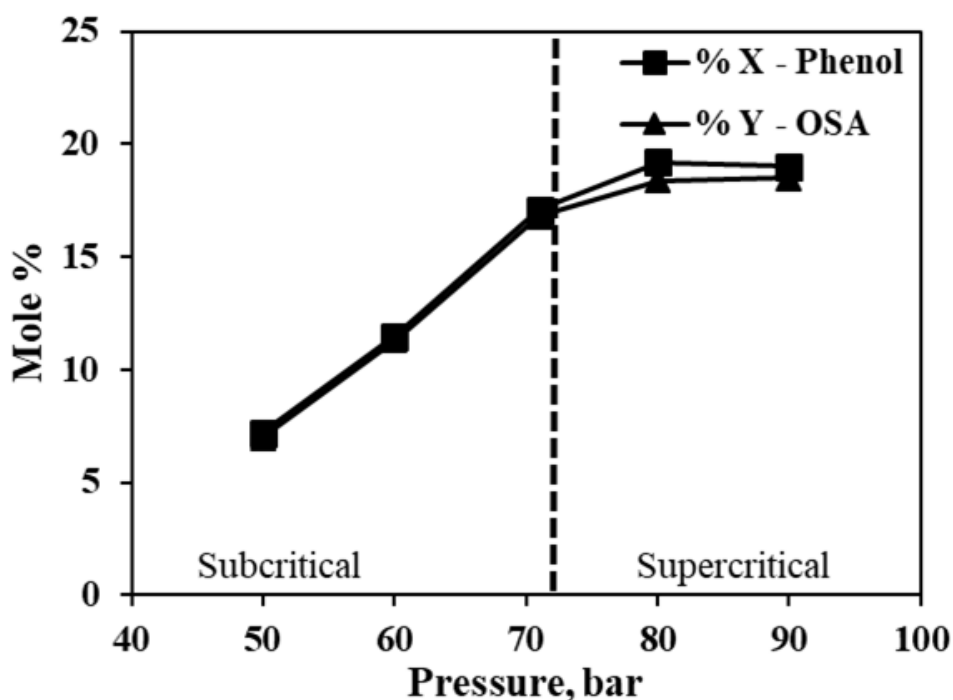


Figure 4.9: Effect of Phase change (pressure). Reaction conditions: Temperature 200 °C, time 5 h, phenol 2 gms, catalyst K/NaX zeolite.

3.5.3.4 Effect of reaction time

The study of reaction yield with time suggests slow reaction rate as shown in figure 4.10 a & b. The reaction were performed at 200 oC in the presence of K/NaX zeolite under 80 bar pressure. It was observed that the rate of salicylic acid decreased with time and after 5 hours, reaction attains its equilibrium. This could be due to the low solubility of salicylic acid in scCO₂ as studied by Iijima et al¹³. Figure 4.10 b compares the phenol conversions at 200 °C and 180 °C with time.

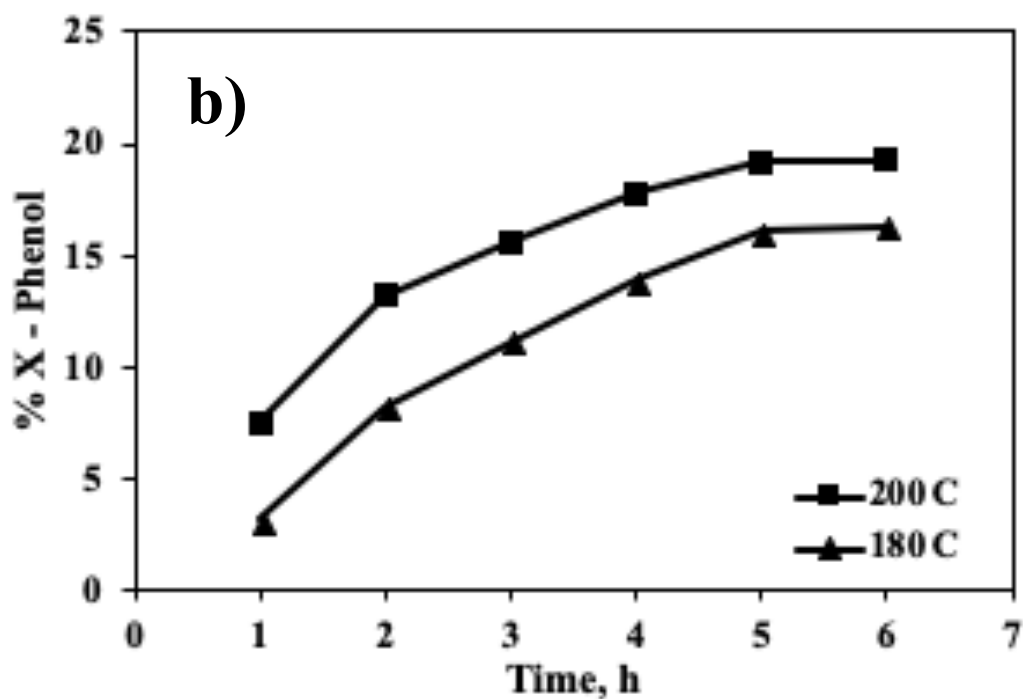
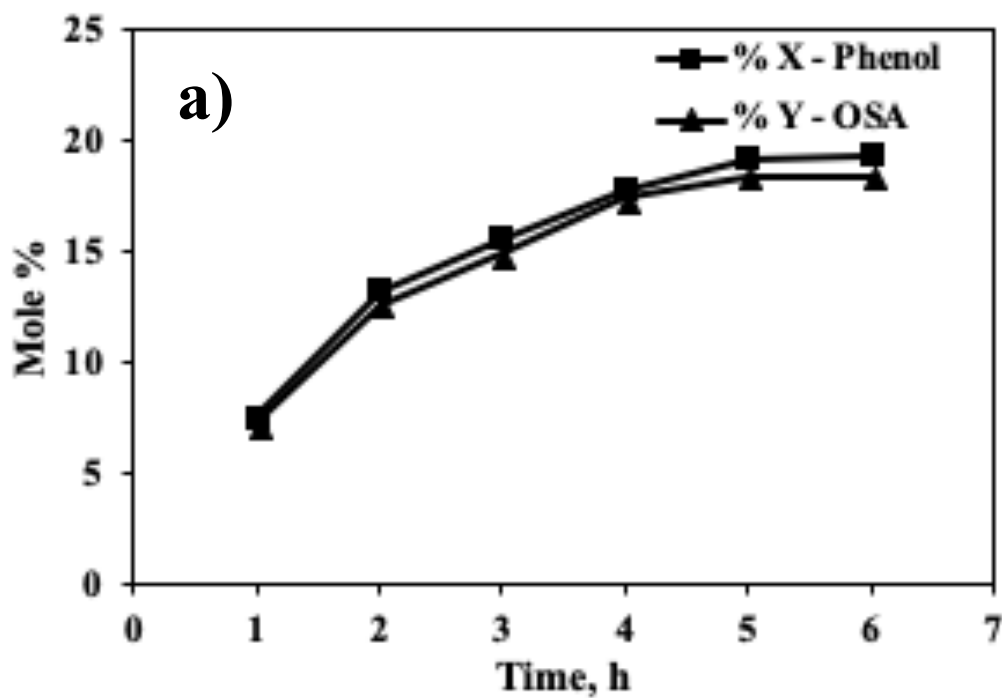


Figure 4.10: a) Effect of reaction time. b) Comparison of reaction conversions at different temperature with time. Reaction conditions: Temperature 200 °C, phenol 2 gms, catalyst 2 gms, pressure 80 bar.

3.5.3.5 Effect of solvent

The effect of solvent for carboxylation reaction is studied with variety of solvents as shown in figure 4.11. With water as a solvent in reaction, phenol conversion was less probably due to chelation of water molecules with loosely impregnated potassium on zeolite or hydrolysis of phenoxide intermediate forms during the reaction. A polar aprotic solvent DMF has great CO₂ solubility³⁴ making the reaction mixture homogenous also did not showed the better activity as it might be blocking the phenol activation on catalyst surface. The solvents like methanol and ethanol with high dielectric constant showed the similar activity towards carboxylation while without the use of any additional solvent than only CO₂, which acts as reactant as well as solvent showed the maximum activity towards carboxylation of phenol as shown in figure 4.11.

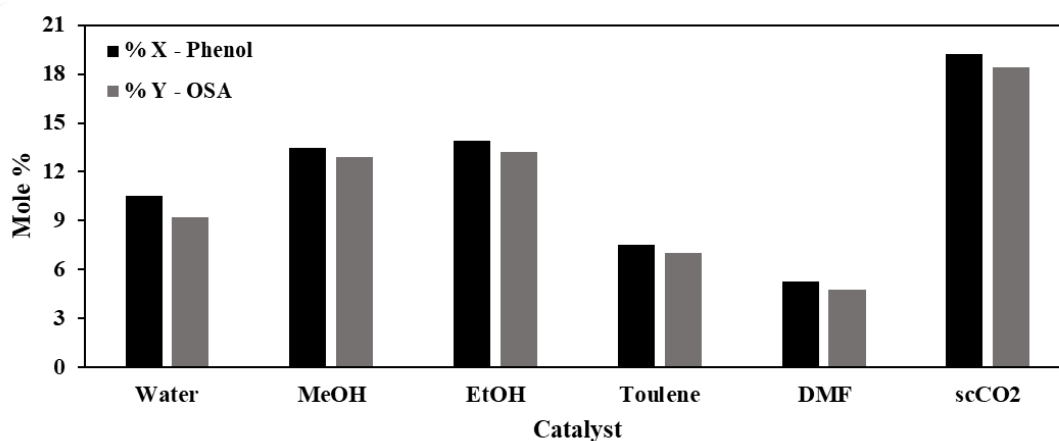


Figure 4.11: Effect of solvent. Reaction conditions: Temperature 200 °C, pressure 80 bar, time 5 h, phenol 2 gms, catalyst 2 gms.

3.6 Conclusion and the path forward

The demand for salicylic acid is increasing due to its wide range of applications in pharmaceutical, cosmetic, and chemical industries. The industrial synthesis process offers a good reaction efficiency but the process is multistep and obtaining the desired purity intermediates is the main challenge with the formed salt as a by-product. Additionally the recovery of alkali requires further process.

In the present work, single pot synthesis of salicylic acid is achieved using potassium impregnated NaX zeolites. The modified zeolite offers high surface area, greater CO₂ adsorption and higher selectivity for salicylic acid. The detailed catalyst characterization and process optimization is carried out and at optimized conditions; more than 98 % selectivity of

salicylic acid is obtained with 20 % conversion at 200 °C within 5 hours under supercritical conditions of CO₂ and without the use of any additional solvent. The CO₂ above its critical point offers several advantages in terms of higher product solubilities, enhanced diffusion and lower mass transfer limitations.

As the process potentials sustainable method to synthesize salicylic acid, process intensification, product separation and catalyst recovery studies are the next aim for development of pilot scale. Also, the reaction mechanism needs to understand for development of kinetic models.

3.7 References

- (1) Global Salicylic Acid Market <https://www.skyquestt.com/report/salicylic-acid-market> (accessed Jun 27, 2023).
- (2) Sambyal, K.; Singh, R. V. Production of Salicylic Acid; a Potent Pharmaceutically Active Agent and Its Future Prospects. <https://doi.org/10.1080/07388551.2020.1869687> **2021**, *41* (3), 394–405. <https://doi.org/10.1080/07388551.2020.1869687>.
- (3) Arif, T. Salicylic Acid as a Peeling Agent: A Comprehensive Review. *Clin. Cosmet. Investig. Dermatol.* **2015**, *8*, 455. <https://doi.org/10.2147/CCID.S84765>.
- (4) Ranganathan, S.; Mukhopadhyay, T. DANDRUFF: THE MOST COMMERCIALY EXPLOITED SKIN DISEASE. *Indian J. Dermatol.* **2010**, *55* (2), 130. <https://doi.org/10.4103/0019-5154.62734>.
- (5) Teimouri, A.; Chermahini, A. N.; Ghorbani, M. H. The Green Synthesis of New Azo Dyes Derived from Salicylic Acid Derivatives Catalyzed via Baker's Yeast and Solid Acid Catalysis.
- (6) Darbre, P. D.; Harvey, P. W. Regulatory Considerations for Dermal Application of Endocrine Disrupters in Personal Care Products. *Endocr. Disrupt. Hum. Heal.* **2015**, 343–361. <https://doi.org/10.1016/B978-0-12-801139-3.00019-3>.
- (7) Koo, Y. M.; Heo, A. Y.; Choi, H. W. Salicylic Acid as a Safe Plant Protector and Growth Regulator. *Plant Pathol. J.* **2020**, *36* (1), 1. <https://doi.org/10.5423/PPJ.RW.12.2019.0295>.
- (8) Lindsey, A. S.; Jeskey, H. The Kolbe-Schmitt Reaction. *Chem. Rev.* **1957**, *57* (4), 583–620. <https://doi.org/10.1021/cr50016a001>.
- (9) Zhang, X. B.; Liu, Y. X.; Luo, Z. H. Kinetic Study of the Aqueous Kolbe-Schmitt Synthesis of 2,4- and 2,6-Dihydroxybenzoic Acids. *Chem. Eng. Sci.* **2019**, *195*, 107–119. <https://doi.org/10.1016/j.ces.2018.11.045>.
- (10) Stanescu, I.; Achenie, L. E. K. A Theoretical Study of Solvent Effects on Kolbe-Schmitt Reaction Kinetics. *Chem. Eng. Sci.* **2006**, *61* (18), 6199–6212. <https://doi.org/10.1016/j.ces.2006.05.025>.

- (11) Cheng, C. Y.; Brinzari, T. V.; Hao, Z.; Wang, X.; Pan, L. Understanding Methyl Salicylate Hydrolysis in the Presence of Amino Acids. *J. Agric. Food Chem.* **2021**, *69* (21), 6013–6021. <https://doi.org/10.1021/ACS.JAFC.1C00958>.
- (12) Singh, L.; Gupta, A. K.; Singh, R. T.; Verma, D. K.; Jha, R. C. Effect of DMSO on the Kinetic Behavior of Alkali Catalyzed Hydrolysis of Methyl Salicylate. *React. Kinet. Catal. Lett.* **1984**, *241* **1984**, *24* (1), 161–165. <https://doi.org/10.1007/BF02069621>.
- (13) Iijima, T.; Yamaguchi, T. K₂CO₃-Catalyzed Direct Synthesis of Salicylic Acid from Phenol and Supercritical CO₂. *Appl. Catal. A Gen.* **2008**, *345* (1), 12–17. <https://doi.org/10.1016/j.apcata.2008.03.037>.
- (14) Tsuji, H.; Okamura-Yoshida, A.; Shishido, T.; Hattori, H. Dynamic Behavior of Carbonate Species on Metal Oxide Surface: Oxygen Scrambling between Adsorbed Carbon Dioxide and Oxide Surface. *Langmuir* **2003**, *19* (21), 8793–8800. https://doi.org/10.1021/LA0342666/SUPPL_FILE/LA0342666SI20030623_085146.PDF.
- (15) Iijima, T.; Yamaguchi, T. Efficient Regioselective Carboxylation of Phenol to Salicylic Acid with Supercritical CO₂ in the Presence of Aluminium Bromide. *J. Mol. Catal. A Chem.* **2008**, *295* (1–2), 52–56. <https://doi.org/10.1016/j.molcata.2008.07.017>.
- (16) Gu, M.; Yan, X.; Cheng, Z. Hybrid Catalytic Effects of K₂CO₃ on the Synthesis of Salicylic Acid from Carboxylation of Phenol with CO₂. *Res. Chem. Intermed.* **2016**, *42* (2), 391–406. <https://doi.org/10.1007/s11164-015-2025-2>.
- (17) Rahim, M. A.; Matsui, Y.; Kosugi, Y. Effects of Alkali and Alkaline Earth Metals on the Kolbe-Schmitt Reaction. *Bull. Chem. Soc. Jpn.* **2002**, *75* (3), 619–622. <https://doi.org/10.1246/bcsj.75.619>.
- (18) Boer, D. G.; Langerak, J.; Pescarmona, P. P. Zeolites as Selective Adsorbents for CO₂ Separation. *ACS Appl. Energy Mater.* **2022**. <https://doi.org/10.1021/acsaem.2c03605>.
- (19) Kosawatthanakun, S.; Pansakdanon, C.; Sosa, N.; Chanlek, N.; Roessner, F.; Prayoonpokarach, S.; Wittayakun, J. Comparative Properties of K/NaX and K/NaY from Ultrasound-Assisted Impregnation and Performance in Transesterification of Palm Oil. *ACS Omega* **2022**, *7* (11), 9130–9141. <https://doi.org/10.1021/acsomega.1c04912>.
- (20) Georgiev, D.; Bogdanov, B.; Markovska, I.; Hristov, Y. A Study on the Synthesis and Structure of Zeolite NaX. *J. Chem. Technol. Metall.* **2013**, *48* (2), 168–173.
- (21) Xie, W.; Huang, X.; Li, H. Soybean Oil Methyl Esters Preparation Using NaX Zeolites Loaded with KOH as a Heterogeneous Catalyst. *Bioresour. Technol.* **2007**, *98* (4), 936–939. <https://doi.org/10.1016/j.biortech.2006.04.003>.
- (22) Montalbo, K. D.; De Leon, R. L.; Sophiphun, O.; Manadee, S.; Prayoonpokarach, S.; Wittayakun, J. Characterization and Catalytic Performance of Potassium Loaded on Rice Husk Silica and Zeolite Nay for Transesterification of Jatropha Seed Oil. *Quim. Nova* **2013**, *36* (8), 1116–1120. <https://doi.org/10.1590/S0100-40422013000800007>.
- (23) Rakmae, S.; Keawkumay, C.; Osakoo, N.; Montalbo, K. D.; de Leon, R. L.; Kidkhunthod, P.; Chanlek, N.; Roessner, F.; Prayoonpokarach, S.; Wittayakun, J.

- Realization of Active Species in Potassium Catalysts on Zeolite NaY Prepared by Ultrasound-Assisted Impregnation with Acetate Buffer and Improved Performance in Transesterification of Palm Oil. *Fuel* **2016**, *184*, 512–517. <https://doi.org/10.1016/J.FUEL.2016.07.035>.
- (24) Peña, R.; Romero, R.; Martínez, S. L.; Natividad, R.; Ramírez, A. Characterization of KNO₃/NaX Catalyst for Sunflower Oil Transesterification. *Fuel* **2013**, *110*, 63–69. <https://doi.org/10.1016/j.fuel.2012.07.072>.
- (25) Lavalley, J. C. Infrared Spectrometric Studies of the Surface Basicity of Metal Oxides and Zeolites Using Adsorbed Probe Molecules. *Catal. Today* **1996**, *27* (3–4), 377–401. [https://doi.org/10.1016/0920-5861\(95\)00161-1](https://doi.org/10.1016/0920-5861(95)00161-1).
- (26) Manadee, S.; Sophiphun, O.; Osakoo, N.; Supamathanon, N.; Kidkhunthod, P.; Chanlek, N.; Wittayakun, J.; Prayoonpokarach, S. Identification of Potassium Phase in Catalysts Supported on Zeolite NaX and Performance in Transesterification of Jatropha Seed Oil. *Fuel Process. Technol.* **2017**, *156*, 62–67. <https://doi.org/10.1016/J.FUPROC.2016.09.023>.
- (27) Thommes, M.; Kaneko, K.; Neimark, A. V.; Olivier, J. P.; Rodriguez-Reinoso, F.; Rouquerol, J.; Sing, K. S. W. Physisorption of Gases, with Special Reference to the Evaluation of Surface Area and Pore Size Distribution (IUPAC Technical Report). *Pure Appl. Chem.* **2015**, *87* (9–10), 1051–1069. <https://doi.org/10.1515/PAC-2014-1117/MACHINEREADEABLECITATION/RIS>.
- (28) Itoh, S.; Kumei, H.; Nagatomo, S.; Kitagawa, T.; Fukuzumi, S. Effects of Metal Ions on Physicochemical Properties and Redox Reactivity of Phenolates and Phenoxyl Radicals: Mechanistic Insight into Hydrogen Atom Abstraction by Phenoxyl Radical-Metal Complexes. *J. Am. Chem. Soc.* **2001**, *123* (10), 2165–2175. https://doi.org/10.1021/JA0036110/SUPPL_FILE/JA0036110_SB.PDF.
- (29) Wesółowski, M. Thermal Decomposition of Salicylic Acid and Its Salts. *Thermochim. Acta* **1979**, *31* (2), 133–146. [https://doi.org/10.1016/0040-6031\(79\)85001-7](https://doi.org/10.1016/0040-6031(79)85001-7).
- (30) Bourns, A. N.; Buccini, J.; Dunn, G. E.; Rodewald, W. Mechanism of Decarboxylation of Substituted Salicylic Acids. II. Kinetics and ¹³C-Carboxyl Kinetic Isotope Effects in Nitrobenzene–Quinoline Mixtures. *Can. J. Chem.* **1968**, *46* (24), 3915–3917. <https://doi.org/10.1139/v68-646>.
- (31) Olah, G. A.; Török, B.; Joschek, J. P.; Bucsi, I.; Esteves, P. M.; Rasul, G.; Prakash, G. K. S. Efficient Chemoselective Carboxylation of Aromatics to Arylcarboxylic Acids with a Superelectrophilically Activated Carbon Dioxide–Al₂Cl₆/Al System. *J. Am. Chem. Soc.* **2002**, *124* (38), 11379–11391. https://doi.org/10.1021/JA020787O/SUPPL_FILE/JA020787O_S.PDF.
- (32) Iijima, T.; Yamaguchi, T. The Improved Kolbe–Schmitt Reaction Using Supercritical Carbon Dioxide. *Tetrahedron Lett.* **2007**, *48* (30), 5309–5311. <https://doi.org/10.1016/J.TETLET.2007.05.132>.
- (33) Fujita, S. I.; Bhanage, B. M.; Ikushima, Y.; Arai, M. Synthesis of Dimethyl Carbonate from Carbon Dioxide and Methanol in the Presence of Methyl Iodide and Base Catalysts

under Mild Conditions: Effect of Reaction Conditions and Reaction Mechanism. *Green Chem.* **2001**, *003* (002), 87–91. <https://doi.org/10.1039/B100363L>.

- (34) Jo, M.; Pe, Ivaro; Kamps, rez-S.; Maurer, G. An Experimental Investigation of the Solubility of CO₂ in (N,N-Dimethylmethanamide + Water). **2012**. <https://doi.org/10.1021/je300105q>.

Chapter 5
Conclusion and future scope

“This chapter concludes the processes developed for conversion of carbon dioxide to value-added chemicals, and future work directions have been proposed.”

Chapter 5

Conclusion and future scope

Conclusions

As the energy demand is rising daily, CO₂ emissions are increasing exponentially, and the total emission of CO₂ per year has crossed 37 billion tons. CO₂ is considered one of the main contributors to global warming, and the average temperature rise from the pre-industrial era has crossed 1 °C. To address the concern of global warming, renewable energy sources and substantial reduction in CO₂ emissions should be adopted.

There may need to be more than just reducing CO₂ emissions alone to meet global climate crises; there is a significant need to utilise and convert it into value-added chemicals. Currently, CO₂ is being consumed in industries to prepare certain chemicals, in food industries and for oil recovery. The yearly consumption of CO₂ is only 250 million tons, which accounts for less than 1 % of total emissions. Using CO₂ for value-added chemicals can provide a helping hand in the battle against global warming, and it has enormous potential for economic growth and innovation.

In the proposed work, processes for three industrially important molecules: dimethyl formamide (DMF), styrene carbonate (SC), and ortho-salicylic acid (OSA), have been developed using CO₂ as a reactant. The current industrial synthesis of these compounds needs significant improvement in terms of efficient and green catalysts, restricted use of toxic substrates, development of an efficient process, single pot synthesis, and process intensification to maximise product viability in the market. The research findings are summarised below:

- Dimethyl formamide is an essential compound with broad applications in chemical industries, mainly as a solvent. The reaction mechanism for hydrogenation of CO₂ to formic acid and dimethyl formamide suggests the need for basic sites in the catalyst for CO₂ activation and conversion. The heterogeneous, recyclable, and green catalyst is developed in the thesis work using metal precursors. The developed mixed metal oxide catalyst showed notable activity towards direct hydrogenation of CO₂. A detailed catalyst characterisation was performed to understand its properties, and the process was developed in a batch reactor. At the optimised reaction conditions, more than 92

% yield of DMF is obtained. Additionally, the process intensification was done using a reaction kinetic study and the development of proof of concept for continuous flow synthesis in a fixed-bed reactor.

- Styrene carbonate is a five-membered cyclic carbonate with various applications, mainly in polymer industries and as a polar aprotic solvent in chemical industries. For the synthesis of styrene carbonate, batch and continuous synthesis processes are developed using CO₂ and styrene oxide as reactants in the presence of tetrabutylammonium bromide as a catalyst. At optimised reaction conditions in a batch process, complete conversion of styrene oxide is obtained with more than 85 % product selectivity. Additionally, the reaction kinetic study suggested the fast reaction dynamics and was used to estimate reaction conversions with a good fit between experimental and calculated values. Process intensification was done by developing a continuous flow reactor, and the process was optimised at mild reaction conditions.
- Salicylic acid has a range of applications in the pharmaceutical and chemical industries. The work presents a single-pot synthesis of salicylic acid from phenol and CO₂ using potassium-impregnated NaX zeolites having high CO₂ adsorption capacities, larger surface areas and volume. The catalyst characterisation was performed to understand its properties, and the process was developed in a batch reactor. At the optimised conditions, more than 98 % salicylic acid selectivity is obtained with 20 % phenol conversion under supercritical CO₂ conditions. The CO₂ above its critical point offers several advantages in terms of higher product solubility, enhanced diffusion, and lower mass transfer limitations

Although the thesis work provides a significant fundamental understanding of the process and catalyst system, there is a need to expand this study further for sustainable commercial-scale production of the proposed chemicals. The future work directions are summarised below:

- The study on hydrogenation of CO₂ suggested a slower reaction rate and proof of concept for continuous flow synthesis was developed. For feasible industrial-scale production, a pilot plant of the continuous reactor and its process development studies are needed to be carried out.
- The continuous flow synthesis process is developed for the synthesis of styrene carbonate, while the development of downstream processes for the separation of

products and recyclability of solvent is the future scope of study needed for industrial plant development.

- The comprehensive reaction kinetics need to be studied considering mass transfer limitations for better validation of continuous reaction data.
- To synthesise salicylic acid, a batch process using a zeolite catalyst has been developed. Process intensification, product separation and catalyst recovery studies are the following goals for developing industrial-scale production and replacing existing processes.
- Understanding and reaction mechanism for salicylic acid preparation over potassium doped NaX zeolite is a major challenge for future research and development.

Annexure A

Supporting information

Chapter 2: Hydrogenation of carbon dioxide to dimethyl formamide

The reaction products quantification was done using an external calibration method on Gas Chromatography (GC) supplied by Agilent technologies. The detailed GC method is presented in table S-1.1, while the GC separation chromatograph and calibration curves are shown in figures S-1.1 & S-1.2.

Table S-1.1: Gas chromatography method for detection of DMA, DMF and TMA

Column	Carbowax	
Column Dimensions	30m x 0.25 mm x 0.25 μ m	
Mode	Split ratio- (50:1)	
Detector	Flame Ionization Detector (FID)	
Mobile phase (gases)	Nitrogen	
Flow rate	1mL/min	
Total run time	8.3 min	
Oven temperature ramp		
Rate, $^{\circ}$ C/min	Temperature $^{\circ}$ C	Hold Time min
	80	3.0
40.0	125	1.0
20.0	150	2.0

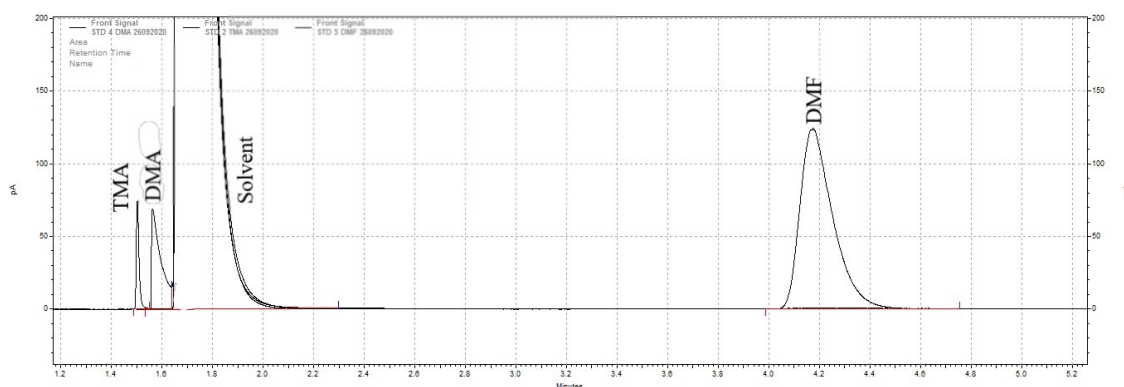


Figure S-1.1: GC separation of DMA, TMA, and DMF

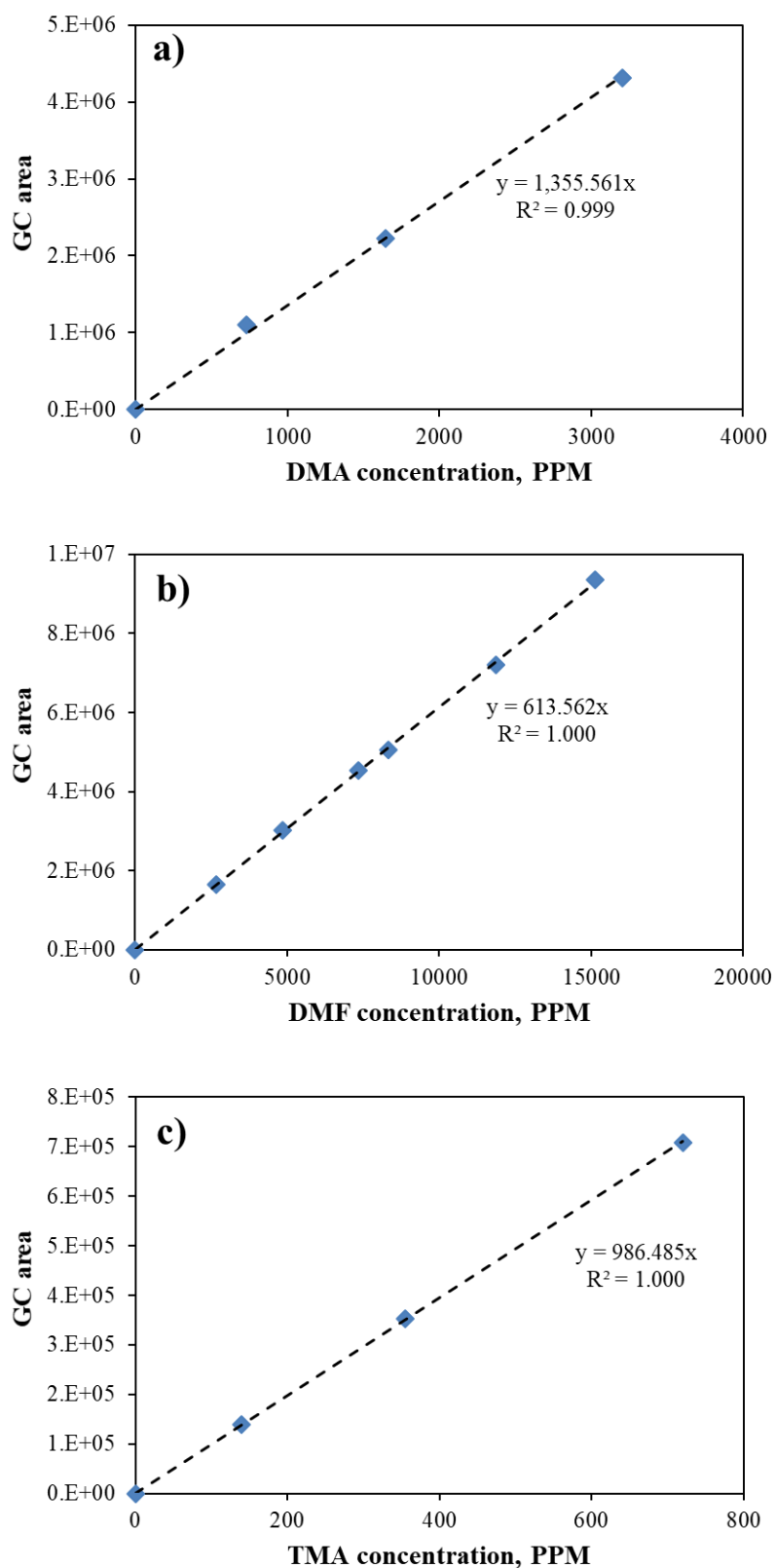


Figure S-1.2: Calibration curve for a) DMA, b) DMF, and c) TMA

The LHHW model developed for reaction kinetics was solved in MATLAB and regressed to fit the experimental values. The detailed MATLAB code is given below:

// Defining rate equation

```
function dcdt=model170(T,C,K)
KZ=K(1);
KH=K(2);
KC=K(3);
KD=K(4);

dcdt=-
((KZ*((KH*C)^(0.5))*(KC*C)))/((1+(KH*C)^(0.5))*(KC*C+KD*(0.112
-C)+1));
```

// Defining Error function (least mean square)

```
function lsqe=errfunc170(K)
C0=0.112;
Ts=[0 60 120 180 300 360];
[T,C]=ode45(@(T,C) model170(T,C,K),Ts,C0);
Cexpt=[0.112 0.07572 0.05892 0.04814 0.04015 0.03654];
Cexpt=Cexpt';
R=(C-Cexpt).^2;
lsqe= sum(R);
end
```

```
// Sover using ODE45
```

```
KZ=0.5844;
```

```
KH=0.03355;
```

```
KC=0.178;
```

```
KD=2.86;
```

```
K0=[KZ;KH;KC;KD];
```

```
fun=@errfunc170;
```

```
[K,fval]= fminsearch(fun,K0);
```

```
KZ=K(1);
```

```
KH=K(2);
```

```
KC=K(3);
```

```
KD=K(4);
```

```
disp(['KZ: ' num2str(KZ)]);
```

```
disp(['KH: ' num2str(KH)]);
```

```
disp(['KC: ' num2str(KC)]);
```

```
disp(['KD: ' num2str(KD)]);
```

```
K=[KZ;KH;KC;KD];
```

```
Ts=[0 60 120 180 300 360];
```

```
C0=0.112;
```

```
[T,C]=ode45(@(T,C) model170(T,C,K),Ts,C0);
```

```
Cexpt=[0.112 0.07572 0.05892 0.04814 0.04015 0.03654];
```

```
plot(Ts,Cexpt,'blue',Ts,C,'red')
```

Chapter 3: Cycloaddition of CO₂ in styrene oxide

The reaction product quantification was done using an external calibration method on Gas Chromatography (GC) supplied by Agilent technologies. The detailed GC method is presented in table S-1.2, while the GC separation chromatograph and calibration curves are shown in figures S-1.3 & S-1.4

Table S-1.2: Gas chromatography method for detection of SO, SC, and SG

Column	HP 50+	
Column Dimensions	30m x 0.25 mm x 0.25 μ m	
Mode	Split ratio- (50:1)	
Detector	Flame Ionization Detector (FID)	
Mobile phase (gases)	Nitrogen	
Flow rate	1mL/min	
Total run time	25 min	
Oven temperature ramp		
Rate, $^{\circ}$ C/min	Temperature $^{\circ}$ C	Hold Time min
	100	1
10	200	2
10	270	5

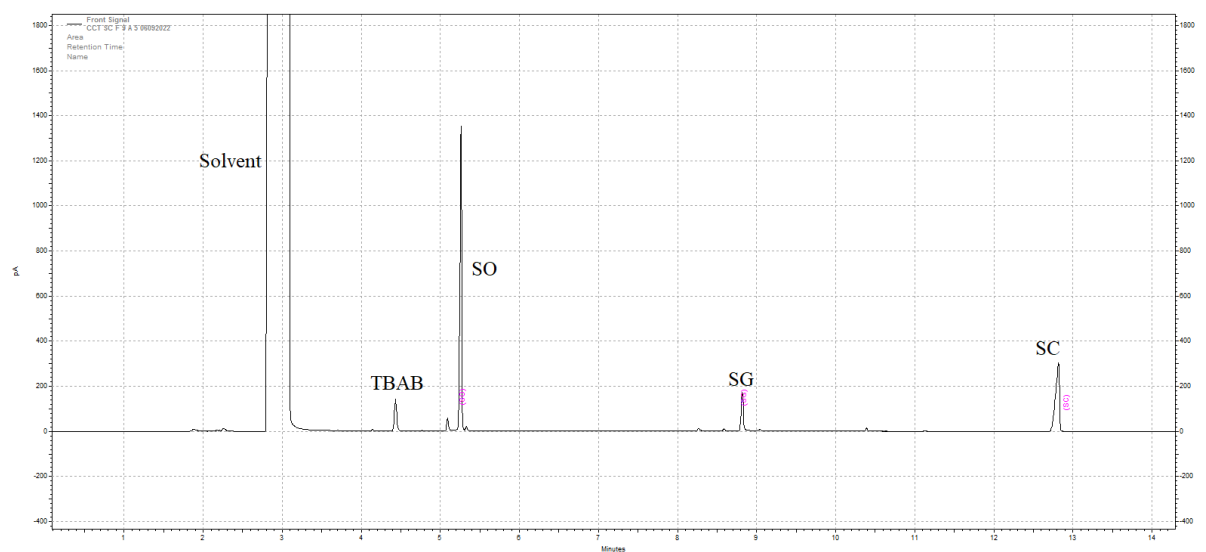


Figure S-1.3: GC separation of SO, SC, SG

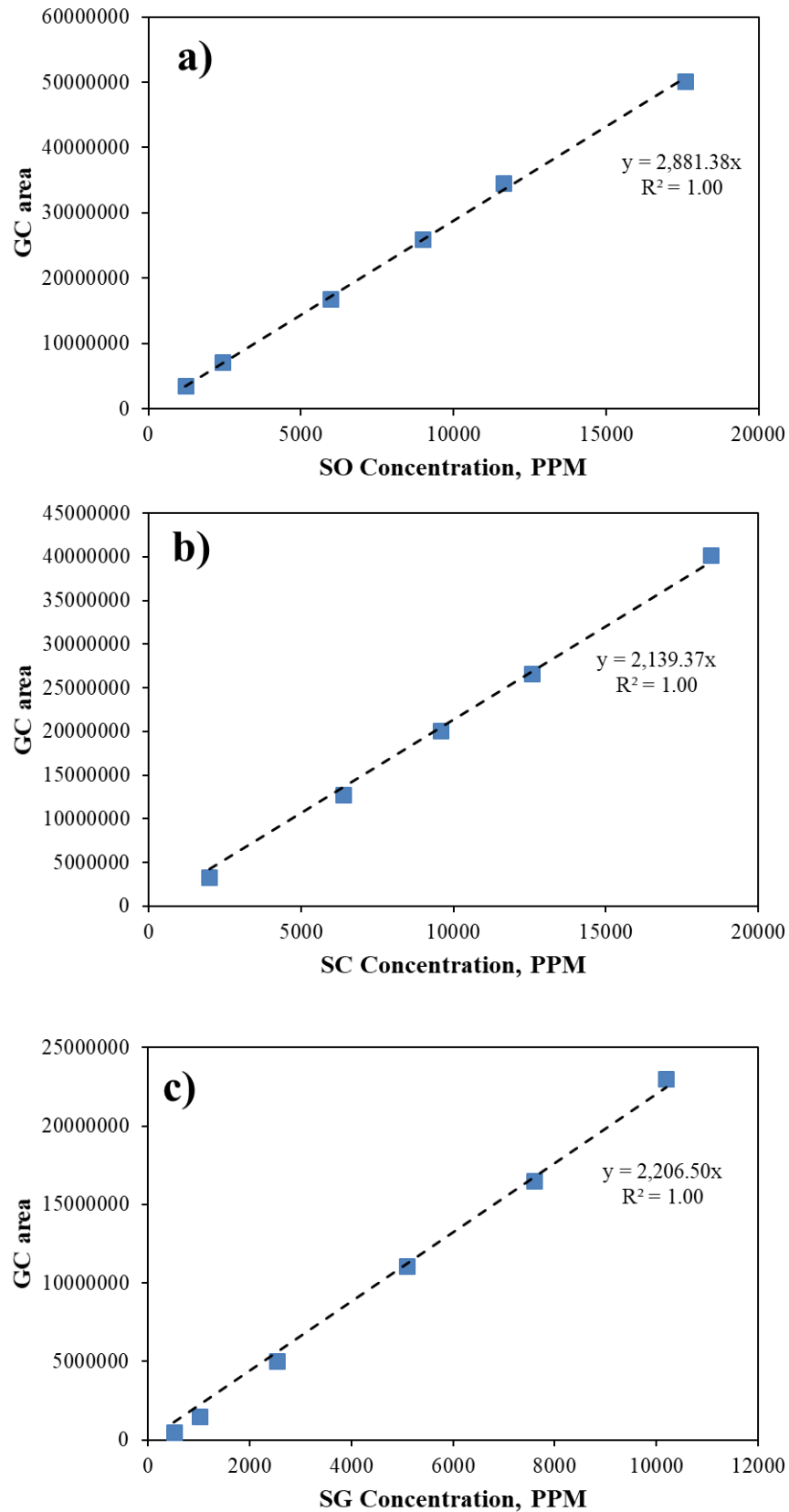


Figure S-1.4: Calibration curve for a) SO, b) SC, and c) SG

Chapter 4: Carboxylation of phenol to salicylic acid

The reaction product quantification was done using an external calibration method on high-pressure liquid chromatography (HPLC) supplied by Agilent technologies. The detailed HPLC method is presented in table S-1.3, while the HPLC separation chromatograph and calibration curves are shown in figures S-1.5 & S-1.6.

Table S-1.3: HPLC method for detection of Phenol, OSA, and PSA

Column	C18
Column Dimensions	150 mm x 4.6 mm x 2.5 μ m
Mode	Isocratic
Detector	UV – 210 nm and 236 nm
Mobile phase	Phosphate buffer (A) : MeOH (B) 50:50
Solution A	2.5 mmol Na ₂ HPO ₄ + 10 mmole H ₃ PO ₄
Solution B	Methanol
Flow rate	0.5 mL/min
Total run time	20 min

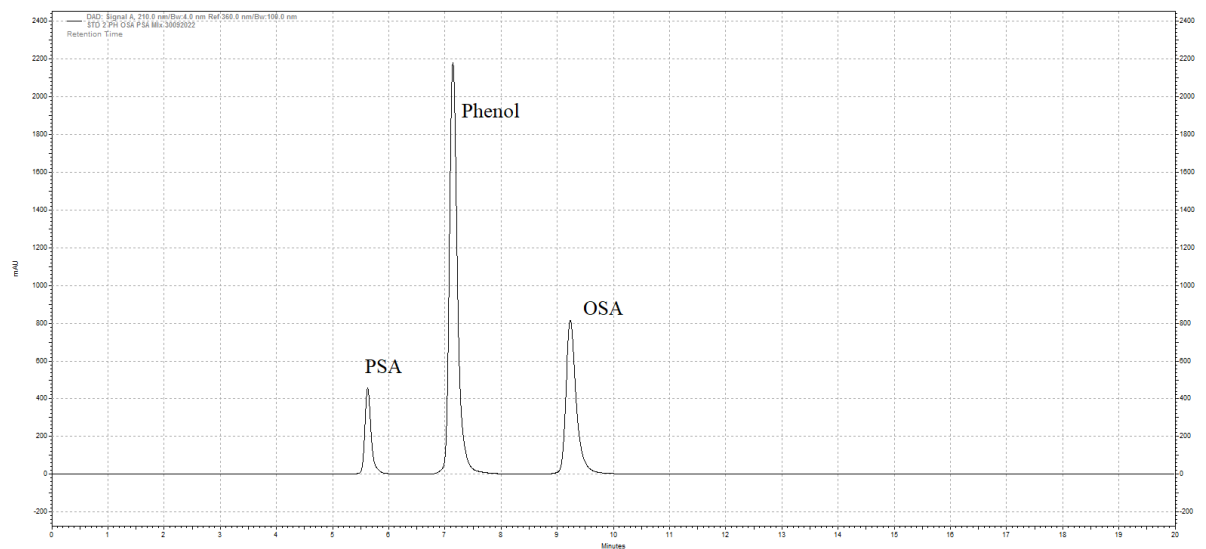


Figure S-1.5: HPLC separation of Phenol, OSA, and PSA at 236 nm UV wavelength.

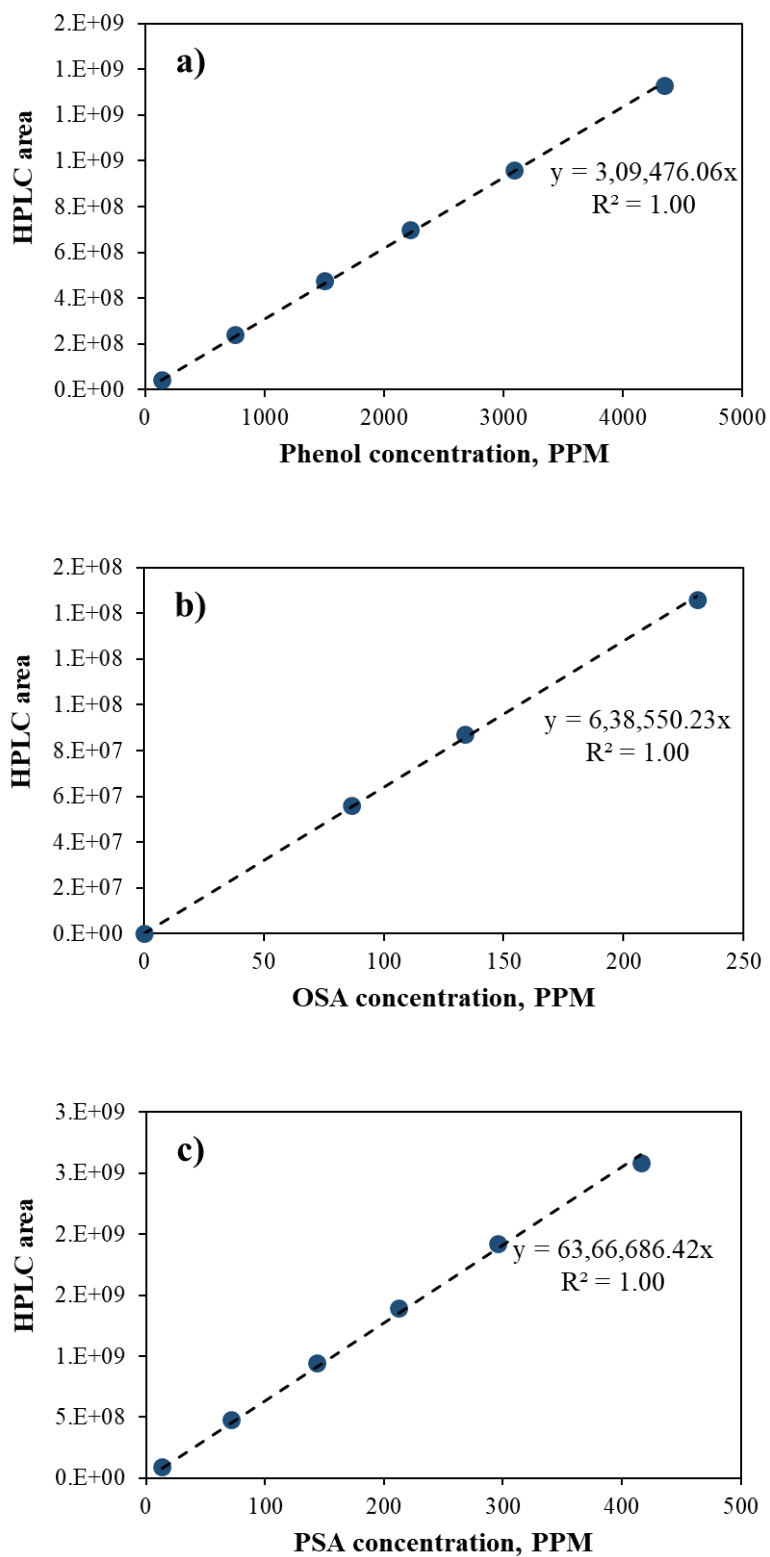


Figure S-1.6: Calibration curve for a) Phenol, b) OSA, and c) PSA

ABSTRACT

Name of Student: Sagar Dattulal Chaudhary **Registration No.: 20EE17A26032**
Faculty of Study: Engineering **Year of Submission: 2023**
AcSIR academic centre/CSIR Lab: NCL, Pune **Name of Supervisor(s):**
 Dr. Nilesh A. Mali (Supervisor)
 Dr. Sunil S. Joshi (Co-supervisor)
Title of thesis: Catalytic conversion of carbon dioxide to value added chemicals

The 21st century is experiencing enormous development in every sector and at the same time demand for energy is rising. Although renewable energy is promising, the main sources of energy are still coal, oil, and natural gas which accounts for 81 % of total energy supply. The excessive use of these resources are increasing CO₂ concentration in the atmosphere. CO₂ is considered as one of the main greenhouse gases causing global warming and the average rise in Earth's temperature has exceeded 1 °C mark. Reducing CO₂ emissions alone may not be sufficient to meet global climate crises, there is a significant need to remove CO₂ from the atmosphere and convert it into viable and valuable products. Also, CO₂ utilization has huge potential for economic growth and innovation. The circular economy can be adopted by converting CO₂, minimizing waste generation, and reducing reliance on finite sources.

In the proposed thesis, sustainable processes for three industrially important products: dimethyl formamide (DMF), styrene carbonate (SC), and ortho-salicylic acid (OSA) were developed which has wide range of applications. The current synthesis methods for these compounds needs a significant modification in terms of process intensification, sustainable and green catalyst, restrict the use of toxic chemicals, development of single pot synthesis, process for continuous flow manufacturing, and improvement of process efficiency for economic stability.

The work mainly focuses on development of heterogeneous catalyst, process optimization, and reaction kinetics for the synthesis of DMF by CO₂ hydrogenation at supercritical conditions. The process optimization resulted in complete conversion of reactant with more than 90 % selectivity of DMF. Also, for the synthesis of styrene carbonate, a continuous flow reactor is developed based on reaction kinetic studies. The continuous reactor promises hassle free synthesis with maximum conversions at mild reaction conditions. The salicylic acid production is carried out in multiple steps by industries with tedious downstream process for catalyst recovery. Single pot synthesis is developed with zeolite catalyst and detailed process development is carried out.

The thesis work, along with intensified processes for valued chemicals, provides significant fundamental understanding of process and catalyst system necessary for sustainable commercial scale production.

List of Publications:

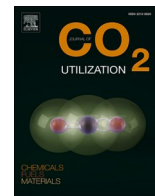
1. Sagar D. Chaudhary, Shardul S. Rahatade, Sunil S. Joshi, Nilesh A. Mali, “Reduction of carbon dioxide to dimethylformamide using ruthenium doped Mg/Al hydrotalcites under supercritical conditions”, Journal of CO₂ utilization, 102055, 2022. <https://doi.org/10.1016/j.jcou.2022.102055>
2. Sagar D. Chaudhary, Shardul S. Rahatade, Sunil S. Joshi, Nilesh A. Mali, “Process development for cycloaddition of CO₂ in styrene oxide, a batch and continuous synthesis approach” (Manuscript under process)

List of Conferences presented:

1. **S. Chaudhary**, S. Joshi, “Hydrogenation of CO₂ to formic acid and its derivatives under supercritical conditions”, Carbon capture and utilization, Dec 2018, CSIR – NCL, Pune (Oral Presentation).



Contents lists available at ScienceDirect

Journal of CO₂ Utilizationjournal homepage: www.elsevier.com/locate/jcou

Reduction of carbon dioxide to dimethylformamide using ruthenium doped Mg/Al hydrotalcites under supercritical conditions

Sagar D. Chaudhary^{a,b}, Shardul S. Rahatade^a, Sunil S. Joshi^{a,b,*}, Nilesh A. Mali^{a,b}

^a Chemical Engineering and Process Development, CSIR-National Chemical Laboratory, Pune 411008, India

^b Academy of Scientific and Innovative Research (AcSIR), Ghaziabad 201002, India

ARTICLE INFO

Keywords:

Hydrotalcite
Supercritical carbon dioxide
Hydrogenation
Dimethylformamide
Langmuir-Hinshelwood-Hougen-Watson model

ABSTRACT

The utilization of carbon dioxide is one of the developing areas due to its significant contribution to global warming. Reducing carbon dioxide (CO₂) to formic acid and its derivatives has gained importance because of its thermodynamic limitations and high industrial demand. In this article, we report the synthesis of dimethylformamide (DMF) using ruthenium doped Mg/Al calcined hydrotalcite by CO₂ hydrogenation in the presence of dimethylamine (DMA). At optimized conditions, complete conversion of dimethylamine was achieved with more than 92% product yield at 170 °C and 13 MPa pressure with a reaction time of 6 h. Key catalyst properties were determined using X-ray powder diffraction (XRD), X-ray photoelectron spectroscopy (XPS), CO₂-temperature programmed desorption (TPD), H₂ temperature-programmed reduction (TPR) and Fourier transform infrared (FTIR). The determination of surface morphology was carried out using field emission scanning electron microscope (FE-SEM) and high-resolution transmission electron microscopy (HR-TEM). At the same time, the chemical composition was verified by energy-dispersive X-ray (EDS). In addition, kinetic modeling is performed using the two site Langmuir-Hinshelwood-Hougen-Watson model. The regressed kinetic parameters gave an appropriate fit with experimental concentration values and activation energy is calculated as 413 kJ/mol K⁻¹.

1. Introduction

With the advent of global warming, increasing levels of CO₂ are the primary concern, and at this alarming rate, the pre-industrial CO₂ concentrations will double by the end of the 21st century [1]. Due to the demand for alternative carbon sources and high carbon dioxide concentration levels, CO₂ to value-added chemicals like methanol, ethers, carbonates, formates, etc, is a competent and engaging route [2,3].

CO₂ hydrogenation to formic acid and its derivatives has been a field of interest for researchers and industrialists due to its thermodynamics and industrial value. It is a highly reversible endergonic reaction with Gibbs free energy of 32.9 kJ/mol [4]. DMF has mainly been used as a solvent for many chemical processes and is currently produced by carbonylation of DMA at 70–100 °C and 2–10 MPa [5]. Many routes for the production of DMF via hydrogenation of CO₂ and DMA have been explored by various authors. In this context, substantial evolution has been made in recent years, and different transition metal-based homogeneous catalysts have been reported with high turnover numbers (TON) and frequencies (TOF) [6–10]. Haynes et al. reported the mechanistic information of hydrogenation of carbon dioxide to DMF using

transition metal phosphine complexes, in which, the moles of DMF produced per mole of catalyst was found to be high [11]. Jessop et al. reported a very efficient method of synthesizing DMF by hydrogenation of CO₂ in a supercritical phase (scCO₂) using Ruthenium chloro-phosphine complex RuCl₂[P(CH₃)₃]₄ [9], where scCO₂ was used as a reactant as well as the reaction medium. In comparison with conventional solvents, scCO₂ improved reaction yields due to its high complex solubility, hydrogen miscibility, and increased diffusion and mass transfer rates [12–15]. Krocher et al. prepared a more active silica hybrid gel containing RuCl₂(dpe)₂ catalyst and obtained TOF up to 110,800/h [16]. However, the formation of water as a side product resulted in a poor interaction between Ru-complexes and amine, which affected the conversion of DMA. To overcome the problem of phase separation, a series of water-soluble Ru-complexes were reported by Kayaki et al. producing TON ranging from 2100 to 9000 [17]. Several reports hypothesized the presence of water promotes CO₂ hydrogenation as a supplementary ligand on a metal-based transition catalyst. Infusion of CO₂ into a metal-hydrogen bond can be accelerated due to water molecules resulting from hydrogen bonding [18–20].

Numerous efforts have been made to prepare heterogeneous

* Corresponding author at: Chemical Engineering and Process Development, CSIR-National Chemical Laboratory, Pune 411008, India
E-mail address: ss.joshi@ncl.res.in (S.S. Joshi).

<https://doi.org/10.1016/j.jcou.2022.102055>

Received 10 February 2022; Received in revised form 2 May 2022; Accepted 4 May 2022

Available online 11 May 2022

2212-9820/© 2022 Elsevier Ltd. All rights reserved.

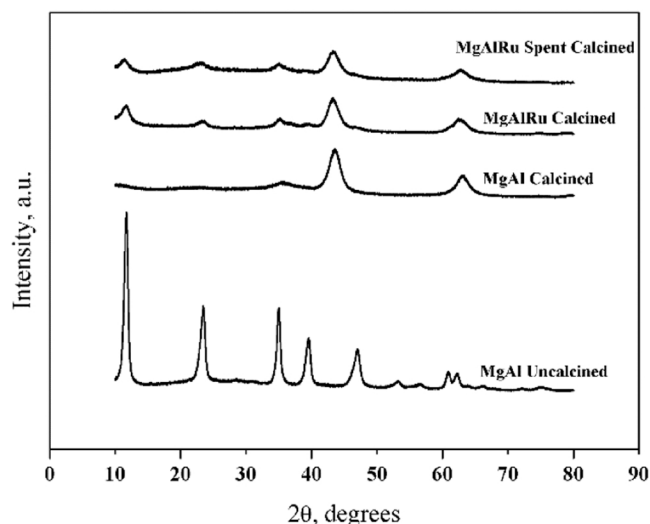


Fig. 1. XRD pattern of Mg:Al and Ruthenium doped Mg:Al hydrotalcites.

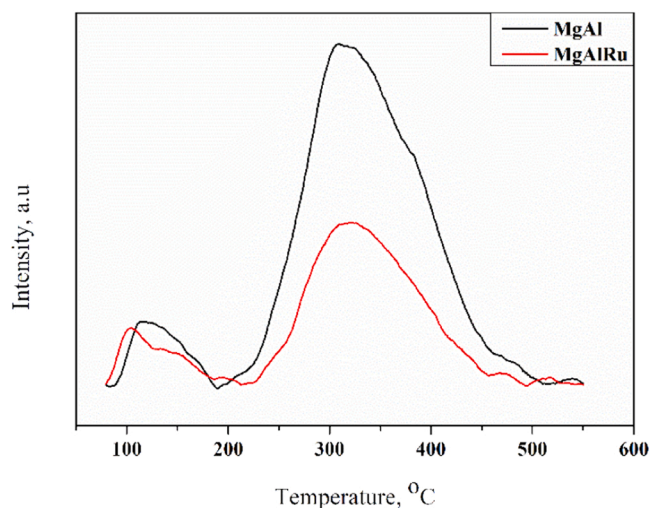


Fig. 2. CO₂ – TPD profiles of Mg:Al and Mg:Al:Ru calcined hydrotalcite.

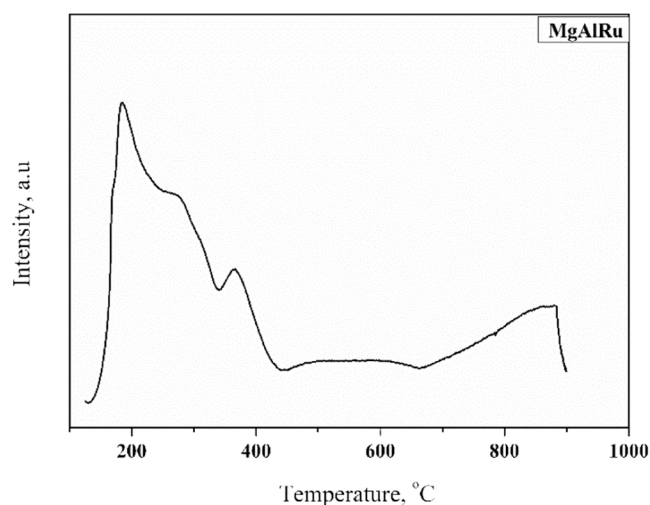


Fig. 3. H₂- TPR for calcined Mg:Al-Ru hydrotalcite.

catalysts using various supports to conquer the constraint of separation and recovery of a homogenous catalyst. Considerable TOF values and recyclability of silica and aerogel-supported Ruthenium complexes were reported by Baiker et al. [16,21–23]. Hydrophilic and recyclable cross-linked graft copolymer resin-supported Ruthenium complex was prepared and studied for hydrogenation of CO₂ to DMF by Kayaki et al. [24]. These catalysts were recycled after drying with a moderate loss of activity. Liu et al. reported the synergistic effect of Cu/ZnO catalyst in solvent-free conditions, where copper is used for hydrogen activation and generation of formate species that migrate on ZnO and form DMF by dehydration dimethylamine formate [25].

Nearly all of the catalysts investigated for hydrogenation of CO₂ to DMF contain transition metal complexes with halides or hydrides and phosphine ligands. A few heterogeneous catalytic systems without halides and phosphine have been reported in the literature [2,25]. Although these catalysts proved better for higher conversion and yield, they are limited by economic considerations and toxicity. Hence, there is a need to develop efficient, less toxic, cheap, and green catalysts. Concerning the selective hydrogenation of CO₂ and DMA to DMF, many catalyst systems have been reported, which involve noble metal complexes and supported metal complexes. Many of these transition metals are well known as active in hydrogenation reactions [3,9,20,25–27]. In the current work, Ruthenium doped Mg:Al calcined hydrotalcite (CHTLs) is proposed as a phosphine-free heterogeneous catalytic system for the hydrogenation of CO₂ to DMF.

Hydrotalcites are a basic anionic layered clay material. These are the types of lamellar ionic compounds used as adsorbents, ion-exchangers, stabilizers, and catalyst precursors [28]. Hydrotalcites have a greater CO₂ adsorption capacity than other basic materials. The structure of hydrotalcite resembles the form of brucite Mg(OH)₂ with fractional change in M(II) ions replaced with M(III). A positive charge is balanced by balancing anions in the inter-lamellar space apart from water molecules. The composition of hydrotalcites can be varied by replacing M(II) with isomorphs M(III) cations having nearly the same size [29]. The dependency of adsorption capacity for CO₂ on microporous volume, interlayer spacing, and charge density of hydrotalcite has been explained by Alirio E. Rodrigues et al. [30,31]. Basicity of hydrotalcite can be tuned by changing the nature and ratio of M²⁺/M³⁺ metal or by replacing a suitable anion between the interlayer. It can also be achieved by doping various elements or controlling thermal activation. Mg:Al CHTLs have intermediate basic sites that form bi-dentate carbonates on the adsorption of CO₂. High surface area, uniform distribution of cations, and high thermal stability make hydrotalcite-based metal oxides a suitable catalyst. The Hydrotalcite structure can hold significant variations in the type of interlayer anions and different cations with + 2 and + 3 oxidation states [32]. The present study aims to compare the effectiveness of noble metals as promoters of Mg:Al CHTLs catalysts for CO₂ hydrogenation to DMF in the presence of DMA. The effects of these promoters on catalyst activity and selectivity have been explored.

2. Experimental

2.1. Materials

Dimethylamine (40% solution) was supplied by Loba chemicals, Mumbai, India, the metal precursors (>99% assay), KHCO₃ (99.5%), methanol HPLC grade (>99.5%), and sodium carbonate(99.5%) were procured from Merck India. Vadilal gases supplied the hydrogen gas cylinder, and the Liquid CO₂ cylinder (99.9%) was procured from Deluxe Industrial gases, Pune, India. Deionized water with a conductivity of 0.055 μs/cm was used to synthesize the catalysts.

2.2. Catalyst preparation

The Mg:Al:M CHTLs were prepared using the co-precipitation method at constant pH [28,33]. For the preparation of CHTLs, Magnesium nitrate

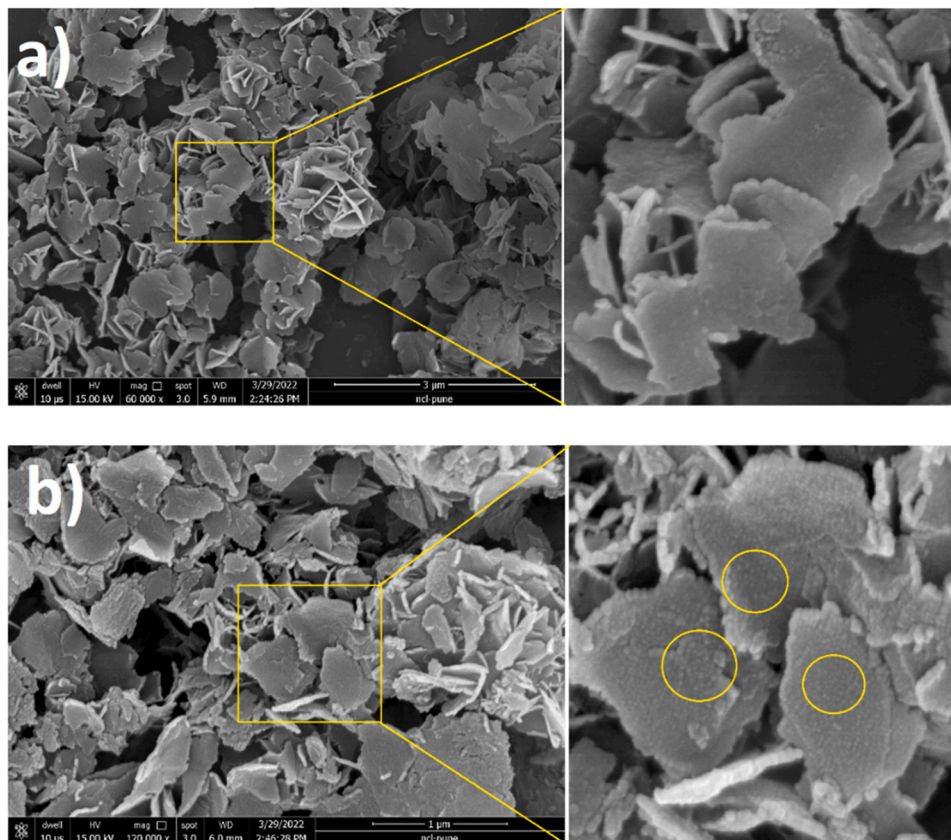


Fig. 4. FE-SEM images of a) Mg-Al and b) Mg-Al-Ru calcined hydrotalcite.

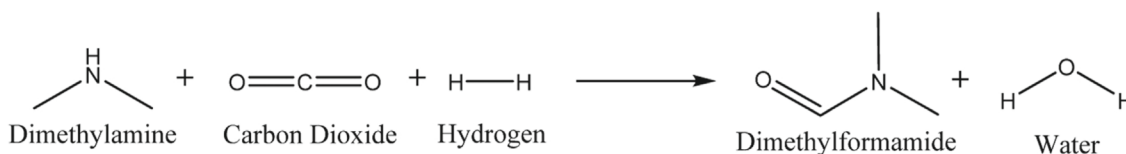
hexahydrate (40 mmol) and Aluminium nitrate nonahydrate (10 mmol) supplied by Merck limited and Ruthenium (III) chloride hydrate (0.5 mmol) supplied by Sigma-Aldrich was dissolved in 100 ml of water. The second solution of 0.5 M Na₂CO₃ was prepared and added dropwise to the nitrate mixture at 80 °C. The blend was aged for 24 h at 80 °C. After filtration, the solid cake was washed with water and dried at 100 °C for 12 h. The resulting catalyst was calcined at 550 °C in the air for 4 h.

2.3. Catalyst characterization

X-ray diffraction (XRD) patterns of the catalysts were measured by Rigaku Dmax 500 diffractometer using nickel filtered Cu K α radiation. The sample was rotated to minimize the textural effect. The diffractometer was recorded in a range between 10° to 80° 2 θ at a scanning rate

resolution transmission electron microscope (HR-TEM) on the Jeol JEM 200 model operated at an accelerating voltage of 200 kV. Catalyst surface composition was confirmed by Energy dispersive X-ray (EDS) analysis coupled with HR-TEM observations. X-ray photoelectron spectroscopy (XPS) measurements were performed on Thermo Fisher Scientific Instrument equipped with Al K α source and multichannel plate (MCP) detector. The Infrared (IR) spectra were recorded in 600–4000 cm⁻¹ using Perkin Elmer Spectrum One Fourier transform infrared spectrometer.

2.4. Catalytic reaction procedure



of 0.01°/s at a temperature of 25 °C. The surface areas of the catalyst samples were determined by nitrogen adsorption with the Thermo-Scientific Surfer instrument at -196 °C and calculated using the Brunauer-Emmett-Teller (BET) surface area analysis method. Basic sites of the catalyst were determined by CO₂ – temperature programmed desorption (TPD) and reducibility of the catalyst were quantified by H₂ – temperature programmed reduction (TPR) studies. Surface morphology studies were performed using a field emission scanning electron microscope (FE-SEM) at an accelerating voltage of 10 kV and a high-

Resolution transmission electron microscope (HR-TEM) on the Jeol JEM 200 model operated at an accelerating voltage of 200 kV. Catalyst surface composition was confirmed by Energy dispersive X-ray (EDS) analysis coupled with HR-TEM observations. X-ray photoelectron spectroscopy (XPS) measurements were performed on Thermo Fisher Scientific Instrument equipped with Al K α source and multichannel plate (MCP) detector. The Infrared (IR) spectra were recorded in 600–4000 cm⁻¹ using Perkin Elmer Spectrum One Fourier transform infrared spectrometer.

Reduction of CO₂ to DMF was carried out in a 300 ml stainless steel high-pressure batch reactor supplied by Parr instruments. In a specific experiment, 80 mmol of 40% aqueous DMA, 1 wt% of catalyst, 4.5 mmol KHCO₃, and 100 ml of methanol as solvent were charged into the reactor. After purging with hydrogen, the reactor was pressurized to 5–10 MPa with H₂:CO₂ (3:1) and heated to the required temperature. The reaction mixture was then kept for stirring at a constant temperature for a pre-determined time. The products were analyzed using Agilent

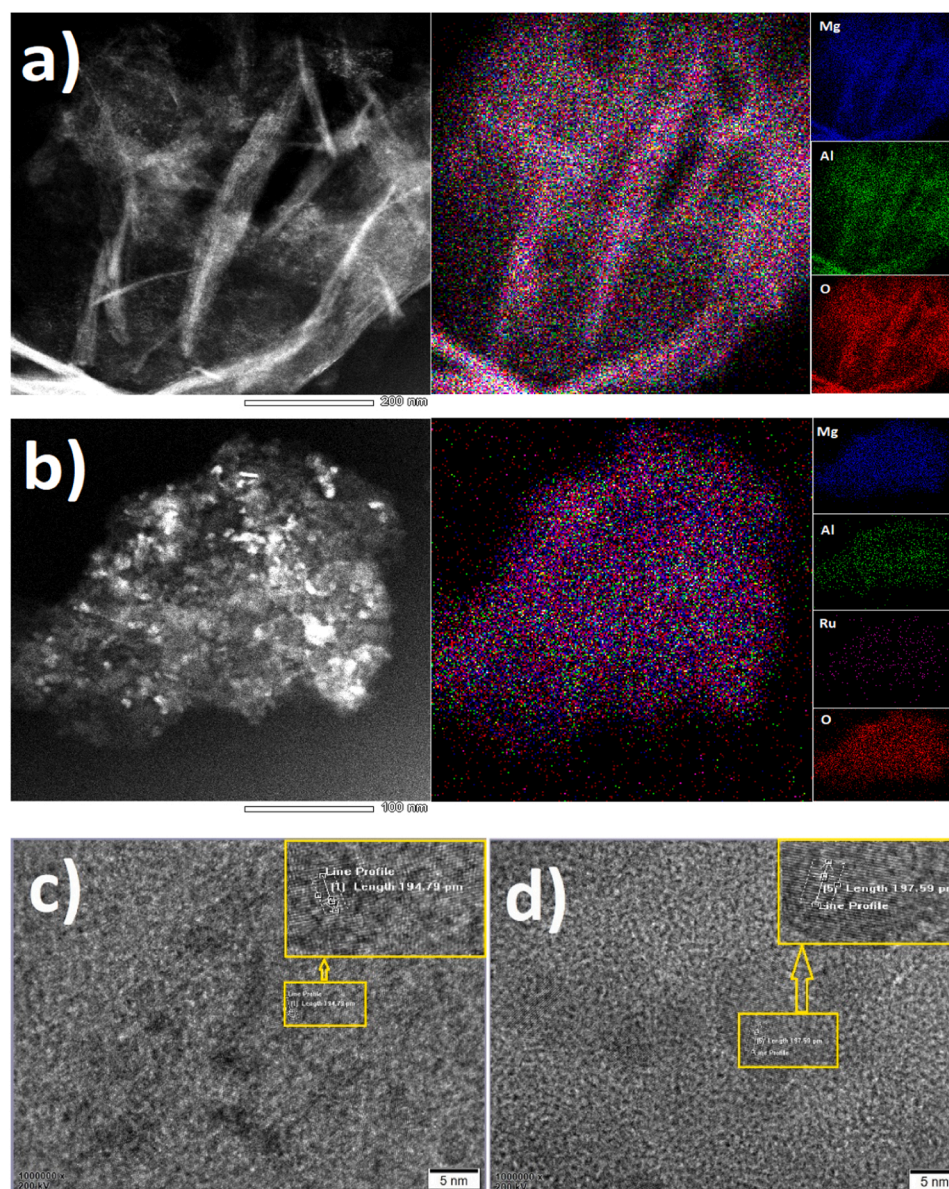


Fig. 5. HR-TEM elemental mapping of a)Mg:Al and b)Mg:Al:Ru calcined hydrotalcite, d-spacing values of c)Mg:Al and d)Mg:Al:Ru calcined hydrotalcite, respectively.

7890B gas chromatography installed with a carbowax 30 m capillary column connected to a flame ionization detector.

3. Results and discussion

3.1. Catalyst characterization

The hydrotalcite structure was stable below 300 °C and transformed into a distorted sheet of Mg/Al mixed oxides after calcination to 550 °C. It is known that the hydrotalcite structure was demolished upon calcination and can be regenerated by the addition of water or being exposed to the atmosphere [34,35]. Powder XRD pattern of uncalcined Mg:Al hydrotalcite (Fig. 1) depicted all representative peaks of pure carbonate-containing hydrotalcites [36]. A comparison of the XRD spectra of Mg:Al (4:1) hydrotalcite and after doping with ruthenium is shown in Fig. 1. The absence of any additional peak in ruthenium doped hydrotalcite confirmed the original crystalline nature. The spent catalyst in the reaction was washed with water and re-calcined at 550 °C for 4 h, and its XRD pattern showed no loss in crystalline nature (Fig. 1).

The basic sites on ruthenium doped Mg:Al calcined hydrotalcite were quantified by CO₂-TPD at different desorption peaks at 100 – 190 °C and 200 – 500 °C, representing weak and medium sites. As shown in Fig. 2, Mg-Al catalyst has a large amount of medium basic sites while, after insertion of ruthenium on Mg/Al oxide support, medium basic sites are decreased due to the acidic nature of ruthenium. These basic sites on Mg/Al oxide layer are responsible for CO₂ activation, while ruthenium helps in hydrogenation. According to Shen et al. [37], calcined Mg-Al hydrotalcite at higher temperatures possess stronger basic sites than acidic ones. With the increase in calcination temperature up to 600 °C, acidic sites are reduced to a minimum while basic sites attain a peak.

Reduction of Mg:Al:Ru calcined hydrotalcite was studied using H₂-TPR. Major Peaks at 200 – 400 °C and small, broad peak at 450 – 600 °C shows the reduction of Ru₂O with different degree of interaction on Mg-Al oxide support [38].

BET surface area of calcined Mg:Al HT and Mg:Al:Ru HT is found to be 851.3 m²/g and 337.7 m²/g, respectively. The loss of interstitial water and carbon dioxide in calcined hydrotalcite leads to amorphous oxide with a high surface area [39]. A decrease in surface area after

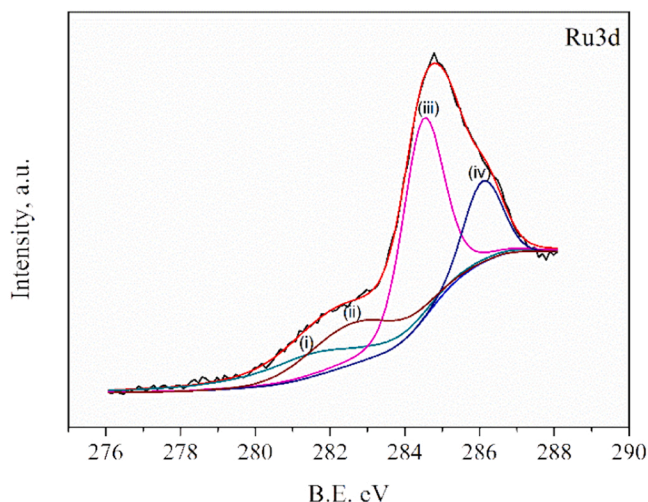


Fig. 6. XPS scan for Ru 3d in Mg:Al:Ru calcined hydrotalcite.

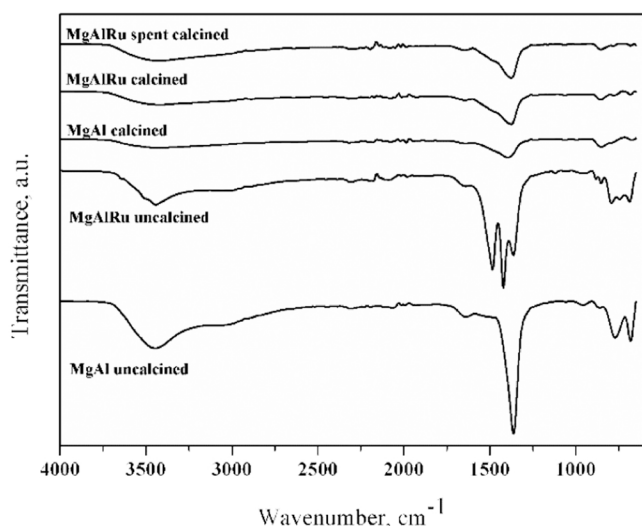


Fig. 7. FTIR spectrum of Mg:Al and Ruthenium doped Mg:Al hydrotalcites.

ruthenium doping is due to meal blocking by large size ruthenium particles on the catalyst's external edge surface, which can be seen from FE-SEM images (Fig. 4). A similar decrease in surface area and pore size after insertion of ruthenium is observed by Maru et al. [40].

The surface morphology studies performed using FE-SEM showed distorted sheet morphology for calcined Mg:Al hydrotalcite (Fig. 4a-b). These conclusions about morphology align with those obtained by Venugopal et al. [41]. As shown in Fig. 4a, distorted sheets of Mg/Al oxide are observed with a planer surface whereas as shown in Fig. 4b, deposition of particles observed on the surface of Mg/Al support which features of the ruthenium oxides.

Evenly dispersed ruthenium particles on the monolayer surface of the catalyst can be seen from elemental mapping and HR-TEM (Fig. 5a-b). Also, the *d*-spacing value (Fig. 5c-d) shows no difference in inter lattice after insertion of ruthenium which also concurs with the doping on the surface of Mg/Al oxide. Energy dispersive X-ray (EDS) analysis confirmed the atomic percentage of ruthenium as 1.3% of total metals present in the catalyst.

Electronic states of catalyst were confirmed using XPS analysis of Ru doped Mg:Al calcined hydrotalcite. The characteristics binding energy values confirms presence of metal oxide in calcined hydrotalcite. Ru 3d scan shows the different oxidation states of ruthenium (Fig. 6). Peak(i) at

B.E 280.3 eV shows the Ru(IV)O₂, peak(ii) at 282.5 contributes to Ru (VI)O₃, peaks(iii and iv) at B.E 284.5 and 286.1 show that the presence of homogeneous ruthenium oxide formation along with other metal incorporation[42] and Ru(II)O[40] respectively. The marginal shifting in binding energies of ruthenium could be due to the stress of metal (M²⁺/M³⁺) incorporation in the catalyst. These observations can also be cross-linked with FE-SEM morphological study and even dispersion of ruthenium in elemental mapping, as described in Figs. 4 and 5.

The FTIR spectrum of the uncalcined Mg:Al:Ru hydrotalcite is shown in Fig. 7. The concentrated broadband between 3800 and 3000 cm⁻¹ represents vibrations of structural OH- groups, physically adsorbed water, and vibrations of carbonate-hydroxyl and hydroxyl-hydroxyl groups in hydrotalcite. The band at 1360 cm⁻¹ represents the presence of carbonate ions and some impurities of nitrate ions due to synthesis solution in uncalcined hydrotalcite. Finally, the broadband at 663 cm⁻¹ was implied in reports as a superposition of the characteristic bonds of hydrotalcites [43]. Upon calcination of HT, it is observed that carbonate and water peaks have vanished, and the loss of hydrotalcite structure is confirmed by the absence of broadband at 663 cm⁻¹. FTIR spectrum of spent calcined hydrotalcite showed the intact nature of the catalyst.

3.2. Mechanistic aspect

The formation mechanism of DMF requires cooperation between both the acidic and basic sites. Base catalyzed hydrogenation was observed with heterolytic dissociation of hydrogen in H⁺ and H⁻ species, whereas amination involves DMA dissociating into ⁻NR₂ and H⁺. In the reaction, basic Mg/Al oxides sites are responsible for CO₂ activation, whereas Ru²⁺ and O²⁻ act as hydrogenation sites.

In the first step, hydrogenation or hydrogen adsorption takes place on the ruthenium surface, followed by activation of CO₂ by creating carbonate species on Mg/Al calcined hydrotalcite (Fig. 8)[44,45]. Further, the lone pair on oxygen atom from carbonate species attacks hydronium ion of ruthenium surface and meanwhile, hydride ion attacks on electrophilic carbon center releasing formic acid and catalyst. Further reaction with DMA forms dimethyl formate, which can be easily dehydrated to form DMF.

3.3. Catalytic CO₂ hydrogenation

In initial studies, a series of calcined hydrotalcites were tested with the general formula M(II): M(III), where M(II) = Mg, Cu, and Zn, and M(III) = Al and Cr with atomic ratio 4:1. Among the catalyst studied, Mg:Al and Cu:Al HT showed a considerable yield of DMF (Table 1). This suggests that appropriate basic sites in Mg and Cu systems contribute to mediating the reaction. The basicity of HT can be adjusted by varying Mg/Al molar ratio or activation at a suitable temperature [46]. The basicity of the HT is mainly due to their O²⁻ (Lewis basicity) and hydroxyl groups (Bronsted basicity) present in it. The increased Mg content in HT resulted in higher DMF selectivity due to the increased basic character of HT. A trace amount of trimethylamine (TMA) was formed in the reaction as a side product by methylation of dimethylamine [47], and in the case of a lesser extent of CO₂ hydrogenation, DMF yield is low, and DMA conversion is higher due to formation of dimethylammonium dimethylcarbamate (DIMCARB) with excess CO₂ in the reaction [48].

Further, different transition and noble metal (1 mol%) doped Mg/Al HT were studied. According to Basile et al., Al³⁺ ions may partially replace by Rh³⁺, Ru³⁺, and Ir³⁺, having in octahedral coordination ionic radius values in the range required for the synthesis of HT phases, whereas Mg²⁺ ions may be substituted by Pd²⁺, Ni²⁺, Co²⁺ and Cu²⁺ [49]. Comparing the results obtained with Ru, Ir, Pd, and Rh-containing catalysts (Table 1, entry 12–15) with other transition metal catalysts (Table 1, entry 7–11) makes it perceptible that preferential coordination is possible to play a more critical role than the ion size. Ruthenium forms a strong coordinated covalent bond in the form of Lewis acid-base

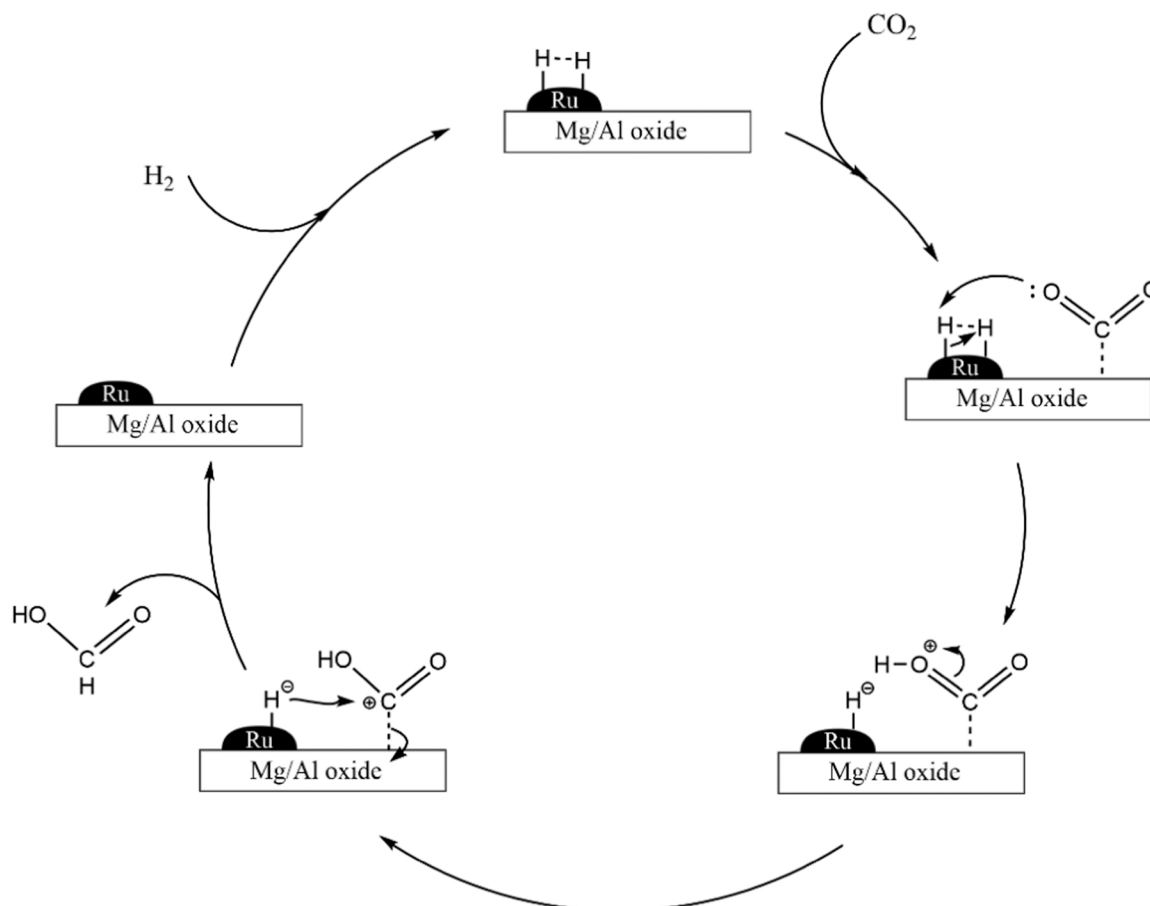


Fig. 8. Proposed reaction mechanism over Ru doped Mg:Al calcined hydrotalcite.

Table 1

Catalyst Screening. Reaction conditions: DMA 80 mmol, solvent MeOH 100 ml, temperature 170 °C, H₂:CO₂ 3:1, reaction pressure 10 MPa, time 3 h, catalyst amount 1 wt%, additive KHCO₃ 4.5 mmol.

Entry	Catalyst (HT)	DMA conversion (%)	DMF yield (%)
1	Cu:Al(4:1)	33.0	7.6
2	Zn:Al(4:1)	6.7	0.3
3	Mg:Cr(4:1)	1.2	0.2
4	Mg:Al(4:1)	24.2	7.0
5	Mg:Al(2:1)	23.3	4.2
6	Mg:Al(6:1)	22.7	2.4
7	Mg:Al:Cu(4:1:0.05)	11.1	6.8
8	Mg:Al:Ni(4:1:0.05)	5.2	2.2
9	Mg:Al:Zn(4:1:0.05)	5.7	0.4
10	Mg:Al:Co(4:1:0.05)	2.1	1.5
11	Mg:Al:Cr(4:1:0.05)	4.5	0.3
12	Mg:Al:Pd(4:1:0.05)	7.9	3.5
13	Mg:Al:Rh(4:1:0.05)	20.3	8.6
14	Mg:Al:Ir(4:1:0.05)	57.3	46.1
15	Mg:Al:Ru(4:1:0.05)	88.4	78.8

interaction, which promotes the hydrogenation step in the reaction mechanism. Higher selectivity and conversion with Ru-HT show that ruthenium has major active sites for the reaction (Table 1, entry 15).

The reaction temperature and time greatly influence catalyst activity and product yield. Fig. 9a shows the reaction yield at different temperatures with ruthenium doped Mg:Al HT. DMF yield increases with temperature up to 170 °C, and a further increase in temperature results in increased TMA due to methylation of DMA, which is a temperature-driven reaction as reported [50,51]. Gradual increase in conversion

and yield is observed at 170 °C with time, and within 6 h, complete conversion with 92.5% yield of DMF is achieved (Fig. 9b).

The total pressure in the reaction plays a significant role in the diffusion of reactants on solid catalyst surfaces. Bertuccio et al. reported the benefits of hydrogenation of CO₂ in the supercritical phase indicating higher reaction yields due to lower mass transfer limitations [52]. The same trend of DMF yield is observed in the proposed study. With increased pressure up to 13 MPa, complete conversion of DMA is observed with 92.5% DMF yield. As shown in Fig. 9c, reaction yield and conversion is comparatively low in the subcritical phase than in the supercritical phase of CO₂.

The catalyst amount reliability on reaction conversion and yield is shown in Fig. 9d. DMF yield is gradually increased with catalyst amount up to 1 wt% of DMA at 170 °C for 6 h. Further increase in catalyst loading does not have any effect on product yield. In addition, the experimental studies show that the reaction does not proceed in the absence of the catalyst.

The addition of a small amount of solid base potassium bicarbonate (KHCO₃) as an additive showed a radical effect on the reaction yield. This is due to basic ions preventing the decomposition of formic acid produced during the reaction back to hydrogen and carbon dioxide [53]. The yield of 92.5% was obtained with the addition of 4.5 mmol of KHCO₃ while 74% yield of DMF was observed without the addition of base at 170 °C in 6 h as shown in Fig. 10.

4. Kinetic model

The experiments were performed to understand the kinetics of the process at temperatures of 150 °C and 170 °C, and the kinetic model was developed according to the Langmuir-Hinshelwood-Hougen-Watson.

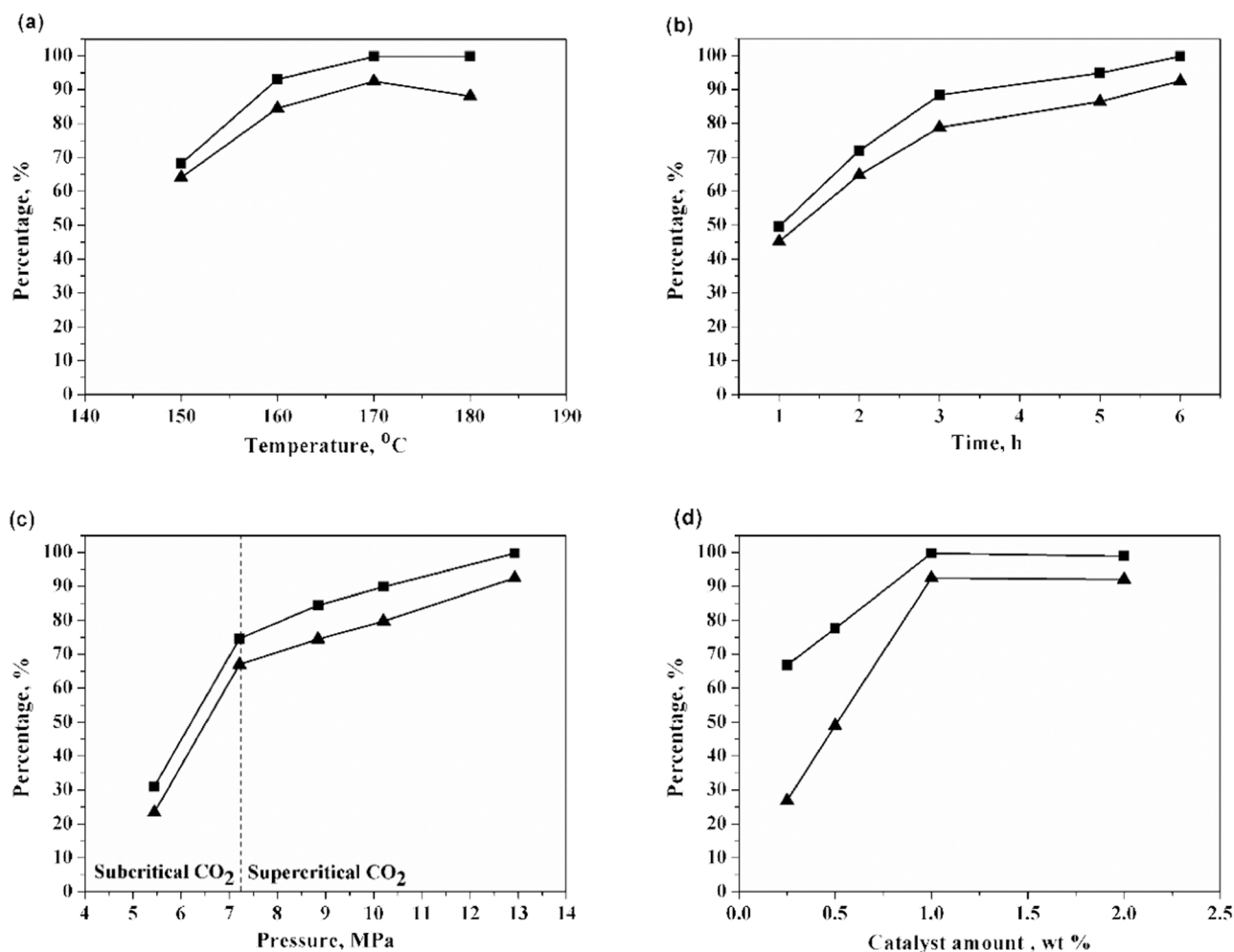


Fig. 9. ■ DMA conversion; ▲ DMF yield. (a) Effect of temperature for 6 h, 13 MPa pressure, and 1 wt% catalyst loading (b) Effect of time at 170 °C at 13 MPa pressure and 1 wt% catalyst loading (c) Effect of pressure at 170 °C for 6 h at 1 wt% catalyst loading (d) Effect of catalyst loading at 170 °C for 6 h and 13 MPa pressure. Other reaction conditions: DMA 80 mmol, solvent MeOH 100 ml, H₂:CO₂ 3:1, additive KHCO₃ 4.5 mmol.

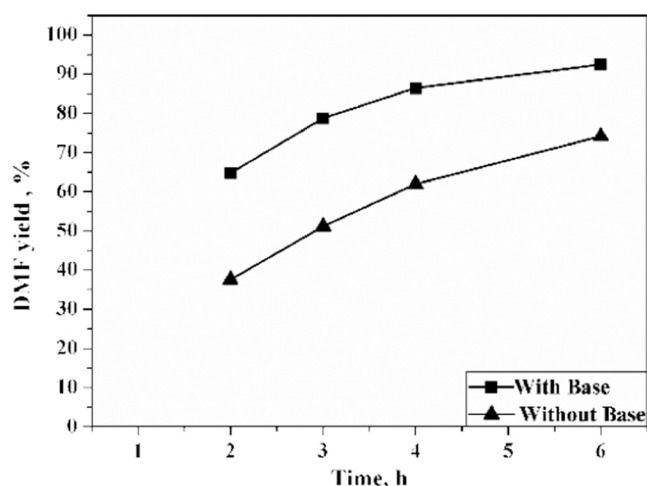


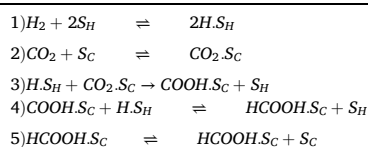
Fig. 10. Effect of Base addition. Reaction conditions: DMA 80 mmol, H₂:CO₂ 3:1, time 6 h, temperature 170 °C, reaction pressure 13 MPa, catalyst Mg:Al:Ru HT (1 wt%),.

The following surface mechanism considers the non-competitive adsorption of CO₂ and H₂ on two types of active sites.

Steps (i) and (ii) are the H₂ and CO₂ adsorption steps, while step (v) is

Table 2

Surface reactions over Mg:Al:Ru hydrotalcite.



the formic acid desorption step from the surface of the catalyst. The irreversible surface reaction considered rate-limiting is step (iii). Under this assumption, the rate equation can be generated for hydrogenation as follows:

$$r_R = K_R S'_H S_{CO_2.C} \quad (1)$$

Where,

Occupied Hydrogen Sites: $S'_H = H.S_H$

Unoccupied Hydrogen Sites: S_H .

Occupied CO₂ sites: $S_{i.C}$.

Unoccupied CO₂ sites: S_C .

The concentration of Components' i : C_i

The equilibrium constants for the surface reaction mentioned in Table 2 are stated as follows:

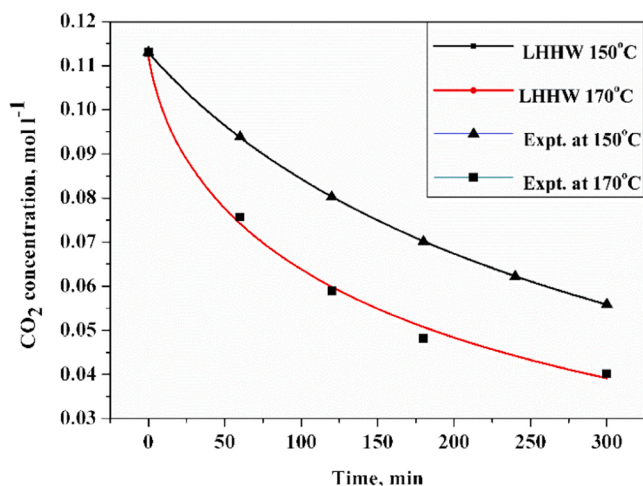


Fig. 11. Comparison between batch reaction data and model results at 150°C and 170 °C.

Table 3
Estimated Kinetic LHHW Parameters.

Temperature	150°C	170°C	Units
Parameters			
K_i	0.3717	0.00018	$\text{mol.mol}_{\text{cat}}^{-1}.\text{min}^{-1}$
K_{ii}	0.7109	0.5329	$\text{mol.mol}_{\text{cat}}^{-1}.\text{min}^{-1}$
K_v	9.98	63.805	$\text{mol.mol}_{\text{cat}}^{-1}.\text{min}^{-1}$
K_R	0.03153	7.68	$\text{L.mol}^{-1}.\text{min}^{-1}$
E_a	413.1		$\text{kJ.mol}^{-1}.\text{K}^{-1}$

$$K_i : \text{H}_2 \text{ adsorption constant} = \frac{S_H^2}{C_H S_H} \quad (2)$$

$$K_{ii} : \text{CO}_2 \text{ adsorption constant} = \frac{S_{\text{CO}_2.C}}{C_{\text{CO}_2} S_C} \quad (3)$$

$$K_{iv} : \text{Reaction rate constant of step iv} = \frac{S_{\text{HCOOH.C}} S_H}{S_{\text{COOH.C}} S_H} \quad (4)$$

$$K_v : \text{Formic acid desorption constant} = \frac{S_{\text{HCOOH.C}} S_H}{S_{\text{COOH.C}} S_H} \quad (5)$$

The fractional coverages of active sites S_H' and $S_{i.C}$ are derived from the mass balances as given by Eqs. (6) and (7).

$$S_H + S_H' = 1 \quad (6)$$

$$S_{\text{CO}_2.C} + S_{\text{HCOOH.C}} + S_{\text{COOH.C}} + S_C = 1 \quad (7)$$

The Eqs. (2) and (6) are combined to yield,

$$S_H' = \frac{\sqrt{K_1 C_H}}{\sqrt{K_1 C_H} + 1} \quad (8)$$

$$S_H = \frac{1}{\sqrt{K_1 C_H} + 1} \quad (9)$$

Similarly, Eqs. (3)–(5) are combined with Eq. (7) to yield,

$$S_{\text{CO}_2.C} = \frac{K_2 C_{\text{CO}_2}}{(K_2 C_{\text{CO}_2} + K_5 C_{\text{HCOOH}} + 1)} \quad (10)$$

Finally, Eqs. (8) and (10) are substituted in Eq. (1) to deduce the final rate equation as,

$$r_R = K_R \times \frac{\sqrt{K_1 C_H}}{\sqrt{K_1 C_H} + 1} \times \frac{K_2 C_{\text{CO}_2}}{(K_2 C_{\text{CO}_2} + K_5 C_{\text{HCOOH}} + 1)} \quad (11)$$

The above kinetic model is solved according to appropriate initial conditions by the ODE45 solver of MATLAB. Regression is performed using the *fminsearch* to minimize the error between the experimental and calculated concentration values. The coefficient of determination (R^2) between the calculated and experimental concentration values for 150°C and 170 °C experimental runs is 0.9997 and 0.9967, respectively. The model accurately describes the observed trends with changes in operating temperature, as shown in Fig. 11. The kinetic parameters were optimized with good precision after multiple iterations. The general procedure for solving the LHHW model is performed as described by Vernuccio et al. [54].

The estimated kinetic parameters are known to follow the Arrhenius temperature dependence (Eq. (12)) and are depicted in Table 3.

$$K_R = k_0 \exp\left(\frac{-E_a}{RT}\right) \quad (12)$$

k_0 : Pre-Exponential Factor ($\text{L.mol}^{-1}.\text{min}^{-1}$).

E_a : Activation Energy ($\text{kJ.mol}^{-1}.\text{K}^{-1}$).

R : Universal Gas Constant ($\text{J.mol}^{-1}.\text{K}^{-1}$).

5. Conclusions

Different hydrotalcite-like compounds with a molar ratio 4:1 were prepared and have been tested for hydrogenation of CO₂ to DMF under supercritical conditions of CO₂. Results show that the basic sites in the catalyst have a considerable influence on the reaction yield. The optimum yield can be obtained from balancing the number of basic and metallic sites on, and the hydrogenation was favored by a topology of metallic sites. Mg/Al HT with molar ratio 4 was found to be most active within other bimetallic hydrotalcite. The activity of the catalyst increased by impregnating various noble metals on hydrotalcite. The selectivity of DMF increases with the increase in the basicity of catalysts, suggesting that formic acid is the primary product. This might be because catalyst particles have a large surface area and had sufficient basic sites to carry out hydrogenation. Among the four noble metal promoters, the Ruthenium effect is more noticeable than the other promoters. This could be due to the different effects of these promoters on CO₂ adsorption, hydrogenation, or product formation. Thus it is concluded that Mg:Al:Ru CHTs with higher thermal stability and a molar ratio of 4:1:0.05 is a promising candidate for hydrogenation of CO₂ to DMF with 92.5% yield and would be able to replace traditional homogeneous catalysts. The kinetic model developed is in-line with the experimental trends, and the regression performed resulted in kinetic parameters with desirable accuracy.

CRedit authorship contribution statement

Sagar D. Chaudhary: Conceptualization, Methodology, Software, Formal analysis, Investigation, Writing – original draft, Writing – review & editing, Visualization, Project administration. **Shardul S. Rahatade**: Methodology, Software, Formal analysis, Writing – original draft. **Sunil S. Joshi**: Conceptualization, Supervision, Validation, Resources, Data curation, Project administration, Funding acquisition. **Nilesh A. Mali**: Validation, Resources, Data curation, Project administration, Funding acquisition.

Declaration of Competing Interest

The authors declare that they have no known competing financial interests or personal relationships that could have appeared to influence the work reported in this paper.

Acknowledgments

The authors acknowledge the support from the Council of Scientific and Industrial Research (CSIR), Delhi, India, for providing a Research

Fellowship. The authors thank the Academy of Scientific & Innovative Research (AcSIR) and CSIR-National Chemical Laboratory for providing experimental facilities.

Declaration of interests

The authors declare no competing financial interest.

References

- S. Solomon, G. Plattner, R. Knutti, P. Friedlingstein, Irreversible climate change due to carbon dioxide emissions, *Proc. Natl. Acad. Sci. USA* 106 (2009) 1704–1709, <https://doi.org/10.1073/pnas.0812721106>.
- W. Wang, S. Wang, X. Ma, J. Gong, Recent advances in catalytic hydrogenation of carbon dioxide, *Chem. Soc. Rev.* 40 (2011) 3703–3727, <https://doi.org/10.1039/c1cs15008a>.
- P. Jessop, T. Ikariya, R. Noyori, Homogeneous hydrogenation of carbon dioxide, *Chem. Rev.* 95 (1995) 259–272, <https://doi.org/10.1021/cr00034a001>.
- T. Schaub, R. Paciello, A process for the synthesis of formic acid by CO₂ hydrogenation: Thermodynamic aspects and the role of CO, *Angew. Chem. - Int. Ed.* 50 (2011) 7278–7282, <https://doi.org/10.1002/anie.201101292>.
- K. Weissermel, H. Arpe, *Industrial Organic Chemistry*, third ed., Wiley, 1997, <https://doi.org/10.1002/9783527616688>.
- A. Behr, K. Nowakowski, Catalytic hydrogenation of carbon dioxide to formic acid, *Adv. Inorg. Chem.* 66 (2014) 223–258, <https://doi.org/10.1016/B978-0-12-420221-4.00007-X>.
- E. Graf, W. Leitner, Direct formation of formic acid from carbon dioxide and dihydrogen using the $[\{\text{Rh}(\text{cod})\text{Cl}\}_2\text{-Ph}_2\text{P}(\text{CH}_2)_4\text{PPh}_2]$ catalyst system, *J. Chem. Soc. Chem. Commun.* 8 (1992) 623–624, <https://doi.org/10.1039/C39920000623>.
- N. Ezhova, N. Kolesnichenko, A. Bulygin, E. Slivinskii, S. Han, Hydrogenation of CO₂ to formic acid in the presence of the Wilkinson complex, *Russ. Chem. Bull.* 51 (2002) 2165–2169, <https://doi.org/10.1023/A:1022162713837>.
- P. Jessop, Y. Hsiao, T. Ikariya, R. Noyori, Catalytic production of dimethylformamide from supercritical carbon dioxide, *J. Am. Chem. Soc.* 116 (1994) 8851–8852, <https://doi.org/10.1021/ja00098a072>.
- F. Gassner, W. Leitner, Hydrogenation of carbon dioxide to formic acid using water-soluble rhodium catalysts, *J. Chem. Soc. Chem. Commun.* 19 (1993) 1465–1466, <https://doi.org/10.1039/C39930001465>.
- P. Haynes, L. Slaugh, J. Kohnle, Formamides from carbon dioxide, amines and hydrogen in the presence of metal complexes, *Tetrahedron Lett.* 11 (1970) 365–368, [https://doi.org/10.1016/0040-4039\(70\)80086-7](https://doi.org/10.1016/0040-4039(70)80086-7).
- R. Skouta, Selective chemical reactions in supercritical carbon dioxide, water, and ionic liquids, *Green. Chem. Lett. Rev.* 2 (2009) 121–156, <https://doi.org/10.1080/17518250903230001>.
- S. Li, Y. Wang, K. Zhang, C. Qiao, Diffusion behaviour of supercritical CO₂ in micro- to nanoconfined pores, *Ind. Eng. Chem. Res.* 58 (2019) 21772–21784, <https://doi.org/10.1021/acs.iecr.9b04750>.
- C. Wai, F. Hunt, M. Ji, X. Chen, Chemical reactions in supercritical carbon dioxide, *J. Chem. Educ.* 75 (1998) 1641–1645, <https://doi.org/10.1021/ed075p1641>.
- P. Licence, J. Ke, M. Sokolova, S. Ross, M. Poliakov, Chemical reactions in supercritical carbon dioxide: from laboratory to commercial plant, *Green. Chem.* 5 (2003) 99–104, <https://doi.org/10.1039/b212220k>.
- O. Kröcher, R. Köppel, M. Fröba, A. Baiker, Silica hybrid gel catalysts containing group(VIII) transition metal complexes: Preparation, structural, and catalytic properties in the synthesis of N,N-dimethylformamide and methyl formate from supercritical carbon dioxide, *J. Catal.* 178 (1998) 284–298, <https://doi.org/10.1006/jcat.1998.2151>.
- Y. Kayaki, Y. Shimokawatoko, T. Ikariya, Synthesis of ruthenium(II) complexes containing hydroxymethylphosphines and their catalytic activities for hydrogenation of supercritical carbon dioxide, *Inorg. Chem.* 46 (2007) 5791–5797, <https://doi.org/10.1021/ic700470n>.
- F. Hutschka, A. Dedieu, M. Eichberger, R. Fornika, W. Leitner, Mechanistic aspects of the rhodium-catalyzed hydrogenation of CO₂ to formic acid - A theoretical and kinetic study, *J. Am. Chem. Soc.* 119 (1997) 4432–4443, <https://doi.org/10.1021/ja961579x>.
- J. Tsai, K. Nicholas, Rhodium-catalyzed hydrogenation of carbon dioxide to formic acid, *J. Am. Chem. Soc.* 114 (1992) 5117–5124, <https://doi.org/10.1021/ja00039a024>.
- P. Jessop, Y. Hsiao, T. Ikariya, R. Noyori, Homogeneous catalysis in supercritical fluids: Hydrogenation of supercritical carbon dioxide to formic acid, alkyl formates, and formamides, *J. Am. Chem. Soc.* 118 (1996) 344–355, <https://doi.org/10.1021/ja953097b>.
- O. Kröcher, R. Köppel, A. Baiker, Sol-gel derived hybrid materials as heterogeneous catalysts for the synthesis of N,N-dimethylformamide from supercritical carbon dioxide, *Chem. Commun.* 13 (1996) 1497–1498, <https://doi.org/10.1039/CC960001497>.
- L. Schmid, M. Rohr, A. Baiker, A mesoporous ruthenium silica hybrid aerogel with outstanding catalytic properties in the synthesis of N,N-diethylformamide from CO₂, H₂ and diethylamine, *Chem. Commun.* (1999), <https://doi.org/10.1039/a906956i>.
- O. Kröcher, R.A. Köppel, A. Baiker, Silica hybrid gel catalysts containing ruthenium complexes: Influence of reaction parameters on the catalytic behaviour in the synthesis of N,N-dimethylformamide from carbon dioxide, *J. Mol. Catal. A Chem.* (1999), [https://doi.org/10.1016/S1381-1169\(98\)00224-6](https://doi.org/10.1016/S1381-1169(98)00224-6).
- Y. Kayaki, Y. Shimokawatoko, T. Ikariya, Amphiphilic resin-supported ruthenium (II) complexes as recyclable catalysts for the hydrogenation of supercritical carbon dioxide, *Adv. Synth. Catal.* 345 (2003) 175–179, <https://doi.org/10.1002/adsc.200390007>.
- J. Liu, C. Guo, Z. Zhang, T. Jiang, H. Liu, J. Song, H. Fan, B. Han, Synthesis of dimethylformamide from CO₂, H₂ and dimethylamine over Cu/ZnO, *Chem. Commun.* 46 (2010) 5770–5772, <https://doi.org/10.1039/c0cc00751j>.
- C. Tai, J. Pitts, J. Linehan, A. Main, P. Munshi, P. Jessop, In situ formation of ruthenium catalysts for the homogeneous hydrogenation of carbon dioxide, *Inorg. Chem.* 41 (2002) 1606–1614, <https://doi.org/10.1021/ic010866l>.
- P. Munshi, A. Main, J. Linehan, C. Tai, P. Jessop, Hydrogenation of carbon dioxide catalyzed by ruthenium trimethylphosphine complexes: The accelerating effect of certain alcohols and amines, *J. Am. Chem. Soc.* 124 (2002) 7963–7971, <https://doi.org/10.1021/ja0167856>.
- F. Cavani, F. Trifirò, A. Vaccari, Hydrotalcite-type anionic clays: Preparation, properties and applications, *Catal. Today* 11 (1991) 173–301, [https://doi.org/10.1016/0920-5861\(91\)80068-K](https://doi.org/10.1016/0920-5861(91)80068-K).
- J. Bravo-Suárez, E. Páez-Mozo, S. Oyama, Review of the synthesis of layered double hydroxides: A thermodynamic approach, *Quim. Nova* 27 (2004) 601–614, <https://doi.org/10.1016/S0100-40422004000400015>.
- Z. Yong, V. Mata, A. Rodrigues, Adsorption of carbon dioxide onto hydrotalcite-like compounds (HTLcs) at high temperatures, *Ind. Eng. Chem. Res.* 40 (2001) 204–209, <https://doi.org/10.1021/ie000238w>.
- Z. Yong, A. Rodrigues, Hydrotalcite-like compounds as adsorbents for carbon dioxide, *Energy Convers. Manag.* 43 (2002) 1865–1876, [https://doi.org/10.1016/S0196-8904\(01\)00125-X](https://doi.org/10.1016/S0196-8904(01)00125-X).
- D. Debecker, E. Gaigneaux, G. Busca, Exploring, tuning, and exploiting the basicity of hydrotalcites for applications in heterogeneous catalysis, *Chem. - A Eur. J.* 15 (2009) 3920–3935, <https://doi.org/10.1002/chem.200900060>.
- F. Basile, L. Basini, G. Fornasari, M. Gazzano, F. Trifirò, A. Vaccari, New hydrotalcite-type anionic clays containing noble metals, *Chem. Commun.* 21 (1996) 2435–2436, <https://doi.org/10.1039/CC9960002435>.
- A. Corma, F. Fornés, R. Martín-Aranda, F. Rey, Determination of base properties of hydrotalcites: Condensation of benzaldehyde with ethyl acetoacetate, *J. Catal.* 134 (1992) 58–65, [https://doi.org/10.1016/0021-9517\(92\)90209-Z](https://doi.org/10.1016/0021-9517(92)90209-Z).
- D. Tichit, B. Coq, Catalysis by hydrotalcites and related materials, *CATTECH* 7 (2003) 206–217, <https://doi.org/10.1023/B:CATT.0000007166.65577.34>.
- S. Sharma, P. Parikh, R. Jasra, Solvent free aldol condensation of propanal to 2-methylpentenal using solid base catalysts, *J. Mol. Catal. A Chem.* 278 (2007) 135–144, <https://doi.org/10.1016/j.molcata.2007.09.002>.
- J. Shen, M. Tu, C. Hu, Structural and surface acid/base properties of hydrotalcite-derived MgAlO oxides calcined at varying temperatures, *J. Solid State Chem.* 137 (1998) 295–301, <https://doi.org/10.1006/jssc.1997.7739>.
- J. Apuzzo, S. Cimino, L. Lisi, Ni or Ru supported on MgO/γ-Al₂O₃ pellets for the catalytic conversion of ethanol into butanol, *RSC Adv.* 8 (2018) 25846–25855, <https://doi.org/10.1039/c8ra04310h>.
- P. Kustrowski, L. Chmielarz, E. Bozek, M. Sawalwa, F. Roessner, Acidity and basicity of hydrotalcite derived mixed Mg-Al oxides studied by test reaction of MBOH conversion and temperature programmed desorption of NH₃ and CO₂, *Mater. Res. Bull.* 39 (2004) 263–281, <https://doi.org/10.1016/j.materresbull.2003.09.032>.
- M.S. Maru, S. Ram, N.H. Khan, R.S. Shukla, A ruthenium-inserted hydrotalcite (Ru-HT) heterogeneous catalyst: kinetic studies on the selective hydrogenation of carbon dioxide to formic acid, *Mater. Adv.* 2 (2021) 5443–5452, <https://doi.org/10.1039/d1ma00431j>.
- A. Venugopal, A. Venugopalan, P. Kaliyappan, T. Raja, Oxidative dehydrogenation of ethyl benzene to styrene over hydrotalcite derived cerium containing mixed metal oxides, *Green. Chem.* 15 (2013) 3259–3267, <https://doi.org/10.1039/c3gc41321g>.
- C.D. Wagner, A.V. Naumkin, A. Kraut-Vass, J.W. Allison, C.J. Powell, J.R.-Jr. Rumble, NIST Standard Reference Database 20, Version 3.4 (web version) (<http://srdata.nist.gov/xps/>) 2003.
- K. Parida, J. Das, Mg/Al hydrotalcites: preparation, characterization and ketonization of acetic acid, *J. Mol. Catal. A Chem.* 151 (2000) 185–192, [https://doi.org/10.1016/S1381-1169\(99\)00240-X](https://doi.org/10.1016/S1381-1169(99)00240-X).
- M.S. Maru, S. Ram, R.S. Shukla, N.H. Khan, Ruthenium-hydrotalcite (Ru-HT) as an effective heterogeneous catalyst for the selective hydrogenation of CO₂ to formic acid, *Mol. Catal.* 446 (2018) 23–30, <https://doi.org/10.1016/j.mcat.2017.12.005>.
- J. Jia, C. Qian, Y. Dong, Y. Feng Li, H. Wang, M. Ghousoub, K. Butler, A. Walsh, G. Ozin, Heterogeneous catalytic hydrogenation of CO₂ by metal oxides: defect engineering – perfecting imperfection, *Chem. Soc. Rev.* 46 (2017) 4631–4644, <https://doi.org/10.1039/C7CS00026J>.
- T. Kim, M. Sahimi, T. Tsotsis, The preparation and characterization of hydrotalcite thin films, *Ind. Eng. Chem. Res.* 48 (2009) 5794–5801, <https://doi.org/10.1021/ie900371r>.
- I. Alshakova, G. Nikonov, Selective synthesis of secondary and tertiary amines by reductive N-alkylation of nitriles and N-alkylation of amines and ammonium formate catalyzed by ruthenium complex, *ChemCatChem* 11 (2019) 5370–5378, <https://doi.org/10.1002/cctc.201900561>.
- W. Schroth, J. Andersch, H. Schaedler, R. Spitzner, ChemInform Abstract: The dimethylamine-carbon dioxide-complex dimcarb and its preparative use, *ChemInform* 21 (1990) 55–56, <https://doi.org/10.1002/chin.199007144>.

- [49] F. Basile, G. Fornasari, M. Gazzano, A. Vaccari, Synthesis and thermal evolution of hydrotalcite-type compounds containing noble metals, *Appl. Clay Sci.* 16 (2000) 185–200, [https://doi.org/10.1016/S0169-1317\(99\)00053-8](https://doi.org/10.1016/S0169-1317(99)00053-8).
- [50] Y. Kita, M. Kuwabara, S. Yamadera, K. Kamata, M. Hara, Effects of ruthenium hydride species on primary amine synthesis by direct amination of alcohols over a heterogeneous Ru catalyst, *Chem. Sci.* 11 (2020) 9884–9890, <https://doi.org/10.1039/d0sc03858j>.
- [51] D.R. Corbin, S. Schwarz, J.C. Sonnichsen, Methylamines: a review, *Catal. Today* 37 (1997) 71–102, [https://doi.org/10.1016/S0920-5861\(97\)00003-5](https://doi.org/10.1016/S0920-5861(97)00003-5).
- [52] A. Bertucco, P. Canu, L. Devetta, A. Zwahlen, Catalytic hydrogenation in supercritical CO₂: kinetic measurements in a gradientless internal-recycle reactor, *Ind. Eng. Chem. Res.* 36 (1997) 2626–2633, <https://doi.org/10.1021/ie960369q>.
- [53] W. Leitner, E. Dinjus, F. Gaßner, Activation of carbon dioxide. IV. Rhodium-catalyzed hydrogenation of carbon dioxide to formic acid, *J. Organomet. Chem.* 475 (1994) 257–266, [https://doi.org/10.1016/0022-328X\(94\)84030-X](https://doi.org/10.1016/0022-328X(94)84030-X).
- [54] S. Vernuccio, P. Rudolf von Rohr, J. Medlock, General kinetic modeling of the selective hydrogenation of 2-methyl-3-butyn-2-ol over a commercial palladium-based catalyst, *Ind. Eng. Chem. Res.* 54 (2015) 11543–11551, <https://doi.org/10.1021/acs.iecr.5b03424>.